

Development of a device for monitoring Heart Rate during Positive Airway Pressure Therapy

Mark Gardner

BEng (Mechatronics), MEng (Biomedical)

Thesis

Submitted to Flinders University

for the degree of

Doctor of Philosophy

Medical Device Research Institute
College of Science and Engineering

19/08/19

I. Table of Contents

II. Thesis Summary	xiii
II. Acknowledgements	xv
III. List of Abbreviations	xvii
1. Introduction	1
1.1 Context of the study	1
1.2 Problem statement	1
1.3 Aim	2
1.4 Scope	2
1.5 Overview of the study	2
2. Context	5
2.1 Anatomy and Physiology of a Heart Beat	5
2.1.1 General Anatomy and Physiology	5
2.1.2 Normal Variation of the Heart rate	5
2.2 Sleep Apnoea	7
2.3 Positive Airway Pressure Therapy	7
2.4 Sleep	9
2.4.1 Sleep cycles	9
2.4.2 Circadian Rhythms	9
2.4.3 Polysomnography	10
3. Analysis of HR and HRV	12
3.1 Arrhythmia/abnormal heart beat detection	12
3.1.1 Arrhythmias and Sleep Apnoea	13
3.2 Heart Rate Variability	14
3.2.1 Time Domain	14
3.2.2 Frequency domain	15
3.2.3 HRV during sleep	17
3.3 Summary	19
4. Current practices & technologies - Methods for measuring HR	20
4.1 Electrocardiography	20
4.1.1 Introduction	20
4.1.2 Different electrode types	22
4.1.3 Different electrode configurations	30
4.2 Photoplethysmography	38
4.2.1 Measuring PPG signal from forehead	40
4.2.2 Accuracy of PPG HR measurements	41
4.2.3 Examples of wearable devices using PPG	44
4.2.4 Summary	45

4.3	Ballistocardiography.....	47
4.3.1	Examples of wearable BCG devices.....	49
4.3.2	Summary.....	53
4.4	Data fusion techniques.....	54
4.4.1	Previous applications of data fusion methods for physiological monitoring.....	54
4.4.2	Kalman Filter.....	55
4.4.3	Other Data Fusion methods.....	57
4.4.4	Signal quality estimation.....	58
4.4.5	Summary.....	60
4.5	Literature summary.....	61
5.	Device Description.....	62
5.1	Introduction.....	62
5.2	Cardiomask.....	62
5.3	Design Decisions.....	62
5.3.1	Useful information from the sensor.....	63
5.3.2	Minimal discomfort added to the patient by wearing the device.....	63
5.3.3	Sensors/device easy to use.....	63
5.3.4	Low Cost.....	64
5.3.5	Summary.....	64
5.4	ECG.....	65
5.4.1	Setup.....	65
5.4.2	Testing.....	67
5.4.3	Results.....	69
5.5	PPG.....	73
5.5.1	Setup.....	73
5.5.2	PPG heartbeat detection.....	74
5.5.3	Results.....	75
5.6	BCG.....	76
5.6.1	Setup.....	77
5.6.2	Results.....	77
5.7	Discussion.....	81
5.8	Conclusion.....	84
6.	Development of novel beat-to-beat interval correction methods.....	85
6.1	Introduction.....	85
6.2	BBI correction methods used in literature.....	87
6.3	Testing method.....	89
6.3.1	Data.....	89
6.3.2	Signal Corruption.....	89
6.3.3	BBI correction and error analysis.....	91

6.3.4	Statistics	93
6.4	BBI correction algorithms tested	93
6.4.1	Algorithm 1: Pattern Detection algorithm.....	93
6.4.2	Algorithm 2: Wessel algorithm	95
6.4.3	Algorithm 3: Threshold algorithm	96
6.5	Results from Algorithms 1-3.....	96
6.5.1	Correctly detected heartbeats	97
6.5.2	HR error.....	99
6.5.3	HRV error	102
6.6	Combining BBI correction algorithms	105
6.6.1	Algorithm 4: Combined Threshold algorithm	105
6.6.2	Algorithm 5: Combined Wessel algorithm	105
6.7	Results 2: Algorithms 4 & 5.....	106
6.7.1	Correctly detected heartbeats	106
6.7.2	HR error.....	109
6.7.3	HRV error	111
6.7.4	Overall performance	113
6.8	Discussion	114
6.9	Conclusion	117
7.	Experiment Protocol.....	119
7.1	Introduction	119
7.2	Testing Method	119
7.2.1	Reference ECG	121
7.2.2	Movement Detection	122
7.3	HR Analysis	122
7.4	HRV Analysis.....	125
7.5	Signal Quality.....	127
7.5.1	ECG Signal Correlation.....	127
7.5.2	ECG SNR	128
7.5.3	PPG Signal Quality	129
7.6	Pulse Transit Time	129
7.7	Statistical Analysis	130
7.8	Conclusion	131
8.	ECG and PPG analysis.....	132
8.1	Introduction	132
8.2	Results.....	133
8.2.1	Bland-Altman plots of Beat-to-beat Intervals from ECG and PPG signals	133
8.2.2	Sensitivity of heartbeat identification	136
8.2.3	HR window comparison	141

8.2.4	HRV analysis	145
8.2.5	ECG signal quality	157
8.2.6	PPG signal quality	163
8.3	Discussion	164
8.4	Conclusion	169
9.	Combined ECG and PPG analysis.....	171
9.1	Introduction	171
9.2	Category 1 – Combining ECG and PPG data to produce a BBI signal - Methods	172
9.2.1	Method.....	172
9.2.2	Method 1: PPG Fusion method.....	174
9.2.3	Method 2: ECG+PPG data fusion method.....	175
9.3	Category 1 – Combining ECG and PPG data - Results.....	176
9.3.1	BA plots of fused data.....	176
9.3.2	Heartbeat detection sensitivity	178
9.3.3	HR windows comparison	181
9.3.4	HRV analysis	184
9.3.5	Results summary	193
9.4	Category 2 - Generating multiple HR signals - Methods.....	193
9.4.1	Exclusion criteria.....	194
9.4.2	Method 3: Pulse fusion method II.....	194
9.4.3	Method 4: ECG+PPG method II.....	194
9.4.4	Method 5: ECG+PPG+fused method	196
9.5	Category 2 - Generating multiple HR signals - Results.....	196
9.5.1	Mean HR value comparison.....	196
9.5.2	HRV analysis	200
9.5.3	Results summary	210
9.6	Discussion	211
9.7	Conclusion	212
10.	BCG testing	214
10.1	Introduction	215
10.2	Identifying heartbeats in the BCG signal	215
10.3	Experiment method.....	217
10.4	Results.....	218
10.4.1	Examples of BCG signals – Lying on Back.....	218
10.4.2	Examples of BCG signals – Lying on Side	219
10.4.3	Bland Altman plots.....	220
10.4.4	Heartbeat detection sensitivity	222
10.4.5	Results Summary	228
10.5	Data Fusion methods.....	228

10.5.1	CWA Algorithm	229
10.5.2	KF algorithm	230
10.6	Results.....	232
10.6.1	Results summary	235
10.7	Discussion	235
10.8	Conclusion.....	240
11.	Discussion/Conclusion	241
11.1	Restatement of the aim.....	241
11.2	Summary of Contributions.....	241
11.2.1	ECG Electrode position.....	241
11.2.2	BBI correction methods.....	242
11.2.3	Simple methods for rejecting HR and HRV values	242
11.2.4	Data fusion methods for reducing HR and HRV error.....	243
11.2.5	BCG application & data fusion method.....	243
11.3	Future work.....	244
11.3.1	Further development of algorithms developed in thesis	244
11.3.2	Testing on OSA patients who are asleep	245
11.3.3	Replication of results on nasal mask.....	245
11.3.4	Effectiveness of Cardiomask on PAP therapy	246
11.3.5	Effect of Cardiomask on ease of use and comfort.....	246
11.3.6	Practical Design Improvements	246
11.4	Final Statement.....	247
12.	Appendices	248
12.1	Appendix A - General Equations for a Kalman Filter	248
12.2	Appendix B – Individual HRV analysis results	249
12.3	Appendix C –Ethics Submission	269
12.4	Appendix D – Optimisation of data fusion constants	270
12.4.1	Variable optimisation.....	270
12.4.2	Results.....	270
13.	References.....	275

II. Thesis Summary

Obstructive Sleep Apnoea (OSA) is a condition where during sleep a person's upper airway becomes obstructed, limiting breathing and reducing the quality of sleep. OSA is commonly treated using Positive Airway Pressure (PAP) therapy, in which a positive pressure is applied to the person's upper airway via a mask. People with OSA are at a higher than normal risk of developing heart problems. It is thought that by monitoring a person's Heart Rate (HR) and Heart Rate Variability (HRV) long-term, it may be possible to identify if a person's heart health is declining before a serious cardiac event occurs.

Adding HR monitoring to PAP therapy offers a good opportunity for long-term continuous cardiac monitoring as, when used correctly, the PAP therapy is used for several hours every night. This thesis details the development of a device that is able to measure the HR and HRV of people with OSA during PAP therapy.

A PAP mask was modified to be able to measure HR; it was modified such that it can measure Electrocardiography (ECG), Photoplethysmography (PPG) and Ballistocardiography (BCG) signals from the wearer, from which HR values were extracted. The ECG signals were measured using Stainless Steel electrodes which were held in place against the wearer's face and neck by the straps of the PAP mask. The PPG signal was measured using a reflectance pulse oximeter that was located on the wearer's forehead. The BCG signal was measured from a solid-state gyroscope which was attached to the PAP mask.

Signals from the modified mask were recorded from a group of 19 healthy participants who wore the mask whilst lying on a bed, experiencing PAP therapy. A beat-to-beat interval (BBI) correction algorithm was developed for improving the accuracy of the HR and HRV analysis from the measured signals. The analysis of the recorded ECG and PPG signals showed that

HR and HRV values could be accurately measured from the healthy participants, however not consistently. Data fusion methods were developed for combining the HR and HRV information from the ECG and PPG signals, which were able to further increase the consistency of the HR and HRV analysis without a significant decrease in the accuracy. For the BCG signal, the instantaneous HR analysis was only accurate when the participants were lying on their back, as when they were lying on their side there was a decrease in the BCG signal quality. Two data fusion methods were developed to combine the HR information from the 3 axes of the gyroscope to improve the accuracy and consistency of the HR measurements.

These results show that it is possible to accurately monitor the HR and HRV of the Cardiomask wearer. With further development, this technology could be used to monitor the HR and HRV of OSA patients during PAP therapy.

II. Acknowledgements

Firstly, I would like to thank my grandmother (Nanny) who provided me with some money which allowed me to move to Adelaide and to have food to eat and place to sleep before my scholarship came through. Without you I would not be here today.

I would also like to thank my parents for their love and support during my PhD and for helping me move and settle in to Adelaide, and for not nagging me too much about how my writing is going and when I am going to finish.

Another person whose love and support was integral to my success was Bec Lehmann. Thanks for letting me rant about a bad day and help take my mind off things at the end of the day. I'm glad that I could share my PhD journey with you. Also, sorry that I bought home a CPAP device and a bunch of wires and kicked you out of the bed so I could conduct some sleep tests. Hopefully I will never have to do that again.

I would also like to thank Karen Reynolds for her support and guidance during my PhD, and for helping me turn my drafts into something that is PhD-worthy. Thank you for always making time to make sure I was on the right track.

Similarly, I would like to thank Sherry Randhawa for her support and guidance. Talking through different ideas and problems was very helpful, and you and Karen have both made me a better writer.

This project would not be possible without the ResMed Clinical Science and Innovation team. In particular I would like to thank Gordon Malouf who was very helpful in terms of his expertise of the PAP devices, Sleep Apnoea and clinical testing in general, in acquiring different resources to make the prototype testing a possible, and for his mentoring and general guidance through this process.

Similarly, the support and advice from the Medical Device Research Institute was also crucial to the development of this device. In particular Aaron Mohtar was very helpful and was very patient with me when I would burst into his office wondering why things weren't working.

The final group that supported me during my PhD was the engineering services team. Thank you for helping me develop a working prototype and in particular for translating “the thing with the bit that is like this...” into an actual usable part.

I would also like to thank the participants of the prototype testing for taking an hour out of their day to help me out.

Another person who helped me along the way was my housemate Hendrik Wong. Thank you for listening to me talk through my problems, and helping me to alleviate my imposter syndrome by talking through it and realising how silly it is.

I would also like to thank Kate Mulheron for helping me get ready for the phone interview for this PhD position when we were backpacking in Europe.

I would also like to acknowledge the funding I received to help me complete my PhD and travel to different conferences during my candidature from the following sources:

- Australian Government Research Training Program Scholarship
- Institute of Electrical and Electronic Engineers (IEEE) in Medical and Biology Society (EMBS)
- Society of Medical and Biological Engineering (SMBE) – SA chapter
- ResMed

Finally, I would like to thank all of the other PhD students at Tonsley (#nerdsquad) who made this journey bearable. Although the PhD felt like it took forever to complete our time together was too short. Hopefully we can keep in touch after we all finish.

III. List of Abbreviations

Ag/AgCl	Silver/Silver Chloride
AV	Atrioventricular
BA	Bland-Altman
BBI	Beat-to-beat Interval
BCG	Ballistocardiography
BMI	Body Mass Index
BPM	Beats Per minute
CPAP	Continuous Positive Airway Pressure
CV	Coefficient of Variation
CWA	Custom Weighted Average
DRL	Driven Right Leg
ECG	Electrocardiography
ENIG	Electroless Nickel Immersion Gold
HF	High Frequency
HR	Heart Rate
HRV	Heart Rate Variability
IMU	Inertial Measurement Unit
KF	Kalman Filter
LF	Low Frequency
NREM	Non Rapid Eye Movement
NSRDB	Normal Sinus Rhythm Database
OSA	Obstructive Sleep Apnoea
PAP	Positive Airway Pressure
PCB	Printed Circuit Board
PEP	Pre-Ejection Period
PPG	Photoplethysmography
PSG	Polysomnogram
PTT	Pulse Transit Time
PVC	Premature Ventricular Contractions
QRS	Interval between Q and S waves in ECG signal
REM	Rapid Eye Movement
RMS	Root Mean Square
RPC	Reproducibility Coefficient
	R-R Interval - Interval from QRS complex to the beginning of the next QRS complex in ECG signal
RRI	signal
SA	Sinoatrial
SNR	Signal-to-Noise Ratio
SS	Stainless Steel
VPAP	Variable Positive Airway Pressure

I certify that this thesis does not incorporate without acknowledgment any material previously submitted for a degree or diploma in any university; and that to the best of my knowledge and belief it does not contain any material previously published or written by another person except where due reference is made in the text.

Mark Gardner

01/03/2019

1. Introduction

1.1 Context of the study

Obstructive Sleep Apnoea (OSA) is a condition where during sleep, a person's airway becomes partially or fully obstructed, causing a reduction in breathing efficiency. OSA affects 14.3% of males and 5% of females aged 30-70 years old [2]. As well as affecting their quality of life [3], people with OSA are also at a high risk of developing heart problems.

OSA is commonly treated using a Positive Airway Pressure (PAP) device, which as the name suggests, applies a positive pressure to the person's upper airway to limit the amount of obstruction in the upper airway during sleep [4]. Although using the PAP device reduces the number of apnoea episodes an person with OSA has, they are still at risk of developing heart problems because OSA and heart failure share common risk factors, such as obesity and high blood pressure [5].

Although there are many different methods of monitoring cardiac health, one of the most simple and reliable is to monitor how often the heart beats. This is because abnormally high or low Heart Rate (HR) values can be indicative of a heart problem [6]. Additionally by looking at the variability of the HR, acute cardiac events can be diagnosed [7], as well as the person's general cardiac health [8].

1.2 Problem statement

Currently, during regular PAP therapy, no cardiac monitoring occurs. However, since many people with OSA use a PAP device every night for several hours, cardiac monitoring during PAP therapy would allow for large amounts of data to be recorded, and potentially for long term cardiac trends to be measured. Since the PAP device is in contact with the user, this could allow for monitoring of the PAP device user, using contact sensors embedded into the PAP device setup.

Most current HR monitoring devices either prioritise accuracy of the HR information over user comfort or vice versa. Whilst accuracy is important for correct diagnosis of the person's cardiac health, user comfort is also important during sleep. Hence a device is needed that can monitor HR accurately and comfortably during PAP therapy.

1.3 Aim

The aim of this thesis is to develop a device that can accurately and comfortably monitor the heart rate of a person during Positive Airway Pressure therapy.

1.4 Scope

Devices investigated in this research are limited to those that are required to be in contact with the users to accurately measure their HR, and specifically, sensors embedded into the PAP device. This is not the only solution to comfortably and accurately monitoring people during PAP therapy. However, the decision to only investigate sensors that could be embedded into the PAP device setup was made because then users would not have to wear any additional devices to have their HR monitored.

Although this device is designed for people with OSA, the testing of the device in this thesis was conducted on healthy participants. The studies in this thesis were designed to be exploratory, to prove the concept, and were not clinical validation studies. However, if the concept testing is successful, then further testing will need to be conducted on people with OSA undergoing PAP therapy.

In this thesis only heartbeats and associated HR and HR variability (HRV) measures are analysed and compared. Other measures, such as stroke volume, are not explored, but are mentioned in places throughout the thesis.

1.5 Overview of the study

The structure of this thesis follows the development of a device to monitor the HR of people with OSA during PAP therapy. The device has been named the "Cardiomask". The first few

chapters briefly summarise the previously known knowledge, including previous attempts at monitoring HR. In chapter 2, the anatomy and physiology of the heart, sleep and sleep apnoea is briefly summarised. In chapter 3, a more in-depth description of how HR can be used as a diagnostic tool is provided. In chapter 4, previous reports on monitoring HR are reviewed, with a focus on devices where sensors are located in non-traditional places including the head and neck. These devices are divided into three categories: Electrocardiography (ECG), Photoplethysmography (PPG) and Ballistocardiography (BCG).

The remaining chapters relate to the development of the Cardiomask. A flowchart of how each of these chapters fits into the device development is shown in Figure 1-1. The colour of each box indicates a different chapter:

- Green: Chapter 5 - Device description
- Black: Chapter 6 – Development of novel Beat-to-Beat Interval (BBI) Correction methods
- Yellow: Chapter 7 - Experiment protocol
- Light blue: Chapter 8 - ECG and PPG analysis
- Brown: Chapter 9 – Combined ECG and PPG analysis
- Red: Chapter 10 - BCG testing

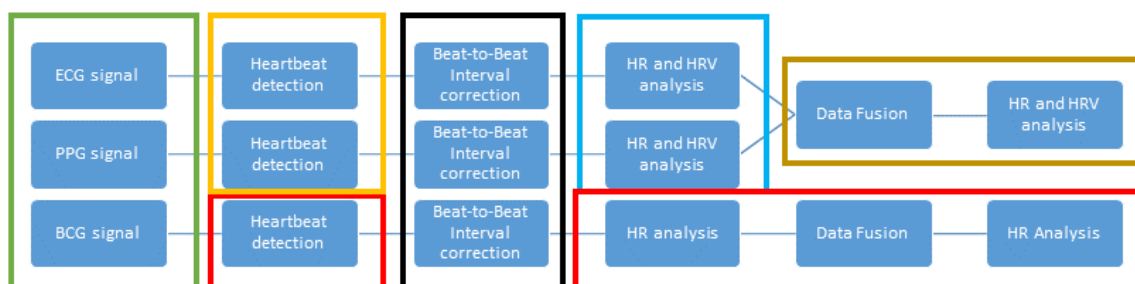


Figure 1-1 – A flowchart of the Cardiomask development. Each thesis chapter is represented as a coloured box.

In chapter 5 (green), the Cardiomask is introduced, as well as an explanation of design of the device. This chapter also includes information on the setup of the ECG, PPG and BCG sensors as well as some preliminary results from these sensors. The results of this preliminary analysis suggest that when sensors are embedded into the PAP mask, there is a

reduction in signal quality compared with normal sensor placement. This prompts the development of an algorithm to identify when a heartbeat has been falsely detected and an erroneous BBI value is measured, and to correct this false value. Several different algorithms are developed and tested in chapter 6 (black), using real patient BBI values from an online database.

The next chapters relate to the testing of the different signals measured from the Cardiomask. In chapter 7 (yellow) the protocol for the experiment is described, including information about the participants of the test and what they were required to do during testing, as well as how the measured signals were analysed. In chapter 8 (light blue), the HR and HRV results of the analysis of the ECG and PPG signals individually are shown. The HR and HRV information from the ECG and PPG signals are combined in chapter 9 (brown), and the combined results are analysed and compared with the individual signal results, as well as the results from the reference ECG signal. In chapter 10 (red) the results of the BCG analysis are shown. These results are shown separately as, unlike the ECG and PPG signals, a reliable instantaneous HR signal could not be obtained using BCG, so alternate methods were used to generate a usable HR signal. The final chapter will bring together all the conclusions from the different chapters to evaluate how well the Cardiomask achieves the aim of this thesis.

2. Context

2.1 Physiology of a Heart Beat

2.1.1 General Physiology

The heart is an organ used to pump blood around the body, allowing cells and vital nutrients to be delivered to the organs and cells in need. One important example of this is oxygen, which is used for energy production in human cells and is transported from the lungs to cells in need through the blood stream.

The heart is divided into four chambers, a left and right ventricle and a left and right atrium. The left side of the heart pumps oxygenated blood around the body via the aorta. The right side of the heart pumps deoxygenated blood to the lungs to be re-oxygenated. The location of these chambers within the heart is shown in Figure 2-1.

Image has been removed due to copyright restrictions

Figure 2-1 - A cross section of the human heart showing the four chambers. Source: <http://www.nlm.nih.gov/>

The muscles of the heart are activated by an electrical signal which controls the timing of when each of these chambers contract. The conduction path of this signal begins with the excitation of the sinoatrial (SA) node located in the right atrium, which then causes the right atrium to contract. Then the conduction path spreads to both the left atrium, and the atrioventricular (AV) node. The AV node is located at the base of the left atrium, and is connected to the wall between the two ventricles. Once the AV node is excited, the conduction path travels through the ventricle walls via the Purkinje fibres. These Purkinje fibres cause the ventricle muscles to contract in the presence of an electric potential. The timing and order of these events allow for a healthy flow of blood around the body.

2.1.2 Normal Variation of the Heart rate

The dominant factor that determines the rhythm with which a person's heart beats is the activity of the autonomic nervous system on the cardiovascular system. Since it is controlled by the autonomic nervous system, the Heart Rate (HR) cannot be directly controlled by a

person, although it is possible to indirectly change HR (for example by varying respiration rate or by exercising).

The two nerve signals that act on the heart to control the HR are the sympathetic and parasympathetic signals. A summary of the effects that these signals have on the HR is shown in Table 2-1. The parasympathetic signal is transmitted to the heart through the SA node and the AV node, and hence it affects the SA and AV nodes. An increase in parasympathetic activity causes a decrease in the rate of excitation of the SA node, and a decrease in conduction rate of the cardiac signal through the AV node. The net result is a decreased HR and a larger interval between the atrial and ventricular contractions.

The sympathetic signal is also transmitted to the heart through the AV and SA nodes, as well as to the ventricular walls. Increased sympathetic activity opposes the parasympathetic stimulation, by increasing the activation rate of the SA node and decreasing the delay in the conduction rate through the AV node. Increased sympathetic stimulation also increases the contraction force of the ventricles, which increases the amount of blood ejected from the ventricles with each heartbeat. The end result is an increase in HR and a decrease in the time difference between atrial and ventricular contraction [6].

Table 2-1 - Effect of sympathetic and parasympathetic stimulation on the heart. Source: [6]

Variable affected	Parasympathetic	Sympathetic
Heart rate	↓	↑
SA excitation rate	↓	↑
AV conduction delay	↑	↓
SA-AV excitation interval	↑	↓
Ventricle contraction force	No significant effect	↑

The heart constantly receives both sympathetic and parasympathetic stimulation, and the HR depends upon the amount of stimulation received from each source. If there is a decrease in sympathetic stimulation, there is also usually an increase in parasympathetic

stimulation, and vice versa. In this way the two signals work as a “push-pull” system to moderate the HR.

Although one might assume the two signals would be balanced at a resting state, the natural frequency of the SA node (that is without any sympathetic or parasympathetic stimulation) is approximately 100 BPM [9]. This implies that at rest there is a dominance of parasympathetic activity at the AV node, as a typical resting HR is around 60 BPM for healthy individuals.

2.2 Sleep Apnoea

Sleep apnoea is a condition where a person stops breathing or has reduced breathing capabilities for a short period of time while sleeping. The most common type of sleep apnoea is **Obstructive Sleep Apnoea** (OSA), which is caused by the upper airway becoming partially or fully obstructed, thus completely stopping the flow of air to and from the lungs [10]. People who have OSA are more likely to develop heart problems than those without OSA, especially in older and middle aged males [11]. This may be due to the increased stress that an apnoea episode places on the heart [12, 13], as well as the amount of overlap between high risk factors for OSA and heart disease (particularly obesity) [10, 14].

2.3 Positive Airway Pressure Therapy

Positive Airway Pressure (PAP) devices are the most common treatment method for OSA. PAP devices work by applying a positive pressure to the person’s upper airway. This helps to prevent the airway from becoming occluded by increasing the pressure inside the airway, keeping the airway open and clear allowing for normal breathing during sleep [4]. Using a PAP device can improve the quality of life of people with OSA who use the device during sleep [4, 15].

PAP devices consist of a mask and a flow generator as shown in Figure 2-2. The flow generator is responsible for generating the positive pressure that ends up in the person’s airway. The flow generator also contains the control systems that are responsible for the

performance of the PAP device. This positive pressure is transferred via airflow through a tube connected to the PAP mask. The mask is worn by the user and directs the airflow into the upper airway.

Image has been removed due to copyright restrictions

Figure 2-2 - An example of a PAP device in use. Source: www.resmed.com

There are two common types of face masks for adults undergoing PAP treatment; the nasal mask, and the full face mask. Examples of these mask types are shown in Figure 2-3. The nasal mask delivers the air flow from the flow generator into the airway through the nose. The full face mask is designed to deliver airflow through both the mouth and nose. The nasal mask is often preferred over the full face mask because the nasal mask is smaller and takes up less area on the face, making it more comfortable for the wearer [15].



Figure 2-3 - An example of a two different types of masks used for PAP treatment for adults: the nasal mask (left) and the full face mask (right)

There are two broad categories of treatment modes that are used during PAP treatment. These modes determine the treatment pressure with respect to time that is applied to the person's airway. These modes are the normal **Continuous PAP (CPAP)** mode, and the **bi-level** or **Variable Positive Airway Pressure (VPAP)** mode. In the normal CPAP mode, the pressure that is applied is constant for the duration of the treatment. This is the more common mode for the treatment of OSA. The typical range of pressures that are used for CPAP therapy is around 6-14cmH₂O. In the bi-level or VPAP mode, the applied pressure from the flow generator varies depending on whether the person is inhaling or exhaling. That is, when the person is inhaling the pressure is increased, and when the person is exhaling

the pressure is decreased. This change in pressure supports the work of breathing and is a form of mechanical ventilation. Bi-level therapy has various applications including Non-compliant OSA [16], Neuro-Muscular Disease [17] and Chronic Obstructive Pulmonary Disease [18].

2.4 Sleep

2.4.1 Sleep cycles

Sleep can be categorised into various sleep stages that the body will cycle through several times a night, in a process known as a 'sleep cycle'. The individual stages in the sleep cycle are classified by changes in brainwave activity, as well as other physiological markers such as HR and body movement. Sleep stages can be divided into Rapid Eye Movement (REM) and Non REM (NREM) stages. There is one REM stage, while there are three levels of NREM stages [19]. Apart from the brainwave activity, there is not much difference physiologically between the different stages of NREM sleep. During NREM sleep there is a decrease in the respiration rate, sympathetic nerve activity, muscle and brain activity as well as HR when compared to wakefulness.

Apart from the movement pattern of the eyes, REM sleep is also characterised by muscle atonia, which is a loss of voluntary muscle contractions in the body. During REM sleep there is an increase in HR and HR variability, blood pressure, respiration, and sympathetic nerve activity [20]. An example of how a healthy person transitions between the various sleep stages during a typical night's sleep is shown in Figure 2-4.

Image has been removed due to copyright restrictions

Figure 2-4 - An example of a typical sleeping pattern. Source: <http://www.howsleepworks.com/>

2.4.2 Circadian Rhythms

Circadian Rhythm is a term used to describe variations in the body that cycle with a period of approximately 24 hours. Although it is mostly associated with controlling when a person falls asleep, it also affects and regulates several other bodily functions including HR [21].

Typically the HR will decrease during the night time, and increase during the day time, with the minimum HR values occurring usually between midnight and 6am, and the maximum values occurring between 10am and 2pm [22, 23]. Although it might appear as though this is just a reaction to the body's inactivity during sleep, insomnia patients and other sleep deprived persons also display similar variations in HR over a 24 hour period [24, 25]. This implies that circadian rhythms are the dominant factor in the 24 hour variation in HR. The time interval between successive SA node activations was found to vary by approximately 10% over a 24 hour period [26]. Similarly the time taken for the ventricles to recover after contraction is increased during the night time, while the shortest time between contractions occurs within 2 hours of a person awakening [27], which may account for the large number of cardiac incidents that occur around this time [28].

2.4.3 Polysomnography

The current process used to monitor the vital signs of a patient while they are sleeping is a **Polysomnogram** (PSG). A PSG comprises of several different sensors, which can measure brainwave activity, respiration rate and HR among other variables. This information is then used to identify the sleep stages of the patient which can be combined with other measured signals such as limb movements to diagnose any sleeping disorders that the patient may have.

Although a PSG is the gold standard for sleep monitoring and diagnosis, it is not a practical solution, especially for long term monitoring outside of a clinical environment. Approximately 22 different electrodes and sensors need to be placed onto a patient in order to perform a full PSG, although this number can vary if specific disorders are being investigated such as sleep movement disorders [19]. This makes the test uncomfortable for the patient being monitored. A PSG is also an expensive test to run, and requires a trained technician to perform the test and interpret the results. There is also usually a long waiting list for a patient

to undergo a PSG due to the resources needed for the test and the time that it takes to complete the test [29].

3. Analysis of HR and HRV

3.1 Arrhythmia/abnormal heart beat detection

By measuring the rate at which a patient's heart beats, abnormalities in the HR can be detected. Abnormalities in HR are called **Arrhythmias**. Although small variations in HR are normal for healthy individuals, an irregular HR value or an irregular variation in HR are often symptoms of an arrhythmia, and can be indicative of cardiac disease or abnormality [7].

Examples of typical arrhythmias are described below.

A Bradycardia is defined as an abnormally slow HR, less than 50 beats per minute at rest. Conversely a Tachycardia is an abnormally fast HR, defined as a resting rate of greater than 100 beats per minute [6]. Bradycardias and tachycardias can be defined as sinus or ventricular depending on the anatomical origin of the arrhythmia. A ventricular bradycardia or tachycardia occurs when there is an abnormal ventricular contraction rate. This can occur even when the sinoatrial (SA) node is stimulating at a regular frequency and usually indicates a problem with the ventricles or with the atrioventricular (AV) node. Sinus bradycardias and tachycardias occur when the frequency of the excitation of the SA node is abnormally low or high, which is usually due to a problem with the autonomic system.

Premature Ventricular Contractions (PVCs) are defined as cardiac signals that originate from the ventricles. This causes an irregular conduction path around the heart, leading to an improper contraction of the heart muscles. Similarly Premature Atrial Contractions (PACs) are irregular heartbeats that originate from an abnormal location in the atrium. While it is common for these types of heartbeats, also known as **ectopic beats**, to occur in healthy people, a high frequency of ventricular stimulation may be a symptom of more serious cardiac disease [6].

AV conduction block occurs when the cardiac conduction signal is impeded through the AV node. In mild cases (defined as first degree AV block) this causes a slight delay between

activation of the atria and ventricles, however in more severe cases (second and third degree AV block) it can result in the AV node blocking the cardiac conduction signal from reaching the ventricles. This causes the ventricular pacemakers to activate, which leads to the atria and ventricles beating independently of each other, reducing the efficiency of the heart [30].

Fibrillation occurs when individual cardiac cells begin to depolarise independently of each other. This causes the cardiac muscle to quiver instead of producing a strong contraction. Fibrillation in the atria (Atrial Fibrillation) can cause a decrease in blood flow and an increase in the likelihood of a blood clot or a heart attack in the future however is relatively benign compared to Ventricular Fibrillation. Ventricular Fibrillation means the heart is no longer able to pump blood around the body, which can lead to serious damage and death within minutes.

A Sinus Arrest occurs when the SA node does not generate a signal to contract the heart. This causes a temporary pause in blood flow, and can have severe consequences for the patient if the pause lasts for more than a few seconds [6].

3.1.1 Arrhythmias and Sleep Apnoea

The Sleep Heart Health Study was a multi-centre study designed to investigate cardiovascular effects of sleep disordered breathing [31]. According to this study, the types of arrhythmia that are common with sleep apnoea are “nonsustained ventricular tachycardia, sinus arrest, second-degree atrioventricular conduction block, and frequent (>2 bpm) premature ventricular contractions”. These arrhythmias are more likely to occur in people with OSA than other people. Additionally, up to 50% of these arrhythmia events occur at night [32]. There is some evidence to suggest that CPAP therapy can reduce the amount of nocturnal arrhythmias that an OSA patient has [33, 34].

3.2 Heart Rate Variability

Heart Rate Variability (HRV) can provide an indication of a subject's autonomic and cardiac health. As the name implies, HRV analysis involves monitoring the dynamics and variability of the HR signal. HRV techniques are typically analysed in one of two different manners; the **time domain, frequency domain**. Non-linear methods have also been developed for HRV analysis but are less commonly used and hence will not be used in this thesis. Typical HRV monitoring periods are classified as either long term or short term. Long term monitoring periods are usually between 18-24 hours, while short term recordings are typically 5 minutes long, however 2 minute and 10 minute time periods have also been used [8].

In most HRV literature, when referring to the time difference between adjacent heartbeats, it is common to refer to these intervals as the NN intervals. The NN intervals represent the time difference between adjacent heartbeats that have been corrected for false positives and false negatives that can occur during heartbeat detection. The NN intervals are used instead of the uncorrected RR interval values, as even missed or extra heartbeats can cause a significant change in the HRV analysis [8, 35, 36].

3.2.1 Time Domain

Time domain analysis of HRV involves using statistical techniques on the NN intervals themselves, or on the time differences between consecutive NN intervals. Common time domain methods are shown in Table 3-1. Of the variables mentioned in Table 3-1, the most commonly used time domain methods are SDNN, RMSSD, and pNN50.

SDNN is the standard deviation of the NN intervals and is the most common time domain variable used for HRV analysis, as it is one of the easiest to calculate [8]. There is significant evidence to suggest that a lower than average SDNN (i.e. < 50ms) is linked to a higher mortality rate [37-39]. SDNN can be used as both a long term (24 hour) and short term (5 minute) measurement of HRV; however SDNN values can only be compared with other

SDNN values calculated from recording periods of the same length, as the variation of heartbeats will naturally increase with a longer recording period [8].

Table 3-1 - Time Domain HRV variables. Source: [8]

Variables	Units	Description
Statistical Measures		
SDNN	ms	Standard deviation of all NN intervals
SDANN	ms	Standard deviation of the averages of NN intervals in all 5-minute segments of the entire recording
RMSSD	ms	The square root of the mean of the sum of the squares of differences between adjacent NN intervals
SDNN index	ms	Mean of the standard deviations of all NN intervals for all 5-minute segments of the entire recording
SDDSD	ms	Standard deviation of differences between adjacent NN intervals
NN50 count	ms	Number of pairs of adjacent NN intervals differing by more than 50ms in the entire recording; three variants are possible counting all such NN intervals pairs or only pairs in which the first of the second intervals is longer
pNN50	%	NN50 count divided by the total number of all NN intervals

RMSSD is the root-mean-square of the differences between adjacent intervals. pNN50 is the percentage of adjacent NN intervals that differ by more than 50ms. RMSSD and pNN50 are useful measurements for short term analysis of HRV variables. It is thought that these variables show the amount of parasympathetic control of the HR, and that changes in these variables can indicate a change in parasympathetic activity [40, 41]. As they both represent similar features, these variables are correlated to each other [8].

3.2.2 Frequency domain

Frequency domain methods involve analysing the NN interval signal in the frequency domain. It is thought that analysis in the frequency domain is able to provide an insight into the amount of stimulation the heart receives from the parasympathetic and sympathetic nervous system, especially if they are stimulating at different frequencies [8]. The

frequencies that are analysed are divided into frequency bands, some of which have a physiological significance. These frequency bands are; Ultra Low Frequency, Very Low Frequency, Low Frequency (LF), and High Frequency (HF). The frequencies that these variables represent are shown in Table 3-2.

Table 3-2 - Frequency components analysed. Source: [8]

Variable	Units	Description	Frequency Range
Total power	ms ²	Variance of all NN intervals	≤0.4 Hz
Ultra Low Frequency	ms ²	Power in the ULF range	≤0.003 Hz
Very Low Frequency	ms ²	Power in the VLF range	0.003-0.04 Hz
LF	ms ²	Power in the LF range	0.04-0.15 Hz
HF	ms ²	Power in the HF range	0.15-0.4 Hz

In long term recordings (i.e. with a recording duration of 24 hours or longer), all frequency domain bands are typically used [8, 42]. For short term recordings the VLF, LF and HF frequency bands are used [8]. The LF and HF bands are often also represented in normalised units. When represented in normalised units the LF and HF values show the relative power of each frequency band, which can be more easily interpreted than in absolute units [8]. The formula for the conversion of the absolute LF and HF power to normalised LF and HF power for short term recordings is:

$$LF_{normalised} = \frac{LF}{Total\ Power - VLF} = \frac{LF}{LF + HF} \quad (3.1)$$

$$HF_{normalised} = \frac{HF}{Total\ Power - VLF} = \frac{HF}{LF + HF} \quad (3.2)$$

Of the different frequency bands, only the HF component has a clear and significant physiological source. The HF component can be seen as a marker of parasympathetic activity [8, 42]. As such, changes in respiration patterns will be reflected in the HF values [42]. There is debate as to the origin of the nature of the LF component, however it is thought to be comprised of both sympathetic and parasympathetic stimulation [8, 40, 42].

What is known is that a reduction in LF power is a good predictor of cardiac failure [43]. The physiological origin of VLF and ULF are not known, however it is still recommended that these variables be monitored, as they can still be used as a predictor for patient mortality [44].

The ratio of the LF/HF components was thought to be able to represent a balance of the level of stimulation from the parasympathetic and sympathetic sources, so that when this ratio is equal, then the stimulation received is also equal. However the opposite is not true. That is, if the LF power is not equal to the HF power, then one cannot approximate the level of parasympathetic and sympathetic stimulation based on the LF/HF ratio [42, 45]. The hypothesis that the LF/HF ratio represents sympathetic and parasympathetic balance has been challenged, as it relies on several assumptions which are not always true [46].

With an evenly spaced signal, to determine the underlying frequencies of the signal, a simple discrete FFT can be used. However, since the NN intervals are not evenly spaced samples, this technique can't be used. Several different techniques have been proposed in order to determine the underlying frequencies of the NN interval signal. These techniques include resampling the NN interval signal to an evenly distributed signal, and fitting the data to an auto-regression equation [8, 42, 47].

The preferred technique uses the Lomb-Scargle periodogram method, which generates a power spectral density estimate of a signal that is sampled at uneven intervals [48]. It has been shown that this technique is superior at estimating the underlying frequencies of an NN interval signal [49].

3.2.3 HRV during sleep

In section 2.4.1 it was mentioned that changes in HR occur during sleep when compared with wakefulness. These changes will affect any HRV analysis on data recorded during the

night time, and it has been found that subjects have a higher normalised HF component during the night time when compared with day time data [50, 51]. Additionally, HR and HRV will also vary depending on the stage of sleep the subject is in. During different stages of NREM sleep, no significant change in HRV has been observed. However, like with HR, most HRV variables are larger in REM sleep than NREM sleep [40].

Long term HRV analysis has also been used for comparing HRV during sleep, mostly using time domain methods [37-39, 52-54]. For these studies, the recording period was divided into 4-6 hour segments to observe HRV differences over a 24 hour period [55]. However caution must be taken using this technique as HRV values measured over different time periods cannot be easily compared [8], because longer recording periods will naturally have more variance than shorter recording periods [56].

In the frequency domain, most HRV analysis has used 5 minute segments, even if the total recording duration was longer. In some cases, only select 5 minute windows were analysed, especially when comparing different scenarios, such as sleep stages and circadian rhythm cycles [44, 57, 58]. However in most cases a sliding window [41, 59, 60], or 5 minute segments in a defined time period [55, 61] were used for HRV frequency analysis.

Erroneous heartbeats can cause significant errors in the calculation of HRV in the frequency domain. As such, pre-processing steps were applied to attempt to avoid corrupt HR data. The most common step was to reject any segments that had a proportion of usable data below a certain threshold, usually 80% [55, 59]. Additionally some studies excluded data that contained a respiratory or other event that may corrupt the HRV calculations [43, 44, 58, 60], or they implemented an algorithm to correct the NN intervals [41, 62, 63].

Respiratory events such as apnoeas are typically excluded from HRV analysis as they can alter the HR in a way which can reduce the accuracy of the HRV analysis. Guilleminault

reported that during an apnoea episode, there was a “progressive brachycardia...followed by abrupt tachycardia” when the patient was aroused from the apnoea episode [64]. However for short term HRV analysis in the frequency domain, an assumption is made that the sympathetic to parasympathetic stimulation levels are constant for the duration of the interval on which HRV analysis is being performed [8]. Hence care should be taken when performing HRV analysis during sleep when respiratory events such as apnoeas may occur, as they may introduce inaccuracies into the HRV analysis [40].

3.3 Summary

In this chapter the importance of measuring and analysing HR was discussed. By analysing HR, some arrhythmias can be identified, which can reveal poor cardiac health. Additionally, by measuring the variability of the HR (HRV), further insights on the patient’s cardiac health can be obtained. HRV analysis can be performed in the time and frequency domain, and the recommended minimum window length for frequency domain analysis is 5 minutes. It is also important that when comparing HRV analysis results, that comparisons be made only with HRV analysis obtained from similar analysis window lengths. Hence for future experiments, any experiment stages should be at least 5 minutes long if HRV analysis is to occur in that stage. Finally, HRV varies with different sleep stages, and can be altered by different respiratory events.

4. Current practices & technologies - Methods for measuring HR

Chapter 3 described how monitoring of HR can reveal information about a person's cardiac health. In this chapter, methods for monitoring HR will be explored with a focus on solutions that would be practical for monitoring during PAP therapy. That is, solutions where the sensor is placed around the face and/or head, which would allow for integration of that sensor into the PAP mask. The different methods that are discussed are

Electrocardiography (ECG), **Photoplethysmography (PPG)** and **Ballistocardiography (BCG)**. This chapter also includes a brief discussion about different data fusion methods and whether they would be applicable to monitoring HR during PAP therapy.

4.1 Electrocardiography

4.1.1 Introduction

One of the variables a PSG (a method for sleep monitoring described in section 2.4.3) is able to measure is HR. This is measured using a method called electrocardiography (ECG). In ECG, the potential difference between two electrodes placed on the surface of the skin is recorded. This potential difference records the electrical activity of the heart caused by the heart muscles contracting and relaxing. The recorded signal can then be compared to a signal measured from a healthy heart to determine a person's cardiac health. A typical ECG signal is shown in Figure 4-1.

Figure 4-1 also shows the annotated features of a typical ECG waveform. Table 4-1 shows how the features in the ECG signal relate to significant events in the contraction and relaxation of the heart muscles during the cardiac cycle. By noting the time of the occurrence of the R peak (ventricles contracting) and measuring the time between successive R peaks, the HR can be measured. Additionally, diagnostic information on the heart can be extracted from comparing the time intervals between the different features shown in Figure 4-1 and the amplitude of those features to the respective values from a healthy heart [7]. For example, an abnormally large PR interval could indicate that there is a delay in the conduction path

between the atria and the ventricles, which is a symptom of Atrioventricular (AV) block. This level of diagnostic information available from an ECG signal is an advantage of an ECG when compared with other methods for monitoring HR which will be discussed in sections 4.2 and 4.3 [65].

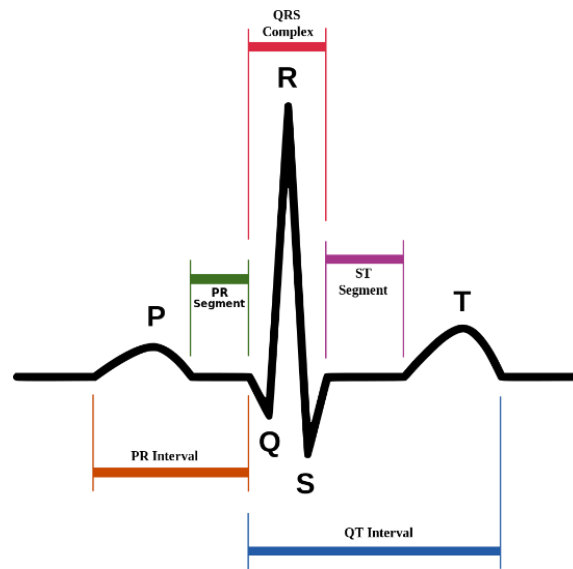


Figure 4-1 – An annotated ECG signal from a healthy patient

Table 4-1 – ECG waveform features and their physiological meaning. Source: [30]

Feature	Event
P wave	<ul style="list-style-type: none"> • Activation of the SA node. • Depolarisation (contraction) of the atria. • Activation of AV node.
QRS complex	<ul style="list-style-type: none"> • Excitation of Purkinje fibres. • Depolarisation (contraction) of ventricles. • Repolarisation (relaxation) of atria.
T wave	<ul style="list-style-type: none"> • Repolarisation (relaxation) of ventricles.

In a standard ECG setup (i.e. for diagnosing cardiac disorders), multiple ECG signals are measured to create many different electrical vectors known as leads. The multiple leads are then used to identify the electrical activity in multiple axes. An example of electrode placement for a simple 3 lead ECG setup is shown in Figure 4-2, where the ECG signal is measured from the potential difference of electrodes placed on a person's arms and left leg [66]. An additional electrode is placed on the person which is used as an indifferent

electrode. This electrode is traditionally placed on the right leg and is known as a Driven Right Leg (DRL) electrode. The purpose of this electrode is to increase the ECG signal quality by reducing the common mode interference in the ECG amplifier [67]. This electrode is required as the human body can pick up large amounts of electromagnetic interference from external sources, such power lines.

Image has been removed due to copyright restrictions

Figure 4-2-Location of electrodes for a 3 lead ECG. Source: [6]

Since a PSG is used to diagnose sleep disorders, and not cardiac disorders, a multi lead setup like Figure 4-2 provides an unnecessary level of information for simply monitoring HR. Hence in most PSG's a single lead setup is used, as this provides sufficient information to measure the HR during a PSG [68]. The location of the electrodes used in a PSG is shown in Figure 4-3, and often a DRL electrode is also attached.

Image has been removed due to copyright restrictions

Figure 4-3 - Electrode placement for a PSG as recommended by the AASM. Source: [19]

4.1.2 Different electrode types

In an ECG, the electrode is able to measure bioelectrical signals due to the the 'half-cell potential', which occurs because of the 'Electrode-Electrolyte' effect in which ion transport occurs between an electrolyte, such as human tissue, and the electrode [69]. The ions flowing from the electrode will 'stick' against the electrode surface, which will lead to a build-up of charged ions on the electrode surface, leading to a capacitive effect known as the Helmholtz layer. Hence the impedance of the electrode-electrolyte interaction can be

modelled as a resistor and a capacitor in parallel, since the impedance of the electrode-electrolyte barrier, which is electrode to skin impedance, is frequency dependent [69].

Another factor that influences the impedance of the electrode-skin interface is the thickness of the skin. Compressed skin has a lower resistance than non-compressed skin, meaning that changes in skin thickness can affect the quality of the measured biopotential signal. This is a source of motion artefacts in biopotential recordings, and means that during ECG recording, subjects should remain still to maximise the quality of the recorded signal.

These electrodes can be categorised as **polarisable** or **non-polarisable**. For a perfect non-polarisable bio-potential electrode, the impedance of the skin-electrode interface is zero and signals measured are noise free. Conversely, for a perfect polarisable electrode, no current flows through the electrode. In reality, all electrodes are some combination of polarisable and non-polarisable electrodes. Most electrodes for measuring bio-potential signals aim to be non-polarisable to measure the most accurate biopotential signal [69].

In a clinical environment, ECG signals are recorded using “**wet**” **electrodes**, which are named because of the conductive gel that exists between the electrode and the measurement subject’s skin. However, “wet” electrodes have some practical limitations which may make them unsuitable in a non-clinical environment. As such, for the potential recording of ECG signals in environments such as in a person with OSA’s bedroom, other types of electrode options need to be explored to choose an electrode that is both accurate and suitable to a non-clinical environment. Hence wet electrodes will be compared to electrode alternatives including **dry electrodes** and **non-contact electrodes**.

4.1.2.1 Wet electrodes

Wet electrodes are made of a silver/silver chloride (Ag/AgCl) electrode, which is attached to a patch of biocompatible material and then placed onto the skin. A conductive gel is placed

in between the electrode and the skin to increase the conductivity between the skin and the applied electrode and increase the signal to noise ratio (SNR) of the measured ECG signal. The gel is also an adhesive which makes precise placement of the electrodes possible and allows for accurate and repeatable measurements. It also ensures the electrode will not move relative to the surface of the skin during recording [69]. These types of electrodes are used in a clinical setting as they provide a high level of accuracy and the mechanisms for any potential errors have been well researched [70]. An example of a Ag/AgCl electrode is shown in Figure 4-4.

Image has been removed due to copyright restrictions

Figure 4-4 - An example of a Ag/AgCl electrode. Source: www.3m.com

While this setup allows for measurement of an accurate ECG signal, it can be uncomfortable for patients, especially during long term use. The gel tends to dry out after a 24 hour period, resulting in a decrease in the conductivity between the electrode and the skin [71], which reduces the quality of the measured ECG signal. To prevent this, wet electrodes are disposable and are replaced after each use or every 24 hours. Thus wet electrodes are unsuitable for long term ECG analysis, especially in a non-clinical environment such as a patient's home, as it would become both expensive and tedious to change the electrodes every night before sleep. Additionally, in some people, the repeated use of wet electrodes can induce skin irritation [72-74].

4.1.2.2 Dry electrodes

Dry contact electrodes work in a similar manner to wet electrodes, however they do not require the conductive gel to measure an accurate ECG signal. Instead dry electrodes use accumulated moisture and sweat from the skin to create a similar effect to the conductive gel, and increase the conductivity between the skin and the electrode [70, 75] . Since there

is no adhesive gel with dry electrodes, the electrodes are usually placed onto or inside some kind of apparatus that holds the electrodes in place [75, 76].

Dry electrodes are typically made of one of three types of materials: stiff materials, soft and flexible materials, or a fabric. The stiff materials used are generally metal, with stainless steel being the most common material used due to its cost, availability and biocompatibility [73]. However other metals have been tested including gold, silver, platinum and titanium [77-79].

Searle and Kirkup demonstrated that when enough time has been allowed for sweat and moisture to accumulate, the impedance between the electrode and skin for dry electrodes was similar to wet electrodes regardless of the electrode material used [70]. This process can take approximately 5 minutes, after which the electrode/skin impedance settles to a point where a high quality ECG signal can be measured. In comparison Searle and Kirkup's results showed that for a wet electrode this process happens almost instantly after the electrode is applied [70]. For long term recordings, especially for sleep monitoring, 5 minutes is a relatively short time to wait for an accurate ECG signal as sleep typically last for several hours.

With the rise of wearable devices, there has have been a growing number of reports of electrodes integrated into clothing. These electrodes are either made of dry electrodes attached to the garment [78] or the electrodes are made of conductive fibres woven into a fabric [80, 81], or regular materials such as cotton [82]. There are also conductive pastes that can be applied to the fabric in order to construct an electrode and electric circuit [83, 84]. The advantage of a wearable device is that it can be worn like a regular garment, and also reduces the discomfort to the wearer caused by the electrodes. However, the typically large contact area distorts the signal and there is usually a greater chance of movement artefacts and noise in the measured signal. To minimise the movement artefacts, compressive garments are typically used to try to reduce the movement of the skin relative to the electrode [80, 81, 83]. Gandhi et al. found that both conductive fabric and cotton when used

as an electrodes had lower quality than electrodes made of other materials [82]; however the quality of the signal for all of the electrode types was still good enough for R peak detection.

As mentioned earlier, dry electrodes do not need to have a gel applied to them in order to measure an accurate signal. This means that the electrodes are easier to apply than wet electrodes, and that they can be used many times without disposal. There are however several disadvantages to using dry electrodes. Firstly, since there is not an adhesive gel to bind the electrode to the skin, the electrode must be held in place in another way. This usually means attaching the electrodes to some kind of frame or device to hold all of the electrodes against the skin such that the position of the electrode relative to the patient doesn't change when the patient moves.

Some examples of these setups are shown in Figure 4-5. The first device, the EEG headset by Cognionics, while not designed to measure an ECG signal, is an example of a frame that holds the dry electrodes in position against the skin. The second device is an example of a chest strap with dry electrodes inside. The chest strap can be tightened to keep the electrodes in contact with the skin and positioned relatively close to the chest. Whilst they keep the electrodes in position these devices all increase the cost of a dry electrode setup, compared with a wet electrode setup.

Images have been removed due to copyright restrictions

Figure 4-5 - examples of devices to hold dry electrodes. (From left to right) An EEG headset by Cognionics (Source: <http://www.cognionics.com/>), a chest strap by Polar (source: www.maximfitness.net).

Since the precise location of the electrodes cannot be guaranteed for any medium to long term experiments, it is more difficult to produce a repeatable ECG signal using dry electrodes. This is because small differences in the location of the electrodes can have a significant differences on the quality and shape of the ECG signal [85]. Furthermore, an improperly positioned electrode could incorrectly show a cardiac abnormality, particularly in diseases where the symptoms involve abnormal QRS complex lengths or QT or PR intervals [73, 75, 85].

4.1.2.3 Non-contact electrodes

Non-contact electrodes are, as the name implies, electrodes that can detect biopotential signals without being in contact with the skin. These electrodes work by creating a capacitive coupling between the electrode and the skin, with either an air gap or some kind of insulating material acting as a dielectric material between the electrode and the skin. Chi et al. showed that the two ways to receive zero input noise in an ideal skin/electrode interface is to have either zero resistance or infinite resistance [75]. While contact electrodes work on reducing the resistance between the skin and the electrode, the capacitive principle of the non-contact

electrode aims for the maximum amount of resistance, which in theory allows for a noise free signal without contact.

Non-contact electrodes are similar to dry electrodes in that they require some kind of device or frame to keep the electrodes in the required position. Several examples of ECG signals measured from non-contact electrodes to detect HR have been developed. These include placing an array of non-contact electrodes in a chair [86, 87] for monitoring vital signs while driving or working in an office, and a bed [88, 89] for monitoring vital signs while sleeping.

The advantages of these systems come from the sensor not having to be in contact with the patient. This means that the discomfort of the patient while their HR is being measured is reduced, when compared with the discomfort of using contact electrodes and associated devices. Similar to dry electrodes, since no gel is needed for accurate ECG signal measurement non-contact electrodes are re-usable, and the impedance will not increase over time as happens with wet electrodes.

Non-contact sensors are not without disadvantages. Since the skin/electrode interface works in a similar manner to a capacitor, a large capacitance is needed in order to produce a signal with a large magnitude. The relationship between the capacitance of a capacitor (C) and the distance between the two capacitive elements (d) is:

$$C \propto \frac{1}{d} \quad (4.1)$$

Thus the larger the distance between the electrode and the skin, the smaller the capacitance and the amplitude of the signal, and the lower the SNR. Hence non-contact electrodes still need to be positioned relatively close to the skin in order to obtain a good quality ECG signal.

Non-contact sensors are also more sensitive to motion artefacts than contact sensors. An example of this was shown in the results recorded from a device designed to measure an ECG signal from non-contact electrodes by Lim et al. [88]. In this design they created an array of non-contact electrodes which were embedded into a bed which participants slept on. Lim et al. discovered that the motion artefacts in the ECG signal measured from non-contact electrodes led to the R-peaks in the ECG signal being unable to be detected for a period of approximately 10 seconds following the movement. This is due to the high-pass nature of the non-contact setup causing the system to have a large time constant. These results are not unusual for non-contact sensors [75]; however it means that for non-contact ECG monitoring, every time the patient moves, there will be a gap in the HR information while the system waits for the ECG signal to settle.

Additionally, if the patient changes to a different sleeping position, then the non-contact electrodes will measure the ECG signal from a different location on the patient's body compared with before movement [90], which will change the shape and the quality of the measured signal [85]. It may also change the distance between the skin and the electrodes, changing the capacitance of the electrode/skin interface and hence the signal quality. This could prove a problem for sleep monitoring, as it is common for movement to occur during sleep, particularly during the NREM stage [20], and repeated movements could make consistent HR monitoring difficult during this stage.

4.1.2.4 Electrode type summary

The main advantages and disadvantages of the different electrode types are summarised in Table 4-2.

Table 4-2 – Advantages and disadvantages of different ECG electrode types

Electrode type	Advantages	Disadvantages
Wet electrodes (Ag/AgCl)	<ul style="list-style-type: none"> • Can measure a good quality ECG signal almost instantly • Will stay in the location they are placed 	<ul style="list-style-type: none"> • Can cause skin irritation • Disposable electrodes

Dry electrodes (Metal, textile)	<ul style="list-style-type: none"> • Reusable electrode • Less likely to cause irritation than wet electrodes 	<ul style="list-style-type: none"> • Require 5 minutes after application for the impedance to reach a low steady state value • Require a device to hold electrodes in position • ECG signals less repeatable than wet electrodes
Non-contact electrodes	<ul style="list-style-type: none"> • Electrodes do not have to be in contact with the patient • Can measure a good quality ECG signal almost instantly • Less likely to cause irritation than wet electrodes • Reusable 	<ul style="list-style-type: none"> • More susceptible to motion artefacts, takes longer for motion artefact to disappear • Require a device to hold electrodes in position • ECG signals less repeatable than wet electrodes

4.1.3 Different electrode configurations

4.1.3.1 Introduction

Electrode configurations can be categorised as **bipolar** or **unipolar**. For bipolar electrode configurations, the biopotential is recorded between two electrodes. An example of a bipolar electrode configuration is shown in Figure 4-2 and 4-3. For unipolar electrodes, the electrical vector from the heart to the measuring electrode is calculated. This allows for the electrical vector of the heart to be measured at certain angles, but requires multiple ECG leads to be measured concurrently to calculate the different electrical vectors. Hence unipolar electrodes are only present in multiple lead ECG configurations.

The recommended placement of the ECG electrodes for measuring HR during a PSG is on the chest, as shown in Figure 4-3 (in section 4.1.1). This particular configuration is chosen to maximise the SNR and magnitude of the R peak of the ECG signal, making HR measurement easier and more accurate. Whilst this positioning is ideal for measurement of a good quality ECG signal, the electrode locations are not practical for long term monitoring or for integrating into a typical PAP therapy setup.

Since a PSG is a diagnostic tool for sleep disorders and not for cardiac disorders, and the main purpose of the ECG signal during a PSG is HR measurement, precise placement of the

electrodes is not necessary [68]. As such, a literature review was conducted on devices to determine if it was possible to measure an accurate ECG signal from electrodes placed in alternate or non-traditional locations. The signal quality of devices that were found were compared to each other and to a “textbook” ECG signal (eg. the signal shown in Figure 4-1). In reviewing the available literature, some alternate locations identified for electrode placement for ECG signal measurement include on the face, behind the head on the mastoid bone, and on the patient’s arm.

4.1.3.2 Different devices

In unpublished work carried out in our laboratory, Chapman et al. determined that it is possible to measure an ECG signal from electrodes placed on the face and neck [91]. They proposed that electrodes could be integrated into a PAP full face mask and a patent was filed [92]. A picture of the proposed setup as described in the resultant patent is shown in Figure 4-6. In this figure, potential locations of the DRL electrode and the negative electrode are shaded, whilst the positive electrode was placed on the back of the neck to maximise the signal magnitude.

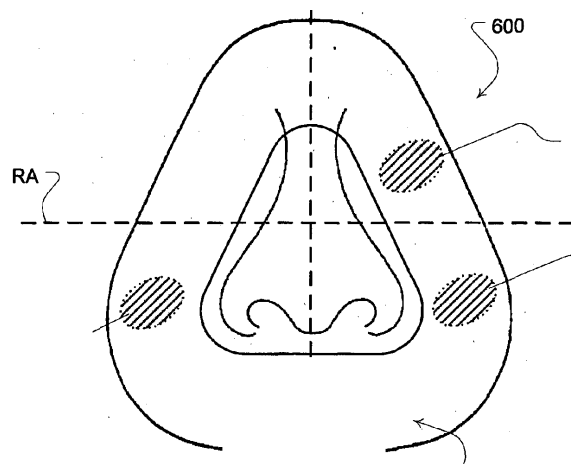


Figure 4-6 – Proposed electrode placement on a face cushion from a full face PAP mask. Electrode locations are indicated by shaded areas. Source: [92]

In preliminary testing of the concept, Farrugia and Chapman reported that the magnitude of the ECG signal measured with Ag/AgCl electrode is in the same order of magnitude as the electric signals from the local muscle and neural activity. This meant that to measure a high-quality ECG signal, a larger gain was needed. The signal was measured again with an ECG

amplifier with a larger gain of 30V/V. This increased gain reduced the SNR compared with a typical ECG signal which meant that some of the features, specifically the P and T waves, were not visible in measured ECG signal. An example of the measured signal is shown in Figure 4-7. There was still a distinct R peak in the measured ECG signal, meaning that the HR could still be reliably measured.



Figure 4-7 – ECG signal measured from electrodes placed on the face and neck. Source:[92]

He et al. [93, 94] designed a device to measure HR from an ECG signal measured from two Ag/AgCl electrodes placed behind the ear (on the mastoid bone) as shown in Figure 4-8. The gain of the ECG amplifier that He et al. used was 7000 V/V, which was because the electrodes were so close together and the ECG signal range was multiple orders of magnitude smaller than a normal ECG signal. An example of the ECG signal measured from the device is shown in Figure 4-8. Similarly to the signal measured by Farrugia and Chapman, He et al. found that the measured ECG signal had a very poor SNR, which may likely be a result of the small magnitude of the ECG signal. Whilst the ECG signal was measured on multiple participants, information about the ECG signal quality was not provided, apart from the example ECG signal shown in Figure 4-8.

Images have been removed due to copyright restrictions

Figure 4-8 - Location of the electrodes as described by He et al. (left) and an example of the measured ECG signal (right) Source: [93]

According to He et al., the quality of the measured ECG signal decreased significantly when the wearer was moving. To compensate for this, an accelerometer was embedded into the device. The accelerometer was used to detect when the participant was moving so that signal analysis could temporarily stop during this time.

He et al. decided to use digital filtering in place of a DRL electrode, due to the limited space available. They showed that it is possible to measure an ECG signal from the head without the use of a DRL electrode, as long as digital filtering is used to improve the signal quality. However this may only work for wet electrodes, and may not be as effective for an ECG signal measured from dry electrodes, especially during or after movement.

Similarly to the device designed by He et al., Zhang et al. designed a wearable device that was worn behind the ear that could measure an ECG signal [95]. Zhang et al. also noticed that the ECG signal had significant motion artefacts even after small movements. To compensate for this, a machine learning approach was applied to reduce the effect of the motion artefacts on the HR measurement. This machine learning algorithm was able to reduce the error of the HR estimation, however some HR measurements were still contaminated by motion artefacts. Similarly to the other devices previously mentioned, the SNR of the measured ECG signal was reduced in comparison to a reference ECG signal.

A device for measuring the ECG signal has been described in unpublished report by Yang et al. which uses electrodes placed on the patient's arm [96]. The electrodes were made of a "Flexible Print Circuit" (FPC) and the configuration is shown in Figure 4-9. No information was provided about the surface finish of the FPC. The width of each electrode was 25mm with a 30mm space in between each electrode. The electrode configuration was tested on the upper and lower arm, as well as the elbow, but was only tested on one participant.

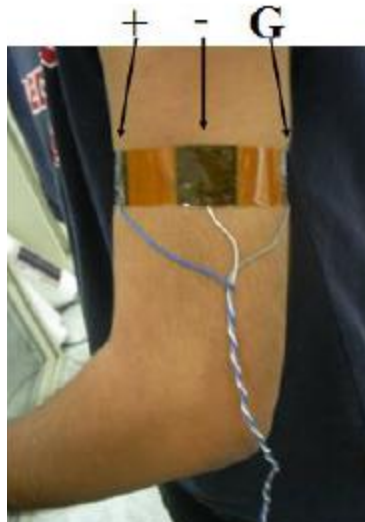


Figure 4-9 -Location of the electrode setup as described by Yang et al. Source: [96]

Examples of the measured signals are shown in Figure 4-10. This figure shows that the further a device is placed away from the torso, the worse the signal quality becomes. Similarly to the other devices earlier measured, the ECG signals in Figure 4-10 have distinct R peaks, however there is limited evidence of any P or T waves. The signals were only recorded for one participant, so it is not known what kind of variation in signal quality there would be between different participants, and whether a clear signal could be measured in the described configuration for different participants. However this demonstrates that an ECG signal can be measured using dry electrodes placed in a non-traditional configuration.

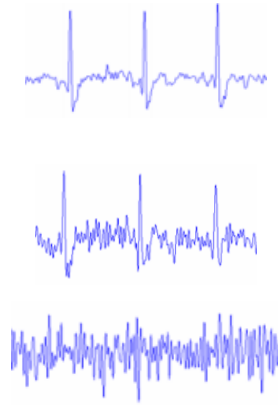


Figure 4-10 - ECG signal measured from the electrode configuration shown in Figure 4-9 placed on the upper arm (top), elbow (middle) and lower arm (right). Source: [96]

Iskandar et al. also developed a device that measures an ECG signal from an uncommon position [1]. The device that they developed contained three dry Ag/AgCl electrodes embedded into a necklace, such that they are in contact with back of the wearer's neck, as shown in Figure 4-11. Iskandar et al. suggested that the electrodes in this configuration will measure a lead I signal with a reduced magnitude compared with a typical ECG signal.

Image has been removed due to copyright restrictions

Figure 4-11 - ECG necklace with electrodes positioned on the back of the wearer's neck. Source: [1]

Iskander et al. included a sample of a recorded ECG signal from preliminary testing on one participant, which is shown in Figure 4-12. Similar to the previous devices, the magnitude of the recorded ECG signal after amplification is at least an order of magnitude smaller than the

Image has been removed due to copyright restrictions

Figure 4-12 - Comparison of an ECG signal measured from the device shown in Figure 4-11 (right) with a reference Lead I ECG signal (left). Source: [1]

reference ECG signal and there is significantly more noise in the recorded signal, which may be a result of the reduced signal magnitude. However Isakandar et al. report that when the participant wasn't moving, the heartbeats can be regularly detected using a standard QRS detection algorithm. Similarly to previous designs, the testing was only conducted on one participant, so the difference in magnitude compared to the reference ECG signal may be different for different participants.

Iskander et al. also described how when the wearer's head moves, either to the left or the right, or up and down, significant motion artefacts occur. These motion artefacts are larger for left to right head movements than up or down head movements. These motion artefacts are possibly a result of a combination of artefacts from muscle contractions in the neck, and the build-up of charge caused by the friction between the dry electrodes and the wearer's skin [75]. These motion artefacts are significantly higher than those occurring in an ECG signal measured from a typical lead I orientation and with wet Ag/AgCl electrodes.

4.1.3.3 Summary

All of these examples demonstrate that it is possible to measure an ECG signal using electrodes placed in non-traditional locations. In particular, several working devices have been developed that measure an ECG signal from electrodes placed on the head or neck [1, 94, 95, 97]. Additionally, there have been successful attempts at measuring an ECG signal from electrodes placed in non-traditional locations using dry electrodes [1, 96]. However the resultant ECG signals measured from the non-traditional electrode positions all had a reduced signal quality in comparison to the reference ECG signal. Whilst there was no quantitative comparison between the ECG signals, features normally present in a reference ECG signal such as a P and T waves were generally not present or easily identifiable in the ECG signals measured from alternate locations. However the R peaks of the alternate ECG signals are generally distinct, and thus identifiable with standard QRS detection algorithms suggesting that HR detection may be possible from these alternate ECG signals.

These examples have also demonstrated that for these non-traditional ECG signals, movement artefacts can have a significant impact on the quality of the measured ECG signal. The electrode material and configurations were compared, however the reviewed ECG signals could have also been affected by the design of the pre-amplifier used, which was not included in all of the surveyed literature. Typically when movement occurs during the recording of an ECG signal from electrodes placed in traditional locations, there is a decrease in the signal quality of the ECG signal, although the R peaks can generally still be identified manually, even if the automatic QRS detection algorithms sometimes misclassify the heartbeats. However for the ECG signals measured from non-traditional locations, movement artefacts cause the quality of the ECG signal to decrease such that it is impossible to identify R peaks. To overcome this issue, several of the reviewed devices used a movement sensor such as an accelerometer to detect when movement occurred. ECG signals were only used when large movements were not happening [94, 95]. This method has been previously used for other monitoring methods where movement causes the signal quality to decrease rapidly, such as detecting HR from vibrations of the patient's body during sleep [98].

4.2 Photoplethysmography

Other non-invasive methods for measuring HR typically identify pulses in blood flow caused by the heart beating. Similarly to the ECG signal, the time interval between successive pulses is used to calculate the HR, which can also be called the pulse rate. An example of a pulse rate signal is shown in Figure 4-13.

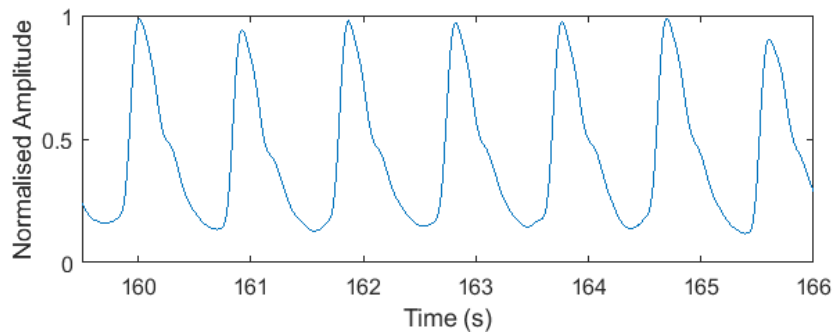


Figure 4-13 - An example of a pulse rate signal

When light is used to detect the pulses, the technique is known as Photoplethysmography (PPG). This is the basis for measurement of HR using a **Pulse Oximeter**. In a Pulse Oximeter, a light is transmitted from the surface of the skin, through blood vessels. The wavelength of the transmitted light is such that a greater amount will be absorbed by oxygenated blood than deoxygenated blood. Another light at a different wavelength is similarly transmitted such that oxygenated and deoxygenated blood are absorbed similarly. By comparing the intensity of the transmitted lights after they have passed through the blood vessels, the percentage of oxygenated blood can be estimated (written as **SpO2** or SaO2) [99, 100].

The measured intensities from the Pulse Oximeter contain a small oscillating component in the raw signal, which is caused by the variation in volume of the blood vessels being measured, coinciding with the beating of the heart

*[99]. The different components that make up a Pulse Oximeter signal are shown in **Image has been***

removed due to copyright restrictions

Figure 4-14. From this oscillating component individual pulses are identified which can be used to measure the HR. The HR from a PPG signal can also be known as the pulse rate to

emphasise the source of the HR measurement, particularly when discussing differences in the HR values from a PPG and ECG signal [101].

Image has been removed due to copyright restrictions

Figure 4-14 - Components of a PPG signal. Components B, C and D represent the absorption due to arterial and venous blood, as well as other tissue. Component A represents the oscillating component that varies with each heartbeat. Source: [99]

The accuracy of the pulse rate from a Pulse Oximeter signal when compared with the HR from an ECG signal varies from study to study. This is because there is no standardised equipment or methodology for testing and extracting a pulse rate from a PPG signal [101], and parameters such as the measurement location, sampling rate and choice of fiducial point differ between examples in the literature.

A Pulse Oximeter signal contains more information about the patient than just the pulse rate. The main purpose of a Pulse Oximeter is to detect periods where the SpO₂ values are low which can indicate that patient is not receiving enough oxygen such as during an apnoea episode [102]. The respiration rate can also be detected from the Pulse Oximeter signal by filtering the signal at typical respiration frequencies [103]. There is also research being conducted into other variables that can be extracted from a Pulse Oximeter signal such as blood pressure and arterial stiffness by examining features of the measured signal [104].

There are two different methods for measuring a Pulse Oximeter signal, both of which are shown in Figure 4-15. The first type is a transmissive Pulse Oximeter (left), which is the most common method. This method involves shining light through perfused tissue (typically a finger or earlobe) and measuring the intensity of the transmitted light on the opposite side of the tissue. The second type is a reflectance Pulse Oximeter (right). This is typically used when the tissue that the sensor is placed on is too large or dense for light to pass through. Instead, the light is reflected by the tissues that is being analysed, and so the receiver and emitter elements of the sensor are placed on the same surface.

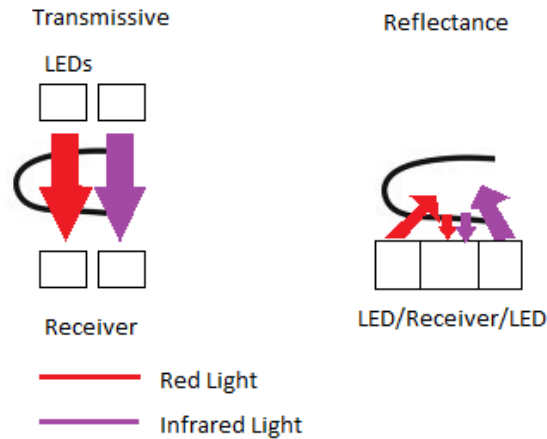


Figure 4-15 - Transmissive vs reflectance pulse oximetry applied on a finger

4.2.1 Measuring PPG signal from forehead

There are many locations where a PPG signal can be measured. The main sites that have been used are the finger, earlobe [99] and forehead [105], although there have been other sites tested [106], particularly for neonatal monitoring [101]. The PPG signals recorded at different measurement sites will have different shapes, amplitudes and signal quality, due to several different physiological factors, including the elasticity of the vessels and the perfusion rate of the tissue close to the sensor [105]. The different measurement sites will also react differently to physiological change. For example, sites that are more central, such as the forehead and the earlobe, will also react faster to a drop in SPO₂ levels [107]. Central sites are also less likely to be affected by other homeostasis functions that are controlled by blood flow, such as the body's temperature control [108]. Additionally, the pulse rate accuracy can also vary with different sensor locations [107]. This means that care must be taken comparing results from a Pulse Oximeter obtained from different measurement sites.

There is evidence to suggest that the forehead is a good location for a PPG measurement. Curative Medical have developed a PAP therapy mask containing a Pulse Oximeter sensor that measures a signal from the forehead. An example of the device is shown in Figure 4-16 [109].

Image has been removed due to copyright restrictions

Figure 4-16 - PAP mask with a Pulse Oximeter attached. Source: [109]

Sugino et al. demonstrated that under general anaesthesia, SpO₂ values measured from the forehead were as accurate as the SpO₂ values measured from a transmissive Pulse Oximeter placed on the finger [110]. It was also shown that for patients in critical care, measuring from the forehead gave fewer inaccurate SpO₂ readings than measuring from the finger [111]. Cheng et al. showed that a forehead Pulse Oximeter was able to detect significant de-oxygenation in patients, but the SpO₂ accuracy differed significantly from a finger Pulse Oximeter in these conditions [112]. Nilsson et al. showed that the pulse rate from the forehead PPG signal agreed well with the HR component from an ECG signal, however for some patients the forehead PPG signal may be contaminated by noise from the veins near the measurement site [113]. Hence there is evidence to suggest that pulse rate and SpO₂ values from a Pulse Oximeter measurement are either as accurate as or potentially more accurate than a finger Pulse Oximeter.

4.2.2 Accuracy of PPG HR measurements

There are many sources of variance in the PPG signal that can occur by using the different testing methodologies that are present in the literature. In a PPG signal (such as Figure 4-13 and Figure 4-17), it is difficult to reliably and consistently define a fiducial point on the pulse wave, as there is not as obvious a candidate as the R peak in an ECG wave. This has led to several different algorithms being developed to extract an inter-pulse interval from different features on the pulse wave, which all have different levels of accuracy and variability [114,

115]. Some examples of these fiducial points are shown in Figure 4-17, and include the local maximum, local minimum, and maximum of the 1st derivative of the PPG signal. Other algorithms rely on using the R peak from an ECG signal as a starting point to detect a fiducial point on the pulse wave signal [95]. While this technique might work well for calculating some cardiac and blood vessel parameters, it is not useful when there is no ECG signal to reference.

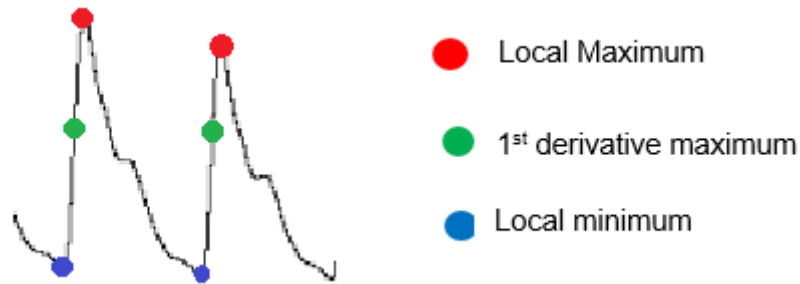


Figure 4-17 - A PPG signal showing some of the common fiducial points used in a PPG signal

Several studies have been conducted to compare HRV analysis from an ECG and a PPG signal. They have all come to a similar conclusion regarding differences in the HRV analysis between an ECG and a PPG signal, which is that a Pulse Oximeter is a reliable source of measuring HRV only for healthy patients at rest [101, 116-118]. They have also noted that there is an increase in the power of the High Frequency (HF) (0.15-0.4Hz) component of the HRV in a PPG signal when compared to the HF component in the ECG signal. There is also common agreement that short term variables derived from a PPG signal, such as RMSSD and pNN50, are not accurate when compared to these similar variables derived from an ECG signal. It is thought that the PPG signal is more strongly influenced by respiration than the ECG signal. There is evidence of this in spectral analysis conducted by Giardino et al, who found that the peak frequency of the variations between the ECG and the PPG signal to be between 0.16Hz and 0.2Hz, approximately the same frequency as a normal respiration rate [116].

The variation in pulse rate, when compared with the actual HR, may also be influenced by the **Pulse Transit Time (PTT)**. PTT is the time taken for the blood to reach a specified part of the body from the heart. This can be measured as the difference between peaks in the ECG wave and the pulse wave (from a PPG signal for example). PTT is mainly affected by arterial contractility, and has been linked to arterial and cardiac health [119]. In a study by Giardino et al. the interbeat interval for pulse rate from a Pulse Oximeter and HR from an ECG were compared [116]. They found that when the instantaneous PTT decreased below the mean PTT, the beat-to-beat intervals for the PPG became longer than the RR intervals for the ECG and vice versa ($r = -.61$). Although compared to the magnitude of the beat-to-beat interval this variation is quite small (maximum of 40ms difference), this is still a source of variation that could also affect the HRV accuracy.

There have been several algorithms developed to identify periods of arrhythmias in a PPG signal. These algorithms aim to identify one particular arrhythmia such as atrial fibrillation [120] or small number of arrhythmias [121]. However, current algorithms for analysing PPG signals cannot reliably classify multiple types of arrhythmias, especially when compared with the performance of an ECG signal. The signal quality of the PPG signal also decreases in the presence of these abnormal beats [101] as well as during a breathing disorder episode such as sleep apnoea [117].

A pulse oximetry signal is also more susceptible to movement artefacts than an ECG signal (measured from wet electrodes) [65]. There have been several papers that attempt to remove these artefacts from the signal in order to improve signal quality. Most algorithms use additional sensors to help compensate for the movement [97, 122-124]. Recent advances in signal processing are able to estimate the HR of a PPG signal corrupted by movement, however these algorithms are not able to measure an instantaneous beat-to-beat HR signal [125, 126]. It should be noted that most of these algorithms were developed and

tested on signals from a finger or a wrist Pulse Oximeter. It is unclear whether they would be applicable to signals from a forehead Pulse Oximeter.

For reflectance Pulse Oximeters, the quality of the measured PPG signal is dependent on the force applied by the sensor to the skin and is one of the main sources of motion artefacts [113, 122]. This would also imply that the force between the sensor and the skin needs to remain constant during measurement to generate a good quality signal. This is an important factor for the sensor placement, as during sleep it is common for movement to occur, which may cause motion artefacts. Hence for a PPG sensor mounted on the forehead, the mounting method must be set up to attempt to keep the application force of the sensor constant at all times to ensure a consistent signal quality for different sleeping positions and during movement.

These results suggest that, although the PPG signal may be able to be used to measure HR and HRV, these additional sources of variation need to be considered, as they can affect the accuracy of the HR and HRV measurements. Additionally, methods for coping with movement artefacts need to be developed or previously developed methods adapted to suit a forehead PPG sensor.

4.2.3 Examples of wearable devices using PPG

With these limitations in mind, a survey was undertaken of literature reporting a pulse rate extracted from a PPG signal measured from the head or neck. Sites where wearable devices have been able to measure a PPG signal from include the forehead [123, 124, 127], neck [128] and ear [95, 129, 130].

Wearable PPG devices are all able to accurately measure the pulse rate of the wearer, however like with the ECG signal measured from the face and neck, the PPG signals measured from the head are sensitive to motion artefacts. Zhang et al. reported that both the

ECG and PPG signals were sensitive to small motion artefacts [95]. Kim et al. were able to reduce the RMS error of the HR estimation caused by motion artefacts using an adaptive filter, however the HR error was at times approximately 10-15 BPM different to the reference HR value [123]. This suggests that similarly to the ECG signals, a method for dealing with motion artefacts in the PPG signal should be implemented to reduce the error of motion artefacts.

He et al. proposed another setup similar to the setup mentioned in section 4.1, in which a reflectance Pulse Oximeter was positioned behind the ear [130]. Testing from this device showed that for a healthy patient at rest, there is a good correlation between the reflectance pulse oximetry signal and the normal pulse oximetry signal taken from the left index finger. However the delay between the ECG and the PPG signal from the finger was longer than the delay between the ECG signal and the PPG signal measured from behind the ear. This is because the blood has further to travel to reach the finger than to behind the ear.

PPG sensors were integrated into headphones by Poh et al [131]. The location of the sensors was such that when the headphones were worn, the PPG sensor was measuring from inside the ear canal. The HR was measured from multiple healthy participants during rest and whilst walking on a treadmill. During rest, the error of 95% of the measurements when compared with the HR from an ECG signal was ≤ 5 BPM. As with the previous examples described, when the participants were walking the error of the HR signal increased.

4.2.4 Summary

It is possible to measure an accurate pulse rate signal from a reflectance Pulse Oximeter positioned on the head. The HRV analysis from a pulse rate signal has good agreement with

HRV results from an ECG signal only when the patient is healthy at rest. However care must be taken when comparing PPG results from different measurement sites as things such as the pulse rate accuracy and PTT can vary in PPG signals from different measurement sites. As with the ECG signal, a PPG signal measured from the forehead is sensitive to motion artefacts, so a method for compensating for motion artefacts needs to be developed if a PPG signal is to be used.

4.3 Ballistocardiography

Ballistocardiography (BCG) is a technique for measuring HR by measuring small movements or vibrations that are caused by the heart pumping. As the heart pumps, a pressure gradient occurs between the ascending and descending aorta, which causes small movements of the body [132]. By analysing these small movements or vibrations, heartbeats can be identified in order to calculate HR. As well as measuring HR, other variables such as respiration rate and movement episodes can also be detected by filtering the signal at different frequencies [98].

The most common application of this techniques involves integrating a sensor into the user's bed, on top of or below the mattress [133, 134], or by attaching it to the bed itself [135]. The advantage of this technique is that the device and/or sensor is not in contact with the subject. Non-contact sensors are generally more comfortable than contact sensors and hence are more likely to be accepted for home use.

A less common method of BCG uses a wearable device containing a solid-state gyroscope, accelerometer or similar sensor to measure the BCG vibrations. Most of the research in this area involves embedding accelerometers into a tight fit garment that is worn by the subject [136, 137]. This method is also known as Seismocardiography (SCG). The accelerometers are positioned on the subject's chest, which can detect the heartbeats from chest movements. An example of BCG signals measured from a gyroscope placed on the chest is shown in Figure 4-18.

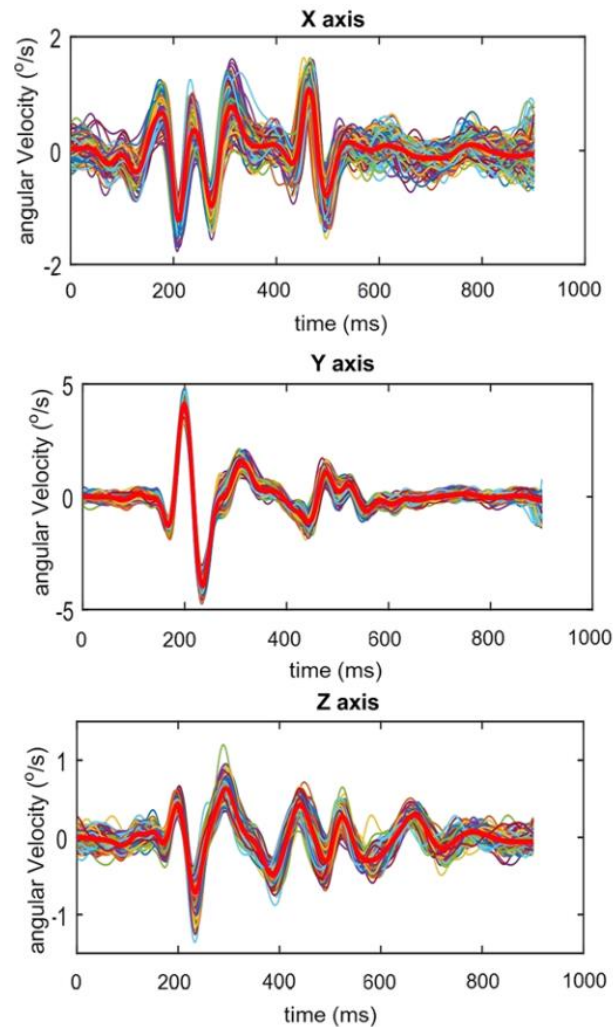


Figure 4-18 – An example of BCG signals measured in the 3 axis a gyroscope located on the chest of nine healthy participants. An averaged signal is shown as a thick red line. Source: [138]

Recent developments have shown that the BCG (or SCG) signal contains more information than just HR. Tadi et al. showed that certain features of a BCG signal measured using a gyroscope placed on the chest correspond to specific cardiac events, including being able to detect when certain heart valves are opening [138]. Wiens et al showed that even when the BCG sensor was placed on distal locations such as the wrist, the aortic valve opening and closing times could still be detected by measuring the delay between peaks of the ECG and the BCG signal [139]. Other cardiac properties that have been researched with regards to BCG signals include stroke volume [140], pulse transit time [132] and blood pressure [141], as well as other cardiac intervals [138], and tissue properties of the heart such as contractility [142]. The RMS value of BCG signals and the time difference between the ECG

and BCG peaks have shown to be linked to clinical outcomes [143]. Differences in the BCG signal measured from the chest before and after exercise have also been used to assess heart failure outpatients [144].

4.3.1 Examples of wearable BCG devices

Similarly to the ECG and PPG setups, it is not practical to locate sensors on the chest for monitoring during PAP therapy as it would require additional devices to be used or a more complicated PAP device setup. There have been several devices that measure a BCG signal from accelerometers or gyroscopes positioned on a subject's head. However instead of measuring small vibrations of the subject's skin, these devices measure small movements of the subject's head caused by the pumping of blood. This concept was first demonstrated by Balakrishnan et al. who used image processing techniques to track the small movements of the subject's head caused by pumping blood [145]. From these movements they were able to estimate the subject's HR.

From this initial work, two examples of wearable BCG devices that are worn on the subject's head were developed by Hernandez et al.[146] and He et al. [94]. In the device developed by Hernandez et al. an Inertial Measurement Unit (IMU), containing a 3 axis accelerometer, 3 axis gyroscope and a 3 axis magnetometer, was embedded into the Google Glass device as shown in Figure 4-19. The IMU that was used was an MPU-9150 (Invensense, USA). The device was designed for estimating the HR of the wearer during normal activities.

Compared with the signals shown in Figure 4-18, the signals measured by Hernandez et al had a reduced signal quality and identifying a peak for heartbeat detection was more difficult. Hernandez et al. were able to develop an algorithm that converted the gyroscope and accelerometer signal into an estimation of the wearer's HR. This algorithm involved filtering the signals and identifying peak frequencies which were assumed to be related to the HR. This algorithm was applied to the signals from both the accelerometer and the gyroscope

signals separately. As well as estimations from the gyroscope and accelerometer signals individually, a simple data fusion method was implemented in an attempt to increase the accuracy of the HR estimation. This method involved using the median value from all of the different sensors for each window. A method for estimating the HR from the onboard camera was also developed but is not relevant in this discussion.

Image has been removed due to copyright restrictions

Figure 4-19 - Sensors included in the Google Glass including the Accelerometer and Gyroscope, which were used to estimate HR. Source: [146]

The accuracy of this algorithm was compared against a PPG sensor worn on the participant's finger which acted as a reference HR sensor. For this sensor the HR was also calculated using the peak frequency over a 20 second window. The algorithm was tested for three different positions: sitting, standing and supine (participant lying on their back). All of the measurements were recorded whilst the participant was stationary, however for some of the recordings, the participants were asked to exercise prior to the recordings, to increase their HR. The results for this experiment are shown in Table 4-3 and Table 4-4.

Table 4-3 – HR estimation (BPM) accuracy by Hernandez et al. over a 20 second window compared with a reference HR measurement. Values being compared are Mean Error (ME) Standard deviation of the error (STD), RMS error (RMSE) and Pearson’s correlation coefficient (CC) Source: [146]

Sensor	ME	STD	RMSE	CC
Gyroscope	0.83	2.02	2.19	0.99
Accelerometer	2.41	6.45	6.88	0.92
Camera	7.89	13.35	15.50	0.59
All	1.21	3.45	3.66	0.98

Table 4-4 - HR estimation mean error (BPM) by Hernandez et al. over a 20 second window in different positions compared with a reference HR measurement. Source: [146]

Sensor	Sitting	Standing	Supine
Gyroscope	1.15	0.91	0.44
Accelerometer	3.30	1.71	2.22
Camera	4.42	10.45	8.80
All	1.49	1.16	0.98

Table 4-3 shows that the gyroscope provided the most accurate signals for estimating HR using the algorithm described, followed by the median estimate (data fusion) and then the accelerometer. These results show that the data fusion method chosen doesn’t improve the accuracy of the HR estimation in comparison with the individual signals. Since the gyroscope signal is the most accurate in estimating the HR, this suggests that for the position of the IMU, the rotational movement caused by the heart pumping is greater than the linear movement.

Table 4-4 shows the accuracy of the HR estimation from the different sensors in different positions. For the estimation from the gyroscope signal, the accuracy of the estimation was higher when the participants were in the supine position (lying on back). For the accelerometer, the most accurate estimation was from when the participants were standing. No reasons or hypotheses were put forward to attempt to explain these results.

The disadvantage of this method is that the estimation of HR is not an instantaneous measurement, but an approximation of the HR over a 20 second overlapping window. Thus any changes in HR values that are measured by the described method may not be an

accurate reflection of the actual changes of the HR. Furthermore, because the beat-to-beat interval is not measured, HRV measurements are not possible using this technique.

The second device was developed by He et al. and comprises a device that is worn behind the ear as shown in Figure 4-20. In this setup an accelerometer is used to measure a BCG signal from behind the ear, superficial to the mastoid bone [94]. The accelerometer used was a BMA180 (Bosch, Germany) which is a MEMS 3-axis accelerometer. Although all 3 axes appear to be recorded, the authors state that the y-axis was the best signal for analysis as “the blood volume movement is mainly is the y-axis” which is in the superior-inferior (upward-downward) direction [94].

Image has been removed due to copyright restrictions

Figure 4-20 - Wearable BCG device developed by He et al. Source: [94]

However similarly to the previous device discussed, the accelerometer signals measured had a reduced signal quality and SNR compared with Figure 4-18. Hence instead of detecting heartbeats from the accelerometer and measuring the HR of the wearer, the accelerometer signal is used in conjunction with an ECG signal to measure the ‘R-J’ interval. The R-J interval is defined as the time difference between the peak of the ECG signal and the peak of the BCG signal. This interval is measured by calculating the delay for signals in an 8 second window using a cross-correlation method. The R-J interval was found to

correlate with the time difference between when the ventricles contract and the aortic valve opens ($R^2=0.96$).

One disadvantage of this technique which would be present in other BCG devices is that measurement is not possible whilst the subject is moving. The author states that the measurements for the R-J interval are made when the magnitude of the accelerometer signal is below a certain threshold [94]. This is because the movements of the wearer will add additional noise to the signal, which may introduce unwanted errors in the detection of heartbeats. Additionally, the magnitude of the acceleration due to movement is typically significantly larger than the acceleration due to heartbeats, so it is likely that the movement artefacts will saturate the acceleration signal, leaving no usable data.

Discarding movement artefacts is a common technique used for BCG monitoring during sleep. The assumption is made that the amount of data discarded during movement artefacts is relatively small, since the proportion of time that is spent moving during sleep is low when compared with the total sleep time. This is argued in [98] by Shin et al. and this strategy has also been used in other BCG sleep monitoring studies [98, 134, 147]. Hence a similar strategy could be applied in the application of a wearable BCG device for sleep monitoring, where the movement sensor is located on the wearer's head.

4.3.2 Summary

Previous work has shown it is possible to measure a BCG signal from movement sensors located on the participant's head. However, the SNR ratio of the BCG signal is reduced in comparison to the BCG signal measured from sensors placed on the chest. As expected, movement artefacts, especially body movement episodes, will have a significant impact on the accuracy of the HR estimation. As well as measuring HR there may be other useful information that can be detected from the IMU signals, such as identifying movement episodes, aortic opening times, and Stroke Volume.

4.4 Data fusion techniques

The review of ECG, PPG and BCG devices that are able to measure a signal from the head or neck of the wearer (sections 4.1-4.3) showed that these devices have a reduced signal quality and SNR in comparison to when these same signals are measured from their traditional locations. This may lead to reduced HR and HRV accuracy, as the heartbeats are more difficult to detect. It is thought that by combining the heartbeat and/or HR information from different signals, accurate HR and HRV analysis may be possible, even when the signal qualities are sub-optimal. Combining sensor information is typically implemented through data fusion algorithms. Hence data fusion methods that have been implemented previously for physiological monitoring scenarios will be compared to determine if any previously used methods are appropriate for this application.

4.4.1 Previous applications of data fusion methods for physiological monitoring

Physiological data fusion has been used in intensive care units (ICUs) or other similar clinical settings [148-153]. In these situations it is important for clinicians to monitor a patient's vital signs, to identify changes such as a rapid decrease in HR or blood pressure, or to determine if the vital signs fall above or below a certain threshold. HRV is not commonly monitored in ICU, so algorithms for HR estimation in ICU tend to prioritise consistent and accurate HR estimation and the rejection of noisy signals and outlier HR values, over instantaneous HR accuracy and accurate detection of heartbeats necessary for HRV analysis.

Data fusion methods can also be used to filter out inaccurate HR measurements from sources that have a relatively poor signal quality [154-156]. With these applications there is an underlying method (such as BCG [156]) which is able to detect HR, however the accuracy and consistency of the HR measurement is poor, causing multiple inaccurate HR values. By using a data fusion algorithm, information (such as HR) from either one signal [155], or multiple channels of the same signal [156] are the input to an algorithm which is

able to discard inaccurate HR information and increase the accuracy and consistency of the HR measurement.

4.4.2 Kalman Filter

One of the most common methods for data fusion is the Kalman Filter (KF), which uses a set of equations used to combine data with known behaviour and variances [157]. Within the equations of a KF the response of the system, which in this case is HR with respect to time, is modelled. The equations for a traditional KF are shown in Appendix A. These techniques are most commonly used in fields such as robotics and telecommunications [158] however recently they have been applied to medical applications, such as the processing of multiple noisy signals for estimation and tracking of physiological parameters.

Traditionally, the system is modelled in a KF using a linear equation [157]. However, there are many factors that can affect the HR, some in a non-linear fashion. When a patient is stationary, the variation in HR is influenced by the different levels of sympathetic and parasympathetic stimulation [8]. HR can also be affected by respiration [159], sleep stages [20], and circadian rhythms [21] as well as spontaneous events such as movement [160], apnoea events [64, 161], and arrhythmias [7]. Since the HR and HRV can be affected by so many different factors, it would be difficult to create a HR model that can account for these different factors, and the potential increase in accuracy over a simple HR model may not be significant. Although it is possible to use non-linear equations in a KF [162], a model to account for so many factors would be complex.

Since there are many factors that can influence the HR, simplified models of the HR have been used in a KF, although more complex HR models have also been attempted [154, 163] with some success. The simpler models either model the HR as constant [148, 164], or use an Auto-Regressive (AR) model in which the HR is modelled as

$$HR_{t+1} = \sum_{i=0}^n \omega_i HR_{t-i} \quad (4.2)$$

where for n of the previous HR values, HR_t is the HR estimation at time t , and ω_i is the associated weighting [165]. These models usually also have a random noise component which is added to the HR model to allow for the natural variation of the HR.

As a pre-processing step, the measured instantaneous HR signal is usually converted into an evenly sampled HR signal. Converting an instantaneous HR signal to an evenly sampled signal can alter the variation in the HR making it not usable for HRV analysis, particularly if the time difference between samples is large.

Li et al. attempted to apply a KF to an instantaneous HR from multiple ECG signals [148]. In their attempt, they picked one ECG signal and identified possible heartbeats using a QRS detection method. Unlike previous methods which output an evenly sampled HR signal, the time of each detected heartbeat was then set as the time points for each iteration of the KF. This allowed for a more instantaneous HR signal as the algorithm will update with each new heartbeat and not after a certain time period. However it relies on the base signal being relatively noise free, as if multiple false heartbeats are detected then the KF algorithm will update multiple times in between each actual beat adding more false variability to the signal. A similar effect would occur if multiple heartbeats are missed. In an ideal data fusion algorithm the quality of one signal should not have a larger influence over the performance of the data fusion accuracy than any other signal.

There have been several KF implementations that use the recorded signals, such as ECG or blood pressure signals, as the input to the KF instead of the HR values. A model of the expected signal shape is modelled instead of the HR, with the HR being a variable in the model of the signal. Many of these models, especially the models using the ECG signals, have come about because of the ability to create dynamic models of physiological signals,

such as the ECG model created by McSharry et al [166]. Using these models, variables such as HR and respiration rate are estimated. These systems contain models that account for the relationship between the different physiological systems, such as how respiration can affect HR [154, 167]. One disadvantage of this method is that the output HR signal is an evenly sampled signal that is an estimation of the HR. While this allows for accurate HR estimation, it once again does not allow for accurate HRV analysis, as the HR dynamics are smoothed out by the KF equations.

Hence a KF can be used to produce an accurate and consistent HR signal from multiple sources, either by creating a simple model of the HR or by extracting HR information from the measured signals. However the nature of the KF algorithm will cause the output HR to be smoothed, which will reduce any variability in the HR signal, reducing the potential for accurate HRV analysis.

4.4.3 Other Data Fusion methods

A KF is not the only method for data fusion of physiological signals. Sometimes more simple approaches can be implemented. Median filters have been used for estimating HR based on HR values from several different sensors, in which the median value from the different sensors is taken as the measured value [146, 153]. This technique is computationally simple and fast, however if the majority of the signals are reporting inaccurately then the median filter will output an inaccurate HR. It also will output a HR signal that is evenly sampled, which would also reduce the accuracy of the HRV analysis.

Another example of a data fusion method was demonstrated by Townsend [168]. In this approach a weighted moving average formula is applied. The weightings were assigned such that an accurate signal is given a higher weighting and an outlier value is given a low weighting. The formula for this is:

$$X_k = \sum_{s=1}^S \left(\frac{\prod_{i=1, i \neq k}^S \sigma_{k,i}^2}{\sum_{s=1}^S (\prod_{j=1, j \neq i}^S \sigma_{k,j}^2)} \cdot x_{k,s} \right) \quad (4.3)$$

where $x_{k,s}$, and $\sigma_{k,s}$ are the independent estimate and the associated uncertainty for the s^{th} sensor at the k^{th} time-step, respectively and S is the number of sensors being fused [169]. This approach has the same advantages as a median filter in that it is not computationally intensive, but is able to reject outlier HR signals more effectively than a median filter, if the weighting values are assigned appropriately.

4.4.4 Signal quality estimation

For most data fusion techniques, a method for comparing the quality of the observations from different signals is needed to determine how accurate the different inputs are. One method for comparing different observation values is to compare different values that represent the quality of the signal the observation came from. For ECG signals, the signal quality can be estimated by comparing the detected heartbeats from different QRS detection algorithms applied to the same ECG signal [148, 170-174]. This is because in theory, for a good quality ECG signal, the number and location of the heartbeats should be the same regardless of the QRS detection algorithm used. However since the QRS detection algorithms all use different methods to identify heartbeats, for a poor quality signal, the performance of the QRS detection algorithms will vary depending on the nature of the noise in the signal. Additionally, using known properties of a good quality ECG signal such as signal kurtosis, skewness and ECG power, the ECG signal quality can also be estimated [172, 174, 175].

For PPG signals, other techniques can be used for estimating signal quality. One such technique compares the signal for one heartbeat to a template generated by previous heartbeats to estimate the signal quality for that heartbeat [176, 177]. However this technique relies on good quality signals occurring previously. This means that if the signal quality is consistently poor, since the adjacent pulses will all have a similar shape the

assigned quality estimation will be high, even though the actual signal quality is poor. Other techniques involve using heuristic values for the shape and size of each pulse to estimate signal quality [176, 178].

When compared with the ECG and PPG signals there has been less research on the features that make up a good quality BCG signal. Brüser et al found that in a smoothed BCG signal the time difference between the maximum and minimum points in one heartbeat and the amplitude of these points could be used to help classify whether a BCG signal was good quality [147]. Another method that has been used is to compare the waveform shape between successive heartbeats [179, 180] in a similar method that was used for the PPG signal. However further research is needed to confirm the signal features and qualities that make up a good quality BCG signal.

One issue that can arise with implementing a data comparison technique is how to compare the quality of different signals. Each of the signal quality metrics described previously are useful for comparing similar types of signals, for example comparing different ECG signals. However, for different types of signals, for example comparing an ECG signal to a PPG signal, most signal quality metrics are difficult to compare, especially for signals of medium to poor quality. For example if a particular quality metric gives a score of 0.6 for an ECG signal and a 0.7 to a PPG signal, one cannot say with certainty that the PPG signal has a better quality and more accurate information than the ECG signal. This is because the scores are only designed for comparing similar signal types, and hence the assigning of scores is relatively arbitrary and only consistent within the same signal type. This means that either some kind of heuristic is needed for comparing quality measurements from different signals, or the signal quality metric should be derived from the HR measurements or identified heartbeats and not the signal itself.

Another method that has been used to attempt to compare the signal quality of different signals (e.g. ECG and PPG signals) involves a signal quality estimate based on the previous HR intervals measured [181]. In this method a higher signal quality is assigned to a signal if the HR is closer to the previous HR signal. This technique will produce a more stable HR signal as false HR signals are less likely to have a significant effect on the algorithm output. However if the HR does change quickly due to an event such as movement, the algorithm may assign relatively low weightings to the correct HR values, which could introduce errors into the HR estimation. Additionally, if the output of the algorithm strays from the actual HR, it can take a longer time for the output to reconverge to the actual HR as the algorithm's measure of HR is incorrect.

Most data fusion methods described previously use the HR values as an input to the data fusion algorithm. To that author's knowledge, there have been no data fusion algorithms that look to combine heartbeat timing annotations from different signals (e.g. combining heartbeat timing information from ECG and PPG signals). There has been an example of using data fusion methods to track HRV variables, but this used the analysed HRV variables as the input [182]. Most publications on HR data fusion algorithms do not include information on the HRV analysis accuracy. Also, most data fusion methods described previously look at combining the HR values from different sources. In a setup where there are potentially multiple signals all able to detect heartbeats, using the heartbeat timing instead of averaged HR values may be a possible approach for combining data from different sources whilst still allowing for accurate HRV analysis.

4.4.5 Summary

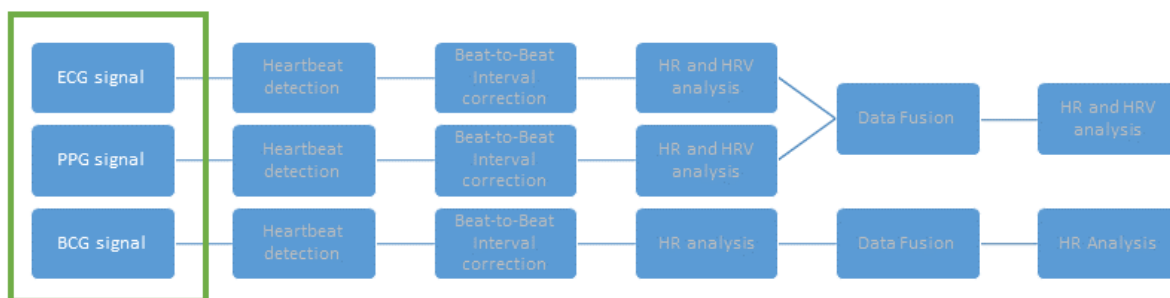
Data fusion algorithms allow for data from several different sources to be combined to increase the accuracy and consistency of the measurement of physiological variables, including HR. Data fusion algorithms such as a KF can turn an inaccurate instantaneous HR into a consistent and accurate HR estimation. Whilst these algorithms are able to produce

accurate HR estimations, the majority of data fusion algorithms produce a smoothed HR signal that is evenly sampled which means HRV analysis cannot be accurately performed. Additionally it can be difficult to compare HR values from different signals, such as an ECG and a PPG signal, especially if the signals have poor quality.

4.5 Literature summary

An analysis of the current literature has shown that it is possible to measure an ECG, PPG, and BCG signal from sensors located on the face and head. Previous iterations of these sensors have shown that motion artefacts can affect the signal quality of the ECG, PPG and BCG signals measured from the head, so methods for reducing the error during movement periods are needed.

In terms of implications for this thesis, the literature suggests that it may be possible to monitor the HR from a PAP mask during PAP therapy from a number of different sensors. Additionally, using data fusion algorithms described in the literature it may be possible to combine the HR information from a number of different signals to produce one accurate HR signal. However this fused HR signal will not allow for accurate HRV analysis, so a new method is needed to combine the HR (and/or HRV) information from different signals such that accurate HRV analysis can be performed on a fused signal.



5. Device Description

5.1 Introduction

Taking inspiration from the devices and solutions discussed in chapter 5, a device was developed that was designed to monitor the Heart Rate (HR) of subjects during Positive Airway Pressure (PAP) therapy. This device was called the **Cardiomask** and was a modified commercial PAP mask. In this chapter the Cardiomask will be introduced including a description of the key design features and an example of the signals measured from sensors embedded in the Cardiomask, obtained from preliminary testing on a small number of participants.

5.2 Cardiomask

The mask that was modified was the ResMed Quattro Air mask, shown in Figure 5-1. A full face mask was chosen rather than a nasal mask as it provided more room on which to attach the sensors. However, there may be potential in the future to take ideas from this design to similarly modify a nasal mask. In accordance with the summary of Chapter 4, sensors selected for inclusion in the Cardiomask were Electrocardiography (ECG) (with dry electrodes), Photoplethysmography (PPG), and Ballistocardiography (BCG). Additional design criteria associated with the sensors in the Cardiomask were selected to maximise the benefits to people with OSA who would potentially use the Cardiomask, and these are described in the next section.

5.3 Design Decisions

Key criteria used to inform sensor choice and placement on the Cardiomask were:

- Useful information can be collected from the sensor

- Minimal additional discomfort to the patient by inclusion of the sensor
- Sensors/device easy to apply/use
- Low cost

Image has been removed due to copyright restrictions

Figure 5-1 - The ResMed Quattro Air PAP mask. Source www.resmed.com

5.3.1 Useful information from the sensor

The primary aim of the Cardiomask was to measure the HR and HRV of the wearer. However, if a sensor/signal was able to provide additional information about the wearer's health, this would increase the clinical value of the device. For example, the PPG signal can not only reveal HR, but also the SPO2 levels of the wearer which could be used to determine if the wearer has had an apnoea event during the night.

5.3.2 Minimal discomfort added to the patient by wearing the device

Uncomfortable devices may stop patients using PAP therapy [183]. Hence to ensure that patients continue to use the therapy as well as having their HR monitored, any modifications that allow for HR monitoring must be comfortable to wear.

5.3.3 Sensors/device easy to use

Following on from this, the modifications to the PAP mask must be also be easy to use. One of the reasons that people with OSA continue to use their PAP device is because of the health benefits of the therapy, such as improved sleep and more energy during the day [4]. However, with the HR monitoring, the immediate health benefit may not be obvious, and thus people with OSA may choose not to use the HR monitoring system if it is difficult to

setup and use. The ideal Cardiomask would not place any additional requirement on the user, and hence sensors should be included as an integral part of the mask.

5.3.4 Low Cost

The masks used for PAP therapy are designed to be reusable. Assuming the sensors are included as an integral part of the mask (to avoid issues associated with setup as described above), then they must be low cost, as patients will be recommended to replace them at regular intervals.

5.3.5 Summary

In line with the comfort and ease of use design criteria, it was decided that sensors (ECG, PPG and BCG) integrated into the mask frame and/or the surrounding mask straps would be the best option for HR monitoring. Furthermore, sensors in the frame or mask straps would not need to be replaced as often as if they were in the mask cushion, which is typically replaced more often.

5.4 ECG

ECG was chosen as a key signal to be measured from the Cardiomask, as it is currently the gold standard for identifying heartbeats and measuring HR [7]. In addition, by analysing the electrical signal of each beat, arrhythmias and other irregular heartbeats can be detected and classified. Furthermore, when combined with a HR detecting method that looks at the blood flow caused by the heart beating (such as PPG or BCG), the ECG signal can be used to calculate the Pulse Transit Time (PTT), which as mentioned in the previous chapter can be linked to other physiological parameters.

5.4.1 Setup

The ECG signal measured from the Cardiomask had electrodes positioned around the wearer's head and face. The positions of the electrodes are shown in Figure 5-2 and were chosen to maximise the magnitude of the ECG signal from possible electrode locations around the face and neck, according to previous work in our laboratory by Farrugia and Chapman [92]. Whilst it had been shown that an ECG signal measured from electrodes in this position can detect heartbeats, it was not known whether arrhythmias detectable in a normal ECG signal would be able to be detected in the ECG setup shown in Figure 5-2.

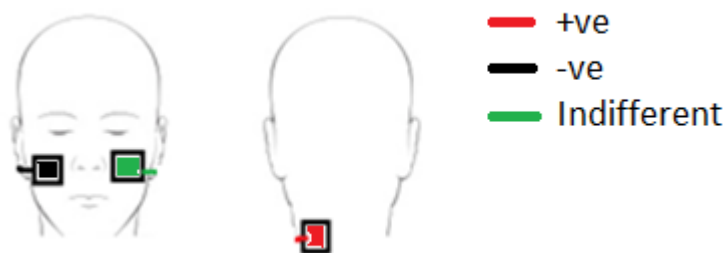


Figure 5-2-Electrode positions that were used to measure the ECG signal in the Cardiomask

The decision was made to measure the ECG signal with dry electrodes, as they do not require a conductive adhesive or conductive gel in between the electrode and the patient's skin and are therefore easier to apply and use.

As well as being easy to use, the same set of dry electrodes can be used for multiple nights, as opposed to most wet electrodes which need to be disposed of after every use, which has

both time and cost implications for the user and is unlikely to be readily accepted. The disadvantage of using a dry electrode is that once the electrode is applied to the patient's skin it takes approximately 5 minutes for the impedance between the skin and the electrode to decrease to a level that is steady and produces a good quality ECG signal [70]. However, compared with the length of a typical night's sleep which is usually several hours, 5 minutes is not a long time, so proportionally there is very little data that is lost or not useable waiting for the skin-electrode impedance to reach the steady state.

Two different materials were used to create electrodes to measure the ECG signal from electrodes located in the positions shown in Figure 5-2. The materials used were stainless steel (SS) and gold plated PCB substrate, which were chosen as they are good conductors and are biocompatible, meaning they are not likely to react with and cause irritation to the wearer's skin. Prototypes of both types of electrodes were made to test which electrode material would provide a superior ECG signal. Both electrodes were designed to be circular and to have an electrode surface with a diameter of 20 mm.

The SS electrodes were made out of a grade 316 SS. The thickness of the electrodes was 0.6mm. Since it is difficult to solder to SS using normal methods, a conductive adhesive was used to attach clips for the ECG leads to the electrode surface. The conductive adhesive used was H20E (EPO-TEK, USA), a silver epoxy mixture. The epoxy was baked at 100°C for 2 hours after mixing to cause it to set. An example of SS electrodes used is shown in Figure 5-3.

The gold plated electrodes were created using an Electroless Nickel Immersion Gold (ENIG) method. This method involves depositing nickel onto a copper plating using a chemical depositing process. This is then covered in a thin gold layer that is deposited onto the nickel layer using an electrochemical process known as immersion. ENIG ensured that the electrode surface had a good conductance, and would degrade little over time compared

with other possible surface finishes. However creating this type of surface finish is an expensive and complicated process compared with other types of surface finishes [184]. The gold plated electrodes (AU electrodes) were attached to a 1.6mm thick prototype PCB. The electrodes had one plate on either side of the PCB; one plate was in contact with the skin of the wearer and the other was used to connect to the ECG leads. Figure 5-4 shows an example of the completed gold plated (AU) electrodes.

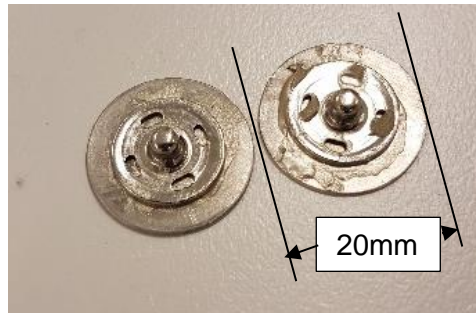


Figure 5-3 - The Stainless Steel electrodes used to measure the ECG signals from the face and neck

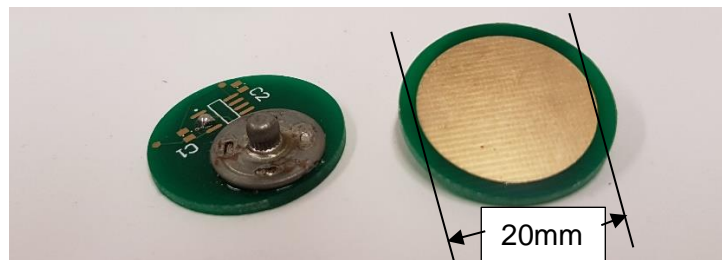


Figure 5-4 - An example of the gold plated electrodes which have an Electroless Nickel Immersion Gold surface finish

5.4.2 Testing

ECG signals using the two different electrode materials were measured from seven different participants and were compared with a reference ECG signal measured from wet electrodes on the same participant. The test electrodes were located in the positions on the face and neck shown in Figure 5-2. Electrodes were attached to existing straps of the PAP mask, however an extra strap was added to ensure the electrode was in contact with the skin on the wearer's neck and that hair from the wearer's head wouldn't be in between the electrode and the skin. This is shown in Figure 5-5.

The reference ECG signal was measured using Red Dot™ Ag/AgCl electrodes (3M, USA), with electrodes in a lead I position, placed on the participant's hands, and a driven right leg electrode on their right leg.

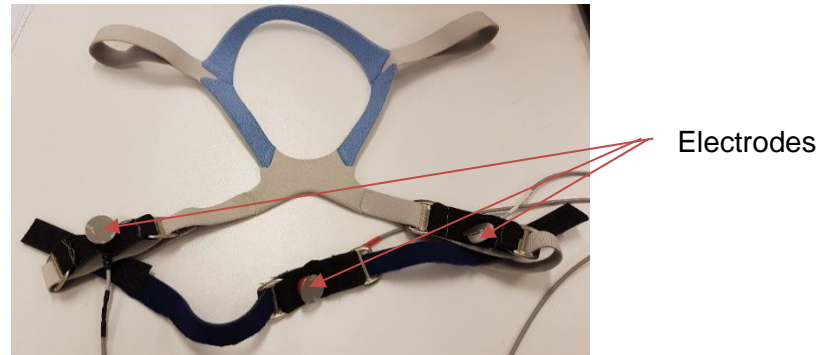


Figure 5-5 - An example of the electrodes embedded into the PAP mask straps

Signals were sampled at 500Hz and amplified at 6 V/V for the reference electrodes and 30 V/V for SS and AU electrodes. 50Hz power line interference noise was filtered out using a digital notch filter in the post processing stage. Heartbeats from the ECG signals were detected using the Pan-Tompkins algorithm [185].

The reference ECG signal and the face ECG signal measured from one of the custom made electrode sets were recorded simultaneously for a period of two minutes. After the two minute period, the procedure was repeated using the other set of custom electrodes. The process of choosing whether the ECG signal was recorded first using the SS or the AU electrodes was randomised, since the participant's skin may have accumulated some sweat after the first recording, which would change the impedance between the electrode and the skin. Additionally, after the electrodes were placed in the positions shown in Figure 5-2, the electrodes were left for a period of 5 minutes before recording commenced to allow enough time for the impedance to decrease and reach a steady state as demonstrated in [70].

The ECG signals were compared by looking at the number of heartbeats successfully detected, and the voltage range of the QRS complexes. The reference ECG signal was used

to identify the location of the QRS complexes which were not identifiable in the face ECG signal.

5.4.3 Results

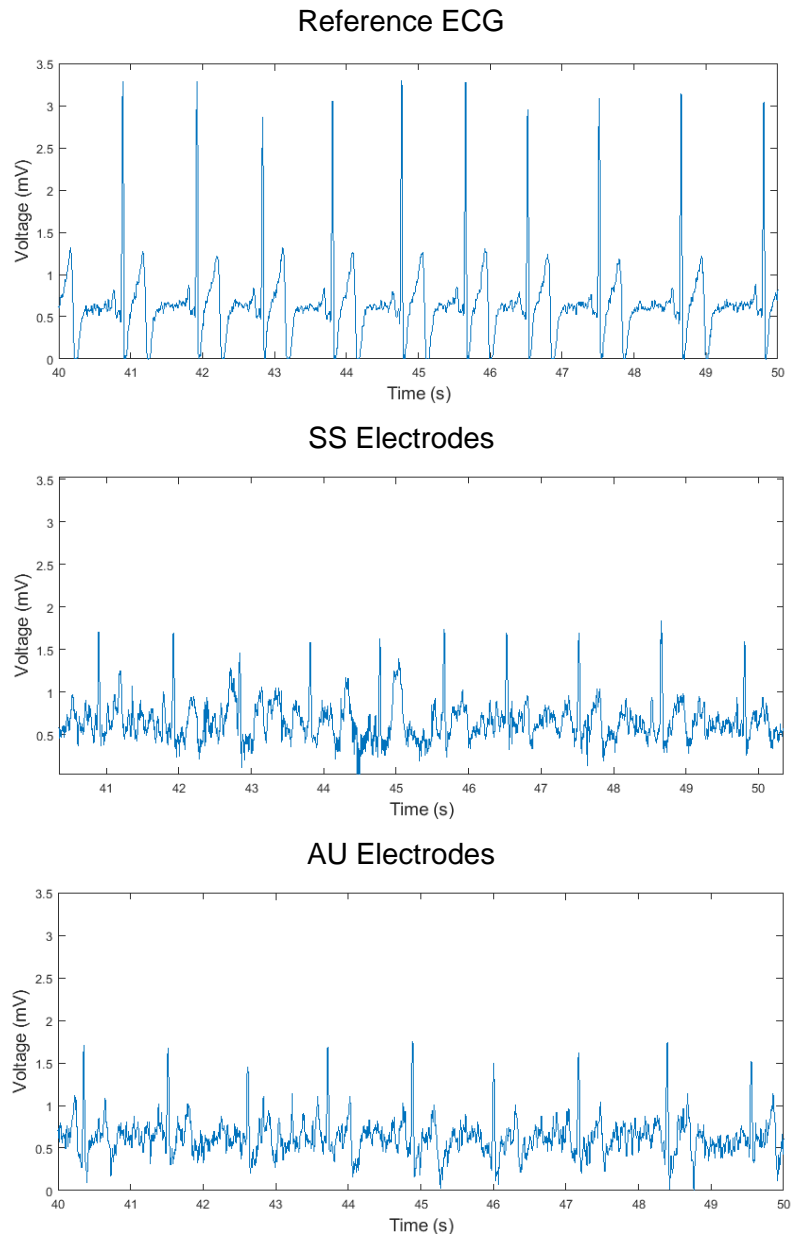


Figure 5-6 - An example of ECG signals measured from the SS electrodes (middle) and the AU electrodes (bottom) measured from the face and neck, compared with a reference ECG signal (top)

Examples of the signals recorded from the SS and AU electrodes are shown in Figure 5-6. Visual inspection of these signals show that the face ECG signal measured from both the SS and AU electrodes contained more noise than the reference ECG signal. These results were consistent for all participants, although the quality of the measured signals varied between

participants. R-peaks were still easily identifiable in most recordings, however much of the remaining detail of the ECG waveform was lost in the noise. This is because, since the magnitude of the signal is much smaller than the reference ECG signal, the gain of the amplifier needs to be higher, which leads to more of the noise being amplified.

The average QRS range (defined as the difference between the maximum and minimum voltage for each QRS complex) of the measured ECG signals for the two different electrode types for each participant is shown in Figure 5-7. This figure shows that interpatient variability has a larger effect on the QRS range than the material that the electrode is made of. This figure also shows that for different participants there was no consistent and clear result in terms of which electrode material performed better in terms of QRS signal amplitude.

The QRS range of the reference ECG signals for each participants are also shown in Figure 5-7. This figure shows that the QRS range is significantly larger in the reference ECG signal than the face ECG signals measured with the SS and AU electrodes, which is also shown in the example ECG signals shown in Figure 5-6.

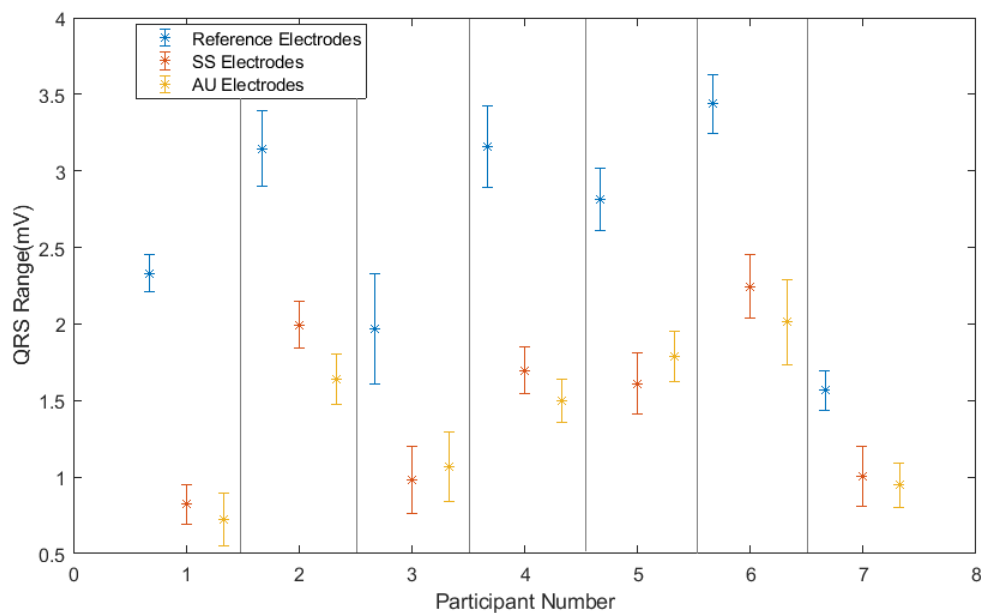


Figure 5-7 - A comparison of the range of the QRS complexes from the ECG signals measured from the face using the SS and AU electrodes, and from the reference electrodes located in traditional ECG locations

The difference in the percentage of missed (false negatives) and extra (false positives) heartbeats detected in the ECG signals measured from the SS and AU electrodes is shown in Figure 5-8. For two of the participants (#4 and #5) there is a large difference in the percentage of missed heartbeats detected in the ECG signal. Of these, the AU electrodes performed worse with up to 30% of missed beats. In terms of extra heartbeats detected (false positives), the electrodes produced similar results, with one participant (#3) experiencing approximately 30% of false positives in the ECG signal measured from both AU and SS electrodes.

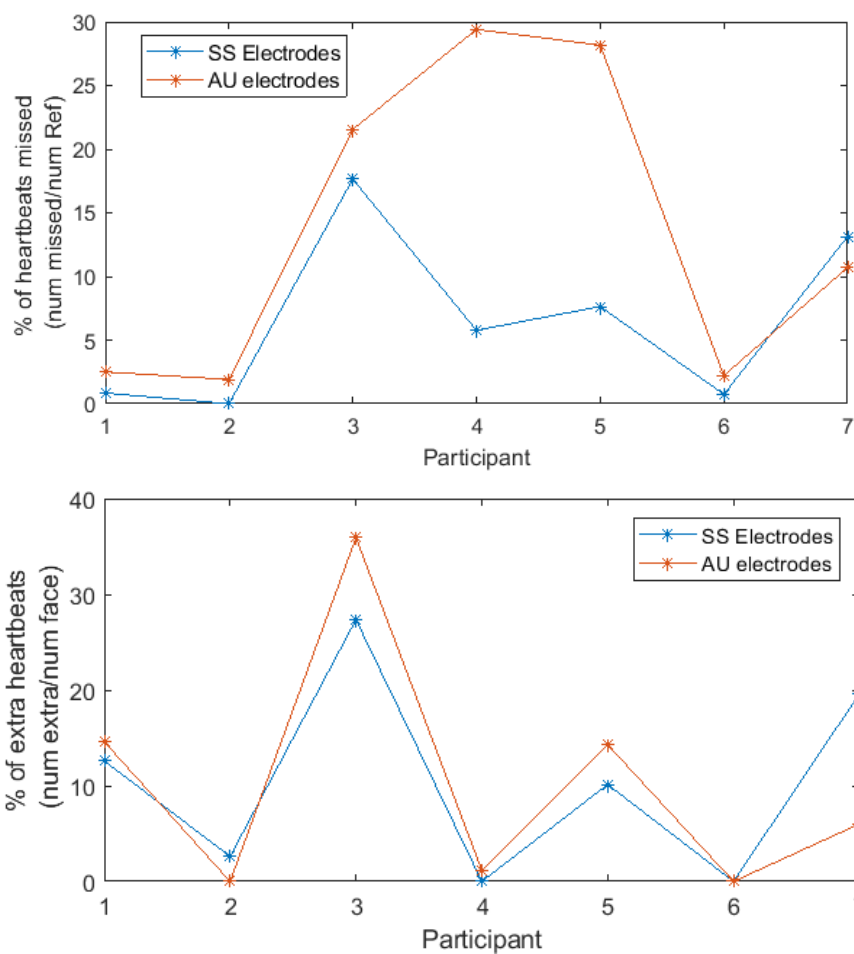


Figure 5-8 - A comparison of the percentage of missed (top) and extra (bottom) heartbeats detected from the ECG signal measured in the SS and AU electrodes AU

In general, these results, as well as the results in Figure 5-7, suggest that the accuracy of the heartbeat detection in the ECG signals measured from the SS electrodes and the AU electrodes is similar. Hence the results in Figure 5-7 and Figure 5-8 suggest that the variability in the ECG signal measured with SS or AU electrodes is less than the interpatient

variability, and there is not a large difference in the ECG quality measured from either electrode. The results also suggest that when attempting to find the heartbeats in the ECG signal measured from the face, there are likely to be missed or extra heartbeats due to the increased noise in the measured ECG signal.

Since the signal quality between electrodes is similar, the decision was made to use SS electrodes in the final design, based on cost. For the AU electrodes, the electrode surface is prepared using ENIG, which is a more costly and technical process than for the SS electrodes which require little preparation of the surface prior to use. There are other surface finish methods that are cheaper than ENIG, however it is not known whether these surface finishes would produce an ECG signal with a similar signal quality to ENIG. SS is also a cheaper than gold, as well as some of the other minerals involved in the ENIG process. Hence using the SS electrodes would result in a cheaper and easier product to manufacture compared with AU electrodes, with no significant difference in the ECG signal quality.

5.5 PPG

5.5.1 Setup

A pulse oximeter was chosen to be included in the Cardiomask because of the additional variables that may be contained within the PPG signal. In addition to measuring HR, the primary purpose of a pulse oximeter is to measure the SpO₂ level of the patient. By measuring the SpO₂ level, apnoea events can be detected, which can determine how effectively the PAP therapy is working. Furthermore, as mentioned in section 5.4, when combined with the ECG signal, the PPG signal can also be used to measure the PTT. Other potential uses of the pulse oximeter signal include respiration analysis and blood pressure estimation [186]. Another advantage of the PPG signal is that it is also relatively cheap, especially with the rise and success of commercial devices that can measure a PPG signal [187]. Finally, a pulse oximeter sensor is typically small, which means its addition would not add too much additional weight and size to the mask or discomfort to the wearer.

A reflectance pulse oximeter was attached to the PAP mask as shown in Figure 5-9 such that the sensor was positioned in the centre of the wearer's forehead. Using a 3D printed component the sensor was fixed to the Cardiomask. This design was based on a similar concept by Curative Medical Devices [188] and requires no extra set-up by the wearer.

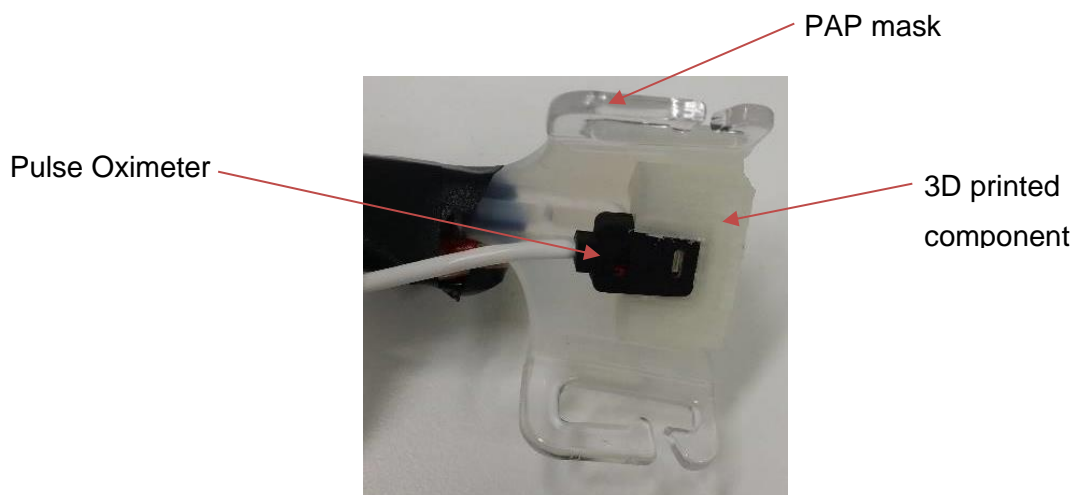


Figure 5-9-The pulse oximeter attached to the PAP mask, such that the sensor was located on the wearer's forehead

The PPG sensor chosen for the Cardiomask was the Nonin 8000R Reflectance Pulse Oximeter Sensor (Nonin, USA) because of its reported accuracy in HR and SPO2 measurements [189]. The sensor was connected to a Nonin Xpod® Model 3012LP which filters the PPG signal and calculates SPO2 and HR. The sampling rate of the Xpod is 75Hz, however the sampling rate of the sensor is unknown. Given the described accuracy of the various Nonin sensors that are compatible with the Xpod, it is assumed that the sampling rate of the sensor is much higher than 75Hz.

5.5.2 PPG heartbeat detection

The traditional fiducial point for heart rate (HR) detection from the PPG signal is the local maximum point as shown in Figure 5-10. However there have also been examples of using other fiducial points on the PPG signal with varying degrees of success [115, 190-192], including the foot of the pulse wave (or the minimum point), and the maximum of the 1st derivative (or steepest rise) of the PPG signal, both of which are also shown in Figure 5-10.

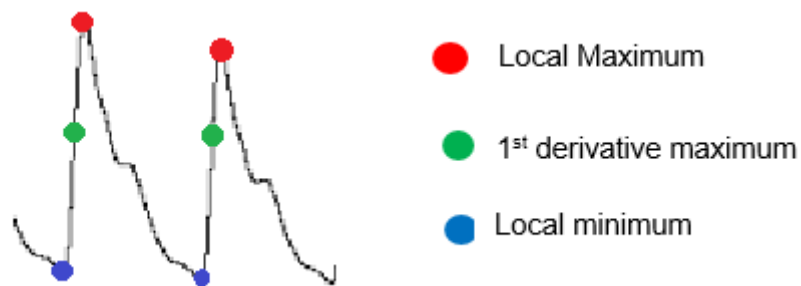


Figure 5-10-A PPG signal showing the fiducial points that were used to find each heartbeat

The three different fiducial points were compared to determine which point is best suited to detecting HR from the PPG signal measured from the forehead. As well as finding the best fiducial point to use, having three different measures of HR allowed data fusion to be performed to investigate the creation of a HR signal with improved accuracy. This will be detailed in chapter 9.

5.5.3 Results

An example of the PPG signal that was measured from the forehead is shown in Figure 5-11, with a pulsatile signal corresponding to heartbeat clearly visible. This figure also shows that for each pulse the maximum, minimum and 1st derivative points were found.

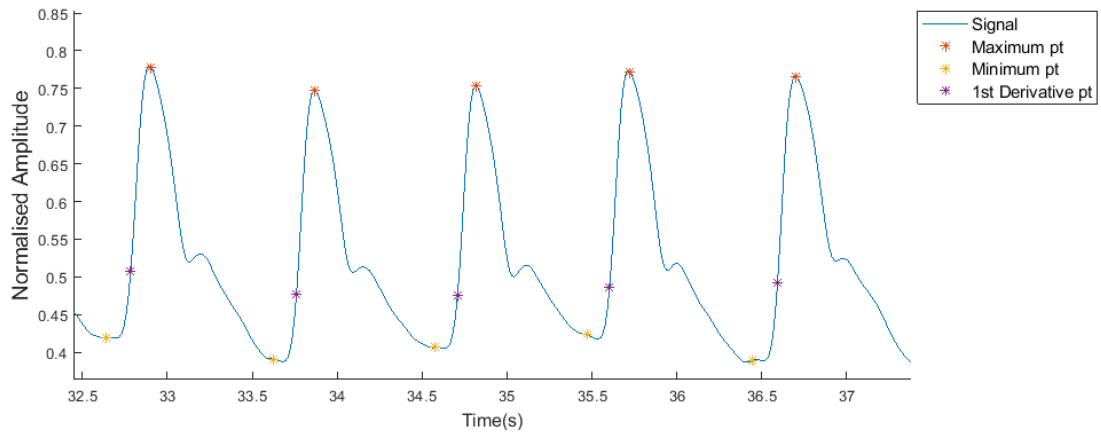


Figure 5-11 - An example of the PPG signal measured from the reflectance pulse oximeter positioned on the forehead, as well as the detected heartbeats from the different fiducial points

5.6 BCG

The final signal to be measured from the Cardiomask was a BCG, in the form of an Inertial Measurement Unit (IMU) attached to the mask. Similarly to the ECG and PPG sensors, the IMU is mounted in such a way that requires no extra set-up from the user. Unlike the ECG and PPG sensor, the BCG sensor is attached to the mask frame and is not in contact with the wearer, which means it does not add any additional discomfort to the wearer.

One of the problems with measuring HR from BCG is that the cardiac portion of the signal is orders of magnitude smaller than other movement signals when large whole body movement occurs. During these movement episodes, HR detection is not possible. One common method of reducing the error caused by whole body movements is to discard all signals during movement, and resume HR detection when movement has ceased [98]. Hence by detecting when movement episodes occur, the accuracy of the HR estimation immediately after movement has ceased can be increased.

Movement data may also be useful in estimating sleep stages for diagnosis of sleeping disorders such as insomnia, such as is now possible using wrist-worn devices and actigraphy [193]. It is hypothesized that a similar principle might be applied to Cardiomask BCG data to estimate sleep staging during PAP therapy.

Over long periods of time, IMU signals can 'drift' in which the propagation of small errors can cause a shift in the baseline signal values of the IMU. This will not have a significant effect on high-frequency or short-term signal analysis, but can could affect any threshold that are used for signal analysis and would have to be considered if the IMU is used to estimate the body orientation during sleep. Methods have been developed for correcting bias, including having short initialisation periods or the use of a Kalman Filter [194].

In addition to containing information about HR and movement, the BCG signal also allows estimation of other cardiac parameters. Stroke volume may be estimated from the amplitude of the BCG signal [94]. Additionally, by looking at the PTT between the ECG and the BCG signal, the pre-ejection period of the patient can be estimated [94]. However further testing will be needed to determine whether these variables can be replicated using the Cardiomask.

5.6.1 Setup

To measure a BCG signal in the Cardiomask, an IMU was attached to the mask as shown in Figure 5-12. The IMU used was an MPU-9150 (Invasense, USA), which includes a 3-axis accelerometer, a 3-axis gyroscope and a 3-axis magnetometer. Although the gyroscope and magnetometer can be measured from the sensor, only the gyroscope signals were analysed as the literature (described in chapter 4) showed that gyroscope signals are the most accurate for HR measurement. The sampling frequency of the sensor was 50Hz.



Figure 5-12 - The prototype PAP mask with the IMU attached and the gyroscope axes labelled

5.6.2 Results

Figure 5-13 shows the raw gyroscope signal measured from a participant who was lying on their back. This figure shows that there is evidence of a cardiac component in the gyroscope signals, particularly in the Y component and the normalised gyroscope signal. However, this figure also shows a large amount of high frequency noise that is present in all gyroscope signal components, which will need to be filtered out before further analysis can begin.

Figure 5-14 shows a comparison of the signals measured by the gyroscope in the Cardiomask (left) to the BCG signals published by Tadi et al. (right) from the chest [138]. Similarly to Tadi et al, the gyroscope signals in Figure 5-14 were filtered using two 4th order bandpass filters with frequency ranges of 1-20Hz and 4-45Hz respectively to eliminate the high frequency noise shown in Figure 5-13. The main peaks shown in the signals measured by Tadi et al appear to be present in the BCG signals measured from the head. These peaks correspond to key events of the cardiac cycle such as the aortic valve opening [132]. However, the smaller features in the measured BCG signal are not as easily identifiable. Additionally, the magnitudes of the gyroscope signals measured from the head are smaller than the magnitudes of the signals measured by Tadi et al. This suggests that the propagation of the vibrations that cause the BCG movements are attenuated in the head, leading to a lower SNR for the BCG signals, and loss of the smaller features in the signal. There may also be some dampening of the signal from the cushion of the PAP mask. Differences in the signals could also be due to the differences in sampling rates. The sampling rate of the gyroscope used in this paper was 50Hz, subsequently resampled to 500Hz. The gyroscope signals measured by Tadi et al. [138] had a sampling frequency of 800Hz. This difference in sampling frequency may also explain the loss of definition of the smaller features of the BCG wave.

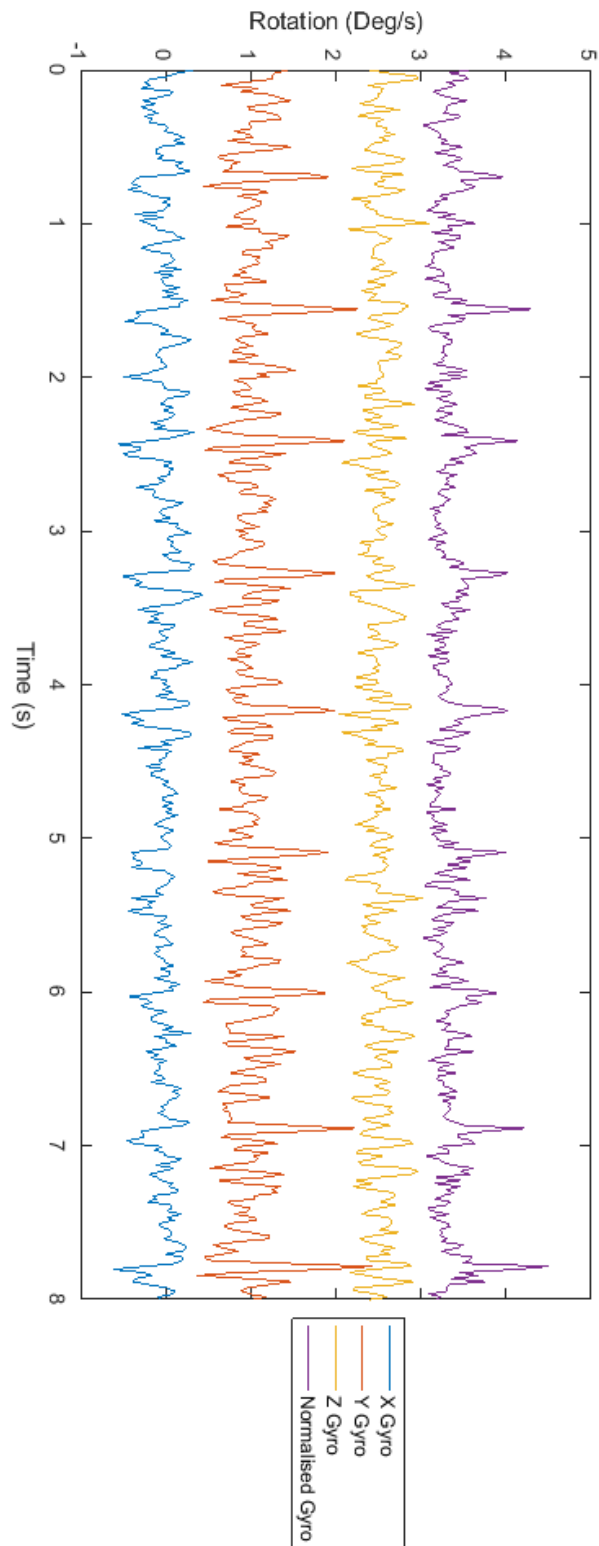


Figure 5-13 - Raw signal from the gyroscope measured from the location shown in Figure 5-12 from a participant lying on a bed. Constant values have been added to the gyroscope signals only to make it easier to differentiate the signals in this figure.

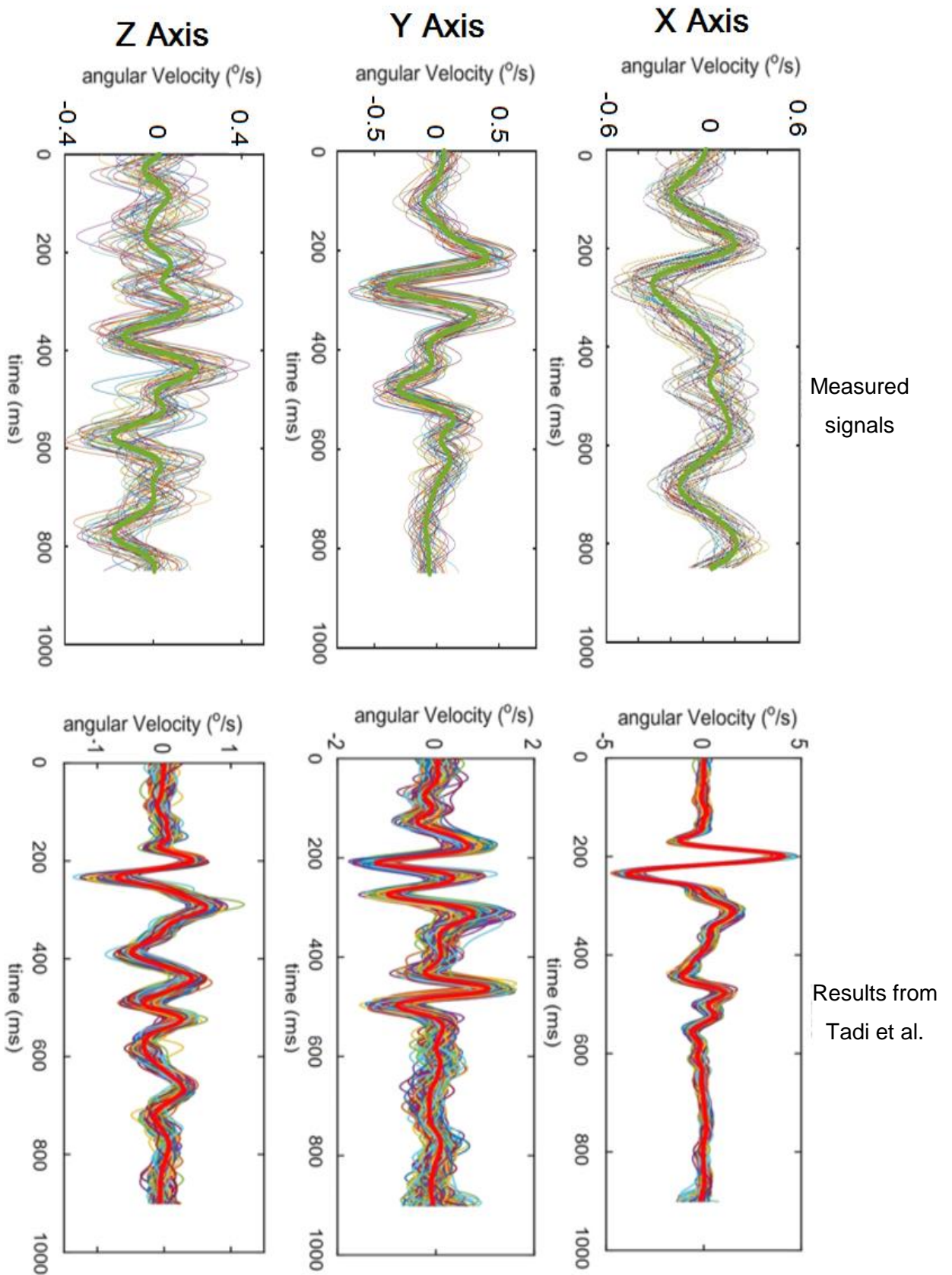


Figure 5-14 - BCG signals measured when the participant was lying on their back (left column), as well as the averaged waveform (shown as the bold green line), compared with signals measured from the chest as described in [138] (right column). Axes have been paired with the equivalent axis from the other setup.

5.7 Discussion

A device, named the Cardiomask, was developed that was able to record an ECG, PPG and BCG signal from sensors integrated into a PAP mask. The sensors were all designed to be comfortable for the wearer, easy to use, relatively low cost, and have potential to measure or estimate other parameters in addition to HR.

All of the individual sensors have shown they are able to identify heartbeats, and it is feasible therefore that the Cardiomask could be developed to only contain a single sensor (ECG, PPG or BCG). However, the decision was made to include all three signals for several reasons. Firstly, there are some physiological variables that can be measured from combining the different signals, such as the PTT (using information from the ECG and PPG signal). Additionally, by combining multiple signals there is the possibility of developing data fusion methods which combine the HR information from different signals to increase the accuracy of the HR measurements. Finally, only larger scale testing will be able to reveal which sensors are not needed and which sensors are the most important, not only for HR monitoring but also for the estimation and measurement of other variables relating to the Cardiomask wearer's health.

The heartbeats in the face ECG signal were detected using the same algorithm as the reference ECG signal, which was the Pan-Tompkins algorithm. This was so that the quality of the ECG signals could be compared. It is possible that another QRS detection algorithm would be able to detect heartbeats in the face ECG signal more accurately than the Pan-Tompkins algorithm. Future work could determine alternate methods for detecting heartbeats in the face ECG signal.

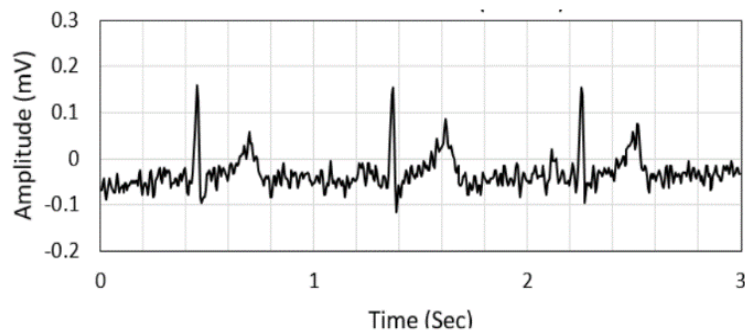
The testing of the PPG and BCG signals in this chapter has only been carried out on one healthy male participant. However, the quality of the signals recorded from this one participant are not necessarily representative of the general population, or the OSA

population. Further testing (described in chapter 7) aimed to include a larger population size, with a variation in age, gender and health.

The testing in the current chapter also did not account for conditions common to PAP therapy and sleep in general, such as lying in different sleeping positions and different PAP therapy modes. In testing the ECG and PPG signals, the participant was sitting upright, and only when measuring the BCG signal was the participant lying down. In all signal recordings, the participant tried to remain as still as possible which is not representative of normal sleeping conditions. Lying in different sleeping positions, moving during sleep and different PAP modes could all affect the signal quality by introducing unwanted artefacts. This will all be tested later in the thesis (described in chapter 7).

There have been several other examples of an ECG setup where all the electrodes were located on the patient's head or neck. Some of these examples were described in the

Signal measured by Iskandar et al



Signal measured by Cardiomask

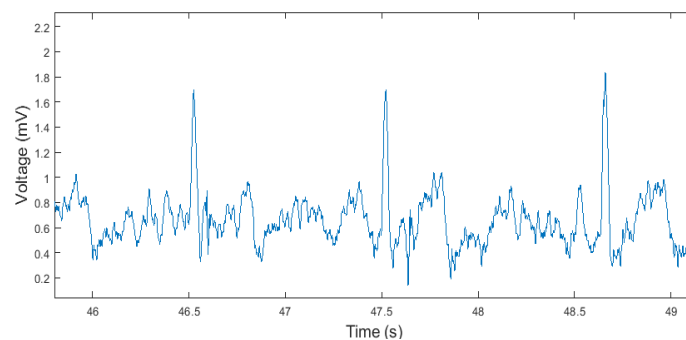


Figure 5-15-A comparison of the ECG signal measured from the device by Iskandar et al (top), with an ECG signal measured using the setup described in this paper. [1]

previous chapter [1, 94, 95]. The closest example to the Cardiomask setup was developed by Iskandar et al. in which three dry electrodes were positioned at the back of the wearer's neck [1]. A comparison of Iskandar's published signal [1] to an ECG signal measured from Cardiomask is shown in Figure 5-15.

In Figure 5-15, the R peak can be easily identified in both signals, and both signals appear to be of a similar quality. In their publication, Iskandar et al. describe how the measured ECG signal has a reduced SNR and signal quality in general when compared a reference ECG signal [1], which is also true for the ECG signal measured by the Cardiomask. In both signals there appears to be some evidence of a T wave and a P wave for each heartbeat, however they are not as clear and easy distinguishable as has been seen in the reference ECG signal.

One difference between the Cardiomask and the device described by Iskandar et al. is the electrode material. Iskander used dry Ag/AgCl electrodes to record the ECG signal shown in Figure 5-15, whereas the Cardiomask used SS electrodes to record the ECG signal of the participants. This suggests that by using the straps of the PAP mask to hold the SS electrodes against the participant's skin and by waiting for the skin-electrode impedance to decrease before measurement, an ECG signal can be measured from the SS electrodes with a similar quality to an ECG signal measured from Ag/AgCl electrodes in similar locations.

As discussed earlier, He et al. also developed a device that measured a BCG signal from the wearer's head [94]. By visually comparing examples of the quality of their signal (as shown in Figure 5-16), to the BCG signals measured with the Cardiomask as shown in Figure 5-14, the signal quality appears similar. Tadi et al. demonstrated that the BCG signal quality is repeatable between different models of sensors [138]. This means that it is possible that the same features can be extracted from the BCG signal from the Cardiomask, as those that were extracted by He et al. – that is, the pre-ejection Period (PEP) and Stroke Volume,

however further research is needed to confirm this. The aortic opening time, which is the finishing cardiac event in the PEP, has also been extracted from the BCG signal [132, 138, 139], and hence might be accessible through the Cardiomask, however this will not be tested in this thesis.

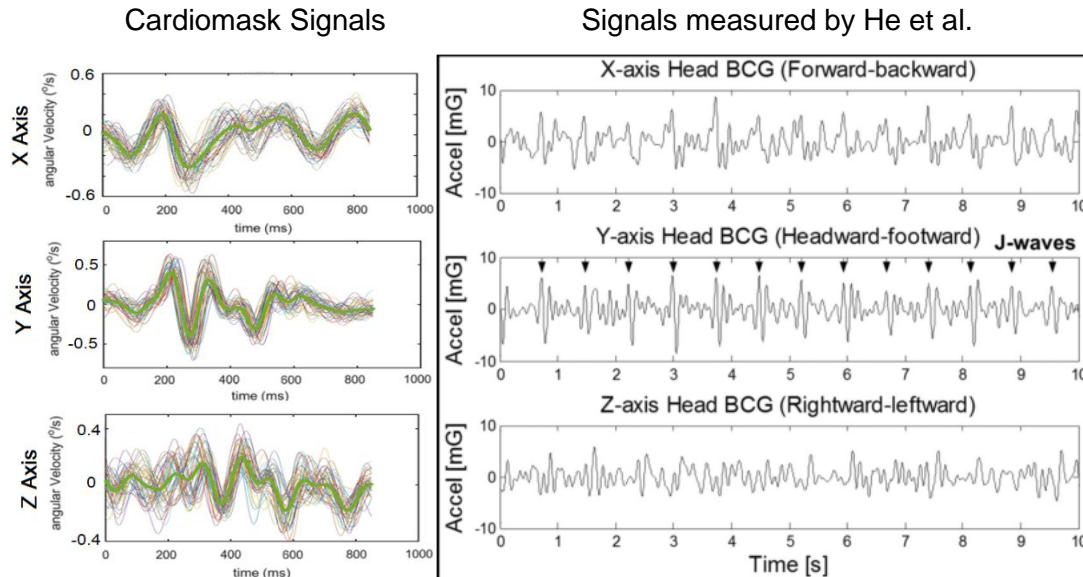
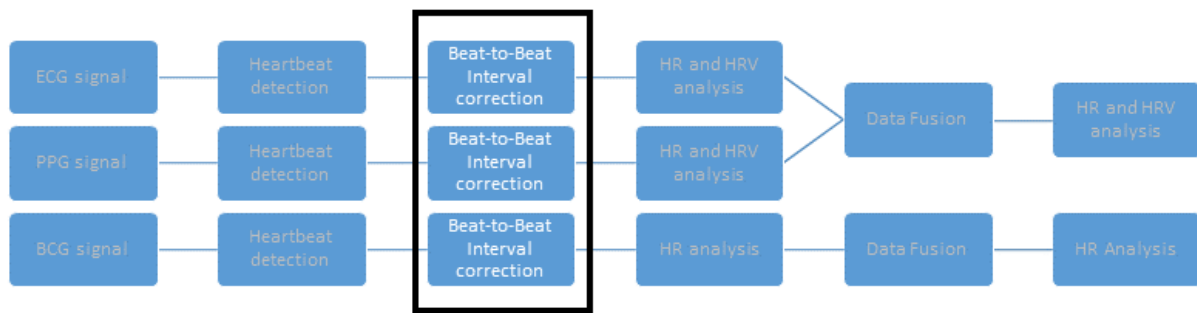


Figure 5-16 – Averaged BCG signals measured when the participant was lying on their back (left column) compared with examples BCG signal measured from an Accelerometer placed behind the wearer's ear from [94] (right column)

5.8 Conclusion

A PAP device has been modified to be able to measure an ECG, PPG and BCG signal, with sensors located on the patient's head and neck. The device, named the Cardiomask, was modified in a way to minimise additional discomfort and set-up burden for the wearer. The Cardiomask was tested on one participant which showed that a heartbeat could be detected in all of the recorded signals. However not all signals were able to detect every heartbeat due to a reduced SNR caused by the non-traditional locations of the sensors. Hence a method for improving the accuracy of the heartbeat detection and HR accuracy is needed. Further testing to confirm the effectiveness of the device on the general population, as well as the effectiveness in more realistic sleeping conditions, will be described in the following chapters.



6. Development of novel beat-to-beat interval correction methods

In Chapter 5, a Positive Airway Pressure (PAP) mask, named the Cardiomask, was modified to be able to record several signals (ECG, PPG and BCG), from which the wearer's Heart Rate (HR) can be measured. However, preliminary testing showed that the Signal-to-Noise Ratio (SNR) of the recorded signals was less than optimal. In the ECG signal measured from the face, this caused falsely detected and missed heartbeats which would introduce errors into the recorded instantaneous HR signal. Hence a strategy for correcting false HR values was needed to ensure accurate HR and Heart Rate Variability (HRV) measurement, not only for the ECG signal but for all signals. In this chapter, HR signals are purposely corrupted. Then, the ability of several different algorithms to correct the corrupted HR signals is compared, and the best algorithm is selected to be used on the signals recorded from the Cardiomask.

6.1 Introduction

As described in chapter 3, analysing HR and HRV can reveal information about a patient's cardiac health [8]. When a HR signal is generated, it is most commonly produced using the time interval between successive heartbeats. For the ECG signal this is known as the R-R Interval (RRI), however for any signal that can measure HR this interval is more generally called the beat-to-beat interval (BBI), and this more general term will be used here forward for intervals measured from all source signals. HR and HRV analysis are sensitive to artefacts in the BBI signal [35, 36, 195]. These artefacts can originate from motion artefacts,

improper sensor placement or poor signal quality, and can cause heartbeats to be missed (false negative) or extra heartbeats to be detected (false positive). Typically in a clinical setting, any artefacts that occur in the recorded BBI signal are manually corrected by a trained physician/technician, as the number of artefacts that may occur will be relatively small compared with the number of total heartbeats in the recording period.

However, HR and HRV analysis is becoming more common in non-controlled environments, where there is a higher risk of artefacts corrupting the BBI signal. Examples of this include wearable devices, implantable cardiac monitoring and sleep monitoring in patients' homes. Signal corruption is particularly a problem for wearable devices, which tend to produce signals that are noisier than clinical signals, leading to errors in the BBI signal and a higher rate of incorrectly detected and missed heartbeats. Wearable devices have the potential to play a larger and more clinically relevant role in assessing a patient's health [196], however algorithms are needed to extract accurate BBI, HR and HRV data from noisy signals.

Additionally, automated BBI correction methods are needed in order to analyse the large amounts of data that can be collected for long term HR monitoring. For example, for sleep monitoring, in which a sleep session may take around 8 hours, it is not feasible to manually correct BBI signals from multiple sleep sessions for multiple patients. Hence when analysing BBI signals measured during sleep (especially if HRV analysis is also included), it is common to apply an automatic BBI correction technique [63, 197] to ensure that the BBI signal is free of artefacts and the HRV analysis is accurate.

Most current BBI correction algorithms prioritise generating a stable BBI signal free of large and sudden deviations, sometimes at the expense of preserving the number of heartbeats originally detected [62, 195, 198, 199]. However this can reduce the accuracy of HRV analysis performed on the corrected BBI signal [200]. The ideal BBI correction algorithm

should be able to correct artefacts within the BBI signal without affecting the accuracy of the HR and HRV information within the BBI signal.

In this chapter, BBI signals will be artificially corrupted to investigate the effect that missed or extra heartbeats have on the accuracy of the HR and HRV analysis. Furthermore, several BBI correction algorithms will be applied to the corrupted BBI signals to determine how well each algorithm is able to increase the accuracy of the HR and HRV analysis. These BBI correction algorithms include algorithms from the literature, algorithms developed by the author, and some combination approaches. From the results obtained, the ability of each BBI correction algorithm to discard artefacts, whilst preserving the HR and HRV data in the BBI signal, will be compared to determine which algorithm is the best for correcting corrupted BBI signals.

6.2 BBI correction methods used in literature

Most BBI correction algorithms in the literature were developed to correct artefacts caused by ectopic beats which cause errors in the BBI signal and HRV analysis in a similar way to missed or extra detected heartbeats [62, 195, 198, 201]. As discussed in Chapter 3, an ectopic beat is a type of arrhythmia such as a Premature Ventricular or Atrial Contraction, and is generally harmless [6]. An example of an ectopic beat (top) and the effect it has on the BBI signal (bottom) is shown in Figure 6-1. The deviation in the BBI signal caused by an ectopic beat is usually smaller than for a missed or extra heartbeat [195], and it is unknown how well these algorithms will be able to correct the larger BBI deviations caused by missing or extra heartbeats.

The most common method for correcting a BBI signal affected by ectopic beats and other artefacts involves deleting any instantaneous HR values where the difference between consecutive BBI values is greater or less than some threshold. This threshold is either a constant value [62] or an adaptive threshold based on either one [198] or several of the

previous BBI values [199]. The disadvantage of this technique is that deleting BBI values can change the HRV analysis derived from the BBI signal [35, 36, 200], especially if multiple BBI values are deleted.

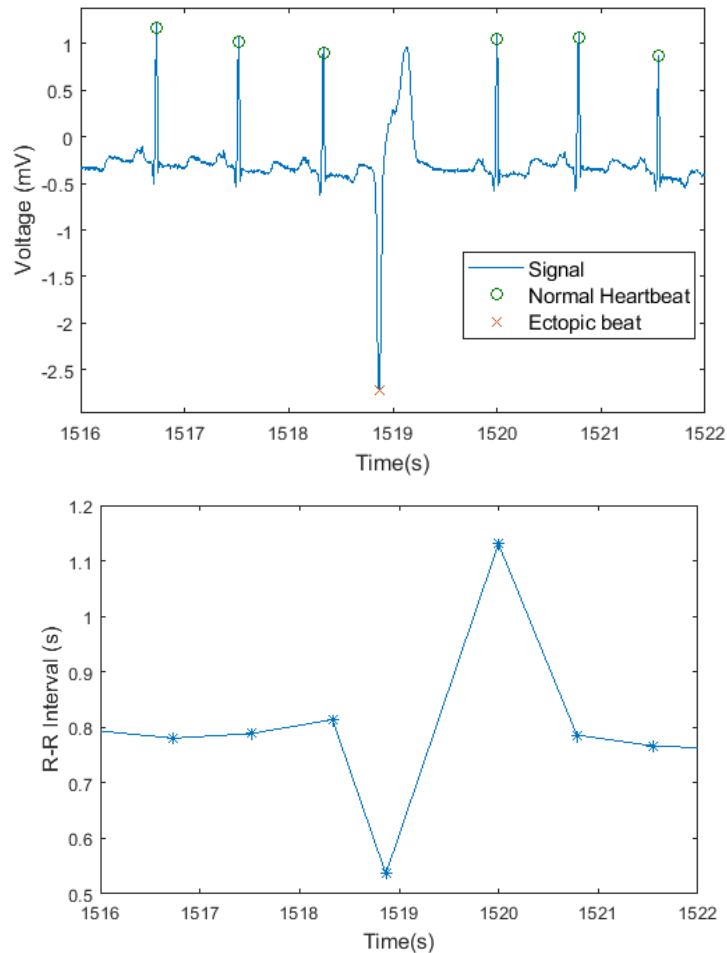


Figure 6-1 – An example of an ectopic beat in an ECG signal (top) and how that effects the BBI between heartbeats (bottom)

Another method for correcting ectopic beats involves replacing artefact affected BBI values with an estimation of the correct BBI value. Methods for estimating BBI values involve using linear interpolation [62, 63] or a cubic spline [195]. However, similarly to deleting BBI values, it has been shown that different estimation processes can also cause errors in HRV analysis [202].

The final method that will be considered was developed by Wessel et al. [201], and is based on adaptive correction. This method is designed to correct the BBI signal such that the

variability of the BBI signal is preserved, allowing for accurate HRV analysis after the artefacts have been removed. Wessel showed that correcting ectopic artefacts in BBI signals using his algorithm was more effective at reducing the HRV error than simply deleting the affected BBI values. However, it is unknown if this algorithm would be as successful on BBI artefacts caused by missed or extra detected heartbeats.

6.3 Testing method

6.3.1 Data

To test the BBI correction algorithms, real patient BBI signals were used and then corrupted. The data were taken from the normal sinus rhythm database (NSRDB) from the Physionet database [203], in which the timing of heartbeats from 18 different participants have been annotated by experts. The reference BBI signal was calculated by measuring the time difference between successive annotated heartbeats, prior to corruption.

The data used were from all 18 participants in the NSRDB. The heartbeats used were the first annotated heartbeats within a 5 minute window where there were no adjacent BBI values that differed by greater than 0.1 seconds. The reference BBI signal was calculated from the time difference between the annotated heartbeats. The sampling frequency of the recorded signals was 128Hz. A window length of 5 minutes was chosen as it is the recommended window length for HRV analysis [8]. Regular adjacent BBI values do not commonly vary by more than 0.1 seconds [7], so the check for no adjacent BBI values that differed by 0.1 seconds was to make sure that no ectopic beats were found which can add significant errors to HRV calculations [195]. This may also exclude some segments where no ectopic beats occur, but there is just naturally a large variation in the BBI values.

6.3.2 Signal Corruption

Previous studies have investigated the effect of artefacts in the BBI signal on the accuracy of HRV analysis [35, 36, 200]. These previous studies used a BBI correction method in which a BBI value that was thought to be inaccurate was simply deleted. However in this chapter,

algorithms are tested that not only attempt to delete false positive values, but also to estimate realistic BBI values if false negatives are detected through addition of extra beats.

To create a “corrupted” BBI signal, some of the NSRDB heartbeats were randomly selected to be deleted and new heartbeats were added at random time intervals. The heartbeats that were added were positioned at random time points that were more than 0.2 seconds from the nearest heartbeat. It is not physiologically possible to have two heartbeats less than 0.2 seconds apart, and this condition is integrated into most heartbeat detection algorithms [185, 201].

The corrupted BBI signal was calculated from this set of new heartbeats. An example of the original BBI values and the artificially corrupted BBI values is shown in Figure 6-2.

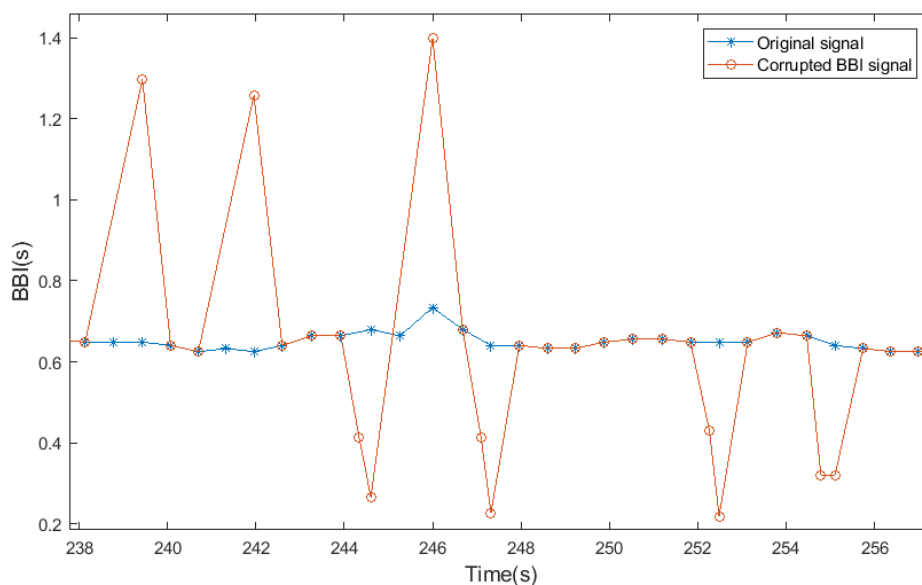


Figure 6-2 - A plot showing the original BBI values and the “corrupted” BBI when 10% of the input heartbeats are corrupted

The number of heartbeats that were added and deleted varied, starting with only 1 added/deleted heartbeat in the 5 minute window increasing to adding an additional 25% of the total number of reference heartbeats and deleting 25% of the original heartbeats. Other values that were used were 1%, 5%, 10%, and 17% of the total number of heartbeats in the

5 minute interval. Each case was repeated 5 times, with different sets of heartbeats added and deleted each time, due to the random nature of the corruption process.

6.3.3 BBI correction and error analysis

Three different BBI correction algorithms were applied to the corrupted BBI signals. For each set of corrupted BBI values, the percentage of correctly identified heartbeats, the HR error and the mean HRV error were calculated and compared with the original and corrupted BBI signals.

6.3.3.1 Percentage of correctly identified heartbeats

The percentage of correctly detected heartbeats in the corrected BBI signal was calculated by comparing the number of correctly detected heartbeats in the corrected BBI signal with the number of correctly detected heartbeats in the original (reference) signal. A heartbeat was classified as “correctly detected” if it was within 0.2s of a reference heartbeat, since it is not possible for two heartbeats to appear within 0.2s of each other [185]. The resulting percentage of correctly detected heartbeats was calculated for the corrected BBI values after each BBI correction algorithm was applied, as well as for the corrupted BBI values (i.e. the BBI values before correction)

6.3.3.2 HR error

For each set of corrected BBI values, the mean HR error (in beats per minute) from the BBI correction algorithms was also calculated. The mean HR error was calculated by resampling the reference BBI signal and the corrected BBI signal at 50Hz, calculating the difference between the reference and estimated HR values, converting the difference to beats per minute (BPM), and then taking the average of the difference. Since the BBI signal is not a regularly sampled signal, resampling the BBI signals to an evenly sampled signal allows for simple calculation of the absolute HR error.

6.3.3.3 HRV values

The HRV variables that were calculated from the reference, corrupted and corrected BBI were described in section 3.2 and are also shown in Table 6-1. To calculate frequency domain variables, the Lomb-Periodogram method was used [48], using an online toolbox

[203, 204] for Matlab (Mathworks, USA). The percentage error was calculated for all HRV variables except for pNN50, in which the absolute error was recorded, and was calculated as (using SDNN as an example):

$$SDNN \% error = \frac{|SDNN_{corrected} - SDNN_{ref}|}{SDNN_{ref}} \times 100 \quad (6.1)$$

Percentage error values were used instead of absolute values to remove any interpatient variability. To make this chapter more succinct the results for the average HRV error will be given instead of the results for all HRV variables. The results for each individual HRV variable are attached in Appendix B. The average HRV error is defined as the average percentage error across all HRV variables. This method was also used by Wessel et al. in comparing BBI correction algorithms [201]. The absolute Low Frequency (LF) and High Frequency (HF) components were excluded from the average HRV calculation as the errors for the absolute frequency components could be up to several orders of magnitude larger than other HRV variables, which would have a significant effect on the average HRV error calculation.

The level of acceptable mean HRV error was based on a review of healthy HRV values by Nunan et al. [205]. In this review, for the overall population the mean Coefficient of Variation (CV) (defined as $\frac{standard\ deviation}{mean} \times 100$) for the normalised LF and HF, SDNN and RMSSD values was approximately 30%. For the mean HRV results in this test, it was decided that an acceptable mean HRV error should be less than the normal amount of variation in the HRV term, defined by the CV value. Hence the mean HRV error was defined as acceptable if it was less than 30% of the reference value.

Table 6-1 - Description of HRV variables used. Source: [8]

Name	Time or Frequency Domain	Description	Units
SDNN	Time	Standard Deviation of R-R intervals	ms
RMSSD	Time	Root-Mean-Square (RMS) values of adjacent R-R intervals	ms
pNN50	Time	Number of adjacent R-R intervals that differ by more than 50ms, expressed as a percentage of the total number of R-R intervals	%
Low Frequency	Frequency	Power in LF range (0.04-0.15Hz)	ms^2
High Frequency	Frequency	Power in HF range (0.15-0.4Hz)	ms^2
LF normalised	Frequency	LF/(total power - VLF)*100, where VLF is 'Very low Frequency' which is < 0.04Hz	Normalised units
HF normalised	Frequency	HF/(total power - VLF)*100	Normalised units
Frequency ratio	Frequency	LF/HF	Normalised units

6.3.4 Statistics

Significance between different results was calculated using a paired t-test, with significance level set at $p=0.05$. Outliers (defined as larger than 1.5 x interquartile range from the upper or lower quartile) were excluded from the statistical analysis.

6.4 BBI correction algorithms tested

Three different BBI correction algorithms were tested initially. These algorithms are a combination of algorithms described in the literature and algorithms developed by the author.

6.4.1 Algorithm 1: Pattern Detection algorithm

This algorithm is designed to correct two basic patterns that can occur due to false heart beat classification, and was developed by the author for simple BBI correction.

The first pattern occurs when an extra heartbeat has been detected that is not a true heart beat (false positive), and the second is when a true heart beat has been missed (false negative). In the first scenario in which an extra beat has been detected (false positive), the following two criteria are satisfied:

$$BBI_i - 0.15s \leq t_{i+2} - t_i \leq BBI_i + 0.15s \quad (6.2)$$

$$|BBI_i - \overline{BBI}| \leq 0.2 \times \overline{BBI} \quad (6.3)$$

where, t_i is the time point where the i th heartbeat occurs, BBI_i is the BBI value associated with the i th heartbeat and \overline{BBI} is the average of the previous 8 BBI values. The first equation identifies an extra beat at $i+1$; a value of ± 0.15 s was determined experimentally to account for the natural variation in BBI values, as it is rare that a BBI value will remain constant between successive heartbeats [8]. The second equation prevents the algorithm from identifying a corrupted BBI value as a correct BBI value and correcting an already correct BBI value, by ensuring that corrections do not differ significantly from previous BBI values. An example of this type of correction is shown in Figure 6-3. In this example, the time difference between heart beats A and B (BBI_B) is approximately equal to the time difference between heart beats B and D ($t_D - t_B$), which would indicate that an extra heartbeat (beat C) has been detected, which can then be removed.

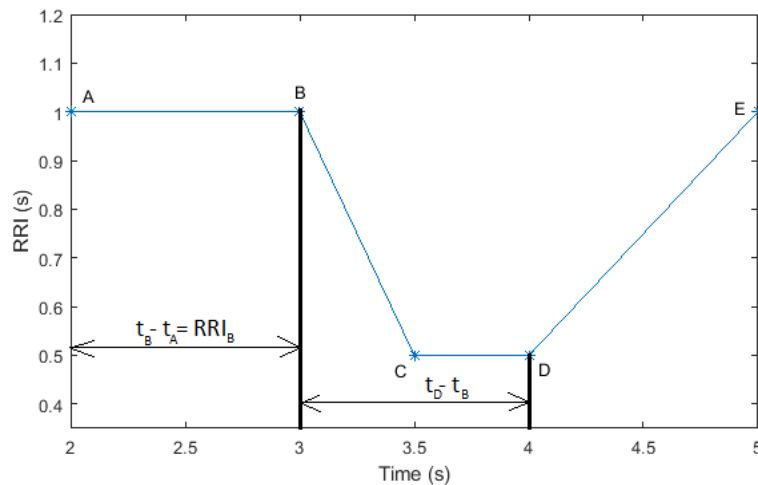


Figure 6-3 - Example of a change in RRI value when an extra beat has been detected.

The second pattern is designed to detect when a heartbeat has been missed (false negative) and to replace it. There are two conditions that need to be met to identify a missing beat:

$$2 \times BBI_{i-1} - 0.15 \leq BBI_i \leq 2 \times BBI_{i-1} + 0.15 \quad (6.4)$$

$$2 \times BBI_{i+1} - 0.15 \leq BBI_i \leq 2 \times BBI_{i+1} + 0.15 \quad (6.5)$$

An example of this scenario is shown in Figure 6-4. In this example the detected BBI value for heartbeat D is approximately twice the value of the adjacent BBI values (BBI_B and BBI_E), which indicates there is a heartbeat missing between heartbeats D and B (which is heartbeat C).

When a heartbeat has been missed as in Figure 6-4, the algorithm adds an extra heartbeat at a time point where it is estimated the missed heartbeat occurs. This estimation is based on linear interpolation and places the heartbeat halfway between the two adjacent heartbeats. Using the example in Figure 6-4 a heartbeat would be added halfway between heartbeats D and B, at $t=4s$.

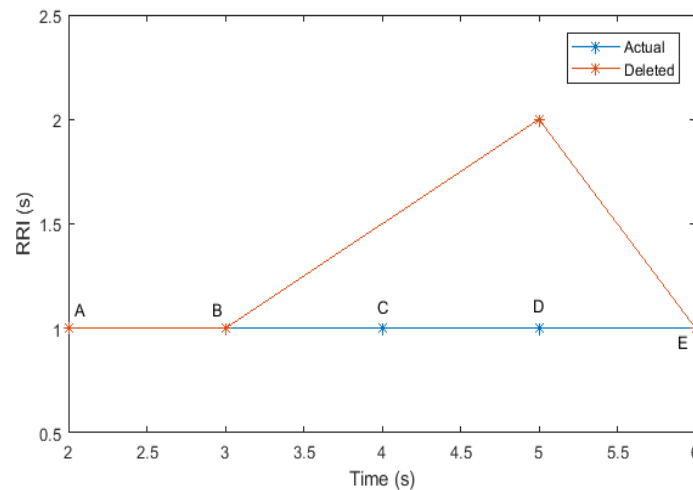


Figure 6-4 - Example of a change in RRI value when a heartbeat (C) has been missed

6.4.2 Algorithm 2: Wessel algorithm

The second algorithm that was implemented was described by Wessel et al. [201]. This algorithm is designed to identify abnormal BBIs where values are classified as abnormal if:

$$|BBI_i - BBI_{i-1}| > \frac{p}{100} RRI_{i-1} + c_f \cdot \sigma_a \quad (6.6)$$

$$|BBI_i - BBI_{iv}| > \frac{p}{100} RRI_{iv} + c_f \cdot \sigma_a \quad (6.7)$$

where p and c_f are constants, BBI_i is the i th BBI value, BBI_{lv} is the last valid BBI value, and σ_a is a variability value derived from the filtering of the BBI signal, as described in [201]. If the BBI value is abnormal, it is replaced with a random number within a specified range of numbers such that the variability of the BBI signal will be preserved. A final check is then conducted, whereby a BBI value is classified as abnormal if

$$|BBI_i - \mu_a(i)| > c_{f1} \cdot \sigma_a(i) + \sigma_b \quad (6.8)$$

where RRI_i is the i th resulting BBI value from the previous checks, μ_a and σ_a are derived from filtering the BBI signal, and σ_b and c_{f1} are constants. Abnormal BBI values are then replaced with values from a binomial filtered series. For this study, the value of c_f and c_{f1} (suggested as between 0 and 1) was set to 0.05 as per [206] and p was set to 10 as suggested in [201].

6.4.3 Algorithm 3: Threshold algorithm

In algorithm 3, BBI values that are significantly different to their respective adjacent BBI values are deleted. Variations of this technique are commonly used [62, 198, 199] as it is able to remove trivial errors in the BBI signal. The criteria that were used to determine if the i th BBI value should be deleted is:

$$|BBI_i - RRI_{last}| > b \times BBI_{last} \quad (6.9)$$

where BBI_{last} is the last BBI value that satisfies equation 6.9, and b is a pre-defined constant. The value of b was set to 0.15 for this experiment.

6.5 Results from Algorithms 1-3

Results from the study to investigate how well the three BBI correction algorithms can preserve the number of correct heartbeats and reduce the HR and HRV error are given in this section. For each parameter, the results are shown over two figures (low level of corruption $\leq 1\%$ and higher corruption $\geq 5\%$) to allow for a change in y-axis scaling (and

easier visualisation at low levels of corruption). A table summarising the overall results can be found at the end of each subsection.

6.5.1 Correctly detected heartbeats

The percentage of original (reference) heartbeats correctly identified for the corrupted signal after each of the BBI correction algorithms has been applied is shown in Figure 6-5 and Figure 6-6. Mean (and standard deviation) values are given in Table 6-2.

After the Wessel algorithm (Algorithm 2) (blue) was applied to the corrupted heartbeats (red), there was no change to the percentage of correctly identified heartbeats. This is because the Wessel algorithm (Algorithm 2) modifies the BBI values by replacing abnormal BBIs with new BBIs, but does not alter the number of beats in the signal.

The Threshold algorithm (Algorithm 3) (black) was the worst performing algorithm in terms of the percentage of correctly identified heartbeats preserved, across all levels of corruption.

Table 6-2 shows that the number of correctly identified heartbeats for the Threshold algorithm (Algorithm 3) was significantly less than the number of correctly identified heartbeats in the corrupted data. This is because the nature of this algorithm is to delete BBI values until there is no longer a large difference in adjacent BBI values, unlike the other BBI correction algorithms which seek to modify BBI values. This effect worsened for larger levels of corruption and when the percentage of corrupted heartbeats was increased to 25%, the algorithm only able to detect 33% of heartbeats correctly.

The Pattern Detection algorithm (Algorithm 1) (purple) was the best performing algorithm for preserving correct heartbeats. Table 6-2 shows that this algorithm consistently improved the proportion of correctly identified heartbeats by up to 5% compared with the corrupted BBI values at higher levels of corruption. Additionally, when the percentage of corrupted input BBI values was $\leq 5\%$, the Pattern Detection algorithm (Algorithm 1) was able to identify $>99\%$ of heartbeats correctly (i.e. heartbeat timing before corruption) for most of the

corrupted BBI signals. However, when there is a larger level of corruption in the input BBI signal, the simple patterns that are being searched for (described in section 6.4.1) become less common, and instead multiple BBI adjacent values that require correction form complex BBI patterns. This leads to less of the corrupted BBI values being corrected as the algorithm cannot correct these more complex patterns. This also suggests that a more complex pattern detection/correction algorithm is needed to increase the performance of these Pattern Detection algorithms for signals with a high degree of corruption.

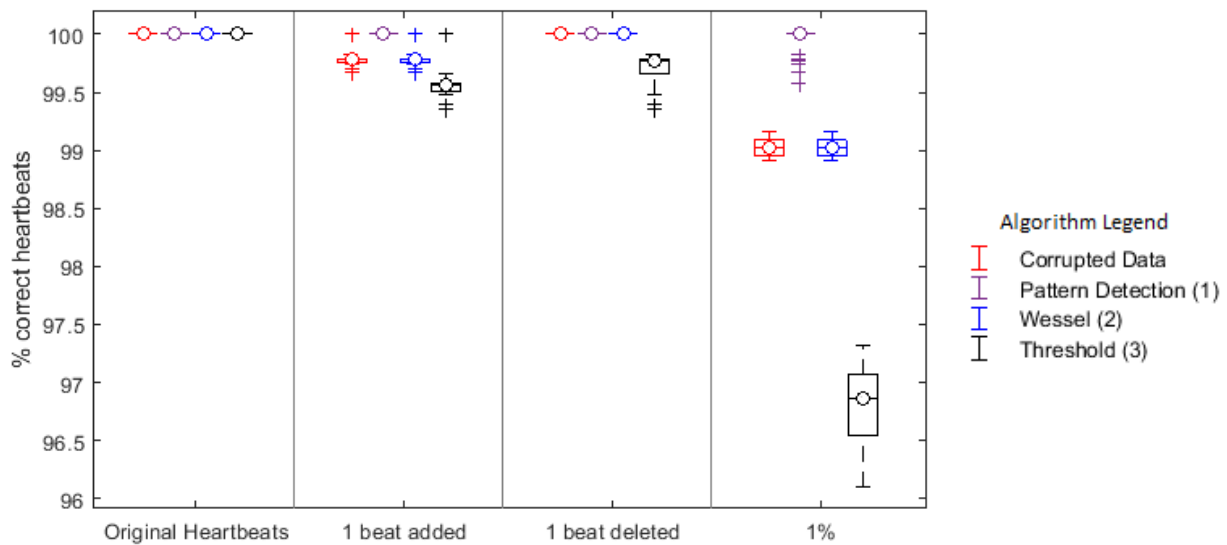


Figure 6-5 – Percentage of correctly identified heartbeats after BBI correction using the Pattern Detection algorithm (Algorithm 1) (purple), Wessel algorithm (Algorithm 2) (blue) and Threshold algorithm (Algorithm 3) (black) compared with the original corrupted BBI values (red). % value on horizontal axis relates to proportion of BBI values corrupted.

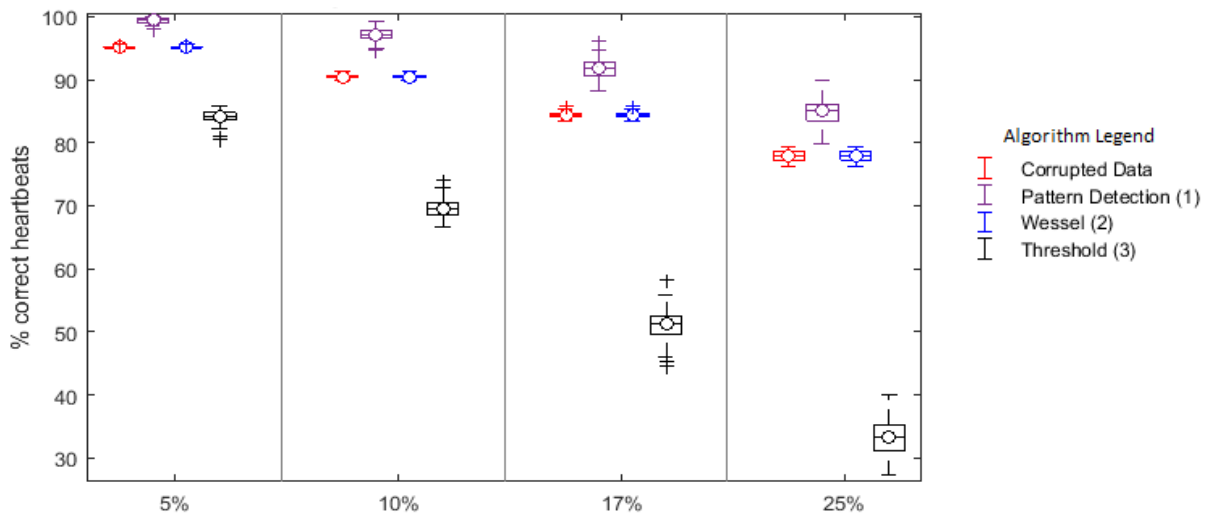


Figure 6-6 - Percentage of correctly identified heartbeats after BBI correction using the Pattern Detection algorithm (Algorithm 1) (purple), Wessel algorithm (Algorithm 2) (blue) and Threshold algorithm (Algorithm 3) (black) compared with the original corrupted BBI values (red). % value on horizontal axis relates to proportion of BBI values corrupted.

Table 6-2 – A comparison of how well the different BBI correction algorithms were able to preserve the proportion of correct heartbeats for different level of corruption. Values are mean% (std%)

	Original heartbeats	1 beat Added	1 beat deleted	1%	5%	10%	17%	25%
Corrupted Data	100 (0)	99.78 (0.02)	100 (0)	99.02 (0.07)	95.134 (0.14)	90.47 (0.31)	84.36 (0.47)	77.86 (0.75)
Algorithm 1	100 (0)	100 (0)*	100 (0)	100 (0)*	99.4 (0.34)*	97.14 (0.95)*	91.64 (1.51)*	84.78 (2.05)*
Algorithm 2	100 (0)	99.78 (0.02)	100 (0)	99.02 (0.07)	95.134 (0.14)	90.47 (0.31)	84.36 (0.47)	77.86 (0.75)
Algorithm 3	100 (0)	99.56 (0.46)*	99.72 (0.10)*	96.79 (0.34)*	84.25 (0.83)*	69.56 (1.47)*	51.07 (2.27)*	33.33 (2.94)*

* indicates significant difference (p<0.05) to corrupted data

6.5.2 HR error

Mean HR error after correction with the different algorithms is plotted in Figure 6-7 and Figure 6-8, and tabulated in Table 6-3. All BBI correction algorithms were able to significantly reduce the mean error in the HR across all levels of corruption. This is shown in Figure 6-7 and Figure 6-8 where, for all cases, the mean HR error of all algorithms was significantly less than the mean HR error of the corrupted input data. Hence as long as $\leq 25\%$ BBI values are corrupted, all of the BBI correction algorithms described are able to reduce the mean HR

error. The data in Table 6-3 also show that when the BBI input signal is not heavily corrupted (when the percentage of added/deleted BBI values is $\leq 1\%$) the average HR error is less than 0.6BPM for all three BBI correction algorithms, compared to an average HR error of up to 1.86BPM for the corrupted data.

The Wessel algorithm (Algorithm 2) was the worst performing algorithm in terms of reducing the HR error of the corrupted BBI signal. Table 6-3 shows that the mean HR error from the Wessel algorithm was significantly larger than the other algorithms for all levels of corruption. Table 6-3 also shows that when the Wessel algorithm (Algorithm 2) was applied to the reference BBI signal, this algorithm modified some of the correct BBI values, causing an error in the HR measurement, although this error was less than 0.01BPM. However as mentioned in the previous paragraph, the mean HR error for the Wessel algorithm (Algorithm 2) was less than 4 BPM when $\leq 5\%$ of the input BBI values are corrupted, which still makes it a potentially usable algorithm for low corruption signals.

When the percentage of corrupted BBI values was $\geq 5\%$ the Threshold algorithm (Algorithm 3) was the best performing algorithm, producing a BBI signal with the lowest mean HR error. At corruption levels $< 5\%$ the Pattern Detection algorithm (Algorithm 1) was the best performing algorithm, although the difference in mean HR error between Algorithms 1 and 3 was less than 0.2 BPM.

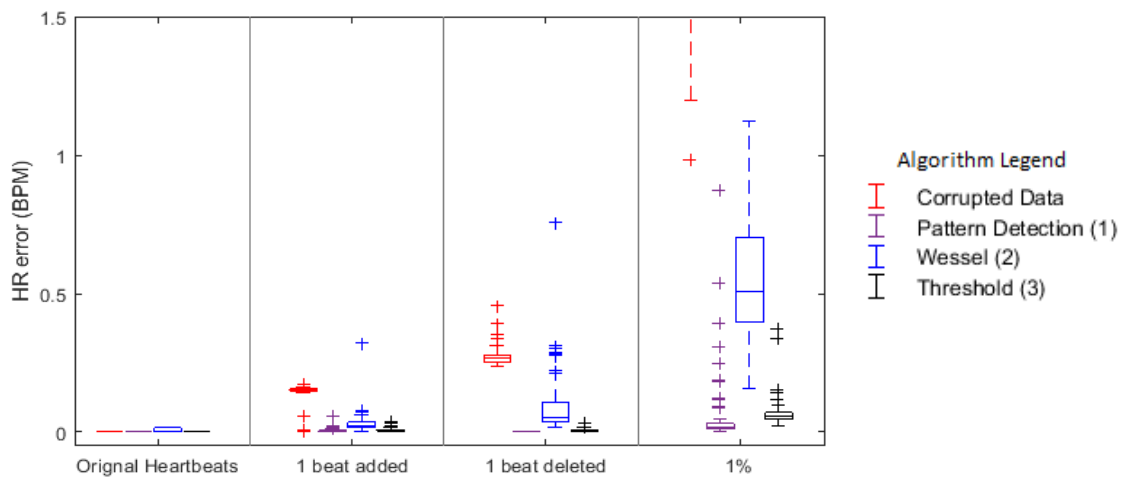


Figure 6-7 – Mean HR error after correction using the Pattern Detection algorithm (Algorithm 1) (purple), Wessel algorithm (Algorithm 2) (blue) and Threshold algorithm (Algorithm 3) (black) compared with the original corrupted BBI values (red)

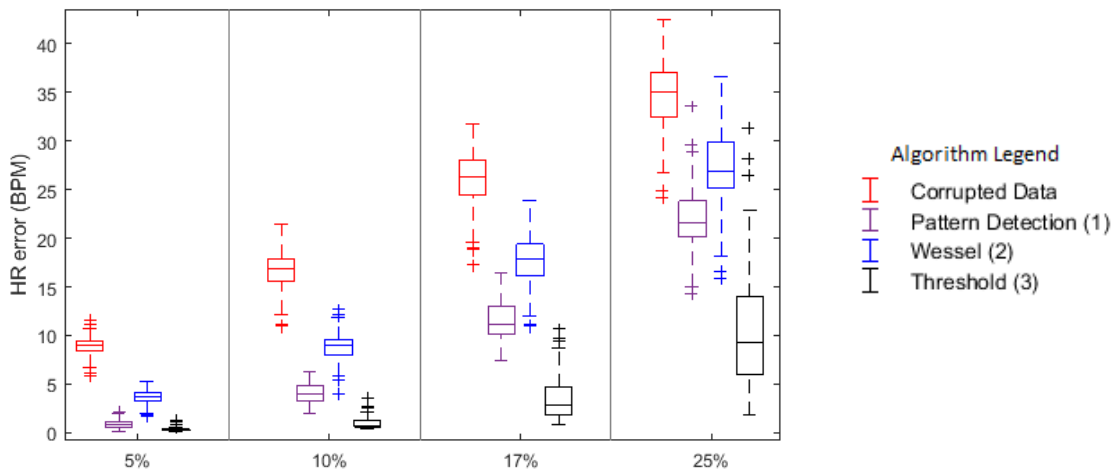


Figure 6-8 – Mean HR error after correction using the Pattern Detection algorithm (Algorithm 1) (purple), Wessel algorithm (Algorithm 2) (blue) and Threshold algorithm (Algorithm 3) (black) compared with the original corrupted BBI values (red)

Table 6-3 - A comparison of the HR error after applying the different BBI correction algorithms for different levels of corruption. Values are mean% (std%)

	Original heartbeats	1 beat Added	1 beat deleted	1%	5%	10%	17%	25%
Corrupted Data	0	0.15 (0.004)	0.27 (0.02)	1.87 (0.30)	8.87 (0.91)	16.8 (2.17)	26.34 (2.85)	34.87 (3.68)
Algorithm 1	0	0.003 (0.003)*	0 (0)*	0.018 (0.01)*	0.91(0.43)*	4.04 (1.02)*	11.51 (1.97)*	21.86 (2.84)*
Algorithm 2	0.008 (0.007)*†	0.026 (0.013)*†	0.07 (0.04)*†	0.57 (0.24)* †	3.68 (0.72) *†	8.87 (1.34) *†	17.77 (2.43) *†	27.27 (3.78) *†
Algorithm 3	0	0.007 (0.004)*†	0.005 (0.003)*†	0.056 (0.02)*	0.31 (0.09) * †	0.89 (0.43) * †	3.21 (1.95) * †	9.78 (5.26)* †

* indicates significant difference ($p < 0.05$) to corrupted data
† indicates significant difference ($p < 0.05$) to Algorithm 1 results

6.5.3 HRV error

The HRV error for each BBI correction algorithm is shown in

Figure 6-9 and Figure 6-10. For all levels of corruption up to 25%, all three BBI correction algorithms reduced the HRV error. However when the percentage of corrupted heartbeats was $\geq 5\%$, only the Threshold algorithm (Algorithm 3) had a mean HRV error of less than 30%, suggesting that the HRV results from the Pattern Detection and Wessel algorithms (Algorithms 1 & 2) would be unusable in these cases (as per Section 6.3.3.3).

Similarly to the mean HR error, Table 6-4 shows that when the percentage of corrupted BBI values was $< 5\%$, the HRV error from the Pattern Detection algorithm (Algorithm 1) was either lower than or equal to the error from other BBI correction algorithms. However, as the proportion of corrupted BBI values was increased, the HRV error for the Pattern Detection algorithm (Algorithm 1) increased at a higher rate than the other algorithms, such that for when $\geq 10\%$ of the BBI values were corrupted, it was the worst performing algorithm. This increase in HRV error is probably a result of the increase in mean HR error seen in the previous section. This means that for BBI signals with a large number of corrupted BBI values, the Pattern Detection algorithm (Algorithm 1) is not suitable for reducing the HRV error.

Table 6-4 shows that the Wessel algorithm (Algorithm 2) was only able to reduce the HRV to an acceptable error (i.e. below 30%) when the percentage of corrupted BBI values was < 1%. This was because when a BBI value is corrected, the Wessel algorithm (Algorithm 2) attempts to preserve the variability of the BBI signal. If there are multiple corrupted BBI values, then the variability of the BBI signal is altered significantly from the true BBI variability, so the corrections made by the Wessel algorithm would not be accurate.

The Wessel algorithm was able to significantly reduce the HRV error of the corrupted BBI signal more effectively than the Pattern Detection algorithm (Algorithm 1) when the proportion of corrupted BBI values was $\geq 17\%$, however the mean HRV error values for these cases were greater than 186%. Similarly to the HR error, when none of the BBI values was corrupted, there still existed a difference between the HRV values from the Wessel algorithm (algorithm 2) and the reference BBI signal, showing that this algorithm will alter some of the BBI values even if they are correct. This Wessel algorithm was developed for the correction of ectopic heartbeats, and these results show that ectopic beat correction algorithms are not necessarily applicable for the correction of corrupted BBI values from missed or extra detected heartbeats.

Based on the results of

Figure 6-9 and Figure 6-10, as well as Table 6-4, the algorithm that is best able to reduce the HRV error is the Threshold algorithm (Algorithm 3), except at very low levels of corruption (<5%) when the Pattern Detection algorithm (Algorithm 1) performs better.

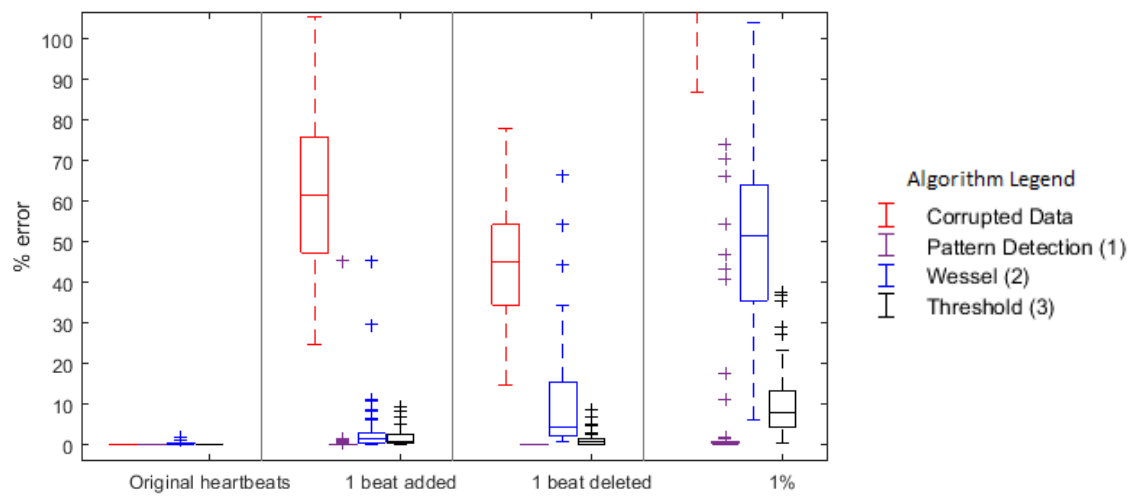


Figure 6-9 - HRV error after correction using the Pattern Detection algorithm (Algorithm 1) (purple), Wessel algorithm (Algorithm 2) (blue) and Threshold algorithm (Algorithm 3) (black) compared with the original corrupted BBI values (red)

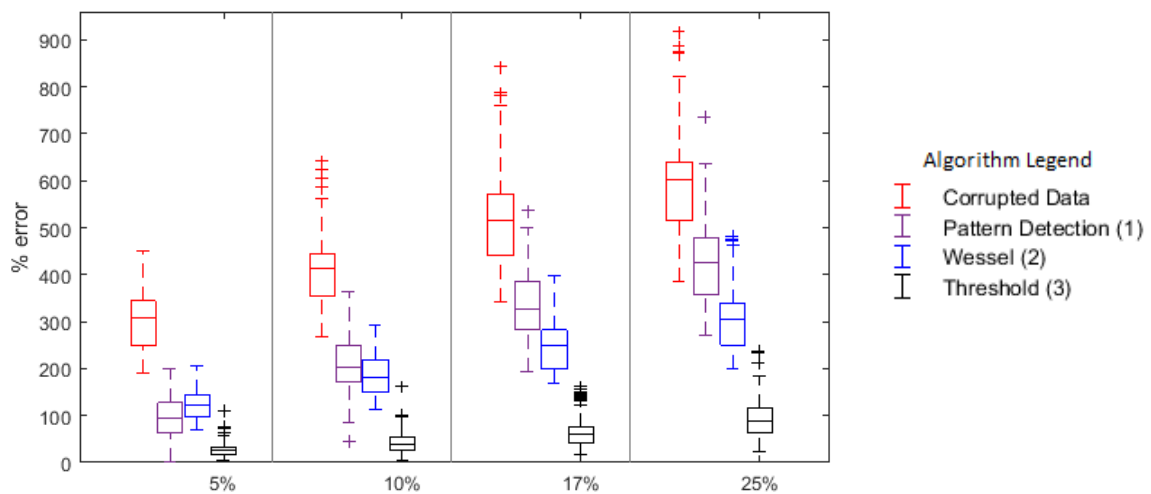


Figure 6-10 - HRV error after correction using the Pattern Detection algorithm (Algorithm 1) (purple), Wessel algorithm (Algorithm 2) (blue) and Threshold algorithm (Algorithm 3) (black) compared with the original corrupted BBI values (red)

Table 6-4 - A comparison of the HRV error from the different BBI correction algorithms for different levels of corruption. Values are mean% (std%)

	Original heartbeats	1 beat Added	1 beat deleted	1%	5%	10%	17%	25%
Corrupted Data	0 (0)	62.89 (18.43)	45.64 (15.57)	150.2 (38.56)	300.37 (64.71)	396.35 (67.42)	505.85 (89)	573.04 (98.72)
Algorithm 1	0 (0)	0.11 (0.10)*	0 (0)*	0.36 (0.31)*	96.81 (46.5)*	209.5 (57.84)*	331.29 (69.6)*	421.35 (88.53)*
Algorithm 2	0.21 (0.16)*	1.6 (1.5)*	8.727 (9.34)*	50.95 (20.27)*	125.57 (34.02)*†	186.2 (46.29)*†	246.85 (56.42)*†	297.61 (58.87)*
Algorithm 3	0 (0)	1.22 (1.28)*	0.71 (0.58)*	8.35 (5.54)*	24.64 (11.58)*†	41.94 (20.4)* †	57.77 (21.82)*†	87.6 (37.46)*

* indicates significant difference ($p < 0.05$ to corrupted data)
 † indicates significant difference ($p < 0.05$) to Algorithm 1 results

6.6 Combining BBI correction algorithms

The results in Section 6.5 showed that the Pattern Detection algorithm (Algorithm 1) was the best algorithm for preserving the number of correct heartbeats, but the Threshold algorithm (Algorithm 3) was the most effective algorithm at reducing the mean HR and HRV error. It was thought that by combining different BBI correction algorithms, the best elements of the different algorithms might work together to improve the effectiveness of the BBI correction. This was tested by comparing the Wessel and Threshold algorithms (Algorithms 1 & 3) with two new algorithms, which were comprised of a combination of the algorithms described in section 6.4. In each of the new algorithms, the Pattern Detection algorithm (Algorithm 1) was used as a pre-processing step, due to its ability to identify missing/added heartbeats (see section 6.5.1).

6.6.1 Algorithm 4: Combined Threshold algorithm

In this algorithm the corrected BBI signal from the Pattern Detection algorithm (Algorithm 1) was used as the input for the Threshold algorithm (Algorithm 3), the best performing algorithm for reducing the mean HR and HRV error.

6.6.2 Algorithm 5: Combined Wessel algorithm

For the second of the combined algorithms the Pattern Detection algorithm (Algorithm 1) was used as a pre-processing step to the Wessel algorithm (Algorithm 2).

6.7 Results 2: Algorithms 4 & 5

6.7.1 Correctly detected heartbeats

The percentage of correctly detected heartbeats for the Combined Wessel algorithm (Algorithm 5) (light blue) and the Combined Threshold algorithm (Algorithm 4) (orange), are shown in

Figure 6-11 and Figure 6-12, alongside the results from the original Wessel (Algorithm 2) (dark blue) and Threshold (Algorithm 3) (black) algorithms. Table 6-4 shows that the Combined Wessel and Combined Threshold algorithms have an equal or higher proportion of correctly identified heartbeats than either the original Wessel or Threshold algorithms. This suggests that applying the Pattern Detection algorithm (Algorithm 1) as a pre-processing step to other BBI correction algorithms will increase the percentage of correctly identified heartbeats in the corrected BBI signal.

Figure 6-11 and Figure 6-12 show that the algorithm that produced a BBI signal with the highest proportion of correctly identified heartbeats was the Combined Wessel algorithm (Algorithm 5). The percent of correctly identified heartbeats for this algorithm was equal to the proportion of correctly identified heartbeats from the Pattern Detection algorithm (Algorithm 1) (see Figure 6-5 and Figure 6-6), as the Wessel algorithm (Algorithm 2) doesn't alter the number of heartbeats in the BBI signal, but only alters the BBI values as shown in section 6.5.1.

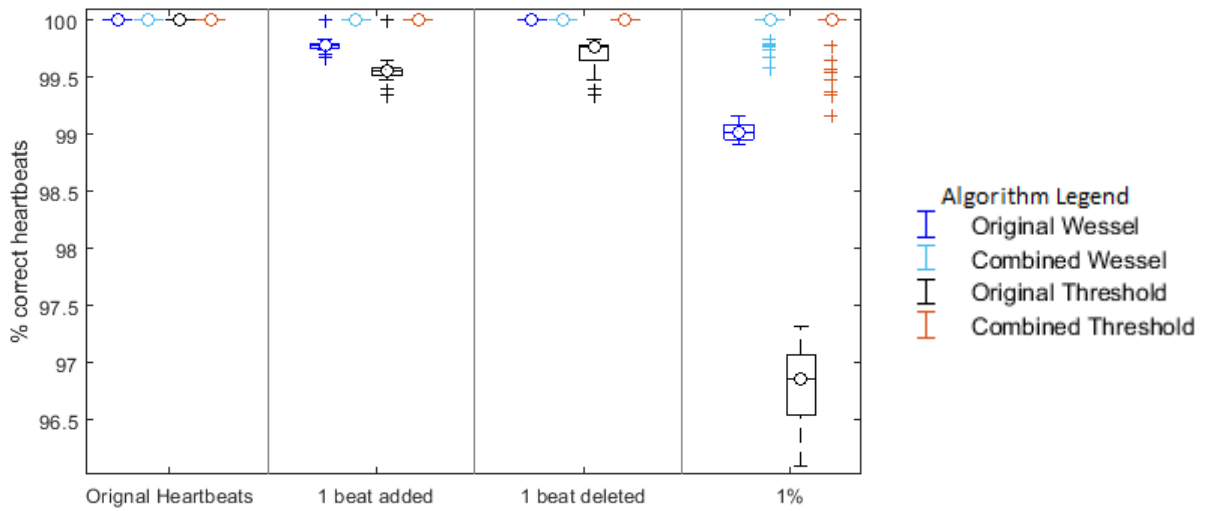


Figure 6-11 – Percentage of correctly identified heartbeats after correction using the original (blue) and Combined Wessel (light blue) algorithm, and the original (black) and Combined (orange) Threshold algorithm

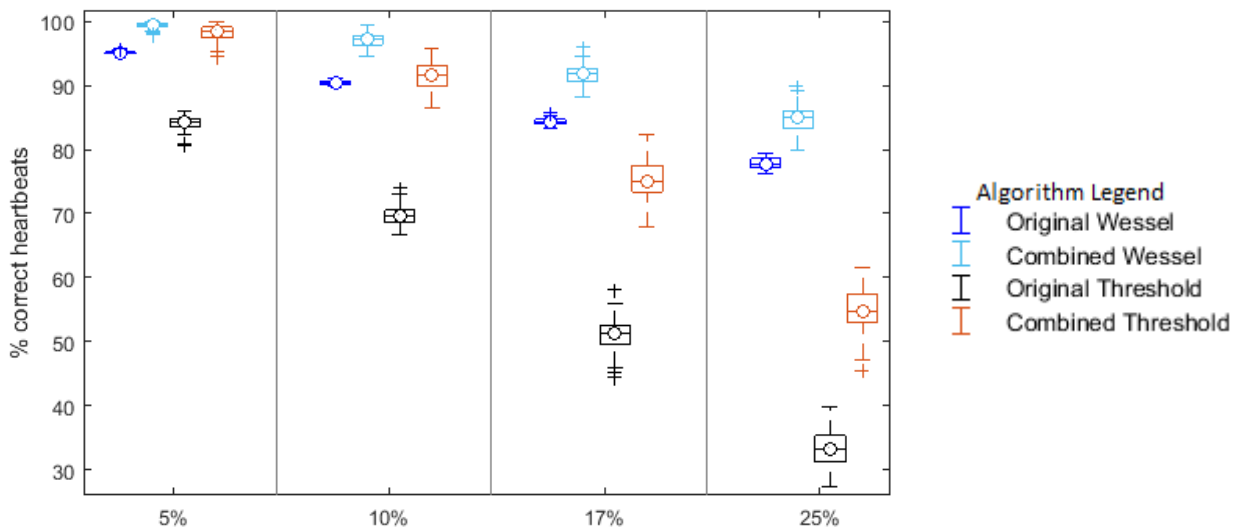


Figure 6-12 - Percentage of correctly identified heartbeats after correction using the original (blue) and Combined Wessel (light blue) algorithm, and the original (black) and Combined (orange) Threshold algorithm

Table 6-5 - A comparison of how combined BBI correction algorithms were able to preserve the proportion of correctly identified heartbeats for different level of corruption. Values are mean% (std%)

	Original heartbeats	1 beat Added	1 beat deleted	1%	5%	10%	17%	25%
Original Wessel	100 (0)	99.78 (0.02)	100 (0)	99.02 (0.07)	95.13 (0.14)	90.47 (0.31)	84.36 (0.47)	77.86 (0.75)
Combined Wessel	100 (0)	100 (0)	100 (0)	100 (0)*	99.4 (0.35)*	97.09 (0.99)*	91.59 (1.51)*	84.63 (1.95)*
Original Threshold	100 (0)	99.56 (0.46)	99.72 (0.10)	96.79 (0.34)	84.25 (0.83)	69.56 (1.47)	51.07 (2.27)	33.33 (2.94)
Combined Threshold	100 (0)	100 (0)*	100 (0)*	100 (0)*	98.2 (1.09)*†	91.48 (2.31)* †	75.42 (3.2)* †	55.18 (3.34)*†

* indicates significant difference ($p < 0.05$) of combined algorithm to original algorithm
 † indicates significant difference ($p < 0.05$) to Combined Wessel algorithm

6.7.2 HR error

The HR errors for the Combined Wessel algorithm (light blue) and the Combined Threshold algorithm (orange), are shown in Figure 6-13 and Figure 6-14, alongside the results from the original Wessel (dark blue) and Threshold (black) algorithms. These figures show that when the proportion of corrupted BBI values was $\leq 10\%$ of the total number of BBI values, the combined Wessel and Combined Threshold algorithms have an equal or lower mean HR error than their respective original Wessel and Threshold algorithms. This shows that use of the Pattern Detection algorithm as an initial step can decrease the mean HR error of a corrupted BBI signal. Additionally, for all levels of corruption, the mean HR error from the Combined Wessel algorithm (Algorithm 5) was less than the mean HR error for the original Wessel algorithm (Algorithm 2).

When the proportion of corrupted BBI values was $\geq 17\%$, the mean HR error from the Combined Threshold algorithm (Algorithm 4) was between 1-4 BPM greater than the error for the original Threshold algorithm (Algorithm 3). This is possibly because the Pattern Detection component of the Combined Threshold algorithm becomes less effective at reducing the mean HR error for larger levels of BBI corruption, as shown in Figure 6-8. However, for these cases (i.e. where the proportion of corrupted BBI values is $\geq 17\%$), the mean HR error for all algorithms is ≥ 3 BPM, regardless of the algorithm used.

The HR error from the Combined Threshold algorithm (Algorithm 4) was less than or equal to the mean HR error from the Combined Wessel algorithm (Algorithm 5) for all levels of corruption, except for 1%. This indicates that the best algorithm for reducing the mean HR error in a corrupted BBI signal is the Combined Threshold algorithm (Algorithm 4).

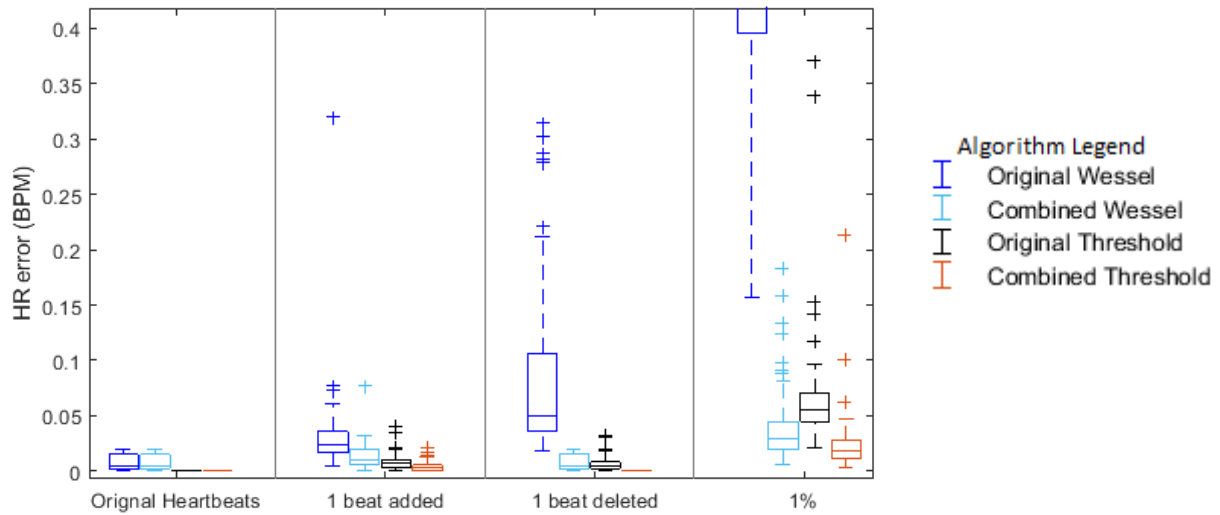


Figure 6-13 – HR error after correction using the original (blue) and Combined Wessel (light blue) algorithm, and the original (black) and Combined (orange) Threshold algorithm

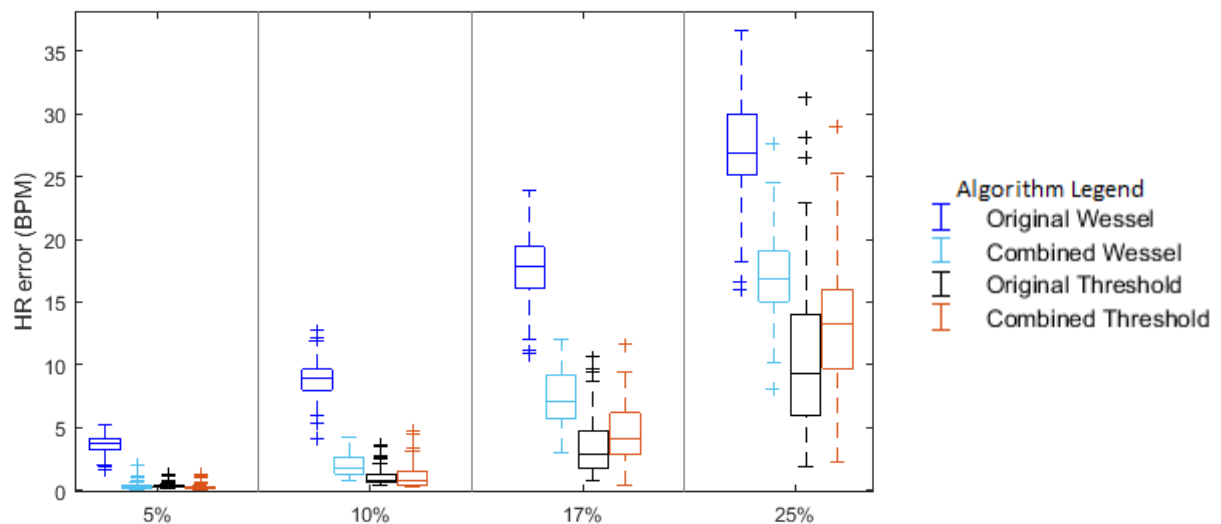


Figure 6-14 – HR error after correction using the original (blue) and combined Wessel (light blue) algorithm, and the original (black) and Combined (orange) Threshold algorithm.

Table 6-6 - A comparison of the HR error from the combined BBI correction algorithms for different levels of corruption. Values are mean% (std%)

	Original heartbeats	1 beat Added	1 beat deleted	1%	5%	10%	17%	25%
Original Wessel	0.008 (0.007)	0.03 (0.01)	0.07 (0.04)	0.57 (0.24)	3.68 (0.72)	8.87 (1.34)	17.77 (2.43)	27.27 (3.78)
Combined Wessel	0.008 (0.007)	0.01 (0.008)*	0.008 (0.007)*	0.29 (0.02)*	0.29 (0.15)*	1.96 (0.84)*	7.26 (2.09)*	16.85 (3.26)*
Original Threshold	0	0.007 (0.004)	0.005 (0.003)	0.06 (0.02)	0.31 (0.09)	0.89 (0.43)	3.21 (1.95)	9.78 (5.26)
Combined Threshold	0 (0)†	0.003 (0.004)*†	0 (0)* †	0.02 (0.01)*	0.15 (0.08)*†	0.98 (0.78) †	4.37 (2.25)* †	12.96 (4.62)* †

* indicates significant difference ($p < 0.05$) of combined algorithm to original algorithm
 † indicates significant difference ($p < 0.05$) to Combined Wessel algorithm

6.7.3 HRV error

Figure 6-15 and Figure 6-16 and Table 6-7 show that the HRV error from the Combined Wessel and Combined Threshold algorithms was less than their respective original Wessel and Threshold algorithms for all cases when the proportion of corrupted BBI values was $\leq 10\%$. Additionally, for all levels of corruption, the Combined Wessel algorithm (Algorithm 5) had a lower HRV error than the original Wessel algorithm (Algorithm 2). This shows that, like the mean HR error, the use of the Pattern Detection algorithm (Algorithm 1) as a pre-processing step for a BBI correction algorithm reduces the HRV error.

Also similarly to the mean HR error, when the proportion of corrupted BBI values was $\geq 17\%$, the HRV error from the Combined Threshold algorithm (Algorithm 4) was larger than the HRV error from the original Threshold algorithm (Algorithm 3). However both of the error values were $> 30\%$ which is too large for accurate HRV analysis, as defined in section 6.3.

Table 6-7 also shows that the HRV error was larger for the Combined Wessel algorithm (Algorithm 5) than for the Combined Threshold algorithm (Algorithm 4). This difference increased from a difference of 0.2% error at very low levels of corruption, to a difference of $\geq 43\%$ in HRV error when the percentage of corrupted BBI values was $\geq 10\%$. Thus the Combined Threshold algorithm (Algorithm 4) is the best algorithm for reducing the HRV error for the corrupted BBI signals.

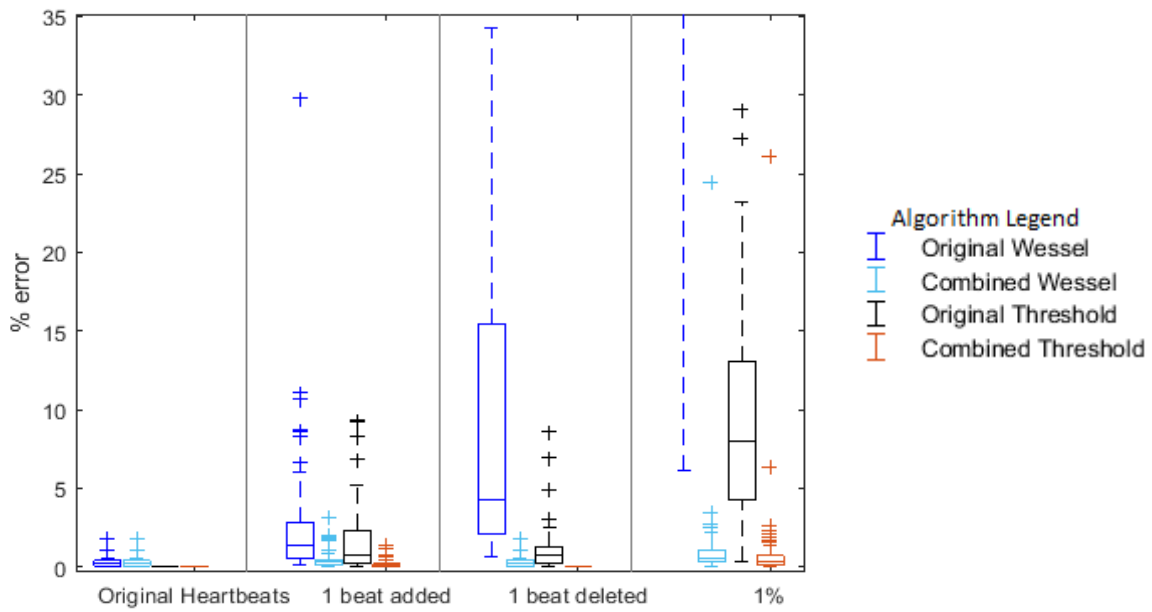


Figure 6-15 – HRV error after correction using the original (blue) and Combined Wessel (light blue) algorithm, and the original (black) and combined (orange) Threshold algorithm

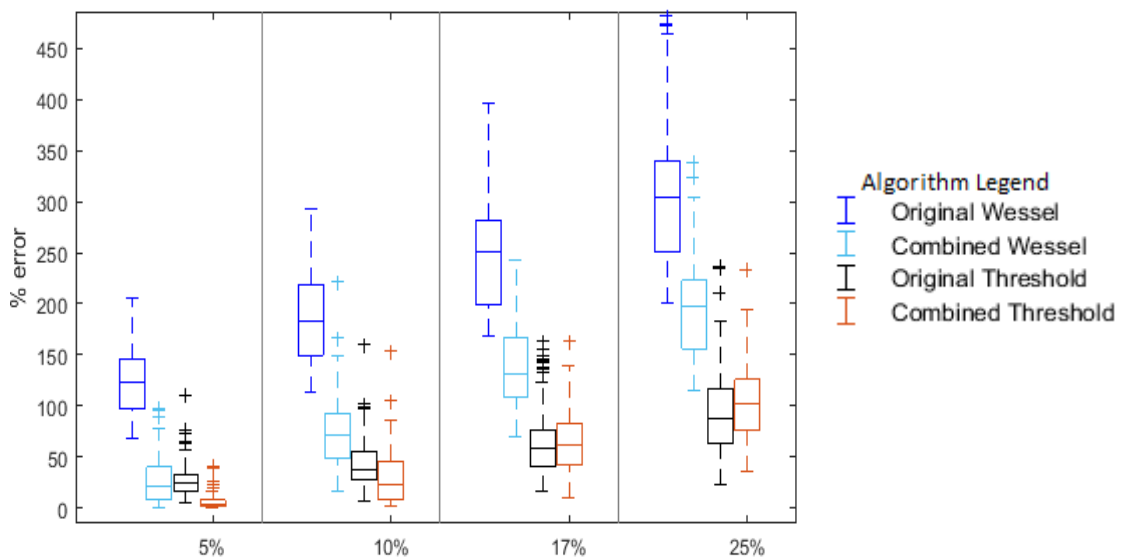


Figure 6-16 - HRV error after correction using the original (blue) and Combined Wessel (light blue) algorithm, and the original (black) and Combined (orange) Threshold algorithm.

Table 6-7 - A comparison of the HRV error from the combined BBI correction algorithms for different levels of corruption. Values are mean% (std%)

	Original heartbeats	1 beat Added	1 beat deleted	1%	5%	10%	17%	25%
Original Wessel	0.21 (0.16)	1.60 (1.50)	8.73 (9.34)	50.95 (20.27)	125.57 (34.02)	186.20 (46.29)	246.85 (56.42)	297.61 (58.87)
Combined Wessel	0.21 (0.16)	0.29 (0.19)*	0.21 (0.16)*	0.642 (0.49)*	25.1 (20.33)*	71.36 (31.68)*	138.15 (40.26)*	192.60 (44.06)*
Original Threshold	0 (0)	1.22 (1.28)	0.71 (0.58)	8.35 (5.54)	24.64 (11.58)	41.94 (20.4)	57.77 (21.82)	87.60 (37.46)
Combined Threshold	0 (0) †	0.11 (0.10)*	0 (0)*†	0.37 (0.32)* †	4.46 (4.28)*†	28.02 (23.4)* †	64.29 (27.46) †	102.93 (35.99) †

* indicates significant difference ($p < 0.05$) of combined algorithm to original algorithm

† indicates significant difference ($p < 0.05$) to Combined Wessel algorithm

6.7.4 Overall performance

Table 6-8 – A summary of the best performing algorithm for percentage of correctly identified heartbeats, HR error and HRV error for different levels of corruption

	Original heartbeats	1 beat Added	1 beat deleted	1%	5%	10%	17%	25%
Correctly identified heartbeats	Pattern Detection Algorithm	Pattern Detection / Combined Wessel						
HR error	Original Threshold/ Combined Threshold/ Pattern detection	Combined Threshold		Original and Combined Threshold	Combined Threshold	Original and Combined Threshold	Original Threshold	
HRV error	Combined Threshold/ Pattern detection	Combined Wessel/ Combined Threshold/ Pattern detection	Combined Threshold				Original and Combined Threshold	

A summary of the best performing algorithms for different levels of corruption is shown in Table 6-8. This table shows the Pattern Detection algorithm was the best single algorithm for preserving correct heartbeats. It was thought originally that the higher the proportion of correct heartbeats, the smaller the mean HR and HRV error, however the results in this chapter prove this hypothesis is not always true. Although the Pattern Detection algorithm was able to preserve the highest proportion of heartbeats, it was not able to reduce the mean HR and HRV error as effectively as other BBI correction algorithms, particularly when the proportion of corrupted BBI values was $\geq 5\%$ of the total number of BBI values.

The results from these tests show that using the Pattern Detection algorithm (Algorithm 1) as a pre-processing step to either the Wessel or Threshold algorithm increases the number of correctly identified heartbeats and reduces the HR error and the HRV error in a corrupted BBI signal. Of the two BBI correction algorithms, the Combined Threshold algorithm (Algorithm 4) was better than the Combined Wessel algorithm (Algorithm 5) at reducing the HR and HRV error.

6.8 Discussion

Five different algorithms were developed to correct any corrupted BBI values caused by falsely detected or missed heartbeats that may be present in the output of automatic heartbeat detection algorithms. BBI values from expertly annotated HR data were purposely corrupted to determine how effective different BBI correction algorithms were in correcting the BBI values with respect to the reference BBI values. This was measured by comparing the proportion of correctly detected heartbeats, the mean error of the HR output, and the error of the HRV analysis calculated from the output of the BBI correction algorithms.

It should be noted that when calculating HRV analysis in the frequency domain, the Lomb-Periodogram method was used. If the frequency components were calculated using another method, such as the Auto-Regressive (AR) method [207] or by resampling the BBI signal [208], the frequency domain HRV analysis and hence the mean HRV error may have produced different results.

The BBI values in this test were artificially corrupted by randomly removing and adding heartbeats. In reality, BBI values containing large numbers of false positives and false negatives would generally come from a reduction in signal quality from a source such as an ECG or PPG signal. This signal corruption could be due to short term factors such as movement artefacts, or longer-term factors, such as poor sensor/electrode placement.

The performance of these BBI correction algorithms could potentially be improved by including some measure of the quality of the signal in the correction algorithm. HR correction techniques have been used previously that estimate the signal quality, which then use this information to delete or correct BBI values when the signal quality is poor [148, 172], such as during movement. Future work could use a combination of the algorithms described in this paper and signal quality estimation methods to improve the effectiveness of the BBI correction methods.

Several of the figures in the results section contain outlier values, symbolised by crosses in the box plots. These outliers occur because the heartbeats are added and deleted randomly. These outliers (defined as larger than 1.5 x interquartile range from the upper or lower quartile) were excluded for the statistical analysis as they can have a large effect on the mean value. However these values are still important as they show the range of values obtained from each BBI correction algorithm.

The BBI correction algorithms were analysed on data that contained no ectopic beats. This decision was made because HRV analysis accuracy is reduced when ectopic beats are present [195]. Thus the comparative performance of these algorithms when ectopic beats are present is not known. Examples exist of the performance of the Wessel algorithm (Algorithm 2) when ectopic beats are present [201, 206, 209, 210]. However, these examples either have no comparison to other BBI correction algorithms, or reference an algorithm similar to the original Threshold algorithm (Algorithm 3) in which the Wessel algorithm has a significantly lower HRV error than the original Threshold algorithm.

The effect of missing BBI values was investigated using both the time and frequency domain by Kim et al. [35, 36]. Kim's HR data were also taken from the NSRDB, as well as HR data collected from their own experiments. In these studies, varying numbers of random consecutive BBI values were deleted and the effect of these deleted values on the time and

frequency domain HRV variables were studied, however no heartbeats or BBI values were added or otherwise modified. There was also no attempt to correct the BBI values, but rather the focus was to study the effect of the corrupted BBI values on the HRV analysis.

Kim et al in [35] reported that the error in the HF power analysis was higher than other frequency bands, an observation also made in this study (see individual HRV variable performance data in Appendix B). However in [4] they reported that the SDNN error was greater than the RMSSD error, albeit only by a small amount. This was not observed in the results in this chapter, as the error for the SDNN values were lower than the RMSSD values for all cases where there was at least one corrupted BBI value. This may be because Kim et al looked at the maximum error for each HRV variable, whereas in this thesis the median and mean error are compared. Additionally, because Kim et al. deleted BBI values, rather than deleting heartbeats and then updating the BBI values, there may be less variation in the BBI values. Although the Threshold algorithm (Algorithm 3) would ideally delete corrupted BBI values, there may be some cases where BBI values are not deleted or the process of deleting the heartbeats causes some additional variation in the signal.

Peters et al. [200] conducted a similar study to that described in this chapter, looking at the effect of artefact correction on frequency domain HRV parameters. The artefact correction method that they studied was similar to the Threshold algorithm (Algorithm 3). However, similar to Kim et al in [35] and [4], they corrupted the signal by deleting random BBI values, instead of the method used in this thesis which was corrupting heartbeats and applying the BBI correction algorithm. The result of this is that the range of error values measured by Peters et al. was lower than the values recorded here. This is because for heavy levels of corruption, not all false BBI values will be deleted/corrected by the algorithms described in this chapter. Hence although Peters et al. recommend that accurate HRV analysis can be conducted for data with $\leq 25\%$ of heartbeats missing, this does not necessarily hold for data when 25% of the BBI values are corrupted.

In their original paper, Wessel et al. describe their algorithm as a method to reduce Premature Ventricular Contractions (PVCs) and other artefacts [201]. In order to test the effectiveness of their algorithm, they used HR data from an unknown number of healthy patients, and added some examples of PVCs and other artefacts to the signal, from which a corrupted BBI signal was measured. They then applied their algorithm to generate time and frequency domain HRV variables from this corrupted BBI signal as well as the original uncorrupted (healthy) BBI signal. They found that the mean error of the HRV variables ranged from 6 to 17.5% depending on the nature of the ectopic beats introduced. This range of values was smaller than the range of error values from the tests described in this chapter. This is most likely due to their different method of signal corruption, based on ectopic beats rather than heartbeat addition and removal used here.

Furthermore, a direct comparison cannot be made between the results from the Wessel algorithm applied here and the results in Wessel's paper [201] since the value of the controlling coefficient (c_f in equations 6.6 and 6.7) is not given in the original paper. The value that is assigned to this coefficient will influence whether any BBI values should be corrected by the Wessel algorithm, so different results will be achieved if different values are used.

Other studies have looked specifically at the effect of correcting ectopic beats (and not other artefacts that can cause false BBI values) on HRV [195, 202, 211-214]. However to the author's knowledge, no studies have looked at the effect on HRV accuracy caused by the effect of missed or extra heartbeats creating artefacts in the BBI signal.

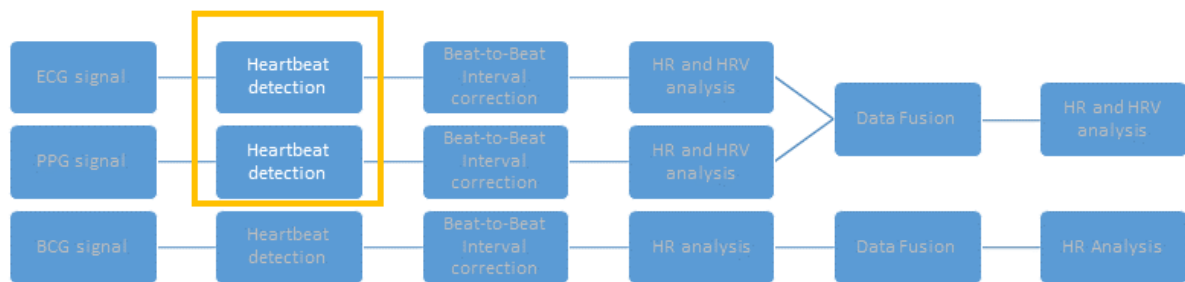
6.9 Conclusion

In this chapter, real HR data were corrupted by randomly removing and adding heartbeats, to compare different BBI correction algorithms. The BBI correction algorithms were

compared by proportion of correctly detected heartbeats, the mean HR error, and the error in the HRV analysis.

All BBI correction algorithms were able to reduce the mean HR error and error for HRV variables when compared with the corrupted BBI values. Additionally, adding the Pattern Detection algorithm (Algorithm 1) as a pre-processing step to other BBI correction algorithms further reduces the mean HR and HRV error. However when the number of corrupted BBI values was larger than 10% of the total number of BBI values, the error of the HRV analysis was larger than 30% of the HRV values from the original signal.

The algorithm that was best able to reduce the mean HR and HRV error was the Combined Threshold algorithm (Algorithm 4). As such, the BBI signals (and other similar HR signals from sources such as the PPG and BCG signals) measured from the Cardiomask in future chapters will be corrected using the Combined Threshold algorithm (Algorithm 4) to remove corrupted BBI values and to reduce the mean HR and HRV error of the measured signal.



7. Experiment Protocol

7.1 Introduction

The Cardiomask device was initially tested on a small number of participants (see Chapter 5). This initial testing showed that for all test participants, not all heartbeats could be accurately detected. In Chapter 6, an algorithm for minimising the Heart Rate (HR) and HRV (Heart Rate Variability) error was developed for application to the signals from the Cardiomask. However, further testing was needed to confirm that the Cardiomask utilising this algorithm was able to accurately measure BBIs, HR and HRV on a range of participants.

This chapter is divided into two sections. In the first section of the chapter (section 7.2), the methods and protocol used to record the signals from the Cardiomask are described. In the second section (section 7.3-7.7), the methods used to analyse the ECG and PPG signals from the Cardiomask are described. Results from the ECG and PPG signals are displayed in chapters 8-9 and the methods for BCG analysis and corresponding results are shown in chapter 10.

7.2 Testing Method

The Cardiomask was tested in a simulated PAP therapy environment by volunteers. 19 participants were recruited for testing, 14 males and 5 females. Each participant was between the ages of 19-48 (mean age: 30.5 ± 8.8). Participants had no known previous or current heart or respiratory diseases, and previous experience with PAP therapy was not required. The protocol of this experiment was granted ethical approval by the Southern Adelaide Clinical Human Research Ethics Committee (SAC HREC EC00188, application number HREC/16/SAC/277, see Appendix C).

During the experiment the participants wore the Cardiomask, which was connected to a PAP device (Lumis 150, ResMed, Sydney, Australia). The participants were asked to lie in the supine position on top of a mattress, with their head resting on a pillow. The experiment setup (with no participant) is shown in Figure 7-1.



Figure 7-1-Experiment setup

The participants were asked to lie in a number of defined sleeping positions whilst they underwent two common PAP therapy modes. This was to determine whether the signal quality of the ECG, PPG and BCG signals were influenced by different sleeping positions or under different PAP modes. It also allowed recording of data during the repositioning movement episodes to determine the effect of movement artefacts on the Cardiomask signals.

The sequence of the different experiment stages and the sleeping positions and PAP modes are listed in Table 7-1. A length of 5 minutes was chosen for each of the 6 experiment stages as this is the recommended HR segment length for HRV analysis [8], which allowed for HRV analysis for the different experiment stages. For the body positions “Left side” and “Right side”, the volunteers were instructed to lie on their left side and right sides in a manner that was comfortable. The two PAP modes, namely the CPAP and bi-level modes, were used. The CPAP mode involves a constant pressure being applied into the PAP mask, which for this test was set at a pressure of 6 cm H₂O. In the bi-level PAP mode, the applied

pressure increased during inspiration and decreased during expiration. In this experiment the bi-level inspiration and expiration pressures were set to 4 and 8 cmH₂O respectively. The pressures that were used for the CPAP and bi-level modes during testing were chosen to be at the lower end of the normal range of PAP pressures (4-20cmH₂O) [215], such that participants who had never used PAP before would not feel too uncomfortable, but were deemed representative as to the artefacts they would introduce to the measurement methods.

From the PAP device, the mask pressure (cmH₂O) and patient flow (L/s), which is an estimation of the patient's respiration activity, were measured and recorded using custom software designed by ResMed. All other signals were recorded using a custom Labview (National Instruments, USA) program and all signals were analysed in the post-processing stage using Matlab (Mathworks, USA).

Table 7-1-Experiment protocol for resting positions and PAP therapies

Stage Number	Body Position	PAP therapy mode	Duration (mins)
1	Supine	None	5
2	Left side	None	5
3	Right side	None	5
4	Supine	None	5
5	Supine	CPAP mode (6 cmH ₂ O)	5
6	Supine	Bi-level mode (4-8cmH ₂ O)	5

7.2.1 Reference ECG

The HR signals measured from the Cardiomask were compared with a reference ECG signal. The reference ECG signal was measured using Red Dot™ Ag/AgCl electrodes (3M, USA), with electrodes in a lead I position, on the back of the participant's hands, and a driven right leg electrode on their right leg. The gain of the reference ECG amplifier was 6 V/V. The 50Hz power line interference noise was filtered out using a digital notch filter in the post processing stage. The reference heartbeats from the ECG signal were detected using

the Pan-Tompkins algorithm [185], and any incorrectly annotated heartbeats were manually corrected.

7.2.2 Movement Detection

Based on the analysis of the literature in chapter 4 and preliminary experiments in chapter 5, it was thought that during movement the signal quality of the signals measured from the Cardiomask would make accurate HR analysis difficult. Movement was detected using the gyroscope signals from the attached IMU, and periods of movement (i.e. excessive peaks in the gyroscope signals) were identified. All ECG, PPG and BCG data within these movement periods were discarded.

Movement periods were detected using a normalised gyroscope signal which was defined as

$$g_n = \sqrt{g_x^2 + g_y^2 + g_z^2} \quad (7.1)$$

where g_x , g_y , and g_z represent the x, y, and z components of the gyroscope, and g_n is the normalised gyroscope component. In the first 5 seconds of recording it was assumed that the participant was not moving. The maximum value of the normalised gyroscope signal during this initialisation period was then multiplied by a heuristic constant to define the movement threshold. During initial testing this constant was set at 7.5, as it was found that this ensured that large movements, including deliberate head movements would exceed this threshold, whilst small movements, such as accidental movements, would not.

7.3 HR Analysis

Preliminary results in chapter 5 had shown a low SNR from the Cardiomask-measured ECG, PPG and BCG signals, and hence it was anticipated that some of the measured signals from the experiment would have a low SNR. This may lead to corrupted beat-to-beat interval (BBI) values, which as shown in the previous chapter, can have a significant effect on the HR and HRV error. The previous chapter also demonstrated that the most successful algorithm for reducing the HR and HRV error for corrupted BBI signals was the combination of two different BBI correction methods (Combined Threshold algorithm). To compensate for

the reduction in the SNR of the measured signals, this BBI correction algorithm was applied to all measured HR signals before all heartbeat, HR and HRV analysis.

The instantaneous HRs from the Cardiomask-measured ECG, PPG and BCG signals were compared with the HR from the reference ECG signal. Any heartbeat detected that was less than 0.2 seconds from a reference heartbeat was discarded. A Bland Altman (BA) plot was generated for all remaining BBIs.

To determine how accurately heartbeats can be detected from the signals measured from the Cardiomask, the sensitivity of the heartbeat detection algorithms in the ECG and the PPG signals was calculated. Sensitivity was defined as:

$$\text{Sensitivity (\%)} = \frac{\text{Number of heartbeats detected in measured signal}}{\text{Number of heartbeats in reference ECG signal}} \times 100 \quad (7.2)$$

The percentage of incorrectly detected beats was also calculated. An incorrectly detected heartbeat was defined as any heartbeat detected in the measured signals that were larger than 0.2 seconds away from any reference ECG heartbeat. This percentage was defined as:

$$\text{Incorrectly detected heartbeats (\%)} = \frac{\text{False positives in measured signal}}{\text{Number of total heartbeats in measured signal}} \quad (7.3)$$

HR error values were compared over fixed time windows. For each window the mean HR value was calculated. Two window lengths were chosen - 30 seconds and 5 minutes. 30 second windows were used, as this is a commonly used epoch length in sleep medicine [68]. A window length of 5 minutes was also used as this was the length of each experiment stage, and also represents the suggested window length for HRV analysis [8].

A method for discarding inaccurate HR windows was implemented. A flowchart showing this process is shown in Figure 7-2. Firstly, any consecutive BBIs that differed by more than 0.4 seconds were deleted. This process was repeated until there were no longer any adjacent BBI values that differed by more than 0.4 seconds, or until there had been 4 iterations of this

procedure. If there were still any consecutive BBIs that differed by more than 0.4 seconds, the whole window was excluded.

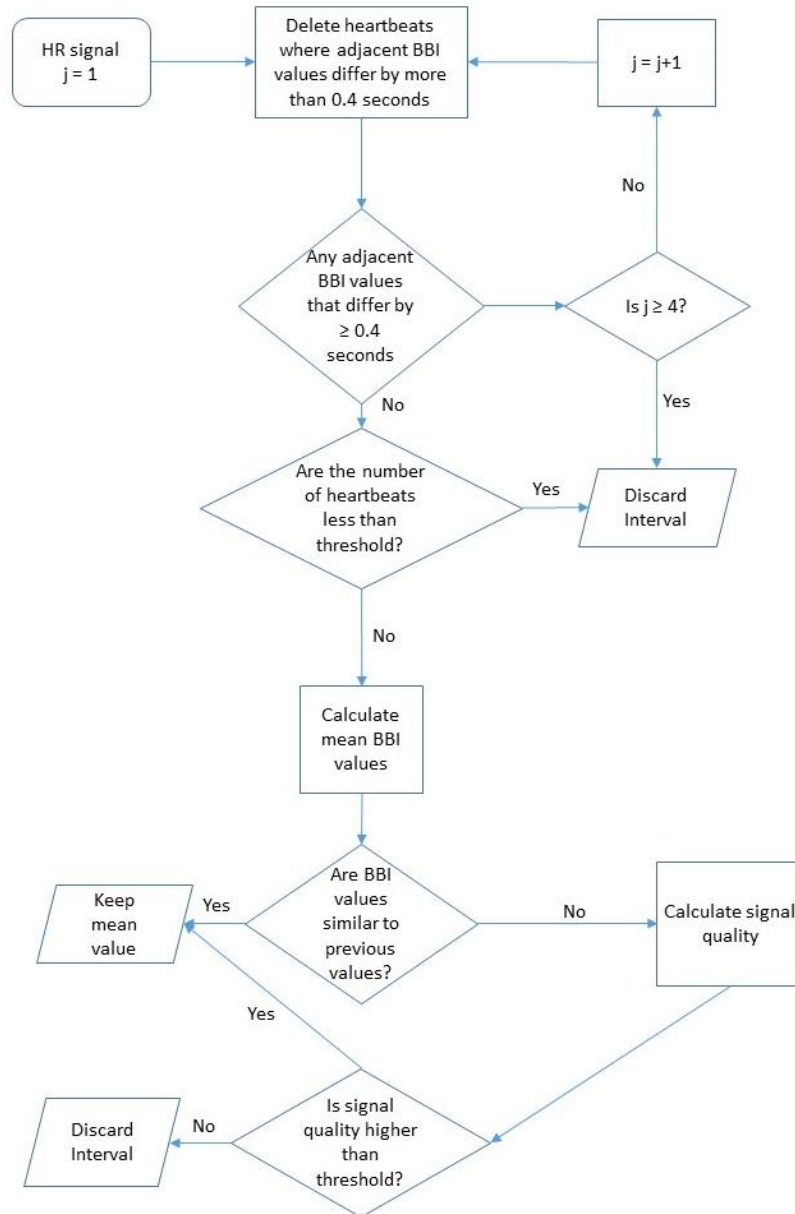


Figure 7-2 - Flowchart for accepting/rejecting time intervals for mean HR calculations

Next, the number of BBIs in each window was counted. If the number of BBIs was less than 15 for a 30 second window, and 150 for a 5-minute window then the interval was assumed not to be accurate. Otherwise the mean BBI value was compared to the values from the previous window. If the mean BBI value differed by more than 0.4 seconds from the previous value, then the signal quality was estimated. For the ECG signal this meant calculating the

kurtosis of the signal. For the PPG signal, the signal quality was estimated using the algorithm described by Li and Clifford [177].

If the kurtosis of the ECG signal was greater than 4, or the median PPG quality value was larger than 0.8, it was assumed to be an accurate signal and the mean HR value for the window was kept and not discarded. A kurtosis value of 4 was chosen as a normal good quality ECG signal has a kurtosis value of greater than 5 [216], however the ECG signal measured from the face has a worse signal quality than a normal ECG signal so a smaller kurtosis value was chosen as the threshold. A pulse quality value of 0.8 was determined experimentally, such that most of the inaccurate HR windows would be discarded, without rejecting too much useful data from the PPG signal.

7.4 HRV Analysis

As well as HR error, the errors in both the time and frequency domain HRV variables were calculated. HRV calculations were only performed on stages 1, 5 and 6 of the experiment (Table 7-1), since these stages involved no change in participant orientation and no movement. A change in orientation or large movement produces a temporarily elevated HR, and the HRV variables calculated for stages 2, 3, and 4 may therefore be significantly affected by the movement [8].

The accuracy of each HRV variable was investigated through a BA plot and by comparing the relative error of that variable to the reference HRV value. If during a particular stage the accuracy of the HR signal was classified as “too corrupted”, then HRV calculations were not performed on the HR signal from that stage. This is because corrupted beats can cause significant errors in the HRV calculations, and the results would not accurately reflect HRV dynamics.

To determine whether data from an experiment stage was “too corrupt”, the HR signal for that window was analysed. Specifically two parameters, the range of the BBI values for the

HR windows and the number of heartbeats in the window divided by the average HR, were used. In a normal and stable situation, particularly during sleep, the HR should remain relatively stable. The only reason the HR may vary markedly during sleep would be if an apnoea or other respiratory event is occurring [64], if the patient is changing between REM and NREM sleep [217, 218], or if the data are corrupted by false HR values. In all of these cases, HRV analysis should not be performed, as the HRV values would be affected either directly by these events [40] or by the inaccuracies in the HR data. For these experiments the BBI range was considered large if it was greater than 0.7s, and in this case the data were considered corrupt and excluded from HRV analysis.

Similarly, if a large number of BBIs are deleted by the BBI correction algorithm, then the accuracy of the HRV calculations will be reduced [35, 36]. To estimate how many heartbeats had been deleted, the number of heartbeats in the 5-minute stage were divided by the average HR in that stage, to provide a rough approximation of the time length of the stage.

$$\text{Estimated stage length (mins)} \approx \frac{\text{Number of heartbeats}}{\text{Average HR (BPM)}} \quad (7.4)$$

Since all experiment stages were 5 minutes long, if only a few BBIs had been deleted or were missing, then the estimated stage length should also be approximately 5 minutes. However if multiple BBIs had been deleted then the estimated stage length will be lower. For these experiments if the estimated HR window length was less than 4.8 minutes then it was classified as having too many heartbeats deleted and the stage rejected for HRV analysis.

If there were any ectopic beats identified in the recorded signals, HRV analysis was not performed on that 5 minute stage, since typically HRV analysis is not performed on HR data that contain ectopic beats [8, 195]. Ectopic beats were identified visually and removed manually.

7.5 Signal Quality

Although the main aim of the Cardiomask is to measure HR and HRV of the wearer there may be other information that can be gained from the ECG, PPG and BCG signals. For example, patterns in an ECG signal can be used to diagnose heart problems. If these features can be shown to be present in the face ECG signal, then this could increase the diagnostic potential of the face ECG signal.

7.5.1 ECG Signal Correlation

Since there has been only limited published research on comparing ECG signals measured from non-traditional electrode locations (see section 4.1.3), several methods were developed to compare the reference ECG signal to the ECG signal measured from electrodes positioned on the face. The first method used a signal correlation technique. To calculate a correlation value a window was created, centred on each heartbeat detected in the reference ECG signal. The window started halfway between the R-waves of the current and the previous heartbeat, identified in the reference ECG signal. Similarly the window ended halfway between the R-waves of the current and the next heartbeat. This would ensure that one window contains one complete ECG signal. The linear correlation coefficient was then calculated between the reference ECG signal inside each window and the face ECG signal inside that same window. This process is shown in Figure 7-3.

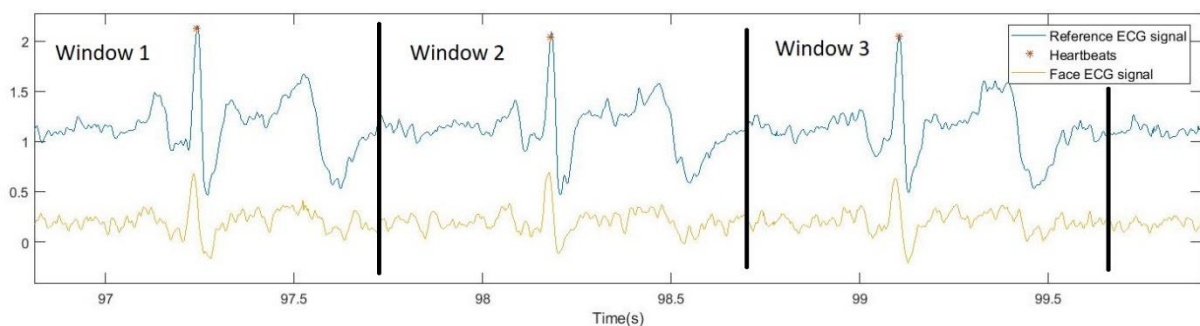


Figure 7-3 - An illustration of how the reference and the face ECG signals are divided into windows to calculate the correlation value. The correlation of the reference signal in window 1 to the face ECG signal in the same window is calculated. A similar process is used to calculate the correlation value for window 2 and 3 and subsequent windows.

The R peaks were then removed from the reference and face ECG signals and the correlation values were re-calculated. The R-peaks were removed by defining a window 0.1

seconds wide centred on each R-peak, and replacing all of the ECG signal within that window with a straight line between the data points at either end of the window. An example of this is shown in Figure 7-4. The reason for removing the R-peaks was to remove the dominance of the QRS complex in the correlation and to more closely investigate the correlation of the smaller ECG features, such as the P and T waves.

Finally, the correlation between the reference ECG signal with the R peak removed and random noise was calculated. These values were compared to previous correlation calculations, to confirm whether the reference ECG signal had a higher correlation value with the face ECG signal than with random noise.

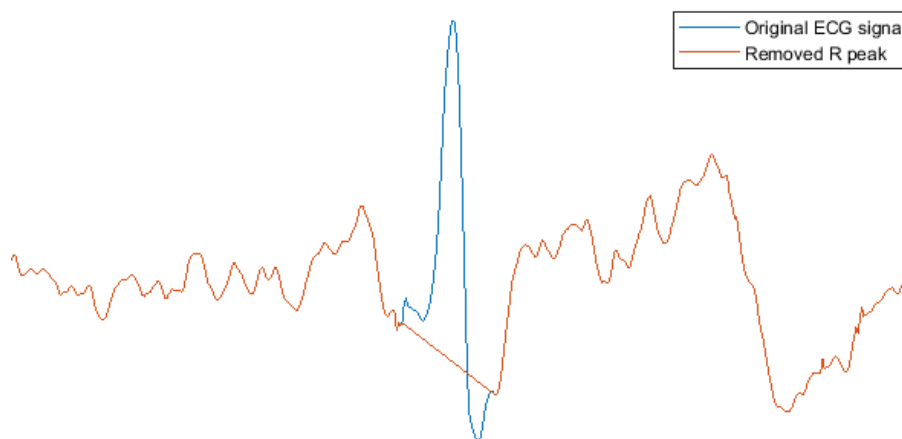


Figure 7-4 - An example of how the R-peak was removed from the ECG signal prior to signal correlation

7.5.2 ECG SNR

The other measure that was used to compare the signal quality of the face ECG signal with the reference ECG was the signal-to-noise ratio (SNR). Typically for SNR calculations, the combined signal is separated into the signal and noise components, for example by filtering the signal at certain frequencies. From these components the RMS values are then calculated. However for an ECG signal there is no trivial way to separate the noise from the signal component.

A method for calculating a 'pseudo' SNR value for the face and reference ECG signal was developed in which the QRS complex was considered 'signal' and the remainder of each heartbeat considered 'noise' as shown in Figure 7-5. The signal segment was centred on the R peaks, with the width of the signal window set at 0.1 seconds. The noise component of the ECG signal was defined as the remainder of the ECG signal, which includes the P and T waves. Because of this, the ideal value for the noise component will not be zero, as that would mean that important features of the ECG signal are missing. Instead, if the SNRs of the face and reference ECG signal are similar, then that would indicate a similar quality for the two signals. A similar method has also been used by Escalona et al. to compare the signal quality of different ECG signals [219].

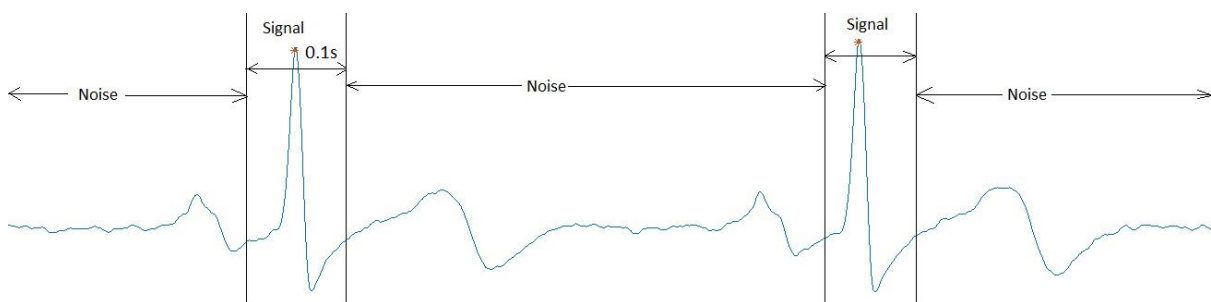


Figure 7-5-To calculate a SNR value the ECG signal is divided into the "signal" and "noise" segments

7.5.3 PPG Signal Quality

The quality of the PPG signal was also calculated, to determine if the different sleeping positions or the different modes on the PAP device caused a change in the PPG signal quality. The quality of the signal was determined using the signal quality algorithm described by Li and Clifford [177]. Briefly, this method compares the shape of a PPG waveform from a single pulse with similar pulses before and after to create a waveform template. For each pulse, the pulse waveform is correlated to the waveform template, and any positive correlation coefficients are used as an estimation of the signal quality with a value of '1' being a good quality signal and '0' a poor signal.

7.6 Pulse Transit Time

Measures of Pulse Transit Time (PTT) were calculated from the time between the R-wave in the ECG signal and the fiducial point in the PPG signal. The main reason for calculating PTT

was to assist in the data fusion methods that will be described in later in chapter 9. The definition of the PTT is shown for each of the fiducial points in the PPG signal in Figure 7-6.

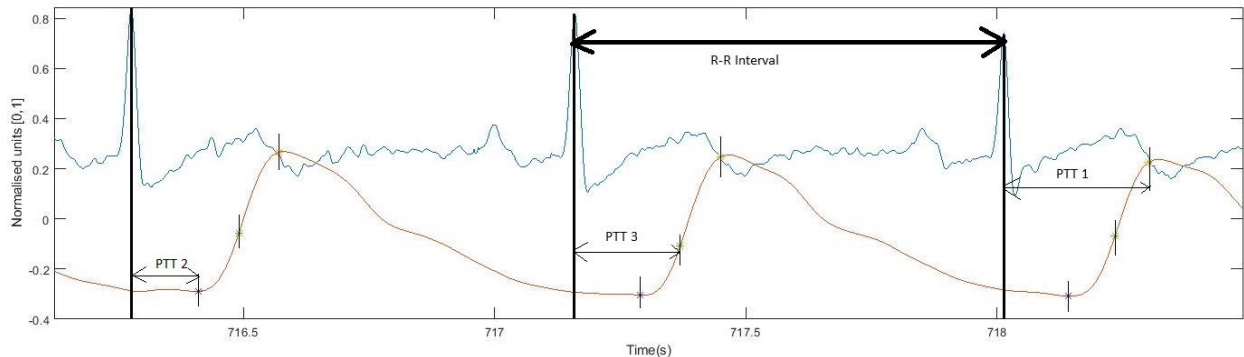


Figure 7-6-A graphical representation of the three different PTT intervals. The ECG signal is shown in blue whilst the Pulse signal is shown in orange. PTT 1 = PTT to maximum PPG point, PTT 2 = PTT to minimum PPG point, PTT 3 = PTT to maximum 1st derivative PPG point

7.7 Statistical Analysis

For each BA plot the following variables were calculated:

- Mean difference: the average of the absolute error between the two measurements compared in the BA plot.
- Reproducibility Coefficient (RPC): the mean difference $\pm 1.96 \times$ standard deviation, which is an estimate of the largest potential absolute error for 95% of subsequent measurements.
- Coefficient of Variation (CV): the ratio of the standard deviation to the mean, and is also used to quantify precision.

To calculate whether a significant bias was present in the BA plots, a t-test was used to determine the probability that the mean difference is 0. A t-test was used, as there was a large number of samples for each BA plot, so a normal distribution of the data could be assumed. If the mean difference was significantly different (significance defined as $p < 0.05$) from 0 then a bias occurred between the two measurements.

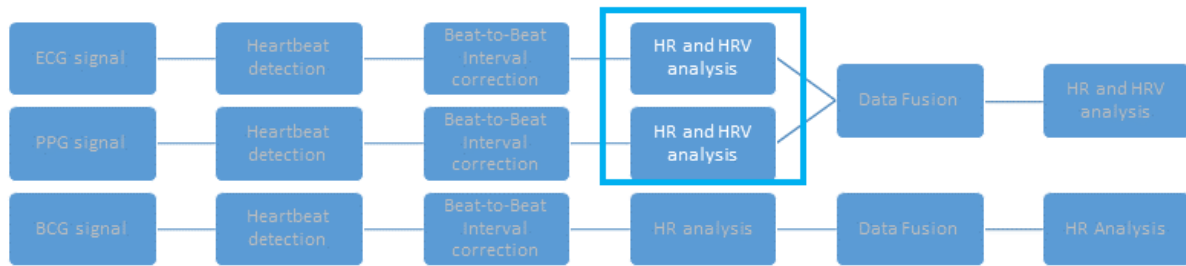
For comparing percentage values, such as the relative HRV error, or the percentage of correctly identified heartbeats, a paired signtest was used. This test was used because of the low number of samples (between 18 – 33 samples for each variable). A signtest was also used, since for variables that are represented as a percentage, a normal distribution cannot be assumed in the data, as the percentages have a defined range of 0-100%.

For determining whether a significant difference occurred between more than two groups, such as comparing the heartbeat detection accuracy from the different methods for detecting heartbeats in the PPG and ECG signals, a Kruskal Wallis test [220] was used. Since percentages were compared, the distributions were not always normal, however normality is not a requirement for the Kruskal Wallis. This test also assumes no relationship between the signal quality of the ECG and the PPG signal, which, since the ECG and PPG signals were measured by different sensors on different parts of the face, was generally true.

For comparing all other values between stages or between different methods, a t-test was used, as the large number of samples mean that the distributions can be approximated as normal distributions.

7.8 Conclusion

In this chapter, methods for recording signals from the Cardiomask are detailed. Results will be presented in subsequent chapters.



8. ECG and PPG analysis

8.1 Introduction

¹A PAP device was modified with the aim of monitoring Heart Rate (HR) from an ECG and a PPG signal. Algorithms were developed that were designed to detect corrupt BBI values and improve the accuracy of the instantaneous HR value estimation. Although some small-scale testing had been conducted (see chapter 5), larger scale testing was needed to confirm that this device could measure HR accurately across a larger sample size. Methods used for larger-scale testing are described in Chapter 7.

In this chapter, the following results will be presented and discussed:

- Bland-Altman (BA) plots of the Beat-to-Beat intervals (BBIs) for the heartbeats detected in the ECG and PPG signal, to evaluate the accuracy and repeatability of the inter-beat intervals measured from the recorded signals (section 8.2.1).
- The sensitivity and percentage falsely detected heartbeats (section 8.2.2).
- The mean HR accuracy over 30 second and 5 minute windows from the ECG and PPG, with a comparison made to the mean HR values from the reference ECG (section 8.2.3).
- The HRV variables calculated from the measured HR from the face ECG and PPG signal, with a comparison to the HRV variables calculated from the reference ECG signal (section 8.2.4).

¹ Excerpts from this chapter have been take from previous publications by the author from the following source:

Gardner, M., et al. *A Modified Mask for Continuous Cardiac Monitoring during Positive Airway Pressure Therapy*. in *2018 40th Annual International Conference of the IEEE Engineering in Medicine and Biology Society (EMBC)*. 2018. IEEE.

- The quality of the measured face ECG and PPG signals (section 8.2.5).

To assist in the interpretation of the results, the heartbeats detected from the maximum points in the PPG signal will be referred to as PPG1, and the heartbeats detected from the maximum points in the 1st derivative of the PPG signal will be referred to as PPG2.

8.2 Results

8.2.1 Bland-Altman plots of Beat-to-beat Intervals from ECG and PPG signals

8.2.1.1 Results

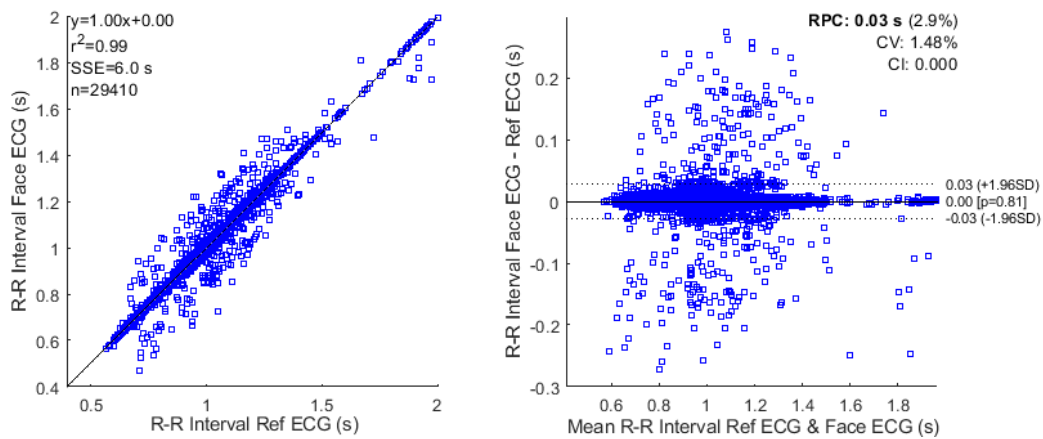


Figure 8-1-Bland Altman plot comparing Beat-to-Beat intervals (written as R-R Intervals) from the Face ECG signal and the reference ECG signal

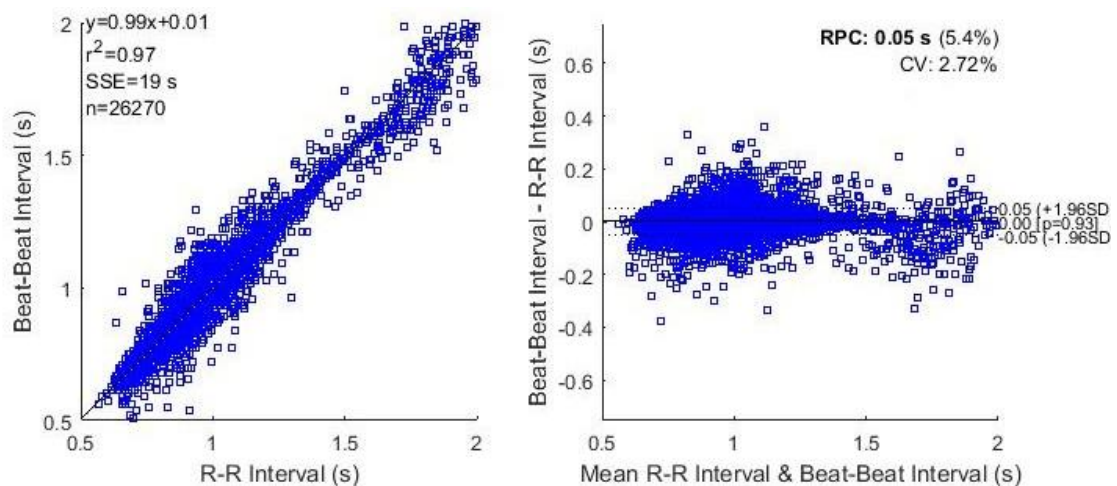


Figure 8-2-Bland Altman plot comparing the Beat-to-beat intervals (BBIs) for PPG1 to the RRIs from the reference ECG signal

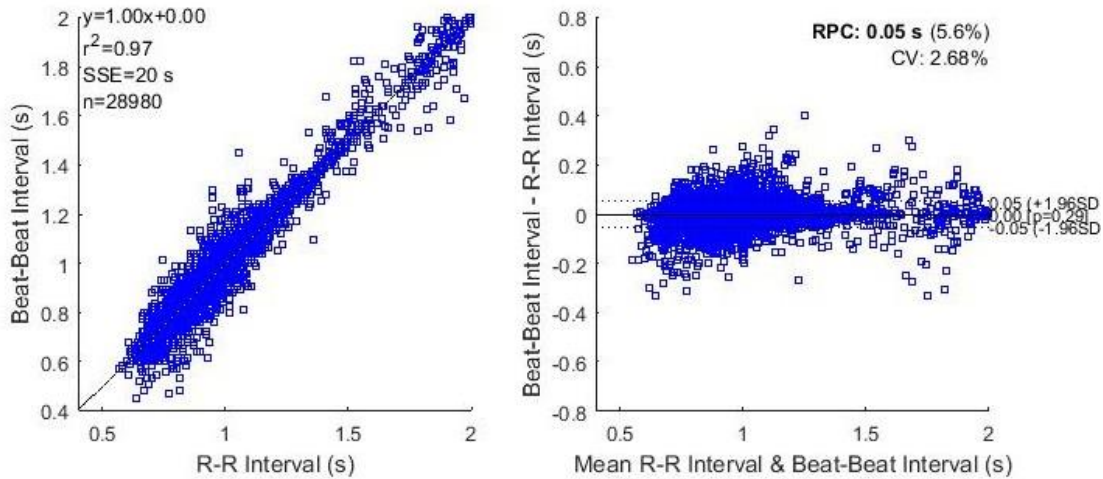


Figure 8-3-Bland Altman plot comparing the Beat-to-Beat intervals (BBIs) for PPG 2 to the R-Rs from the reference ECG signal

Table 8-1 – A summary of the accuracy and repeatability results from the BA plots in Figure 8-1, Figure 8-2 and Figure 8-3

	ECG	PPG1	PPG2
R ²	0.99	0.97	0.97
Number of BBI values	29410	26270	28980
RPC	0.03	0.05	0.05
CV	1.48	2.72	2.68
Mean difference (p value)	0.00 (p=0.81)	0.00 (p=0.93)	0.00 (p=0.29)

8.2.1.2 Analysis and Discussion

In Figure 8-1 the BA plot of BBIs detected in the Face ECG signal in comparison to those in the reference ECG signal is shown. The R² value in Figure 8-1 is 0.99, and the mean difference between the RRI values from the reference and face ECG RRI values is 0.00 (p=0.81), which suggest that the RRI values measured from the face ECG signal accurately reflect the RRI values measured in the reference ECG signal.

Figure 8-1 also shows the spread of RRI values from the face ECG signal. There were some RRI values from the face ECG signal that were up to 0.3s different to RRI values from the reference ECG signal. Most of these points are probably a result of noise or movement

artefacts in the face ECG signal being falsely classified as a heartbeat or from synchronisation errors between the reference and the face ECG signal. However, the low Reproducibility Coefficient (RPC) and Coefficient of Variation (CV) (0.03s and 1.48% respectively) show that the measurements are repeatable.

The BBIs calculated from PPG1 and PPG2 were compared to the RRI values from the reference ECG signal in Figure 8-2 and Figure 8-3. The R^2 value for both the PPG1 and PPG2 heartbeats was 0.97, and the mean difference between both sets of BBIs from the PPG signal and the RRI values from the reference ECG signal was 0.00 ($p=0.29$ for 1st derivative (PPG2) and $p=0.93$ for maximum point detection (PPG1)). This shows that the BBI values from both PPG1 and PPG2 accurately reflect the RRI values from the reference ECG signal. Additionally the reproducibility of the BBI values detected from PPG2 (Figure 8-3) and PPG1 (Figure 8-2) were similar, with RPCs of 0.05 seconds in each case and CVs of 2.7.

However there was a larger number of BBI values in Figure 8-3 from PPG2 ($n=28980$) than for PPG1 ($n=26720$) in Figure 8-2, which indicates that there were more correctly detected heartbeats in PPG2 than PPG1. The reproducibility of the BBIs from both PPG1 and PPG2 is reduced compared with the RRI values from the face ECG signal. The RPC value from the face ECG signal (0.03s) Figure 8-1 was 0.02 seconds lower than the RPC value (0.05s) from PPG1 and PPG2 in both Figure 8-2 and Figure 8-3. Additionally, there were more RRI values detected in the face ECG signal ($n=29410$) (Figure 8-1) than BBI values from PPG1 (26270) (Figure 8-2) and PPG2 (28980) (Figure 8-3) PPG signals. This suggests that the face ECG signal was able to more consistently provide HR data about the wearer of the Cardiomask.

8.2.2 Sensitivity of heartbeat identification

8.2.2.1 Effect of BBI correction algorithm

Table 8-2 shows the heartbeat detection sensitivity before and after BBI correction for each of the three signals at each stage (see Table 7-1 for stage information). In Table 8-3, the median percentage of falsely detected heartbeats before and after BBI correction for each of the three signals at each stage is presented.

Table 8-2 – Median (and IQR) heartbeat sensitivity before and after BBI correction algorithm applied to the heartbeats detected in the ECG and PPG signals.

	Stage 1 (Lying on back)	Stage 2 (Lying on left side)	Stage 3 (Lying on right side)	Stage 4 (Lying on back)	Stage 5 (CPAP on)	Stage 6 (Bi-level on)
ECG						
Before correction	98.01 (7.57)	97.76 (11.98)	95.39 (14.88)	97.03 (9.39)	99.52 (8.03)	98.86 (12.03)
After correction	98.09 (5.80)	98.09 (11.42)	95.47 (15.85)	97.24 (13.49)	99.69 (8.13)	98.60 (8.05)
PPG1						
Before correction	99.55 (2.51)	97.17 (4.98)	97.17 (7.79)	97.29 (7.47)	98.58 (8.21)	98.15 (30.14)
After correction	98.73 (5.69)	98.11 (14.51)	95.04 (54.58)	96.68 (9.31)	97.33 (15.42)	93.09 (51.34)
PPG2						
Before correction	100 (0.57)	99.07 (4.72)	99.01 (3.68)	98.97 (4.22)	99.02 (1.86)	97.83 (16.36)
After correction	100 (0.63)	99.04 (4.72)	96.01 (9.93)	97.89 (4.42)	99.11 (4.46)	96.34 (32.20)

* Difference between before and after correction ($p < 0.05$)

There was no significant difference between the heartbeat detection sensitivity from any of the signals before or after the RRI correction algorithm was applied. This result is similar to the results observed in the initial testing of the RRI correction algorithm, shown in Section 6.6.1. However, the range of sensitivity values (as indicated by the IQR values in Table 8-2) from different participants was greater for the corrected HR signals for all stages for the PPG signals.

Table 8-3 - Median (and IQR) percentage of falsely detected heartbeats before and after BBI correction algorithm applied to the heartbeats detected in the ECG and PPG signals.

	Stage 1	Stage 2	Stage 3	Stage 4	Stage 5	Stage 6
ECG						
Before correction	1.14 (1.90)	0.75 (3.17)	3.14 (8.77)	0.88 (3.76)	0.65 (1.85)	0.63 (8.89)
After correction	0.32 (0.41)*	0.00 (0.91)	0.47 (2.41)*	0.00 (0.80)*	0.00 (0.37)*	0.00 (0.86)
PPG1						
Before correction	0.86 (1.14)	1.04 (2.76)	1.61 (4.01)	1.24 (1.72)	1.11 (3.17)	7.39 (17.62)
After correction	0.36 (0.38)	0.53 (1.14)	0.65 (1.94)*	0.69 (0.86)	0.55 (0.68)*	1.65 (5.54)*
PPG2						
Before correction	0.34 (0.84)	1.28 (3.06)	2.68 (6.82)	0.73 (2.06)	1.19 (1.67)	6.48 (20.82)
After correction	0.32 (0.30)	0.77 (1.44)	0.32 (2.25)*	0.66 (0.76)	0.40 (0.58)*	1.43 (9.14)

* Difference between before and after correction ($p < 0.05$)

Table 8-3 show that the BBI correction algorithm made a significant improvement to the percentage of false positives in the BBI signal from the face ECG signal in all experiment stages except stages 2 and 6. Similarly the BBI correction algorithm was able to make a significant improvement to the percentage of false positives in the PPG1 and PPG 2 signals in stages 3 and 5. This demonstrates the ability of the correction algorithm to improve the accuracy of the BBI signals from the face ECG signal, without reducing the heartbeat sensitivity.

When the bi-level mode was activated on the PAP device (stage 6), the number of false positives that were detected in the PPG signal was significantly higher than other stages ($p=0.0037$ for PPG1 and $p=0.028$ for PPG2). This is likely due to the rapid change in pressure that characterises the bi-level mode. This change in pressure will change the force of the PPG sensor against the participant's skin, causing artefacts in the signal. An example of this artefact is shown in Figure 8-4, compared with a clean signal shown in Figure 8-5.

These artefacts can cause false positives to occur in the heartbeat detection of the PPG signal, especially for the maximum and minimum point detection methods.

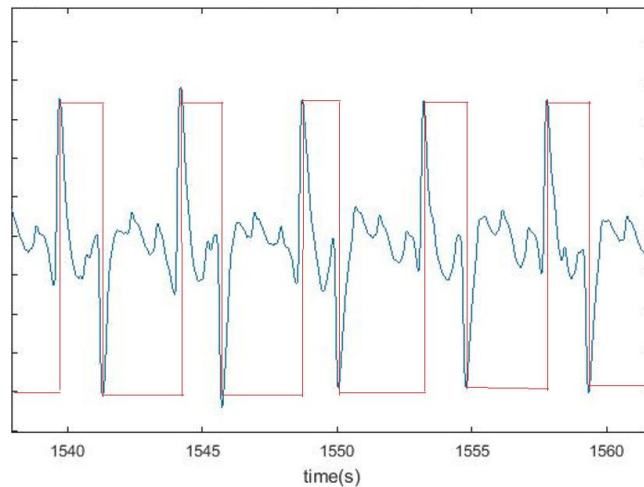


Figure 8-4-An example of the artefacts present in the PPG signal (blue) during bi-level mode (Stage 6) and the bi-level signal (red).

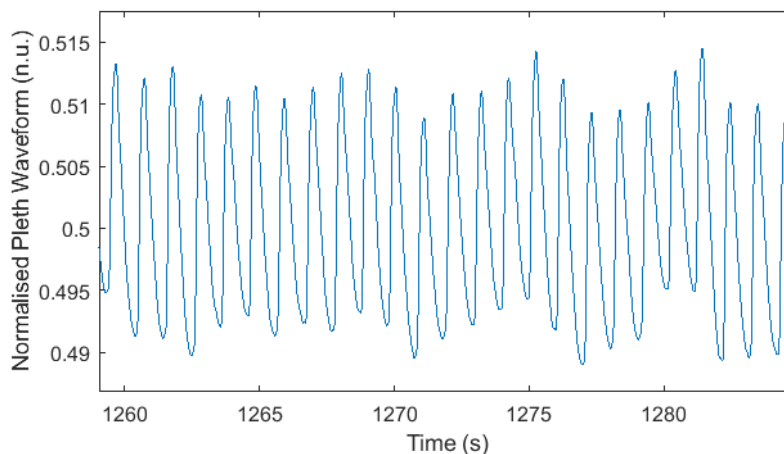


Figure 8-5 - An example of PPG signal free of artefacts. Signal was taken during the CPAP stage (stage 5)

8.2.2.2 Sensitivity after BBI correction algorithm applied

The results displayed in this section refer to the BBI signals and heartbeats after the BBI correction algorithm has been applied. Table 8-4 combines the results of Table 8-2 and Table 8-3 after correction.

There was no significant difference between the heartbeat detection sensitivity from the ECG and PPG signals ($p \geq 0.18$) in any stage. This suggests that after the BBI correction

algorithm was applied, the heartbeat detection algorithms on the ECG and PPG signals were similarly able to detect heartbeats for most of the participants.

However there was a significant difference in the median percentage of falsely detected heartbeats between the ECG signal and the PPG signal (PPG1 and PPG2) in stages 2, 4, 5 & 6 ($p=0.78$ (PPG1) and $p=0.88$ (PPG2) respectively). In stages 1 & 3 where there was no difference, participants were either lying on their back or right side. The percentage of false positives was significantly lower for the heartbeats from the ECG signal than from the PPG signals. The reason for this is not known, however it suggests that the quality of the measured face ECG signal was greater than the quality of the measured PPG signal.

Table 8-4 – Median (and interquartile range) sensitivity and percentage of falsely detected heartbeats in the ECG and PPG signals

	Stage 1	Stage 2	Stage 3	Stage 4	Stage 5	Stage 6
Sensitivity (%)						
ECG	98.09 (5.80)	98.09 (11.42)	95.47 (15.85)	97.24 (13.49)	99.69 (8.13)	98.60 (8.05)
PPG1	98.73 (5.69)	98.11 (14.51)	95.04 (24.58) ^α	96.68 (9.31)	97.33 (15.42)	93.09 (51.34)
PPG2	100 (0.63)	99.04 (4.72) ^α	96.01 (9.93) ^α	97.89 (4.42)	99.11 (4.46)	96.34 (32.20)
Falsely detected heartbeats (%)						
ECG	0.32 (0.41)	0.00 (0.91) ^α	0.47 (2.41)	0.00 (0.80)	0.00 (0.37)	0.00 (0.86)
PPG1	0.36 (0.38)	0.53 (1.14) [*]	0.65 (1.94)	0.69 (0.86) [*]	0.55 (0.68) [*]	1.65 (5.54) [*]
PPG2	0.32 (0.30)	0.77 (1.44) ^{*α}	0.32 (2.25)	0.66 (0.76) [*]	0.40 (0.58) [*]	1.43 (9.14) ^{* †}

* Difference compared to ECG heartbeats ($p<0.05$)

† Difference between stages 5 and 6 ($p<0.05$)

^α Different to Stage 1 ($p<0.05$)

In Figure 8-4 it was shown that the change in pressure during the bi-level mode creates motion artefacts. These motion artefacts affect the sensitivity in the PPG signals. This can be seen in Figure 8-6, where the range of the sensitivity values is larger during stage 6 than all other stages. Similarly in Figure 8-7, the range of false positives in the PPG signal is larger in stage 6 than other experiment stages. The reason that the range is affected more

than the median values, is that for participants with good quality PPG signals, if the signal quality is slightly reduced by motion artefacts, the signal quality is still good enough for consistent and accurate heartbeat detection, similar to the other experiment stages. However for a participant with an average or poor PPG signal, the reduction in signal quality will reduce the sensitivity and increase the number of false positives.

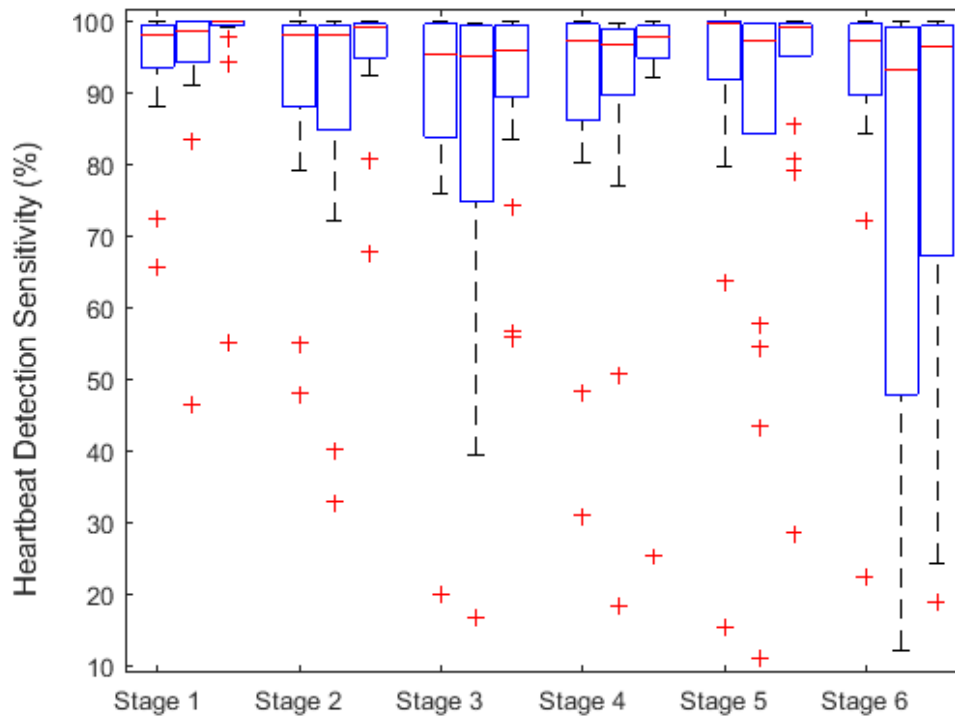


Figure 8-6 - Sensitivity of the ECG signal (left) PPG1 (centre) and PPG2 (right)

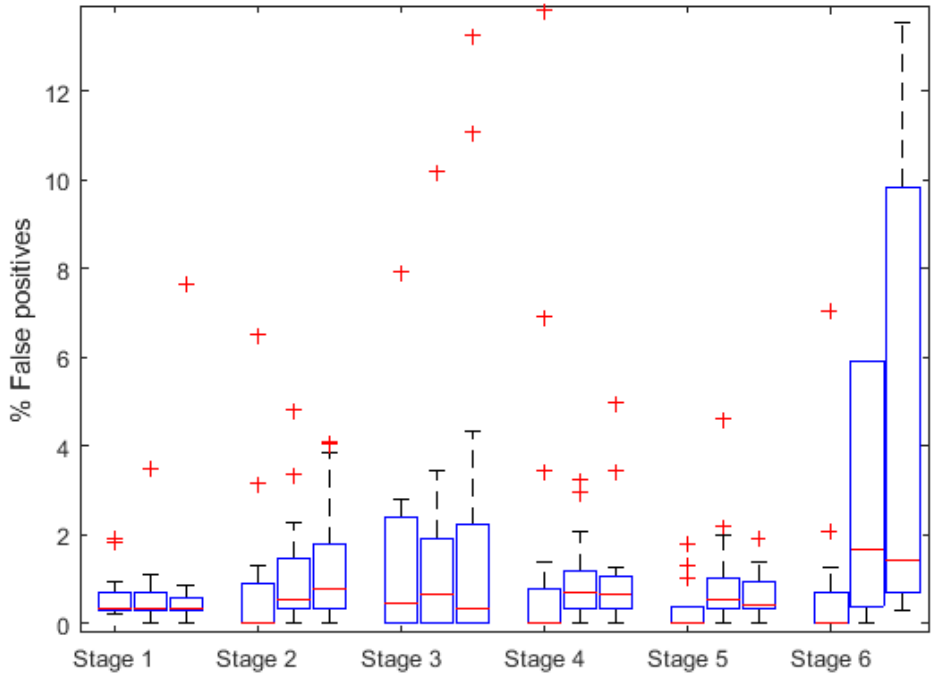


Figure 8-7 - % of falsely detected heartbeats from the ECG signal (left), PPG1 (centre) and PPG2 (right)

8.2.3 HR window comparison

The BA plots comparing the mean HR values from the face ECG and PPG signals to the mean HR values from the reference ECG signal are shown in sections 8.2.3.1-8.2.3.3 and are summarised in Table 8-5 and Table 8-6.

8.2.3.1 Face ECG

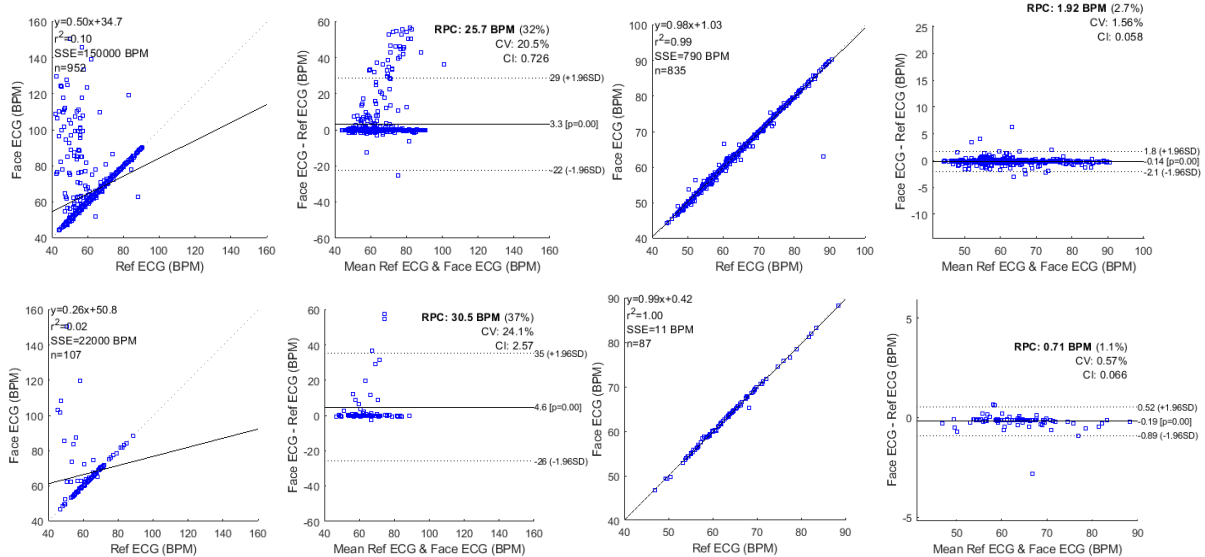


Figure 8-8 – BA plots for the mean HR estimation from the face ECG signal compared to the mean HR from the reference ECG signal. Figures on the left indicate the mean HR values before corrupted mean HR values were removed and figures on the right are after these values were removed. The window length for the top and bottom figures was 30 seconds and 5 minutes respectively

8.2.3.2 PPG1

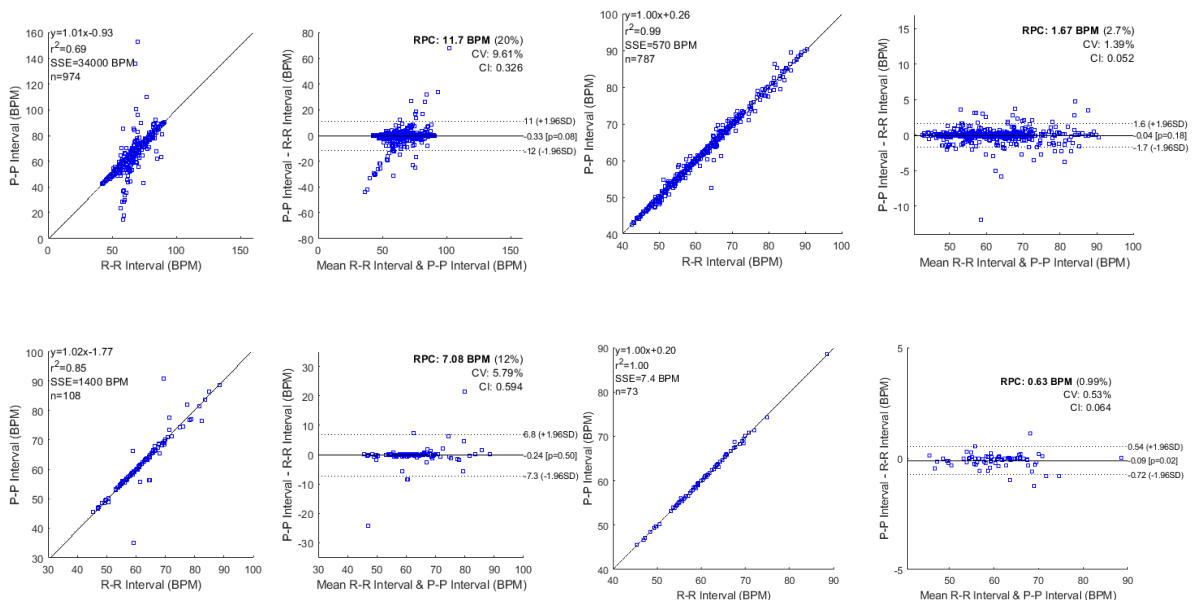


Figure 8-9 - BA plots for the mean HR estimation from PPG1 heartbeats compared to the mean HR from the reference ECG signal. Figures on the left indicate the mean HR values before corrupted mean HR values were removed and figures on the right are after these values were removed. The window length for the top and bottom figures was 30 seconds and 5 minutes respectively

8.2.3.3 PPG2

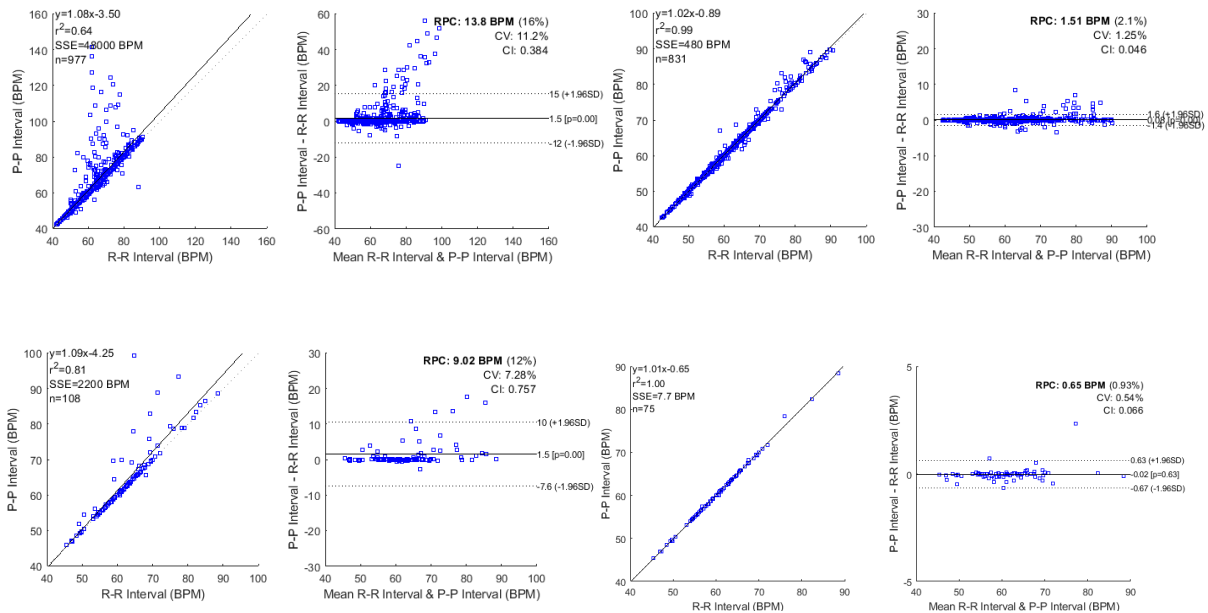


Figure 8-10 - BA plots for the mean HR estimation from PPG2 heartbeats compared to the mean HR from the reference ECG signal. Figures on the left indicate the mean HR values before corrupted mean HR values were removed and figures on the right are after these values were removed. The window length for the top and bottom figures was 30 seconds and 5 minutes respectively

8.2.3.4 BA plot summary

Table 8-5 and Table 8-6 show information on the accuracy and repeatability of the mean HR measurements. The accuracy is shown by the mean difference and the R² values, and the repeatability is shown by the RPC and CV values. As mentioned in the previous chapter windows that are classified as containing inaccurate HR values were discarded, to reduce the error of the mean HR estimations. This means that if the HR values from a particular signal are consistently poor, more HR windows will be discarded. Hence the number of remaining or 'good' windows are also displayed in Table 8-5 and Table 8-6 as well as a percentage of good windows amongst the total number of windows.

Table 8-5 - Comparison of the mean HR values from the face ECG and PPG HR signal over 30 second windows before and after bad HR values were discarded

Before or after	ECG		PPG1		PPG2	
	Before	After	Before	After	Before	After
RPC (CI)	25.7 (0.726)	1.92 (0.058) [^]	11.7 (0.326)	1.76 (0.055) [^]	13.8 (0.384)	1.54 (0.046) [^]
CV (%)	20.5	1.56	9.61	1.47	11.2	1.25
Mean difference	3.3 (p<0.005) †	-0.14 (p<0.005) †	-0.33 (p=0.08)	-0.04 (p=0.17)	1.5 (p<0.005) †	0.08 (p=0<0.005) †
R ²	0.1	0.99	0.69	0.99	0.64	0.99
N of intervals (% kept)	952	835 (87.7%)	974	793 (81%)	977	831 (85.0%)

[^] Significant reduction in RPC value (p<0.05)
[†] mean difference not equal to 0: (p < 0.05)

Table 8-6- Comparison of the mean HR values from the face ECG and PPG HR signal over 5 minute windows

Before or after	ECG		PPG1		PPG2	
	Before	After	Before	After	Before	After
RPC (CI)	30.5 (2.57)	0.7 (0.068) [^]	7.08 (0.594)	0.63 (0.064) [^]	9.02 (0.757)	0.65 (0.066) [^]
CV (%)	24.1	0.56	5.79	0.53	7.28	0.54
Mean difference	4.6 (p<0.005) †	-0.24 (p<0.005) †	-0.24 (p=0.5)	-0.09 (p=0.02) †	1.5 (p<0.005) †	-0.02 (p=0.63)
R ²	0.02	0.99	0.88	0.99	0.81	0.99
N of intervals (% kept)	107	80 (74.7%)	108	73 (66.7%)	108	75 (70.4%)

[^] Significant reduction in RPC value (p<0.05)
[†] mean difference not equal to 0: (p < 0.05)

8.2.3.5 Analysis and Discussion

Table 8-5 and Table 8-6 show that the algorithm for classifying and removing bad HR windows is able to increase the accuracy of the estimation of the mean HR values for both 5 minute and 30 second windows. This is shown by the increase in R² values and the large reduction in the mean difference values in all cases. After bad windows were removed, the mean difference for all HR estimations was < 0.25 BPM. Additionally, there was a significant reduction in all RPC values after bad HR windows were removed, as well as reduction in the CV values. In sections 8.2.3.1-8.2.3.3 the BA plots (Figure 8-8, Figure 8-9 and Figure 8-10) show that most of the outlier mean HR values present before bad windows are discarded (left column) are not present in the corrected mean HR values (right column). Since the outlier values are removed, the repeatability of the mean HR estimations is increased.

The largest difference between the different HR signals (ECG, PPG1 and PPG2) occurred in the number of HR windows that were kept and not discarded. For the HR windows from the ECG signal, Table 8-5 and Table 8-6 show that approximately 88% of 30 second windows and 75% of 5 minute intervals were kept which is larger than the percentage of windows kept for the PPG HR windows (81% and 85% for 30 second intervals and 67% and 70% for 5

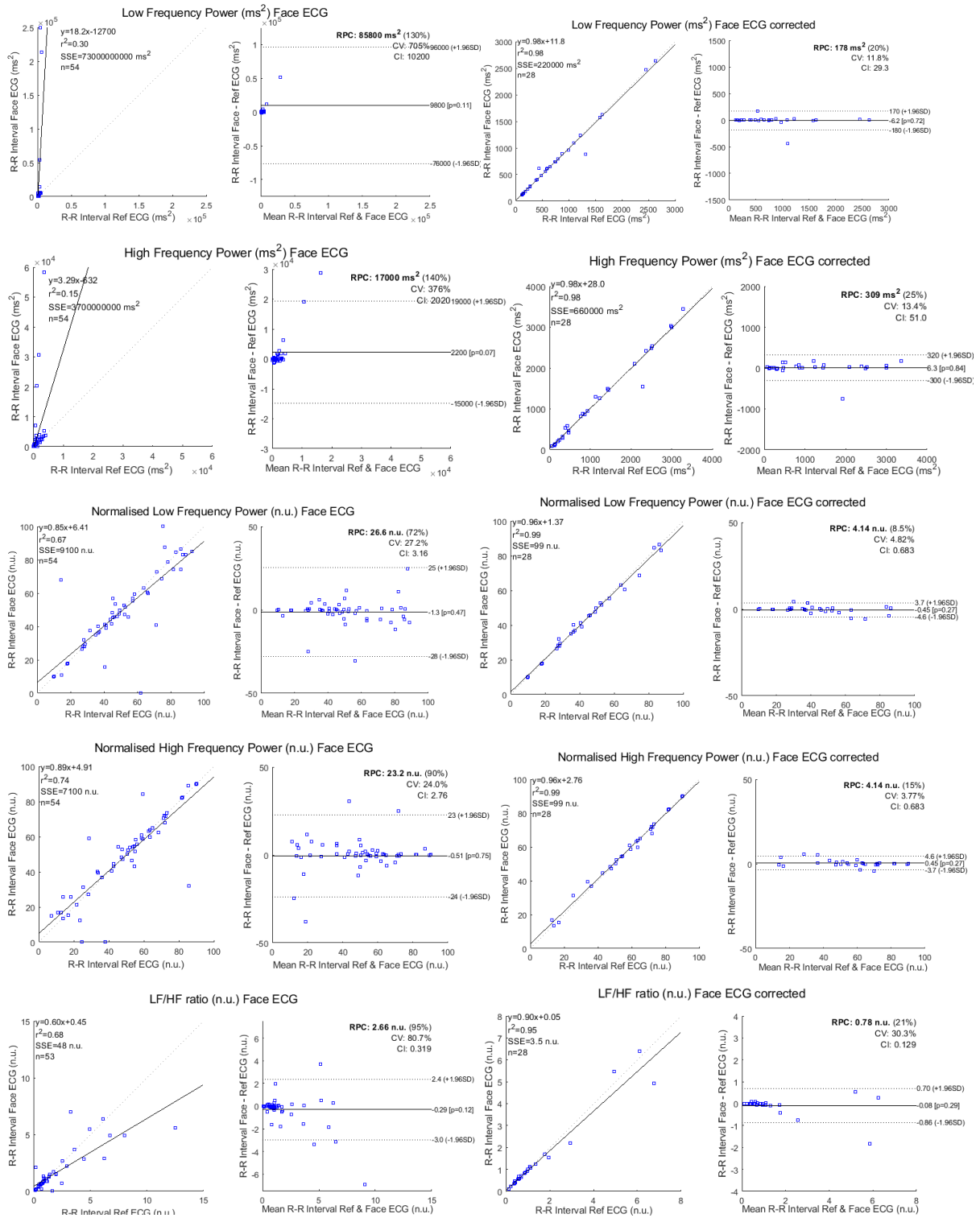
minute windows for PPG1 and PPG2 respectively). This means that the HR windows from the ECG signal met the requirements for a 'good' window more often than the windows from the PPG signal which is probably a result of the lower number of false positive heartbeats detected (Figure 8-7). Table 8-5 and Table 8-6 also show that an accurate mean HR estimation could not be achieved using either the ECG or PPG signal independently for every window, and that future work could focus on combining the ECG and PPG signal to achieve a consistent and accurate HR values.

8.2.4 HRV analysis

BA plots comparing the HRV analysis results from the face ECG and PPG signals to the HRV analysis results from the reference ECG are shown in sections 8.2.4.1-8.2.4.3 and are discussed in section 8.2.4.4.

HRV analysis results are from experiment stages 1 and 5 only for all participants. Stages 2, 3 and 4 were excluded from HRV analysis because the HR during these stages was affected by the participants moving. HRV analysis during stage 6 was excluded for PPG1 and PPG2, as Figure 8-6 and Figure 8-7 show that accuracy of the PPG1 and PPG2 heartbeat detection was significantly decreased during this stage, and hence HRV analysis from PPG1 and PPG2 from this stage would be inaccurate.

8.2.4.1 Face ECG



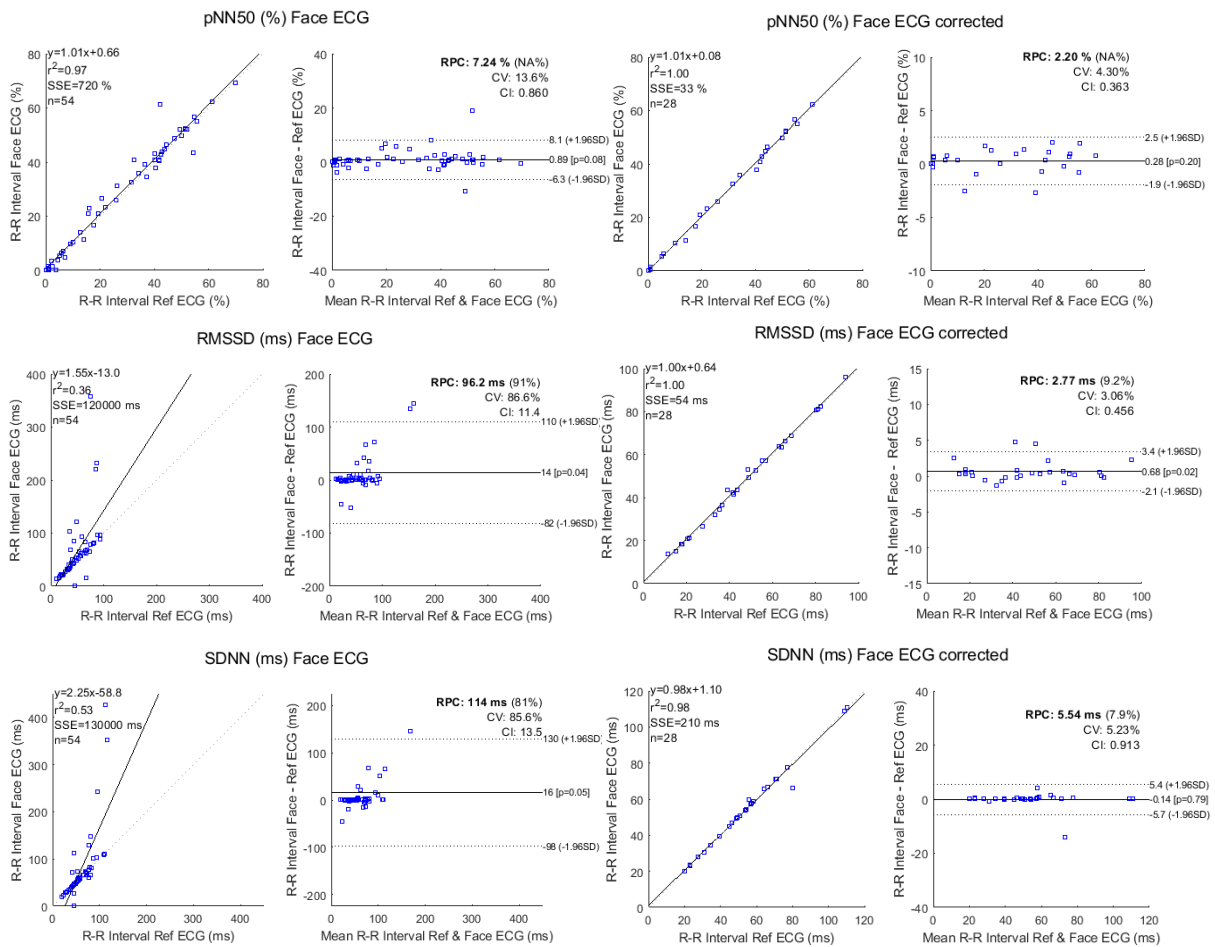


Figure 8-11 - BA plots for different HRV variables from BBI signals from the face ECG signal before (left) and after (right) bad HRV windows are removed.

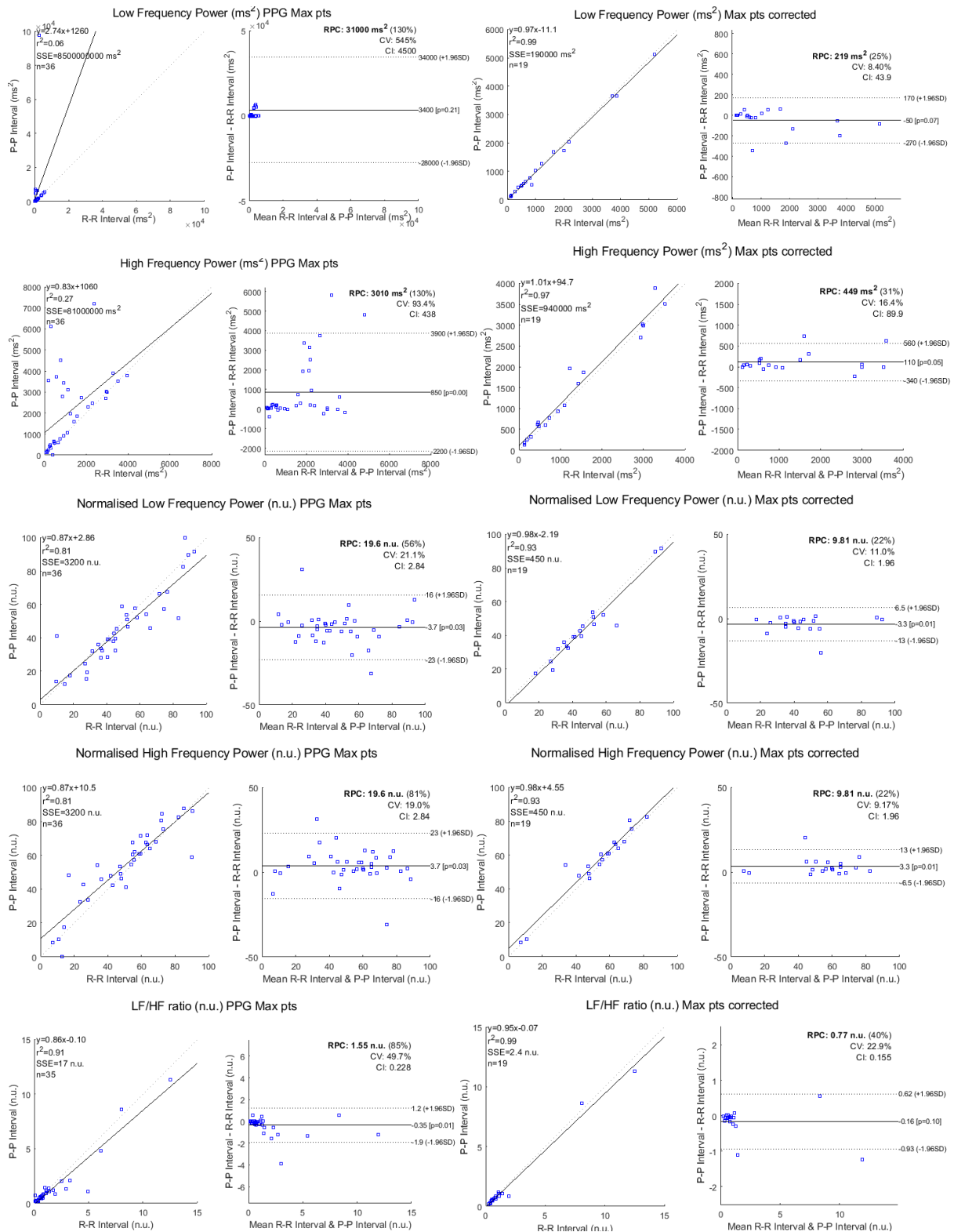
Table 8-7 - The variables from the BA plot for HRV variables from the ECG HR before (n = 54) and after (n = 28) the stages were analysed to remove stages with corrupted BBIs

HRV variable	Before or after stages removed	RPC (CI)	CV (%)	Mean difference	R ²
LF (ms ²)	Before	85800 (10200)	705	9800 (p=0.11)	0.3
	After	178 (29.3)	11.8	-6.2 (p=0.72)	0.98
HF (ms ²)	Before	17000 (2020)	376	2200 (p=0.07)	0.15
	After	309 (51.0)	13.4	6.3 (p=0.84)	0.98
LF n.u.	Before	26.6 (3.16)	27.2	- 1.3 (p=0.47)	0.67
	After	4.14 (0.683)	4.82	-0.45 (p=0.27)	0.99
HF n.u.	Before	23.2 (2.76)	24	- 0.51 (p=0.75)	0.74
	After	4.14 (0.683)	3.77	0.45 (p=0.27)	0.99
LF/HF (n.u.)	Before	2.66 (0.319)	80.7	-0.29 (p=0.12)	0.68
	After	0.78 (0.129)	30.3	-0.08 (p=0.29)	0.95
pNN50 (%)	Before	7.24 (0.860)	13.6	0.89 (p=0.08)	0.97
	After	2.2 (0.363)	4.3	0.28 (p=0.20)	0.99
RMSSD (ms)	Before	96.2 (11.4)	86.6	14 (p=0.04) †	0.36
	After	2.77 (0.456)	3.06	0.68 (p=0.02)	0.99
SDNN (ms)	Before	114 (13.5)	85.6	16 (p=0.05) †	0.53
	After	5.54 (0.913)	5.23	-0.14 (p=0.79)	0.98

^ Significant reduction in RPC value (p<0.05)

† mean difference not equal to 0: (p < 0.05)

8.2.4.2 PPG1



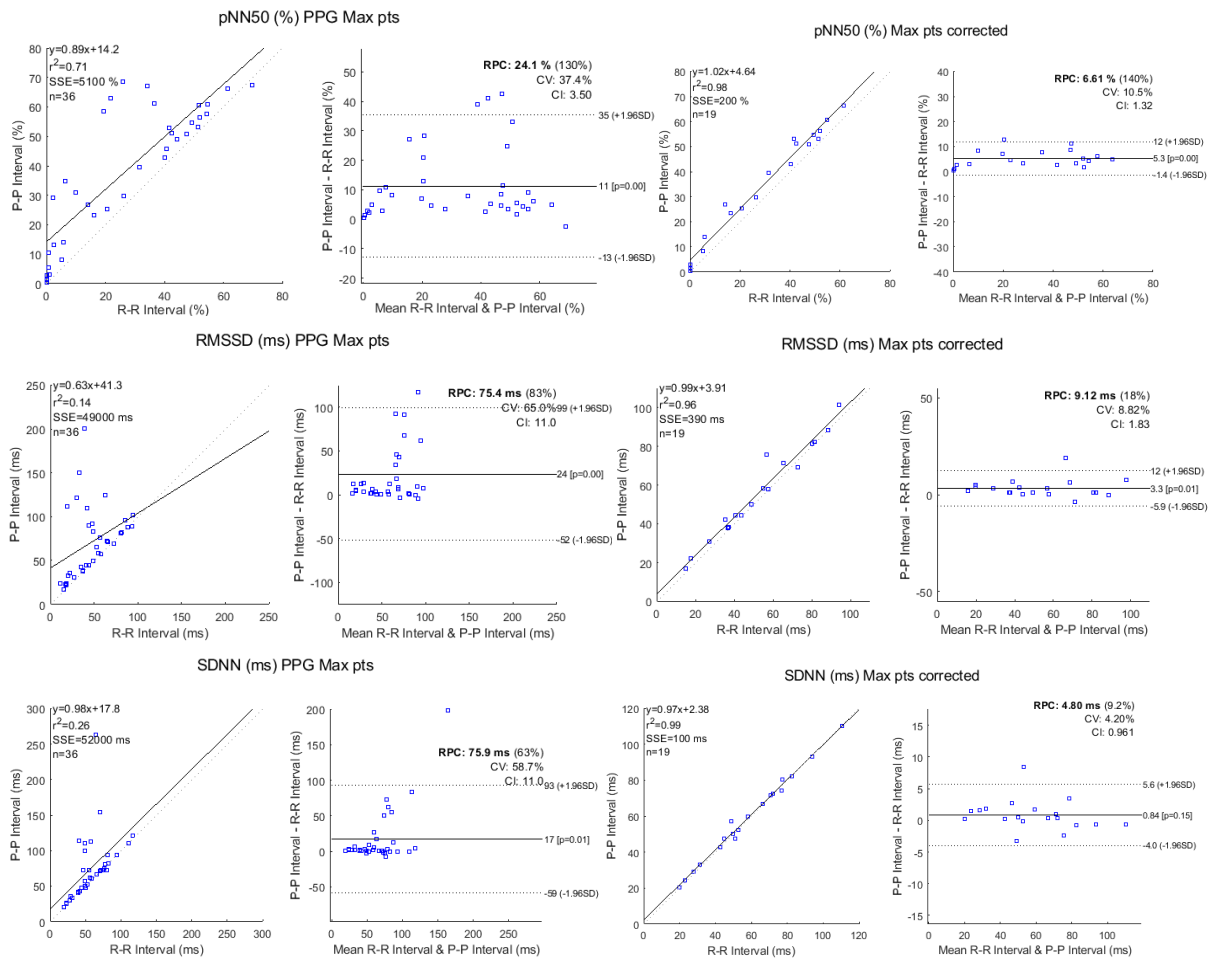


Figure 8-12 - BA plots for different HRV variables from BBI signals from PPG1 before (left) and after (right) bad HRV windows are removed.

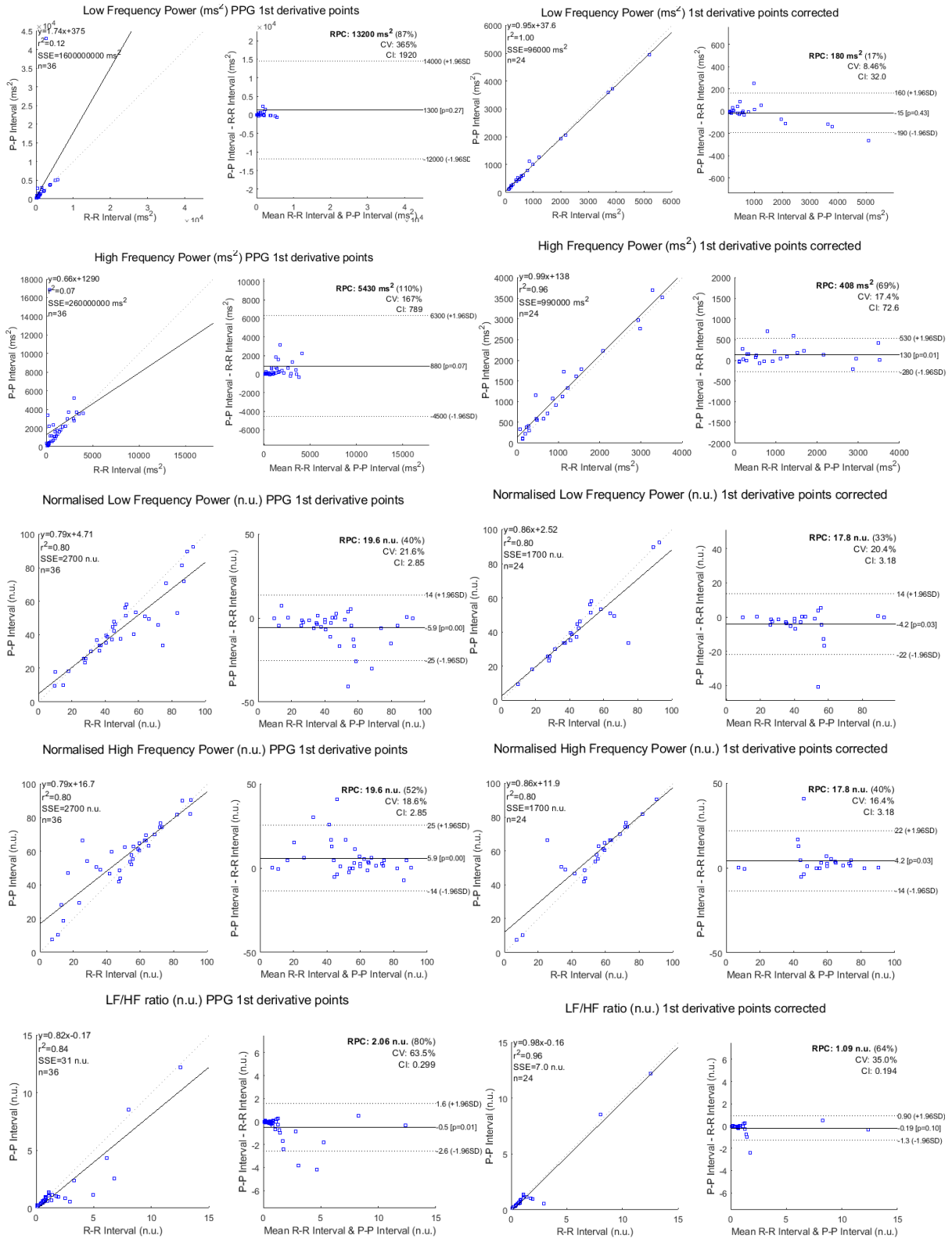
Table 8-8 - The variables from the BA plot for HRV variables from PPG1 before (n = 36) and after (n = 19) the stages were analysed to remove stages with corrupted BBIs

HRV variable	Before or after stages removed	RPC (CI)	CV (%)	Mean difference	R ²
LF (ms ²)	Before	31000 (4500)	545	3400 (p=0.21)	0.06
	After	219 (43.9)	8.4	-53 (p=0.04) †	0.99
HF (ms ²)	Before	3010 (438)	93.4	850 (p<0.005) †	0.27
	After	449 (89.9)	16.4	110 (p=0.05) †	0.97
LF n.u.	Before	19.6 (2.84)	21.1	-3.7 (p=0.03) †	0.81
	After	9.81 (1.96)	11.0	-3.3 (p=0.01) †	0.93
HF n.u.	Before	19.6 (2.84)	19	3.7 (p=0.03) †	0.81
	After	9.81 (1.97)	9.17	3.3 (p=0.01) †	0.93
LF/HF (n.u.)	Before	1.55 (0.228)	49.7	-0.35 (p=0.01) †	0.91
	After	0.77 (0.155)	22.9	-0.16 (p=0.10)	0.99
pNN50 (%)	Before	24.1 (3.5)	37.4	11 (P<0.005) †	0.71
	After	6.61 (1.32)	10.5	5.3 (P<0.005) †	0.98
RMSSD (ms)	Before	75.4 (11)	65.0	24 (P<0.005) †	0.14
	After	9.12 (1.83)	8.82	3.3 (P=0.01) †	0.96
SDNN (ms)	Before	75.9 (11.0)	58.7	17 (P=0.01) †	0.26
	After	4.80 (0.961)	4.2	0.84 (P=0.15)	0.99

^ Significant reduction in RPC value (p<0.05)

† mean difference not equal to 0: (p < 0.05)

8.2.4.3 PPG2



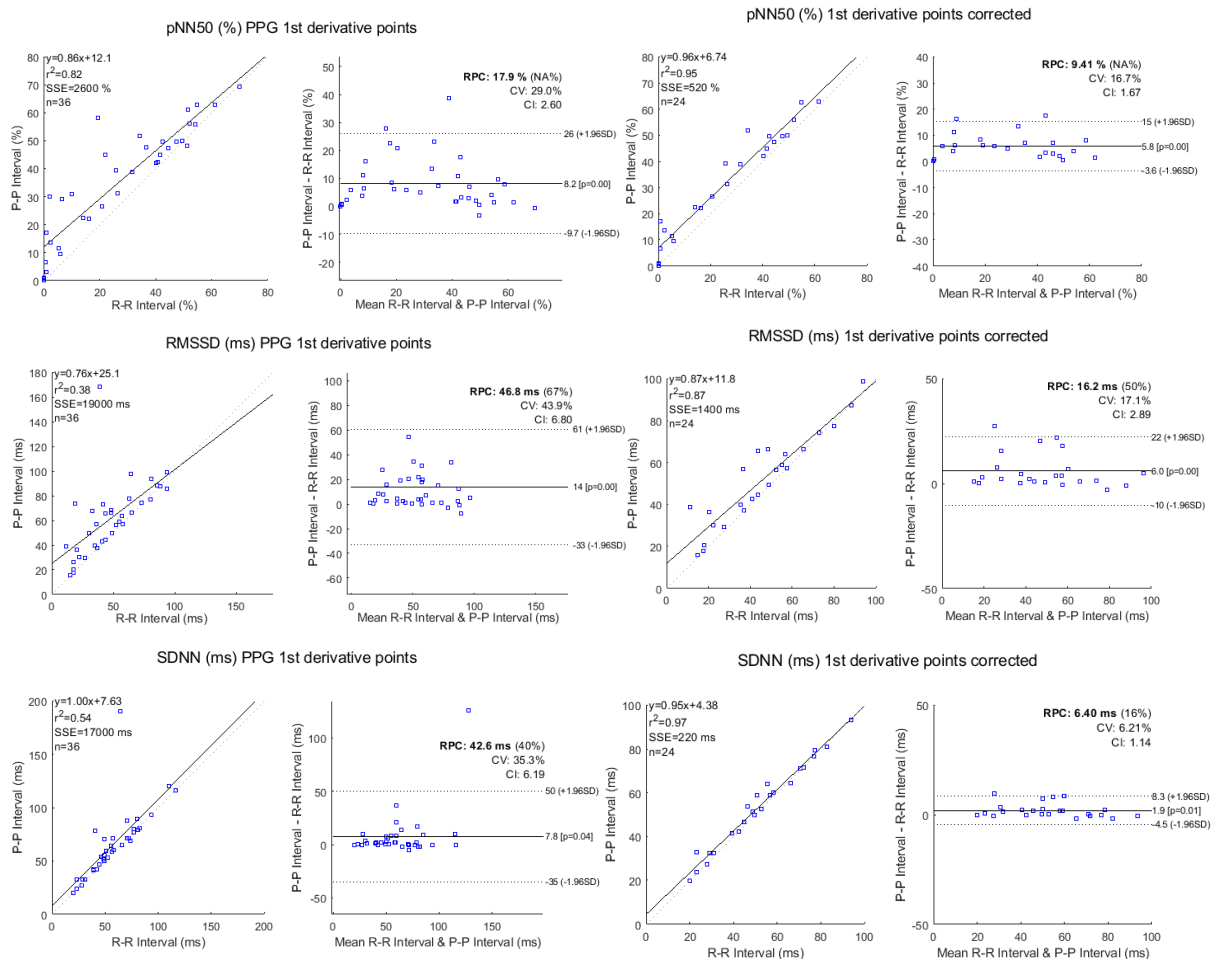


Figure 8-13 - BA plots for different HRV variables from BBI signals from PPG2 before (left) and after (right) bad HRV windows are removed.

Table 8-9 - The variables from the BA plot for HRV variables from PPG2 before (n = 36) and after (n = 24) the stages were analysed to remove stages with corrupted BBIs

HRV variable	Before or after stages removed	RPC (CI)	CV (%)	Mean difference	R ²
LF (ms ²)	Before	13200 (1920)	365	1300 (p=0.27)	0.12
	After	180 (32.0)	8.46	-15 (p=0.46)	0.99
HF (ms ²)	Before	5430 (790)	167	880 (p=0.07)	0.07
	After	408 (72.6)	17.4	130 (p=0.01) †	0.96
LF n.u.	Before	19.6 (2.85)	21.6	-5.9 (p<0.005) †	0.8
	After	17.8 (3.18)	20.4	-4.2 (p=0.03) †	0.8
HF n.u.	Before	19.6 (2.86)	18.6	5.9 (p<0.005) †	0.8
	After	17.8 (3.18)	16.4	4.2 (p=0.03) †	0.8
LF/HF (n.u.)	Before	2.06 (0.299)	63.5	-0.5 (p=0.01) †	0.84
	After	1.09 (0.194)	35	-0.19 (p=0.1)	0.96
pNN50 (%)	Before	17.9 (2.6)	29	8.2 (p<0.005) †	0.82
	After	9.41 (1.67)	16.7	5.8 (P<0.005) †	0.95
RMSSD (ms)	Before	46.8 (6.8)	43.9	14 (P<0.005) †	0.38
	After	16.2 (2.89)	17.1	6 (P<0.005) †	0.87
SDNN (ms)	Before	42.6 (6.19)	35.3	7.8 (P=0.04) †	0.53
	After	6.40 (1.14)	6.21	1.9 (P=0.01) †	0.97

^ Significant reduction in RPC value (p<0.05)

† mean difference not equal to 0: (p < 0.05)

8.2.4.4 Analysis and Discussion

When BBI windows containing a large number of corrupted heartbeats are discarded, HRV analysis could be performed accurately using the BBI values from the face ECG signal and the PPG signal. This is shown by the low relative error values in Figure 8-14 as well as by the low mean difference and high R squared values in the “after” rows in Table 8-7, Table 8-8 and Table 8-9. Additionally, in these tables, the CV values and RPC values are all lower

than the CV and standard deviation values for the range of HRV for a healthy population [205].

The increase in accuracy when corrupted heartbeats were discarded can be seen in the BA plots in Figure 8-11 to Figure 8-13, where initially (left) although most of the HRV values are close to their respective reference value from the reference ECG, there are several outliers that increase the reproducibility coefficient and reduce the R squared value. However, when these points are removed (right) only the accurate HRV values remain and the reproducibility coefficient reduces and the R squared value increases, and hence the accuracy and repeatability of the HRV analysis increases.

Although the accuracy of the HRV analysis was increased by discarding HR signals that were classified as inaccurate, this reduced the number of windows where HRV analysis was performed. This was true for both the ECG signal, in which the number of windows were reduced from 54 to 28, and for the PPG signal in which the 36 windows were reduced to 19 and 24 for PPG1 and PPG2 analyses respectively. This means that when the ECG and PPG signal information was used independently, accurate HRV analysis was not possible for every window analysed and hence not possible in every experiment stage. Work in chapter 9 will look at combining the data from the ECG and PPG signal to increase the consistency of the HRV analysis.

A bias was seen (i.e. a mean difference not equal to zero) in many of the HRV values calculated from the PPG signal, when compared with the HRV values from the reference ECG signal, but not for the HRV values from the face ECG signal. This is shown by the large number of mean difference values that were significantly different from zero shown in Table 8-8 and Table 8-9 and is true for the HR signals taken from both PPG1 and PPG2. The HF (normalised and absolute), pNN50, RMSSD and SDNN values from the PPG signal had a positive mean difference compared with the reference values, and the LF/HF values and

normalised LF had a negative mean difference compared to their respective reference values. The reason this bias occurs in only the PPG signal is possibly due to the sources of variability from the PPG sensor described in section 4.2, including variability in the blood flow from the heart to the PPG sensor location, in this case the forehead. Any variability in the conduction element of the cardiovascular system would also be reflected in the PPG signal and HRV analysis of the PPG.

The HRV values from the face ECG signal had a lower error than the HRV variables from the PPG signal, regardless of the fiducial point used in the PPG signal. As well as the lower mean difference values in Table 8-7, Table 8-8 and Table 8-9, this is shown in Figure 8-14 by comparing the error of the HRV values that were not rejected, with the reference HRV values. A Kruskal-Wallis H test showed that for all stages there was a statistically significant difference between the HRV errors from the face ECG signal and the HRV errors from the PPG signal ($p \leq 0.03$). The larger error for the HRV analysis from the PPG1 and PPG2 heartbeats is probably caused by the larger number of false positives detected in the PPG signal using these methods, as well as the bias in the HRV values from the PPG signal.

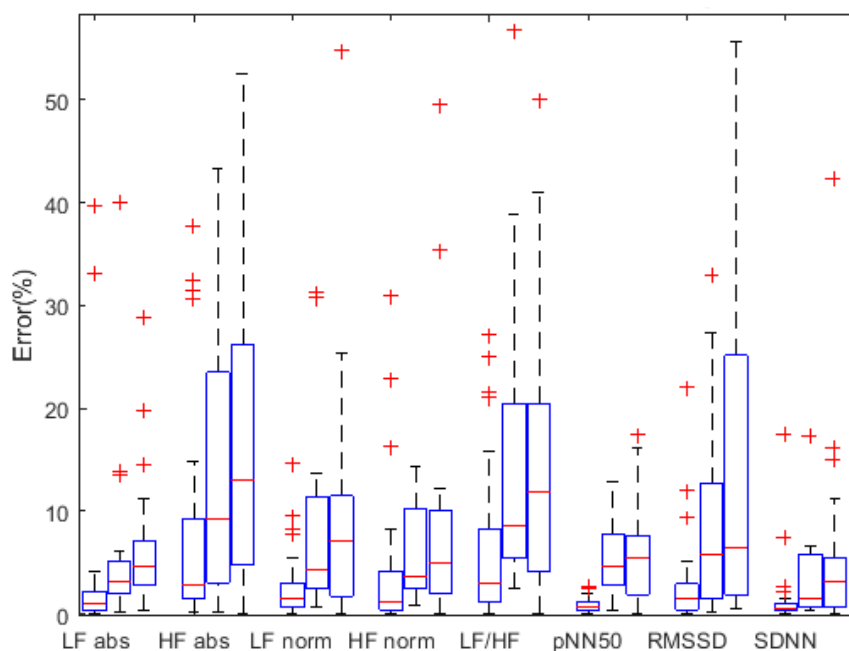


Figure 8-14- % error of the HRV variables from the face ECG (left) heartbeats, PPG1 (centre) and PPG2 (right)

When the corrupted HR stages were removed from HRV analysis, the errors of the HRV analysis from the PPG1 and PPG2 heartbeats were not significantly different, as shown in Figure 8-14 ($p < 0.05$). This suggests that the fiducial point that is used for a PPG signal measured from the forehead does not make a significant difference to the HRV accuracy. However this result is only true for the HR signals after the corrupted HR signals have been removed from HRV analysis, as the HRV error from the PPG1 heartbeats was significantly larger than the error for the PPG2 heartbeats before the corrupted HR values were removed (Table 8-8 and Table 8-9).

The error for the absolute HF, the LF/HF and the RMSSD values were the largest compared with the other HRV variables, for the HRV variables from both the face ECG and PPG signals. This is shown in Figure 8-14 and is possibly a result of the HR correction algorithm. The stages that have been accepted for HRV analysis (stages 1 and 5) did not have large numbers of heartbeats missing. Thus there would have been relatively few subsequent corrections to the HR for these stages. Corrections to a small number of heartbeats would most likely affect the HF and RMSSD components more than other variables, as they relate more to the short term variability between HRs, and less about the overall HR trends. This error in the HF values would also affect the accuracy of the LF/HF ratio similarly.

8.2.5 ECG signal quality

The results for the ECG signal quality measures are displayed in this section. The signal quality metrics that are discussed are the ECG correlation methods, and the SNR estimations using the range and the RMS values.

8.2.5.1 Correlation of ECG signals

The correlation values between the reference and face ECG signal, as well as between the reference and modified face ECG signals (R-peaks removed) and to random noise that were described in section 7.5.1 are shown in Figure 8-15. Figure 8-15 shows good correlation between the ECG signal measured from the face and the reference ECG signal in each stage. When the participants were lying on their side (stage 2 and 3) the correlation values

for the normal and modified face ECG signals were significantly lower than when they were lying on their back (stage 1 and 4) ($p < 0.0013$). This is likely because the RMS noise was larger (Section 8.2.5.3) when the participants were lying on their side than any other experimental stage as shown in Figure 8-22.

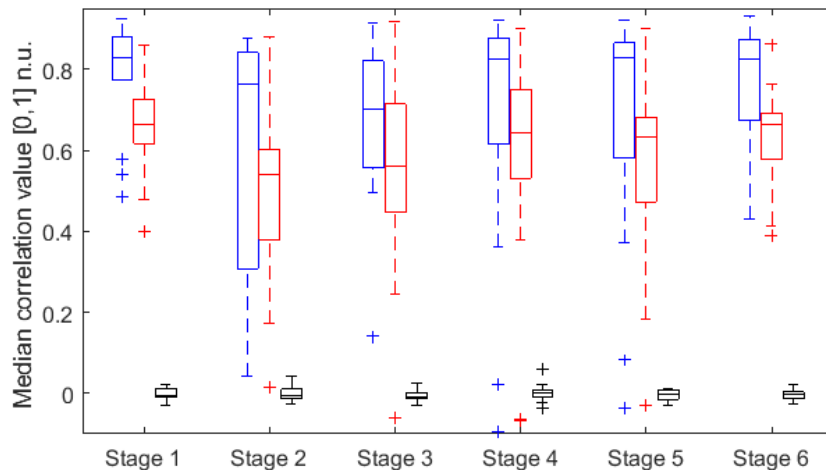


Figure 8-15-Median correlation values for each heartbeat between the face ECG and the reference ECG (blue), and with QRS complexes removed (red), and correlation of reference ECG signal with random noise (black)

When the QRS complexes were removed from the ECG signals the correlation values were significantly reduced ($p < 0.017$). However the correlation values when the QRS complexes were removed were still greater than when the reference ECG signal was correlated with random noise. This shows that the other features of the ECG signal apart from the QRS complex are present in the ECG signal measured from the face, even if they are not as clear and distinct as in the reference ECG signal.

The wide range of correlation values in Figure 8-15 show a large inter-patient variability in the ECG signal quality. For some participants the face ECG signal was of a good quality and the P and T waves could be easily identified, as shown in Figure 8-16. For others the ECG signal components were much less distinct as shown in Figure 8-17.

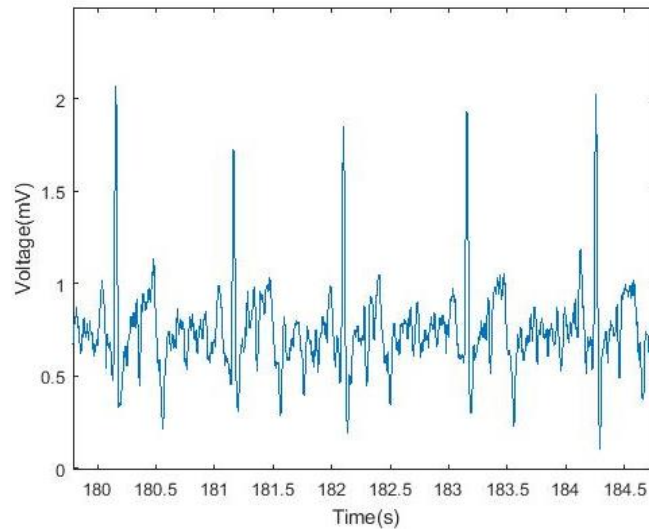


Figure 8-16 - An example of a higher quality ECG signal measured from SS electrodes located on the face and neck

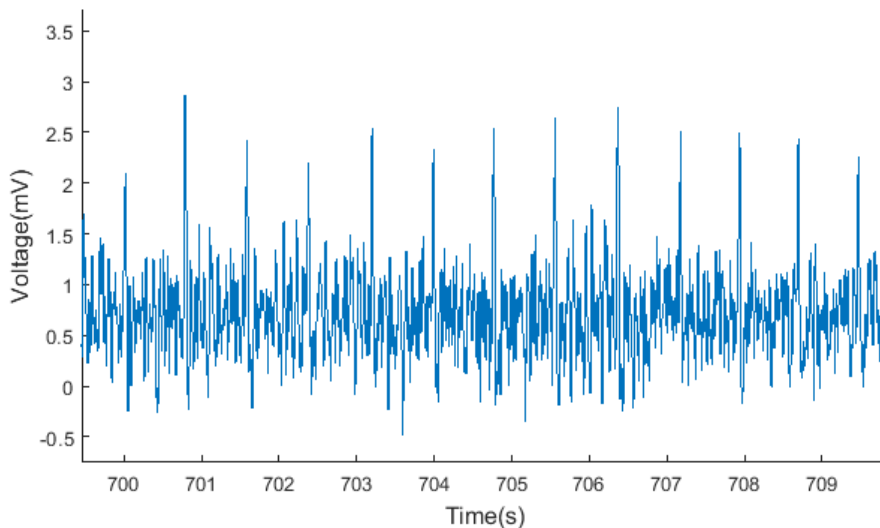


Figure 8-17 - An example of a lower quality ECG signal measured from SS electrodes located on the face and neck

8.2.5.2 SNR-range

When the participants were lying on their back (stages 1, 4, 5, and 6) the voltage range of the signal and noise components were significantly less in the face ECG signal than the reference ECG signal, as shown in Figure 8-18 and Figure 8-19. Additionally, Figure 8-20 shows the ratio of the QRS complex magnitude to the range of the rest of the ECG signal was significantly smaller in the face ECG signal compared to the reference ECG signal for all stages. Notably, $p=0.0481$ for stage 2, but $p \leq 0.004$ for other stages. Since there is a reduced magnitude of the R peak and a smaller difference in range between the signal and

noise components, this could potentially lead to a reduction in the accuracy of the heartbeat detection for the face ECG signal, as the R peaks are not as easily identifiable.

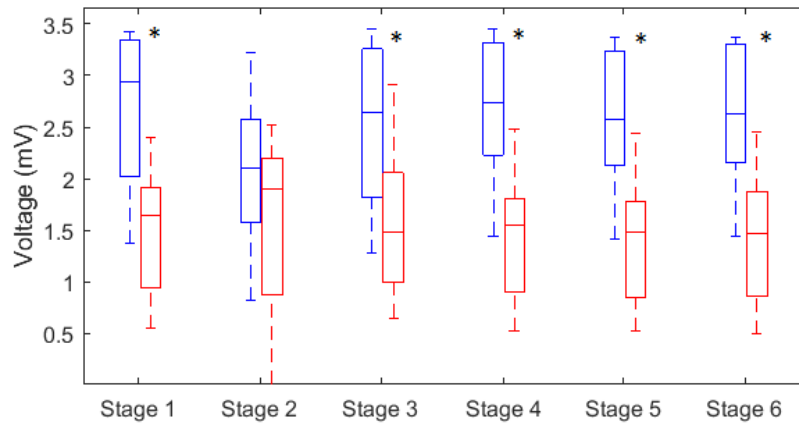


Figure 8-18 – The median voltage range of the signal component of the Reference ECG signal (blue) and the Face ECG signal (red) for each experiment stage. * indicates significant difference between values for face and reference ECG signals ($p < 0.05$).

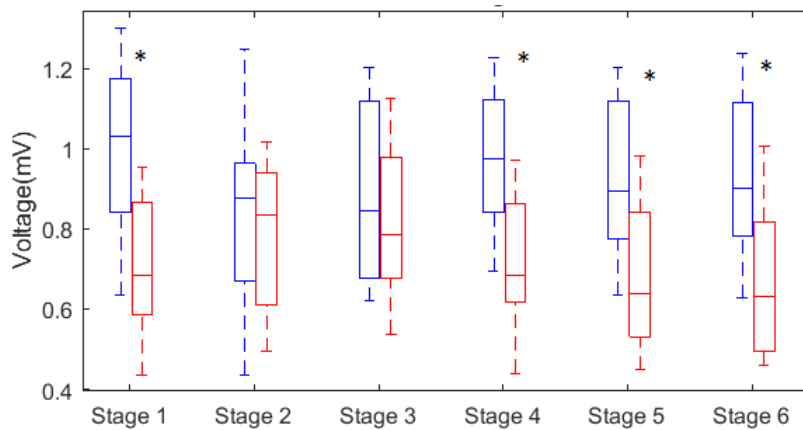


Figure 8-19 - The median voltage range of the noise component of the Reference ECG signal (blue) and the Face ECG signal (red) for each experiment stage. * indicates significant difference between values for face and reference ECG signals ($p < 0.05$).

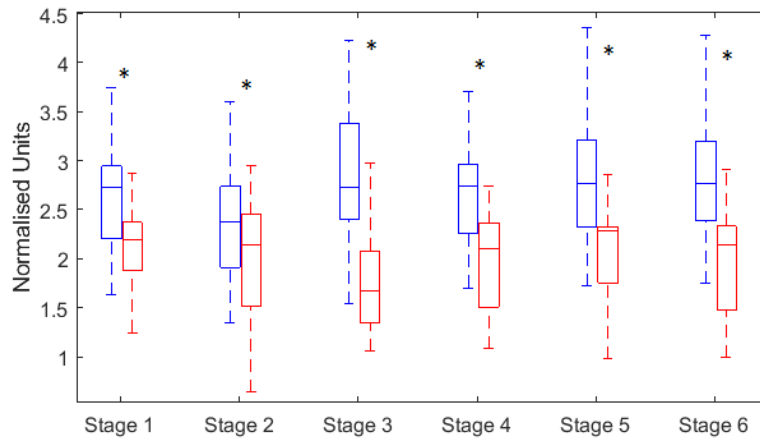


Figure 8-20-SNR (based on range of values in “signal” and “noise” windows) for Reference ECG signal (blue) and the Face ECG signal (red) for each experiment stage. * indicates significant difference between values for face and reference ECG signals ($p < 0.05$).

8.2.5.3 SNR-RMS

Figure 8-21 and Figure 8-22 shows the average RMS values for the “signal” and “noise” components of the ECG signal respectively. Figure 8-22 shows that the average RMS values for the noise components are significantly larger for the face ECG signal than the reference ECG signal. As mentioned in chapter 5, a larger level of amplification is needed to observe an ECG signal from the face than from more traditional electrode locations, leading to the increased noise levels. This increase in the average noise RMS value may lead to an increased difficulty in identifying heartbeats and other features of the ECG signal.

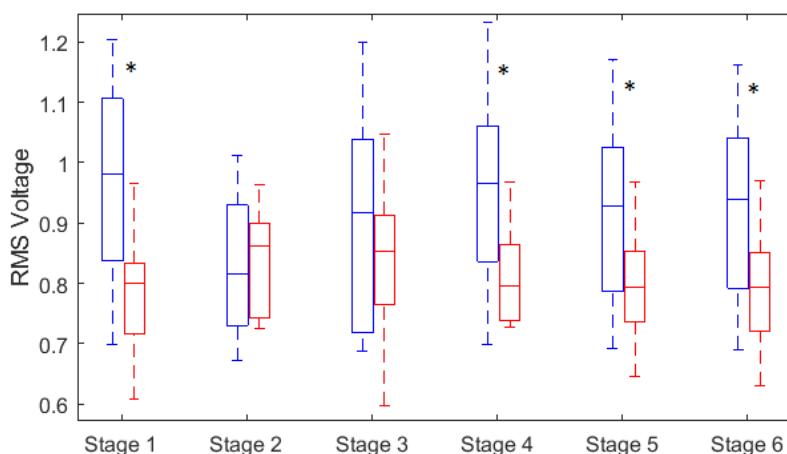


Figure 8-21 – Average RMS values of the “signal” component in the reference ECG (blue) and the face ECG (red) for each experiment stage. * indicates significant difference between values for face and reference ECG signals ($p < 0.05$).

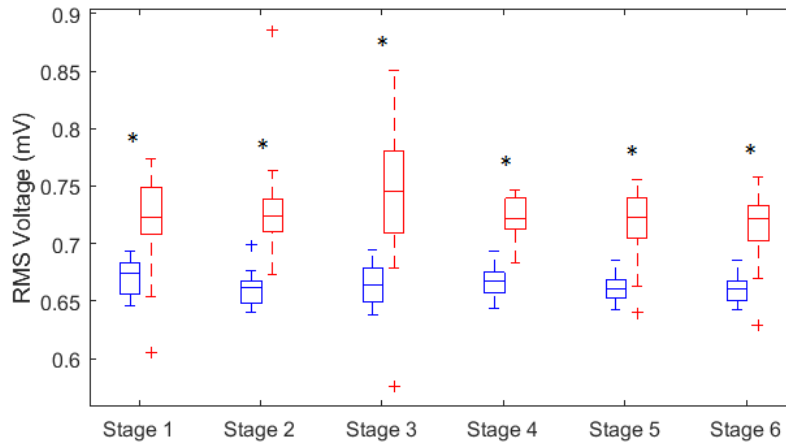


Figure 8-22-Average RMS values of the “noise” component in the reference ECG (blue) and the face ECG (red) for each experiment stage. * indicates significant difference between values for face and reference ECG signals ($p < 0.05$).

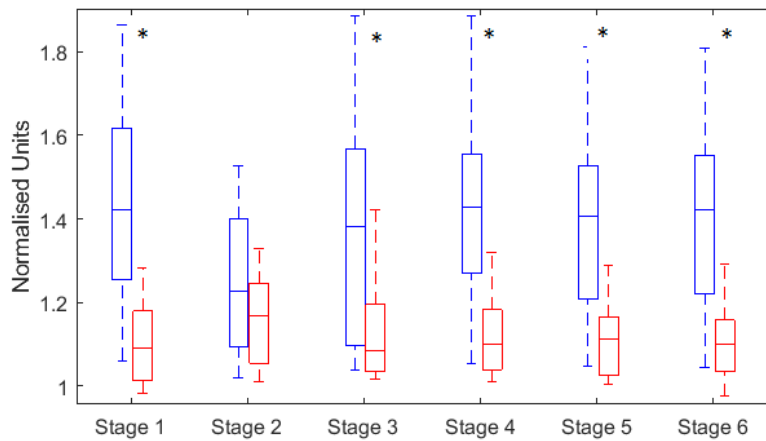


Figure 8-23-Signal to noise (RMS) ratio for the reference ECG signal (blue) and the face ECG signal (red). * indicates significant difference between values for face and reference ECG signals ($p < 0.05$).

Figure 8-22 shows that the only significant variation in the noise RMS values of the face ECG signal was when the participant was lying on their right side (experiment stage 3). In this stage, the average RMS noise value increased compared with other experiment stages ($p < 0.05$). Other than this, for both the face and reference ECG signal there was no significant change in the average RMS values for different PAP modes or different participant orientation. Following on from this, SNR values for the face ECG signal were not significantly different between different experiment stages as shown in Figure 8-23, except for when the participants were lying on their left side (stage 2) ($p = 0.0089$).

8.2.5.4 ECG signal quality summary

The results from section 8.2.5 show that for all PAP modes and all participant orientations, the quality of the face ECG signal is reduced compared to the reference ECG signal.

However the results from section 8.2.2 show that although the signal quality of the face ECG signal is reduced, the quality was sufficiently high for accurate heartbeat detection. These results are similar to the preliminary results in chapter 5.

8.2.6 PPG signal quality

In Figure 8-24, the PPG signal quality is shown, where the signal quality was calculated using a method described by Li and Clifford [177]. Except for the stage where bi-level PAP mode was activated (stage 6), Figure 8-24 shows that the signal quality value of the PPG signal was larger than 0.9 for most participants.

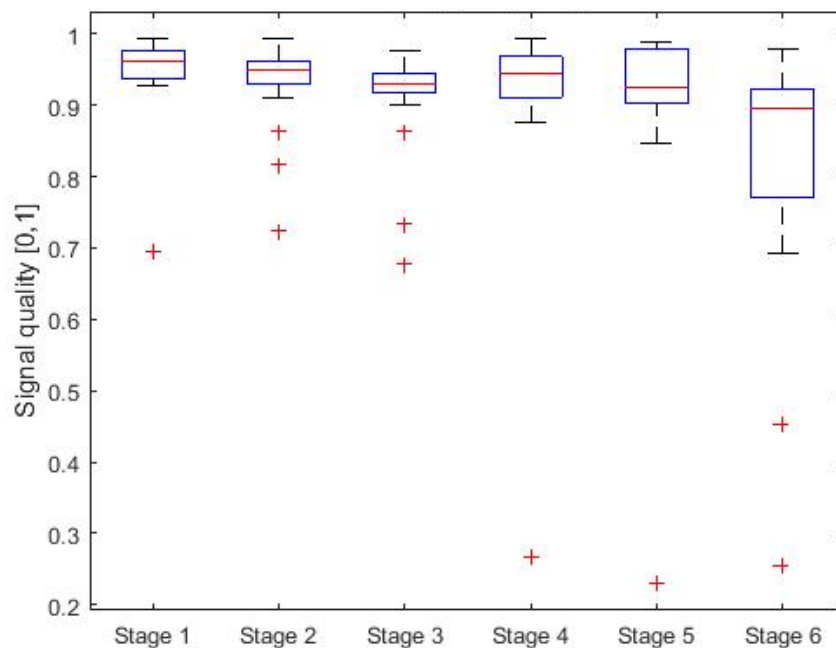


Figure 8-24-The median PPG signal quality values. Signal quality algorithm used was from [19]

Using multiple pairwise comparisons it was determined that the signal quality of the PPG signal was not significantly different between different experiment stages, except when the participants were lying on their right side (stage 3, $p=0.042$), and when the bi-level mode was activated (stage 6, $p=0.0302$). This is shown in Figure 8-24 by the decrease in quality for stage 3 compared with stages 1, 2 and 4, and by the decrease in the median quality value for stage 6 compared with stage 5. The difference in signal quality between stages 5

and 6 (CPAP vs bi-level mode on PAP device) is due to the motion artefacts in the PPG signal caused by the change in mask pressure during the bi-level mode, as discussed previously in section 8.2.2. The reason for the reduction in quality when the participants were lying on their right side (stage 3) (compared with their left side (stage 1) and lying on their back (stage 1 and 4)) is not clearly understood. It is possible that the change in the sleeping position caused the sensor to be improperly positioned when the participants were lying on their side, or that in moving to lie on their right side, tension in the cable was increased, pulling the sensor away from the wearer's skin.

8.3 Discussion

A modified PAP mask designed to measure HR was tested on healthy participants lying on a bed. The mask was able to measure an ECG signal from Stainless Steel electrodes located on the wearer's face and a PPG signal from a reflectance pulse oximeter located on the wearer's forehead. The data from these signals were then used to derive the HR of the participants, estimate the quality of the measured signal, and for HRV analysis.

This study involved healthy participants only. It is unknown whether the heartbeat detection accuracy would be reduced when the participant has an abnormal ECG, or PPG. Future work will look to determine if abnormal ECG signals detected in the reference ECG signal are also present in the face ECG signal.

In chapter 6, a BBI correction algorithm (combined threshold algorithm) was tested on pre-recorded data that had been intentionally corrupted. The results showed that for BBI values that were not significantly corrupted, the sensitivity of the BBI signal was preserved by the HR correction algorithm, whilst the HR and HRV error was reduced. The results in section 8.2.2.1 show a similar result in that whilst there was no significant different reduction in the sensitivity, there was a decrease in the number of false positives, which would lead to a reduction in HR and HRV error. Hence the results of the BBI correction algorithm in this

chapter (in section 8.2.2.1) are similar to the results of the BBI correction algorithm testing shown in chapter 6.

The PPG signal that was analysed was not the raw PPG signal from the reflectance oximeter, but a filtered signal read from the Nonin Xpod. The Xpod is a device that analyses the raw pulse oximetry signal, and extracts the PPG signal and the SpO₂ values. The sampling frequency of the Xpod is only 75Hz, but it is likely that the sampling frequency of the actual pulse sensor is much higher, and that therefore the signal quality and accuracy of HR analysis may be lower than if the raw pulse oximetry signal had been available.

Not having access to the raw signal also may limit the potential to reduce the effect of the bi-level PAP mode on the PPG signal quality, as seen in Figure 8-4. The Xpod does perform some filtering on the PPG signal, in order to remove motion artefacts from the PPG signal. However, this filtering was not designed to remove artefacts caused by a bi-level CPAP mode. This might be accomplished using an adaptive or a high pass filter, however more work is needed to determine if this is possible.

In comparing the mean HR values across different time intervals (i.e. for 30 second and 5-minute intervals) RPC and confidence interval values were used, as well as the mean difference and R² values. However there will be a smaller number of HR values in a 30 second interval than in a 5 minute interval, thus increasing the range of the RPC confidence interval for the 30 second interval. Hence any comparison of values between intervals of different lengths should be done with caution.

Certain features of the measured ECG and PPG signals and corresponding BBI values (such as signal quality or range of BBI values) were used as thresholds for accepting or rejecting HR windows for HR and HRV analysis. However, the values of these variables were heuristic values determined experimentally such that the results produced a high level

of accuracy from the data available. These values may not be the optimum values that produce the best results for other data sets or the general population. To achieve these values, other larger data sets would need to be used so that a larger, more diverse set of HRs could be investigated. Future work could also look at implementing a statistical classifier using machine learning or other technique, to more accurately determine the optimum values for accepting and rejecting HR windows for HR and HRV analysis.

Algorithms were developed to accept or reject HR windows for HR and HRV analysis to increase the HR and HRV accuracy. These algorithms were designed such that any HR windows that were likely to be corrupted would be discarded and so only “good” HR windows would be used. While this approach may be useful for making sure that the bad beats from a good signal do not affect calculations, it may also lead to discarding most HR windows from participants who have a poor face ECG or PPG signal quality. For these patients, HR analyses may not be possible using the methods developed. However, it is better that the corrupted data be discarded, than for it to be falsely interpreted and used for a recommendation or a diagnosis.

The HRV analysis was conducted on the BBI values after the BBI correction algorithm was applied. Although in a previous chapter it was shown that this algorithm has quite a high accuracy rate, especially when intervals with corrupted BBIs are removed, there may be intervals where the HRV calculations were performed where 100% of the heartbeats were not detected, or there were several falsely classified heartbeats. Thus the HRV values that were calculated from the face ECG and PPG signal may not be as accurate as they could be if the heartbeats were manually corrected. However, since this device is designed to monitor patients for several hours at a time, repeated over multiple nights, it is not practical to manually correct all heartbeats.

HR and HRV analysis was performed on the ECG and PPG signals independently. This was to determine if it was possible to achieve consistent and accurate HR and HRV analysis from only one of the signals, either the ECG or PPG signal. Results indicated that whilst accurate HR and HRV analysis was possible from both the ECG and PPG signals, a significant amount of data is discarded to ensure that only good quality HR information remains for accurate HR and HRV analysis. Combining information from both signals might reduce the amount of data discarded and improve the accuracy of HR and HRV analysis. Methods for combining the data will be developed in the following chapter.

HR values collected from the minimum point of the PPG signal were not used because of the poor initial results of the HR and HRV analysis of the minimum point (or the foot) of the PPG signal. This is possibly due to the method used to identify the minimum point, which was to simply identify the point with the smallest value in the pulse wave. Other methods that may prove more reliable include fitting a curve to the foot of the pulse wave using available data from the PPG signal to find the minimum point [191], and finding the intersection point between the line of best fit passing through the maximum 1st derivative point and the tangent of the point with the lowest value [115]. These methods were not implemented here given the relatively good performance of the heartbeats from PPG1 (maximum) and PPG2 (maximum of 1st derivative), however future work could look at the relative performance of these alternate techniques against the fiducial points used in this thesis.

An analysis of HRV variables from differing PPG fiducial points was conducted by Suhrbier et al. [190]. They compared HRV variables extracted from the peaks and maximum 1st derivative points of a blood pressure (BP) signal, which has a very similar shape and physiological origin to the PPG signal. The HRV variables were also compared to HRV variables from an ECG signal, however the ECG HRV variables were detected by finding the maximum 1st derivative points of the ECG signal, not by locating the peaks (R-waves) like in this study. They found that for the HRV variables from the peaks of the BP signal, the

RMSSD and HF error values were larger than the values from the maximum 1st derivative points from the BP signal. Similarly, in this study the RMSSD and HF error values were greater than other HRV variables as shown in Figure 8-14. However, in these results there was no significant difference between the HRV variables from the peak and PPG2 (maximum of 1st derivative of PPG signal). This reason for this difference is unknown however the difference in the HRV variables may just be a function of differences between the PPG signal and the BP signal, used by Suhrbier et al.

Posada-Quintero et al [191] also conducted a similar experiment where the accuracy of HRV variables from a PPG signal were analysed. However, unlike the experiment in this chapter, Posada-Quintero's PPG signal was measured from the finger and not the forehead. They compared the accuracy of HRV variables from the minimum point, the maximum of the 2nd derivative and the tangent intersection method described by Chiu et al [114]. They found that there exists a small bias between the PPG and ECG HRV values for all pulse detection methods. They concluded that the tangent intersection method is the most accurate method for HRV analysis, however all other methods were still relatively accurate. The results in this chapter were similar to the results observed by Posada-Quintero et al [191] in that the LF/HF ratio had the largest error of all the HRV variables for all pulse detection methods.

Schafer and Vagedes concluded that as long as the patient is in supine position (lying on their back) and at rest, there should be good agreement between the HRV variables from the PPG and ECG signal [101]. This was based off a review of PPG literature at the time. Since in this chapter, HRV analysis was only calculated on experiment stages when the participants were in the supine positions, this might explain the relatively good agreement between the corrected PPG HRV values and the reference HRV values. They also concluded that the variables that were most likely to be affected or for a bias to occur were the short term HRV variables, such as HF (and hence LF/HR ratio), RMSSD and pNN50. In this chapter, the HF and the LF/HF ratio were the HRV variables with the highest error. For

the HRV variables from the PPG signal the RMSSD values also have a larger error compared with the other time domain variables, as seen in Figure 8-14. This shows that HRV results that were achieved in this thesis are similar to results that have been achieved in other literature. It is unknown how well the ECG and PPG HRV analysis would agree with each other when participants were lying on their side, and future work could investigate this.

8.4 Conclusion

A PAP mask was modified to be able to measure an ECG and PPG signal from a patient during PAP therapy. The mask, named the “Cardiomask”, was tested on healthy participants in several different sleeping positions and under two different PAP therapies. The results showed that:

- ECG and PPG signals were able to record a HR signal with a relatively high level of accuracy.
- BBI values from the ECG signal is more accurate than the PPG signal.
- There was no significant difference in between the sensitivity of the methods for detecting heartbeats in the ECG and PPG signals, but more false positives in PPG signals compared with the ECG signal.
- PAP device changes in pressure caused motion artefacts in the forehead PPG signal which affected the HR accuracy. This had the largest effect when the bi-level mode was activated.
- Accurate HR and HRV analysis could be performed on both ECG and PPG signals when corrupted HR windows were discarded based on the criteria defined in the previous chapter.
- The accuracy of the HR and HRV analysis from the PPG signal was not significantly affected by the choice of the fiducial point, once the HR correction algorithm was applied.
- Error for HF and LF/HF ratio was largest for all signals, and RMSSD error was also relatively large for PPG signal.

- The HRV from the ECG signal was more accurate than the HRV from the PPG signal for most HRV variables. There was also a bias in some of the PPG HRV variables.
- Data fusion from ECG and PPG signals may be needed to increase consistency of HR and HRV analysis.
- ECG signal from the face had good correlation to reference ECG signal, even when QRS complexes were removed.
- The magnitudes of the QRS complexes in the face ECG signal were smaller in comparison to the reference ECG signal, but the rest of the signal had a higher magnitude.
- The signal quality of the ECG signal and PPG signal varied between participants, and the ECG signal measured from the face had a lower signal to noise ratio than the reference ECG signal.

9. Combined ECG and PPG analysis

9.1 Introduction

Whilst the HR and HRV analysis of the ECG and PPG signals described in the chapter 8 was accurate and repeatable, no one particular HR signal was able to measure HR and HRV for all stages. Given that the Cardiomask measures both ECG and PPG signals, the logical next step was to combine the information from these two signals with the aim of improving the accuracy and consistency of the HR and HRV analysis. In this chapter, methods for integrating and fusing the data from the ECG and PPG signals for HR and HRV analysis will be described, and compared to each other, as well as to the results from the individual ECG and PPG HR and HRV analysis from chapter 8.

As mentioned in Chapter 4, most currently used data fusion methods have generally only been used for approximating the HR or for estimating HR trends, and not for generating an instantaneous HR signal from which accurate HRV analysis is possible. Hence in this chapter, new data fusion algorithms were developed, designed to output an instantaneous HR which could also allow for accurate HR and HRV analysis.

The primary aim of the data fusion methods developed in this chapter was to increase the proportion of the data on which accurate HR and HRV analysis could be performed without a significant decrease in accuracy when compared with the results from chapter 8.

A secondary aim of the data fusion methods was to increase the accuracy of the HR and HRV analysis when compared to the results from the previous chapter (i.e. on the individual ECG and PPG signals). It was hypothesised that by combining the data from the different HR signals, the number of false positives could be reduced, and the heartbeat detection sensitivity could be increased, leading to increased HR and HRV accuracy.

The data fusion methods developed were divided into two categories. The methods in the first category (shown in section 9.2 and 9.3) generated a combined BBI signal using

heartbeat information from both the ECG and the PPG signal, and then applied the HR and HRV calculations on that combined signal. The second category (shown in sections 9.4 and 9.5) involved calculating HR and HRV results from multiple individual BBI signals and using different method to select the most accurate HR and HRV values from these multiple signals.

9.2 Category 1 – Combining ECG and PPG data to produce a BBI signal - Methods

9.2.1 Method

The algorithms in this first category use the heartbeat information from the ECG signal and the PPG signal to generate an integrated BBI signal. HR and HRV analysis is then applied to the integrated BBI signal. Similarly to the last chapter, the accuracy of the BBIs from the integrated BBI signal was determined by looking at a Bland-Altman (BA) plot, the heartbeat detection sensitivity and false positive rate, and the accuracy of the subsequent HR and HRV analysis. These values were compared against the respective values from the reference ECG signal.

9.2.1.1 HR analysis

Similarly to the results in chapter 8, for the HR analysis, the mean HR over a 30 second and 5 minute window was calculated for each data fusion method and windows were rejected for HR analysis using a method similar to what was described in section 7.3, however the signal quality analysis steps were removed as signal quality comparisons across different signal types are less accurate than comparisons for the same signal. The flowchart for rejecting or accepting the mean HR values from the data fusion algorithms is shown in Figure 9-1. Similarly to the methods described in chapter 7, the mean BBI value was converted to BPM to display the results.

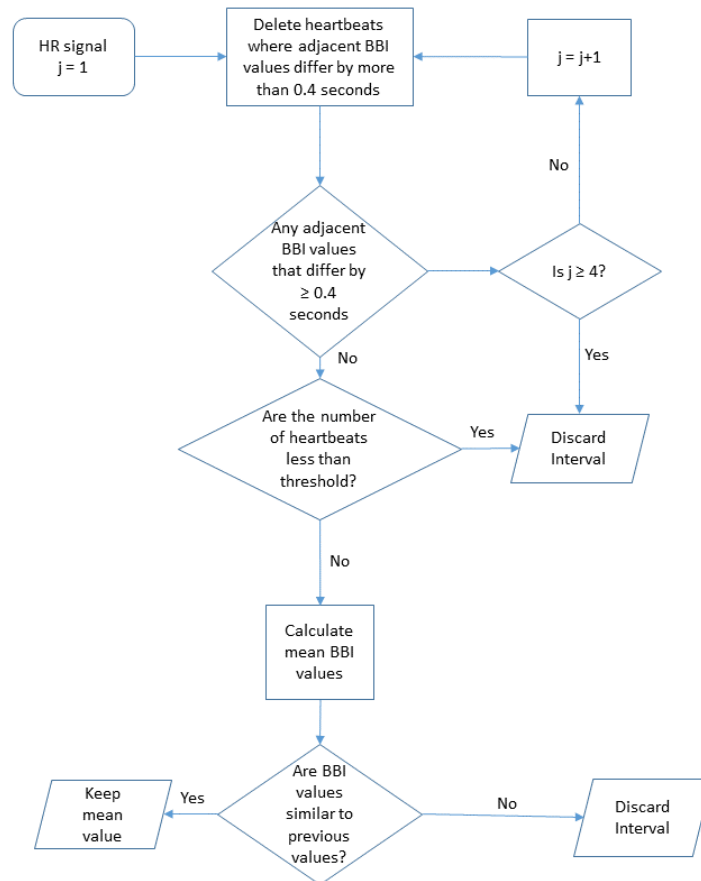


Figure 9-1 - Flowchart for accepting/rejecting windows for mean HR calculations

9.2.1.2 HRV analysis

For the HRV analysis, analysis was performed on experiment stages where the participant did not move to begin the stage (i.e. stages 1, 5 and 6). As before (described in section 7.4), HRV analysis data was excluded if the range of BBI values within the experiment stage was larger than 0.7s. Unlike with the individual ECG and PPG HR windows, dividing the number of heartbeats by the average HR was not an accurate predictor of high HRV error and was hence not used to exclude HRV analysis from the data fusion BBI values. This was possibly because the data fusion methods described in this chapter are designed to find gaps in the BBI signal and fill in these gaps with BBI values from other sources. Additionally, stages containing ectopic beats were excluded for both HR and HRV analysis, as ectopic beats can affect the accuracy of HRV analysis [8].

9.2.2 Method 1: PPG Fusion method

The PPG Data Fusion method used the BBIs from the different fiducial points of the PPG signal. In section 5.5.2. three different fiducial points on a PPG signal were identified (maximum, minimum and 1st derivative), providing three different methods of measuring instantaneous HR. The PPG Data Fusion method attempted to find common heartbeats from the different PPG heartbeat detection methods. If a heartbeat was detected by two or more of the heartbeat detection methods from the PPG signal (e.g. a heartbeat was detected using both the maximum and minimum methods) then that heartbeat was determined to be correct and was included in the fused BBI signal. The median Pulse Transit Time (PTT) for each experiment stage was calculated for the maximum, minimum and 1st derivative heartbeats with respect to the reference ECG signal using the method described in section 7.6. The heartbeats were shifted back by the respective PTTs so that the time of occurrence of the heartbeat was approximately the same as the ECG heartbeats.

A heartbeat was then defined as “common” between two (or all three) signals if the absolute time difference between the time shifted heartbeats was less than 0.2 seconds. Based on the results from chapter 8, the timepoint that was chosen for a “common” heartbeat was taken from the 1st derivative heartbeats (PPG2), as this signal gave more accurate HR and HRV results. If the “common” heartbeat was not detected in the 1st derivative (PPG2) heartbeats, the heartbeat timepoint was taken from the maximum signal heartbeats (PPG1).

After the common heartbeats were found, the BBI correction algorithm developed in Chapter 6 (Section 6.6.1) was applied to improve the accuracy of the fused BBI signal. A flowchart of the PPG data fusion process is shown in Figure 9-2, and an example of its application is shown in Figure 9-3. In Figure 9-3, any heartbeat that was detected by two or more methods is marked by a V. Others (marked X) were rejected, as these were most likely false positives.

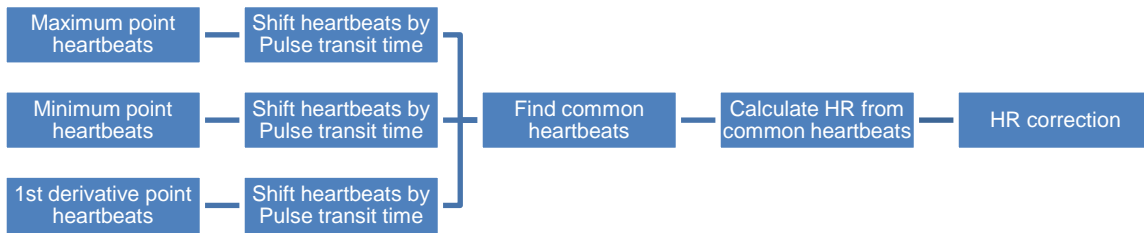


Figure 9-2 - Flowchart of the PPG data fusion method

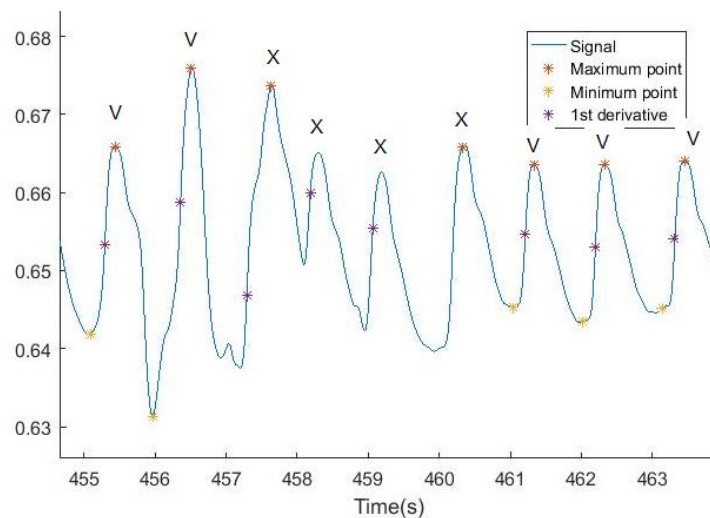


Figure 9-3 - The basic principle of the PPG data fusion method. Coloured stars indicate fiducial points that have been identified. Accepted heartbeats are denoted by V and rejected heart beats denoted by X.

9.2.3 Method 2: ECG+PPG data fusion method

For the second data fusion method, the face ECG was added as an additional component to the PPG data fusion method (Method 1) described in the previous section. The heartbeats from this signal was added because the results in chapter 8 showed that the heartbeats from the face ECG signal were more accurate and provided more accurate results for HR and HRV analysis than the heartbeats from the PPG signal.

In this second method, heartbeats from the face ECG signal were compared to the output of the PPG data fusion method, and 'equivalent heartbeats' identified. An equivalent heartbeat was defined as any heartbeat in the Pulse Data Fusion method that was within 0.2 seconds of a heartbeat from the ECG signal. For any similar heartbeats found, the corresponding BBI values were compared. If the difference between the BBI value from the Face ECG and the

BBI from the output of the PPG data fusion method was less than 0.2 seconds, then the BBI value from the face ECG signal was used. If the difference was larger than 0.2 seconds, then the algorithm discarded the BBI value (from the face ECG HR and the pulse fusion method) that had the largest absolute difference to the two adjacent BBIs. The combined threshold BBI correction algorithm described in chapter 6 was then applied. A flowchart showing this algorithm is shown in Figure 9-4.

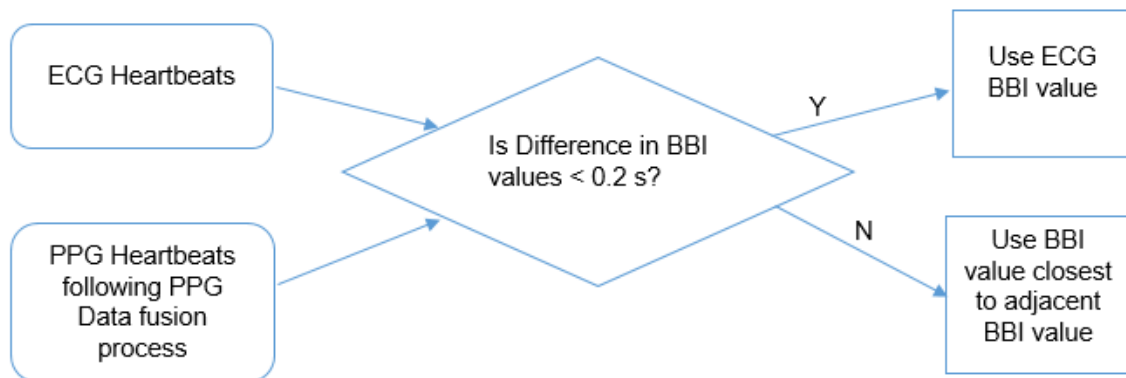


Figure 9-4 - Flowchart of the ECG and PPG data fusion method

9.3 Category 1 – Combining ECG and PPG data - Results

9.3.1 BA plots of fused data

Figure 9-5 and Figure 9-6 show the Bland-Altman (BA) plots of the BBIs for the two fusion methods. Both figures show the ability of the different methods to generate an accurate HR signal as the R^2 values were 0.98 and 0.99 in Figure 9-5 and Figure 9-6 respectively, and the mean difference for both figures was 0.00 ($p=0.38$ Method 1 and $p=0.85$ Method 2). Both methods show good repeatability with RPCs of 0.04 s and 0.02 s for Figure 9-5 (Method 1) and Figure 9-6 (Method 2) respectively. The number of BBIs identified by the two data fusion methods are shown in comparison with the number of BBIs identified by the individual face ECG and PPG signals in Table 9-1. Method 1 (fusing the PPG data) in Figure 9-5 identified a lower number of BBI values in the BA plots from the individual PPG pulse detection methods. Conversely, Table 9-1 shows the number of BBIs identified by Method 2, is greater than the number identified from the face ECG or PPG signal individually.

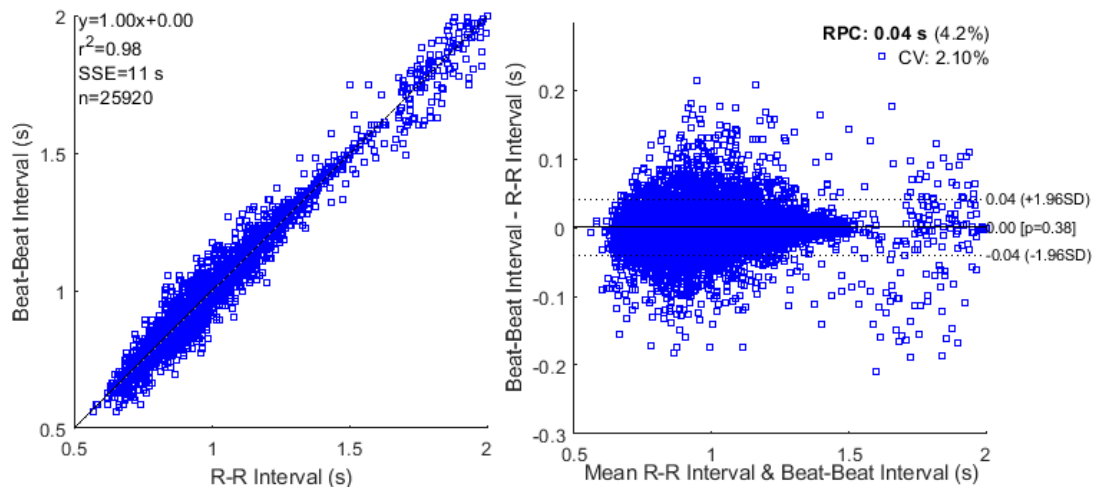


Figure 9-5 - Bland Altman plot of the BBI from the PPG data fusion method (Method 1), compared with the RRI from the reference ECG

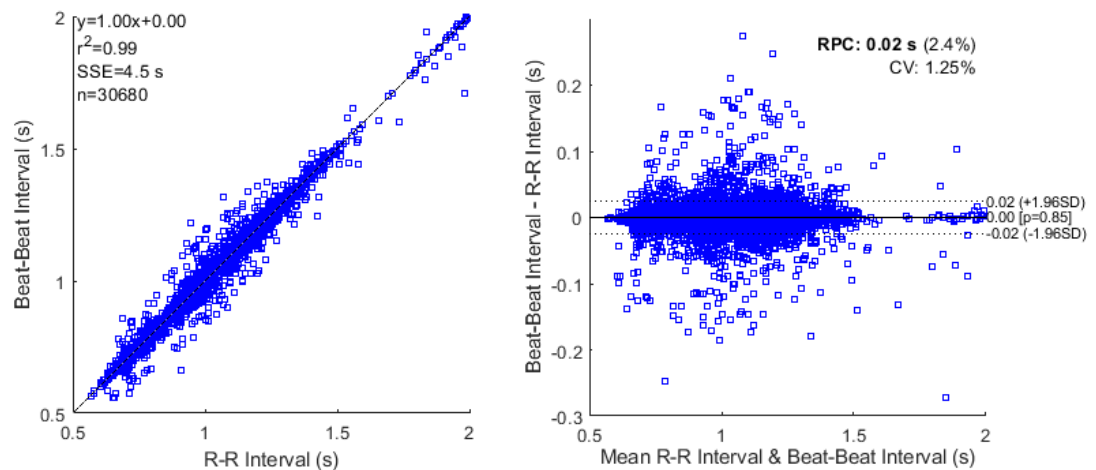


Figure 9-6 - Bland-Altman plot of the BBI from the ECG+PPG fusion method (Method 2), compared with the RRI from the reference ECG

Table 9-1: The number of BBI values identified for data fusion methods described in this chapter, in comparison with the number of BBI values identified in the face ECG and PPG signals (from section 8.2.1.1)

BBI method	Number of BBI values identified
ECG	29410
PPG1	26270
PPG2	28980
Method 1: PPG Fusion	25920
Method 2: ECG+PPG data fusion	30680

9.3.2 Heartbeat detection sensitivity

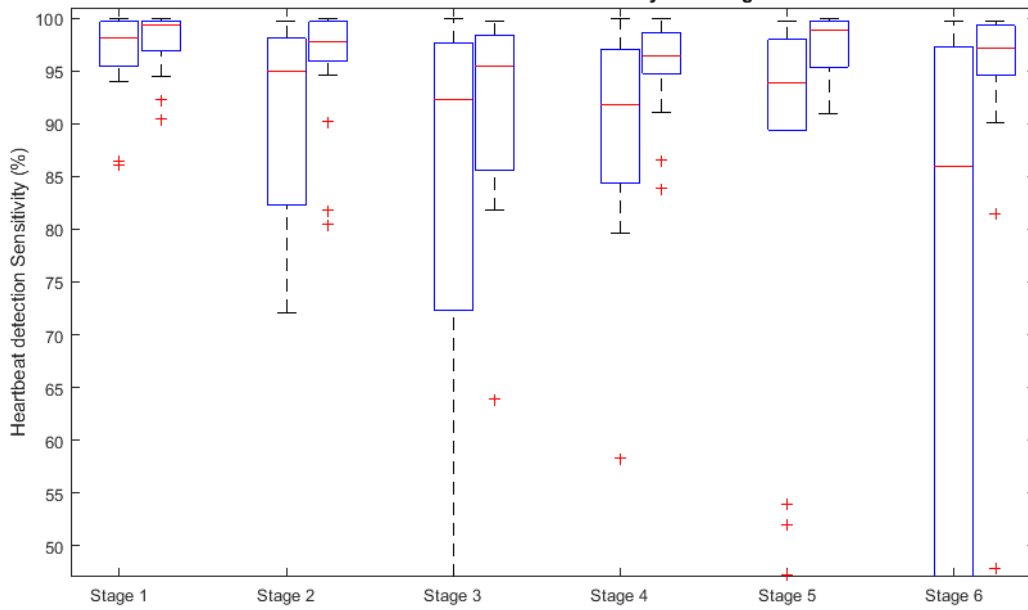


Figure 9-7-Heartbeat detection sensitivity of the PPG data fusion algorithm (Method 1) (left) and by the ECG + PPG fusion algorithm (Method 2) (right)

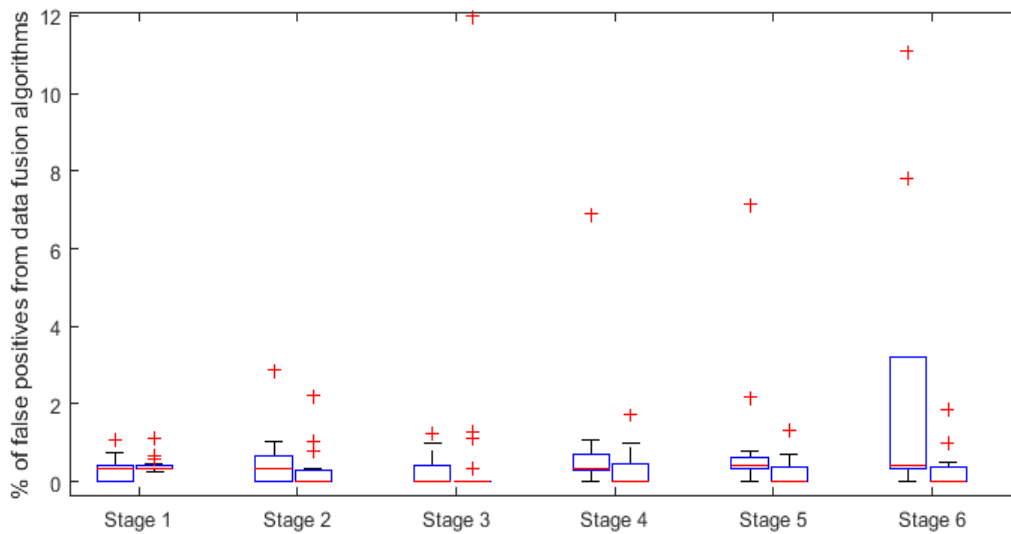


Figure 9-8-Percentage of false positives detected by the PPG data fusion algorithm (Method 1) (left) and by the ECG + PPG fusion algorithm (Method 2) (right)

Table 9-2 – Median (and interquartile range) heartbeat detection sensitivity and false heartbeat rate in the ECG and PPG signals

	Stage 1	Stage 2	Stage 3	Stage 4	Stage 5	Stage 6
Heartbeat detection sensitivity (%)						
PPG data fusion (Method 1)	97.91 (4.22)	94.89 (15.41)*	93.89 (22.21)	93.67 (9.52)	94.20 (8.59)*	92.40 (71.30)*
ECG + PPG fusion (Method 2)	99.34 (2.83)	97.58 (4.27)	95.44 (13.24)	96.47 (3.65)	98.57 (4.60)	97.32 (5.71)
Falsely detected heartbeats (%)						
PPG data fusion method (Method 1)	0.31 (0.42)	0.33 (0.68)	0.00 (0.41)	0.35 (0.40)	0.40 (0.32)*	0.41 (2.91)*
ECG + PPG fusion method (Method 2)	0.32 (0.10)	0.00 (0.29)	0.00 (0.00)	0.00 (0.47)	0.00 (0.37)	0.00 (0.38)

* Method 1 is significantly different to Method 2 ($p < 0.05$)

The heartbeat detection sensitivity and false positive rate from each of the two data fusion methods are given in Figure 9-7 and Figure 9-8 respectively, and results summarised in Table 9-2.

Table 9-2 and Figure 9-7 show that, for all stages, the heartbeat detection accuracy was greater for the ECG+PPG method (Method 2) than for the PPG data fusion method (Method 1), and this difference was statistically significant in Stages 2, 5 and 6. Additionally, Table 9-2 and Figure 9-8 show that the percentage of false positives was significantly lower in stages 5 and 6 using the ECG+PPG method (Method 2). This is perhaps unsurprising, since Method 2 takes the output of Method 1, and uses the face ECG as an additional signal to identify a heartbeat. Thus, when the quality of the PPG signal is low, Method 2 may still be able to identify a heartbeat from the ECG. The largest (and significant) differences occur in stages 2, 5 and 6; this could be due to the significant differences between the percentages of false positives in the heartbeats detected from the ECG and the PPG signal in these stages (see Table 8-4 in section 8.2.2).

In stage 6 (when bi-level PAP mode was activated), the percentage of falsely detected heartbeats for different participants was larger and the sensitivity was lesser using the PPG

data fusion method, when compared with the other experiment stages. This did not hold true using the ECG+PPG fusion method (Method 2). The reduction in the sensitivity of the PPG data fusion method when the bi-level PAP mode was activated is due to the reduction in sensitivity in the PPG signal that was observed in section 8.2.2 (Table 8-4).

Figure 9-9 compares the heartbeat detection sensitivity from the ECG+PPG data fusion method (Method 2) with that from the individual ECG and PPG signals from section 8.2.2 (Table 8-3). A Kruskal-Wallis H test showed that there was no statistically significant difference between the heartbeat detection sensitivity for the ECG+PPG data fusion method (Method 2) and for the individual ECG and PPG heartbeat. This result and Figure 9-9 show that the ECG+PPG data fusion method (Method 2) is able to preserve the heartbeat detection sensitivity from the individual ECG and PPG signals.

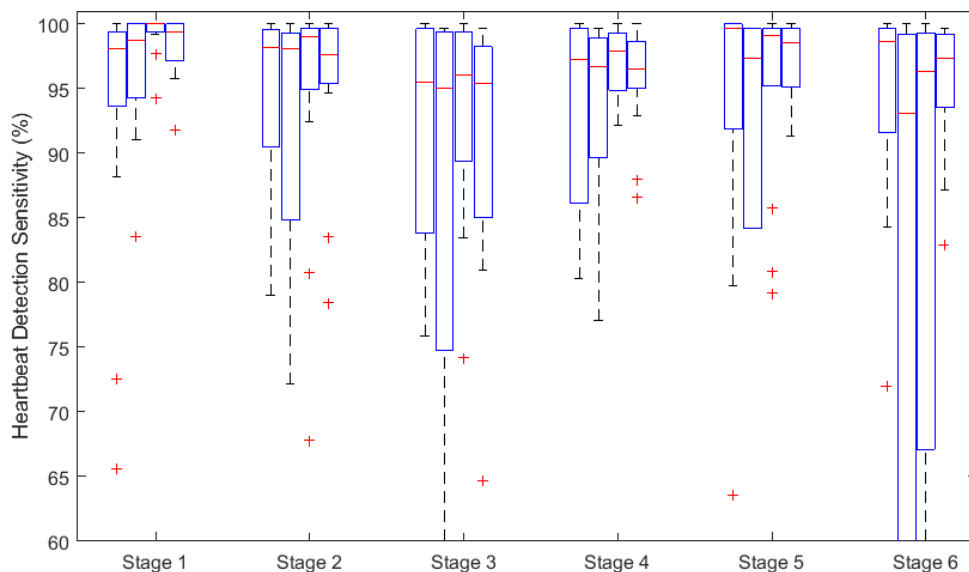


Figure 9-9 - Percentage of correctly detected heartbeats. Signals from left to right are face ECG, PPG1, PPG2, ECG + PPG fused data.

Conversely, the percentage of falsely detected heartbeats in the combined ECG+PPG method (Figure 9-10) was either less than or equal to the percentage heartbeats detected from the individual ECG and PPG signals (section 8.2.2, Table 8-4). A Kruskal-Wallis H test showed that there was a statistically significant difference between the number of false positives for the different methods in all stages except stage 3 and stage 1. This result

shows that (except for stages 1 and 3) combining the heartbeats detected from the ECG and PPG signals provided a greater level of heartbeat detection accuracy than detecting the heartbeats from just the PPG signal.

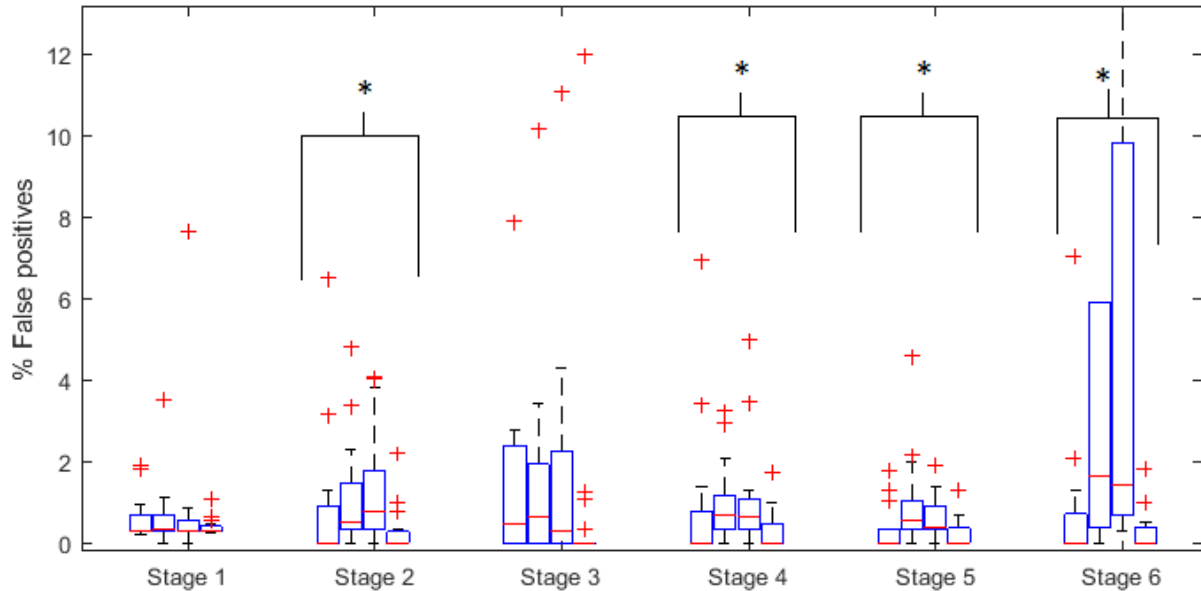


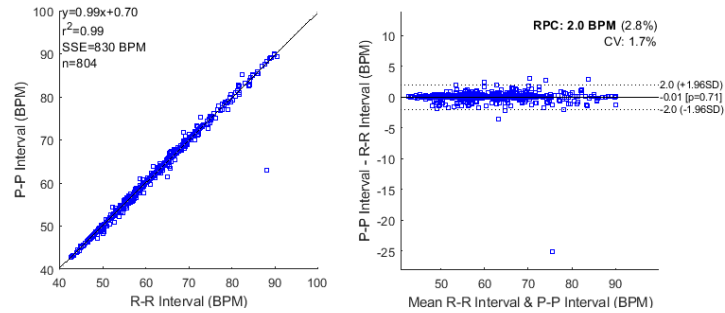
Figure 9-10 - Percentage of false positives in the HR signals. Signals from left to right are face ECG, PPG1, PPG2, ECG + PPG fused data. * indicates significant difference between values for each stage ($p < 0.05$)

9.3.3 HR windows comparison

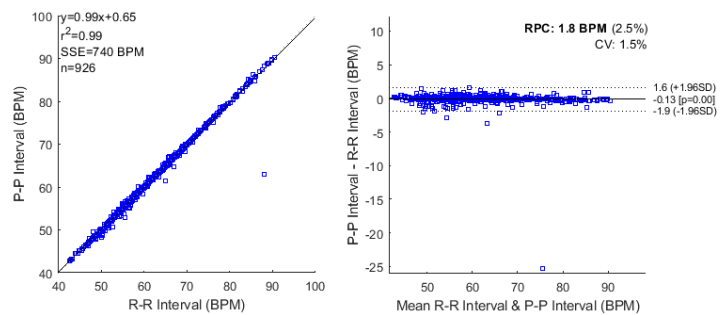
The BA plots comparing the mean HR values obtained from the PPG data fusion method (Method 1) and the ECG+PPG fusion method (Method 2) to the mean HR from the reference ECG signal are shown in section 9.3.3.1. The results are summarised in Table 9-3 in section 9.3.3.2.

9.3.3.1 BA plots of mean HR values

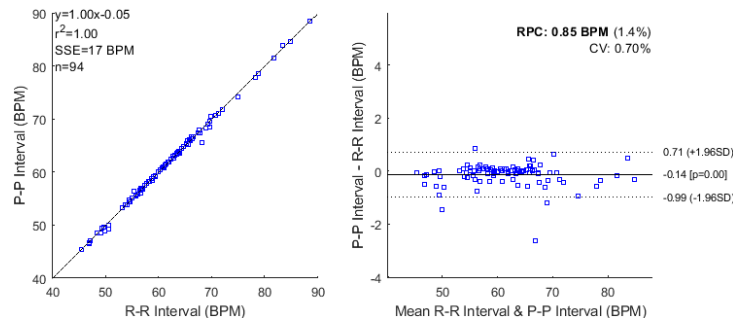
Mean HR for a 30 second window: Pulse Fusion method (Method 1)



Mean HR for a 30 second window: ECG+PPG method (Method 2)



Mean HR for a 5 minute window: Pulse Fusion method (Method 1)



Mean HR for a 5 minute window: ECG + PPG method (Method 2)

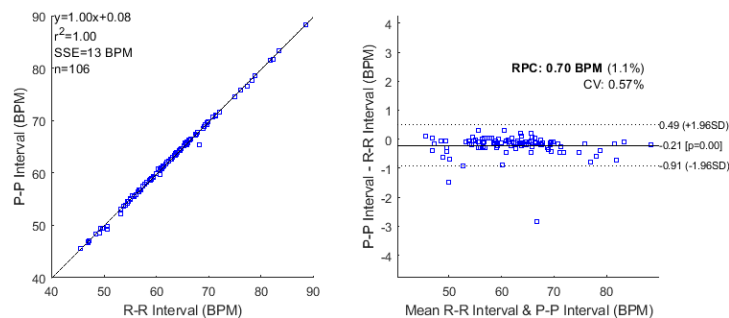


Figure 9-11 – BA plots for the mean HR estimation from the two data fusion methods in comparison to the HR from the reference ECG signal. The window length for the figures were 30 seconds and 5 minutes.

The accuracy and repeatability of the mean HR estimation for a 30 second and a 5 minute window for the two data fusion methods are shown in Figure 9-11 and are summarised in Table 9-3. These values are shown in comparison to the accuracy for the Face ECG signal and 1st derivative points in the PPG signal individually (shown in Section 8.2.3), as these two signals gave the most accurate HR estimation from an individual signal.

Table 9-3 - Mean HR for data fusion methods

	PPG 1 st derivative		PPG data fusion method (Method 1)		Face ECG only		ECG + PPG method (Method 2)	
	0.5	5	0.5	5	0.5	5	0.5	5
Window length (mins)								
RPC (CI)	1.27 (0.038)	0.68 (0.068)	2.00 (0.062) [^]	0.85 (0.076) [^]	1.91 (0.057)	0.71 (0.066)	1.80 (0.051)	0.70 (0.059)
CV (%)	1.05	0.57	1.70	0.70	1.54	0.57	1.50	0.57
Mean difference	0.01	-0.06	-0.01	-0.14*	-0.13*	-0.19*	-0.13*	-0.21*
R ²	0.99	0.99	0.99	0.99	0.99	0.99	0.99	0.99
N	829	76	804	94	836	87	926	106

[^] Significant difference in RPC value for data fusion method compared to individual method (p<0.05)

* Mean Difference not equal to 0 (p<0.05)

9.3.3.2 Discussion and Analysis of results

Figure 9-11 and Table 9-3 show that the mean HR from the Pulse fusion method (Method 1) was as accurate as the HR from the 1st derivative PPG points over a 30 second window, both with mean difference of 0.01 s from the reference signal, while there was a small decrease in accuracy over a 5 minute window. There was a decrease in the repeatability of the HR measurements from the PPG data fusion method (Method 1), as for both 30 second and 5 minute windows, there is a significant increase in the RPC values compared to those from the 1st derivative PPG HR values. The PPG data fusion method was also less successful at increasing the amount of data where accurate HR analysis can occur, as the number of accurate mean HR values for the Pulse fusion method (Method 1) was only greater than for the PPG signal by itself for 5 minute HR windows; less data was identified in the 30 second windows.

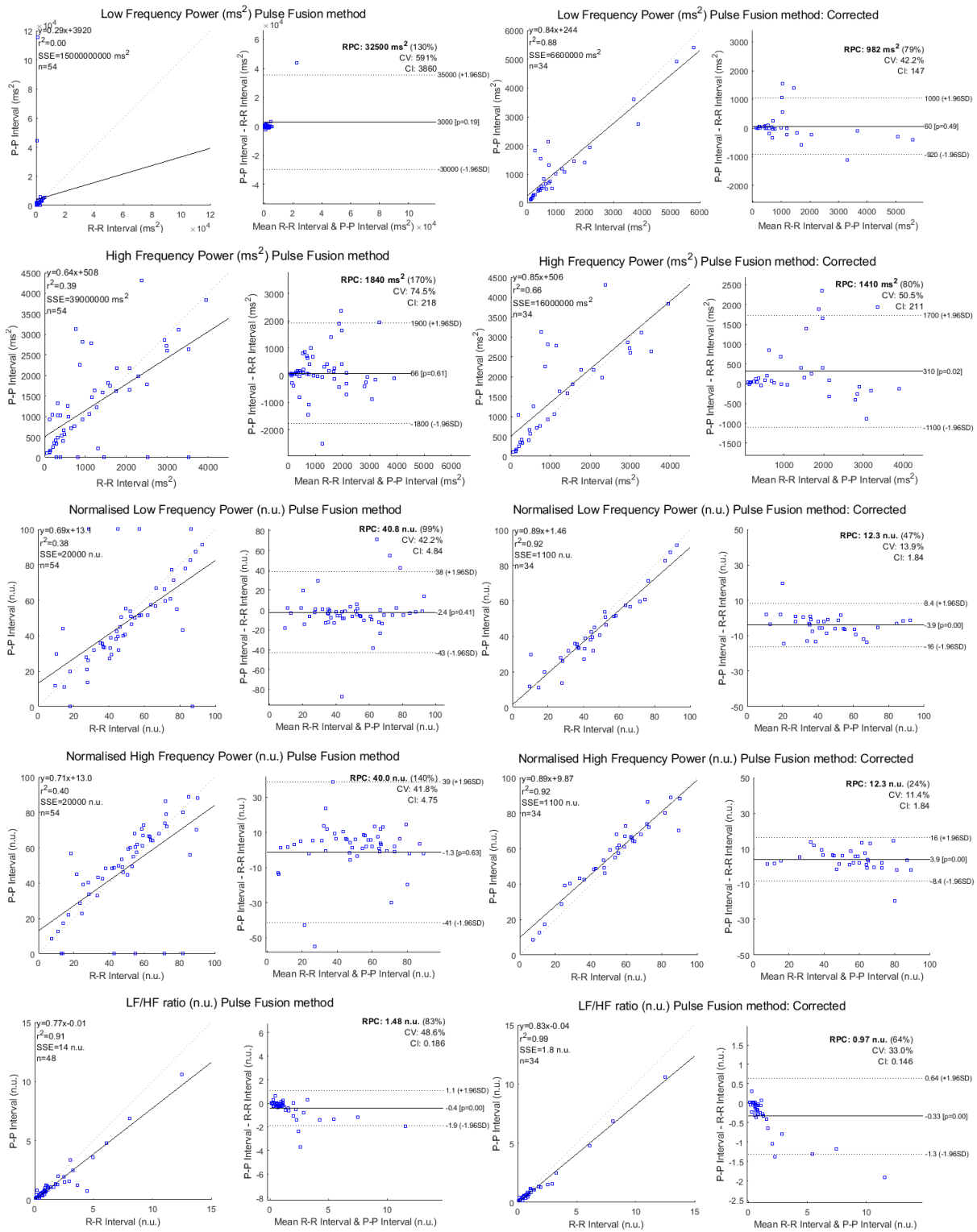
The RPC, CV, mean difference, and R^2 values for the ECG+PPG method (Method 2) are similar to the respective ECG only values for both 30 second and 5 minute windows. However the number of windows (N) where an accurate mean HR estimation can be extracted from the ECG+PPG fusion method (Method 2) is greater than for the ECG signal by itself, showing the ECG+PPG fusion method is able to increase the amount of data where accurate HR estimation can occur for both 30 second and 5 minute windows without a significant reduction in the accuracy of the mean HR value.

9.3.4 HRV analysis

The BA plots comparing the HRV analysis results from the two data fusion methods to the HRV analysis results from the reference ECG are shown in sections 9.3.4.1 and are summarised in Table 9-4 and Table 9-5 in section 9.3.4.2.

9.3.4.1 BA plots

9.3.4.1.1 PPG data fusion method (Method 1)



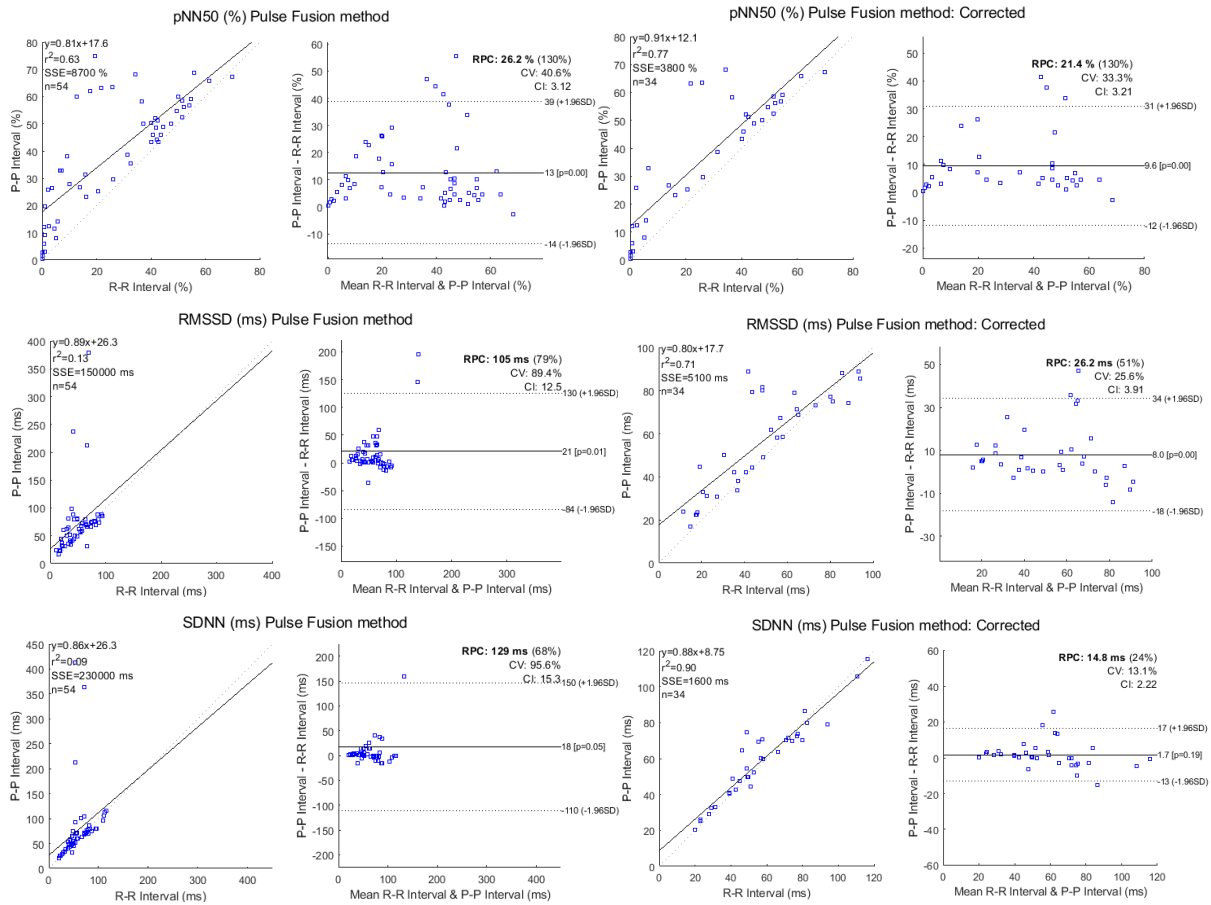
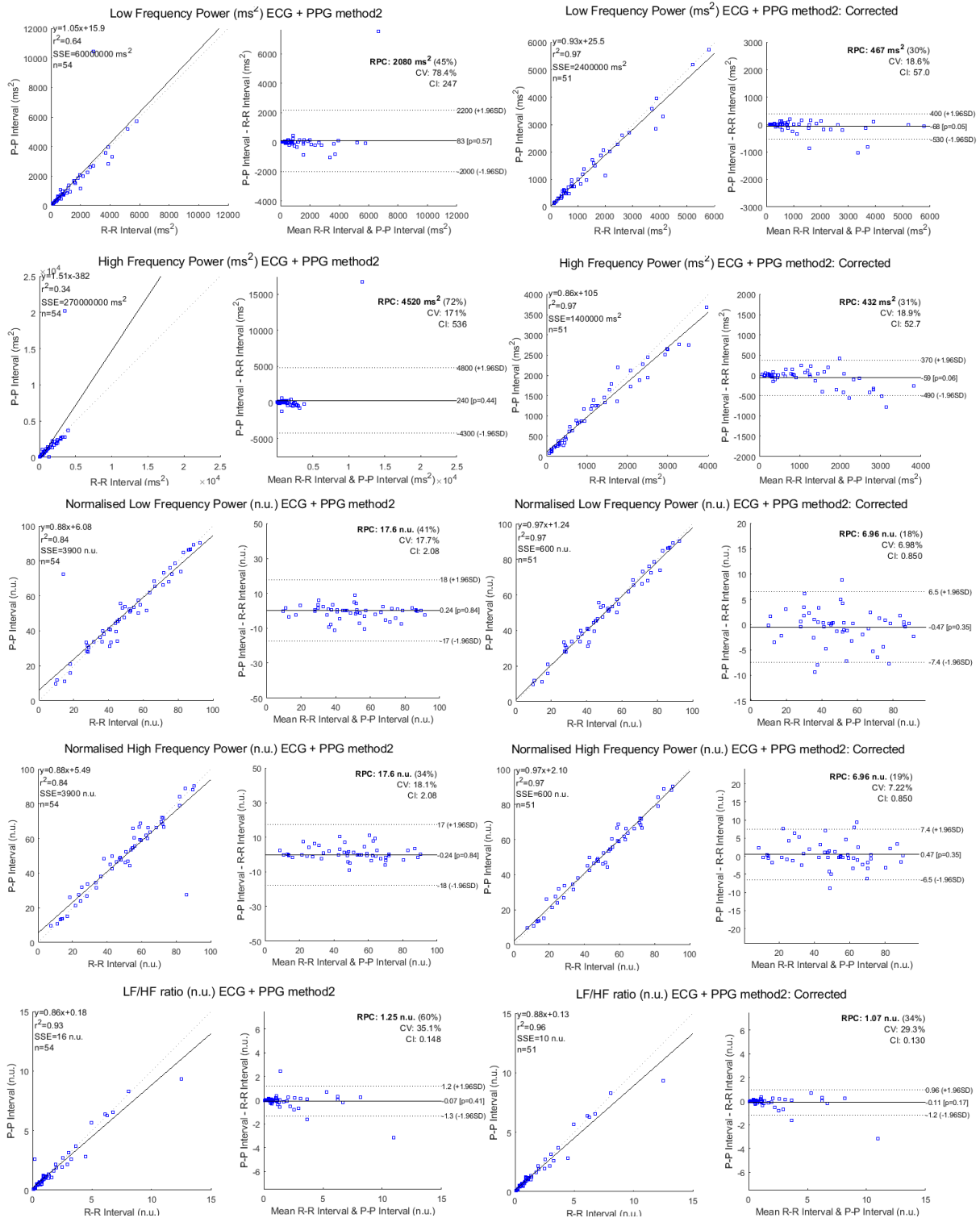


Figure 9-12 - BA plots for different HRV variables from BBI signals from the PPG data fusion method (Method 1) before (left) and after (right) bad HRV windows are removed.

9.3.4.1.2 ECG+PPG fusion method (Method 2)



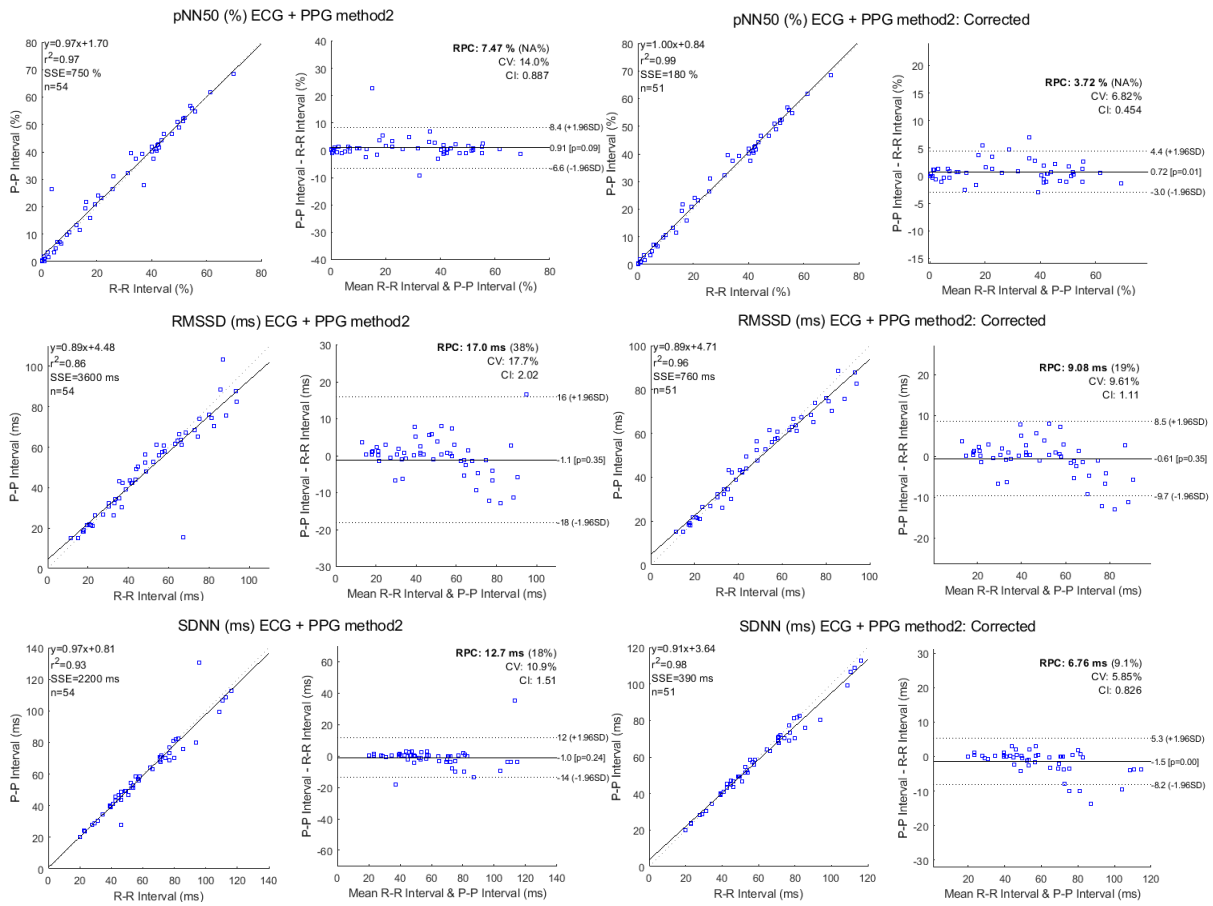


Figure 9-13 - BA plots for different HRV variables from BBI signals from the ECG+PPG data fusion method (Method 2) before (left) and after (right) bad HRV windows are removed.

9.3.4.1.3 Summary of HRV results

Table 9-4 - HRV variables from the PPG data fusion method before (n=36) and after (n=34) the stages were analysed to remove stages with corrupted BBIs

HRV variable	Before or after stages removed	RPC (CI)	CV (%)	Mean difference	R ²
LF (ms ²)	Before	32500 (3860)	591	3000	0.001
	After	982 (147)	42.2	60	0.88
HF (ms ²)	Before	1840 (218)	74.5	66	0.39
	After	1410 (211)	50.5	310*	0.66
LF n.u.	Before	40.8 (4.84)	42.2	-2.3	0.38
	After	12.3 (1.84)	13.9	-3.9*	0.92
HF n.u.	Before	40 (4.75)	41.8	-1.3	0.40
	After	12.3 (1.84)	11.4	3.9*	0.92
LF/HF (n.u.)	Before	1.48 (0.186)	48.6	-0.4*	0.91
	After	0.97 (0.146)	33	-0.33*	0.99
pNN50 (%)	Before	26.2 (3.12)	40.6	13*	0.63
	After	21.4 (3.21)	33.3	9.6*	0.77
RMSSD (ms)	Before	105 (12.5)	89.4	21*	0.13
	After	26.2 (3.91)	25.6	8.0*	0.71
SDNN (ms)	Before	129 (15.3)	95.6	18*	0.09
	After	14.8 (2.22)	13.1	1.7	0.90

* Mean difference = 0 (p≤0.05)

Table 9-5 - HRV variables from the ECG + PPG data fusion method before (54) and after (51) the stages were analysed to remove stages with corrupted BBIs

HRV variable	Before or after stages removed	RPC (CI)	CV (%)	Mean difference	R ²
LF (ms ²)	Before	2080 (247)	78.4	83	0.64
	After	467 (57.0)	18.6	-68*^	0.97
HF (ms ²)	Before	4520 (536)	171	240	0.34
	After	432 (52.7)	18.9	-59^	0.97
LF n.u.	Before	17.6 (2.08)	17.7	0.24	0.84
	After	6.96 (0.85)	6.98	-0.47^	0.97
HF n.u.	Before	17.6 (2.08)	18.1	-0.24	0.84
	After	6.96 (0.85)	7.22	0.47^	0.97
LF/HF (n.u.)	Before	1.25 (0.148)	35.1	-0.07	0.93
	After	1.07 (0.13)	29.3	-0.11	0.96
pNN50 (%)	Before	7.47 (0.887)	14.0	0.91	0.97
	After	3.72 (0.454)	6.82	0.72*^	0.99
RMSSD (ms)	Before	17 (2.02)	17.7	-1.1	0.86
	After	9.08 (1.11)	9.61	-0.61^	0.96
SDNN (ms)	Before	12.7 (1.51)	10.9	-1.0	0.93
	After	6.76 (0.826)	5.85	-1.5*^	0.98

* Mean difference = 0 (p≤0.05)

^ Mean difference significantly smaller than same value in Table 9-4

9.3.4.2 Discussion and Analysis

HRV analysis from the PPG data fusion method (Method 1) was significantly less accurate than the HRV values from the individual signals obtained from the maximum and 1st derivative PPG points. This is shown in Figure 9-12 and summarised in Table 9-4 whereby the mean difference values for the HRV variables from the PPG data fusion method were larger than for the 1st derivative PPG points and the R² were smaller than those in Table 8-9 in section 8.2.4.3 (except for the normalised LF and HF components and the SDNN). The PPG data fusion method was also less repeatable, with the RPC values from all HRV values (except the normalised LF and HF components) significantly larger in Table 9-4 than the RPC values for the HRV values shown in Table 8-9 in section 8.2.4.3. However, the number of stages where HRV was possible was 34, which was larger than the number of stages for the maximum and 1st derivative points individually (19 and 24 respectively). Hence for HRV analysis, the PPG data fusion method is less accurate and repeatable than the HRV analysis from only the maximum or 1st derivative PPG heartbeats, however it gives a larger number of HRV measurements.

The accuracy and repeatability of the HRV analysis from the ECG+PPG data fusion method (Method 2) in comparison to the HRV analysis from the reference ECG signal is shown in Figure 9-13 and summarised in Table 9-5. After the suspected corrupted HRV values are removed, the mean difference is equal to zero for the normalised LF and HF components (and LF/HF ratio), as well as the RMSSD values. Comparing the accuracy of the ECG+PPG data fusion method (Method 2) to the Pulse fusion method (Method 1) for all other HRV values, the mean difference values in Table 9-4 are significantly smaller than the mean difference values in Table 9-5 for all (HRV values except for the LF/HF ratio). Similarly, the R² values for the corrected HRV values in Table 9-5 are significantly larger than Table 9-4 (t-test: $p < 0.05$). These results indicate the ECG+PPG fusion method (Method 2) is more accurate than the PPG data fusion method (Method 1). This is also shown in Figure 9-14, where the HRV error for the pulse fusion method (left) is significantly larger than the error

from the ECG and PPG fusion method (middle) ($p < 0.0185$). This is probably because of the higher number of false positives and the lower number of correctly detected heartbeats shown in Figure 9-7 and Table 9-2, which will have a negative effect on the accuracy of the HRV estimation, particularly in stages 2, 5 & 6.

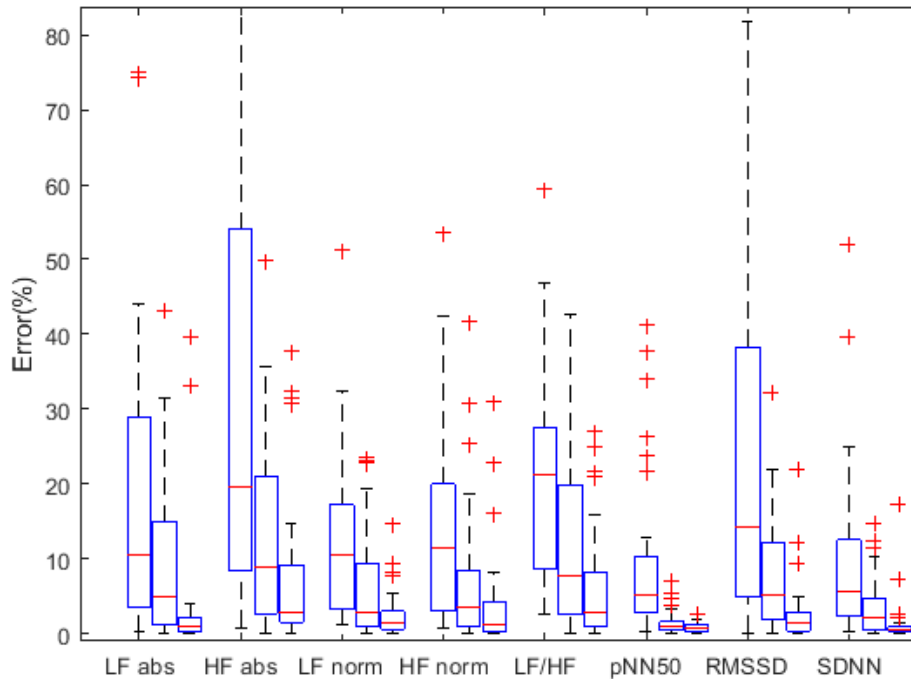


Figure 9-14-HRV Error for the Pulse fusion method (left) and for the ECG and PPG fusion method (middle), compared with the HRV error from the ECG by itself (right)

Table 9-5 shows the ECG+PPG data fusion method (Method 2) has a similar accuracy level as the HRV estimation from the ECG signal by itself (Table 8-7 section 8.2.4.1). This is indicated by the similar mean difference values and R^2 values for both sets of HRV values. However, comparing the repeatability of the two methods, the RPC values were significantly lower for the HRV values from the ECG signal than for the ECG+PPG fusion method (Method 2). Additionally, Figure 9-14 shows that HRV error for the ECG signal individually is lower than the HRV error for the ECG+PPG fusion method (Method 2) ($p < 0.025$, except for pNN50). However, the number of stages where an HRV value was extracted was higher for the data fusion method (51) compared with the ECG signal (28) and the PPG signal (19 and 24 stages).

Thus, although the data fusion algorithm may not improve the accuracy of the HRV value estimations, it does increase the number of stages that are acceptable for HRV analysis. This is because the ECG+PPG fusion algorithm is able to identify heartbeats from both the ECG and PPG signals. Since the HRV accuracy from the PPG signal was less accurate than from the ECG signal, when some of the BBI values from the PPG signal were combined with the ECG signal, the accuracy of the HRV estimation was reduced because of the use of the less accurate heartbeats.

The BBI signal from the ECG+PPG data fusion method (Method 2) provided a more accurate HRV analysis than the BBI signals from the PPG signal by itself. In Table 9-5 the R^2 values are either significantly higher or not significantly different to the R^2 values from the maximum points in the PPG signal in Table 8-5 and 8-6 in section 8.2.3 or the 1st derivative points in Table 8-8 and 8-9 in section 8.2.4. A larger number of HRV values from the ECG+PPG data fusion method (Method 2) had a mean difference not significantly different from zero ($p < 0.05$) in Table 9-5 than for the HRV variables from the 1st derivative PPG heartbeats in Table 8-9 in the previous chapter. A similar result occurs for the HRV RPC values from the ECG+PPG fusion method which were also either significantly lower or not significantly different to the HRV values from the 1st derivative PPG points. This was true for all HRV variables except for the absolute LF component, in which the RPC values were between 250 – 280 ms² lower for the PPG signal than for the ECG and PPG data fusion method.

For the ECG+PPG data fusion method (Method 2) the increase in the accuracy caused by removing inaccurate HR windows was not as large when compared with the individual HR signals from the ECG and PPG signals. This is also shown in Table 9-5. This is due to the increase in accuracy caused by the data fusion. The data fusion methods will, by their nature, remove some of the falsely classified heartbeats, so there are less likely to be false HR values in the fused HRs. This leads to more stages being accepted for HRV analysis,

and hence since less windows are discarded, the step of discarding inaccurate windows has a smaller effect than for the individual HR signals.

9.3.5 Results summary

The PPG data fusion method (Method 1) was able to accurately estimate the HR of the Cardiomask wearer over a 30 second and 5 minute period, however the accuracy and repeatability of the HR estimations, as well as the number of windows where HR estimation was possible was worse than the HR estimation from the 1st derivative PPG signal. The accuracy of the HRV analysis on the PPG data fusion signal (Method 1) was also less accurate and repeatable than for the BBI signals from the ECG and PPG signals individually.

The HR estimation from the ECG+PPG data fusion method (Method 2) was as accurate as the HR estimation from the ECG signal by itself, however the number of windows where accurate HR estimation occurred was higher for the ECG+PPG data fusion method for both 30 second and 5 minute windows. The accuracy of the HRV analysis for the BBI signal from the ECG+PPG data fusion method (Method 2) was less than the individual ECG HRV analysis, however it was more accurate than the PPG signal HRV analysis. Additionally, the number of windows where accurate HRV analysis occurred was largest for the ECG+PPG data fusion method (Method 2) (51) than for the ECG (28) and the PPG signals (19 & 24).

9.4 Category 2 - Generating multiple HR signals - Methods

The results from the previous section have shown that combining the ECG and PPG heartbeats increases the number of windows where accurate HR and HRV analysis can be estimated but also reduces the accuracy and repeatability of the HRV measurements. To attempt to preserve the accuracy of the HRV estimation whilst increasing the number windows where accurate mean HR and HRV estimations can be conducted, a new method of combining ECG and PPG data was implemented. Instead of combining multiple heartbeats into a single signal on which HR and HRV analysis was performed, HR and HRV analysis was calculated for each of the individual ECG and PPG HR signals. The “best” HR and HRV values were then taken as the true HR and HRV values, and the remaining values

were discarded. The reasoning behind this category of data fusion methods is that the HRV accuracy from the single HR source should be preserved, however more HRV values from other (potentially less accurate) sources can be included to attempt to increase the number of windows used. Three different methods were developed for combining multiple HR signals for HRV analysis, described in Sections 9.4.2 – 9.4.4.

9.4.1 Exclusion criteria

The data fusion methods in this Category 2 rely on deciding which mean HR and HRV values are accurate for each experiment stage for each participant, and which values are corrupted. For the ECG and PPG values, mean HR and HRV values were discarded based on the criteria described in section 7.3 and 7.4 for excluding mean HR and HRV values respectively. For mean HR and HRV values from fused HR signals (specifically in Method 5, described below), the inclusion/exclusion criteria described earlier in this chapter in section 9.2.1 were used to decide whether mean HR and HRV were discarded or kept.

9.4.2 Method 3: Pulse fusion method II

In the Pulse fusion method II (Method 3) only the HR and HRV values from the PPG signal are used. A flow chart for deciding the accurate mean HR and HRV values for each experiment stage for each participant for this method is shown in Figure 9-15.

9.4.3 Method 4: ECG+PPG method II

For the ECG+PPG method II (Method 4), HR and HRV values were used from the ECG signal as well as the PPG signal. This algorithm is designed for situations where the signal quality is such that few heartbeats can be found using the maximum minimum or 1st derivative heartbeat detection methods. A flow chart for deciding the accurate mean HR and HRV values for each experiment stage for each participant for this method is shown in Figure 9-16.

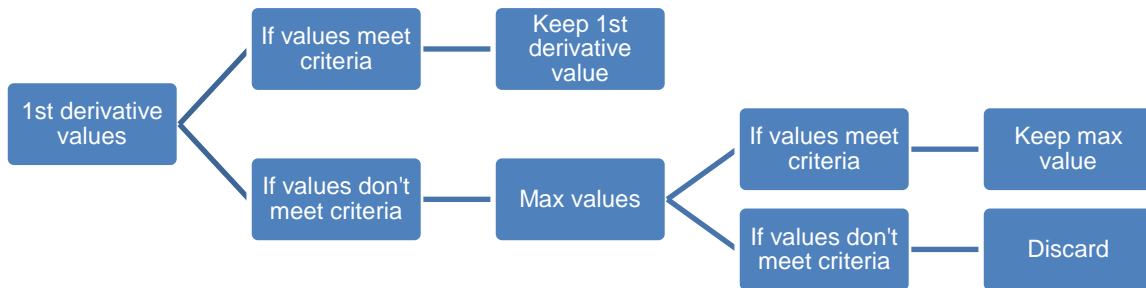


Figure 9-15 - A flow chart for deciding the accurate mean HR and HRV values for each experiment stage for each participant for Method 3: pulse fusion method II

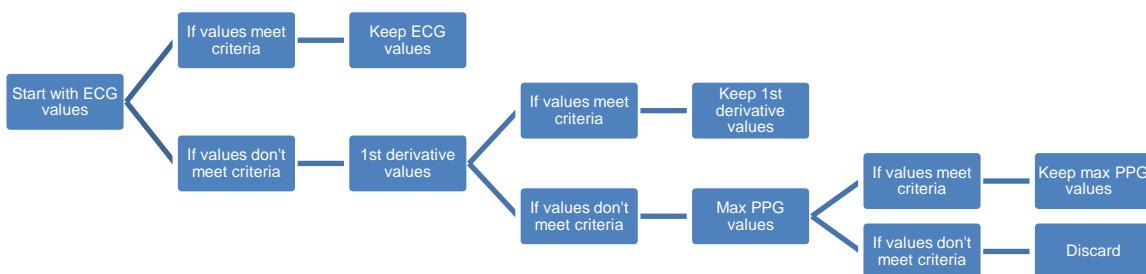


Figure 9-16 - A flow chart for deciding the accurate mean HR and HRV values for each experiment stage for each participant for Method 4: ECG + PPG method

9.4.4 Method 5: ECG+PPG+fused method

The ECG+PPG+fused method (Method 5) used HR and HRV values from the ECG, PPG signals as well as the ECG+PPG fusion method (Method 2) described in section 9.2. A flow chart for deciding the accurate mean HR and HRV values for each experiment stage for each participant for this method is shown in Figure 9-17.

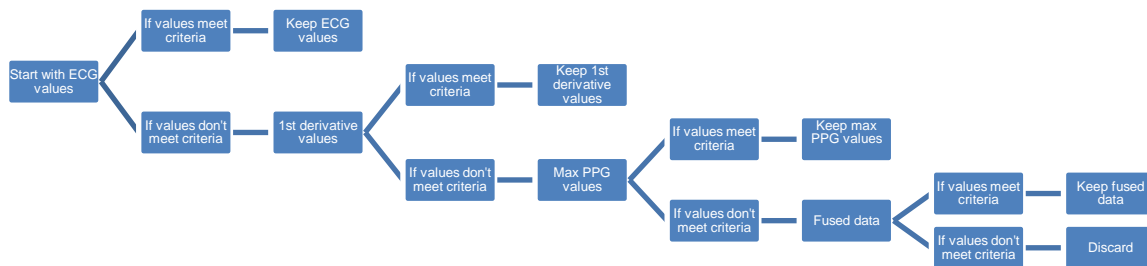


Figure 9-17 - A flow chart for deciding the accurate mean HR and HRV values for each experiment stage for each participant for Method 5: ECG + PPG + fused data method

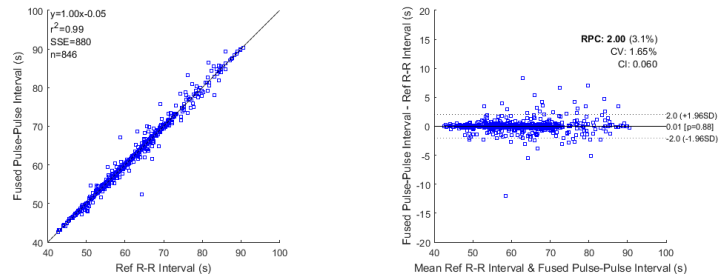
9.5 Category 2 - Generating multiple HR signals - Results

9.5.1 Mean HR value comparison

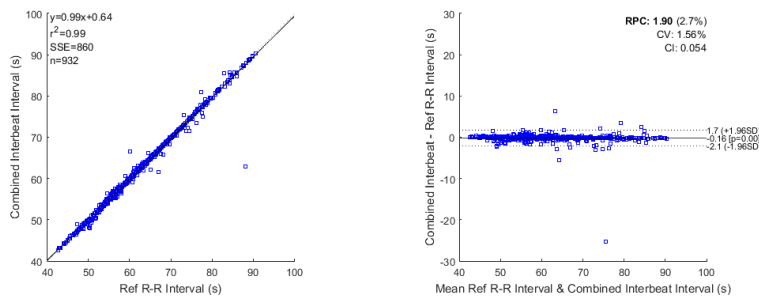
The BA plots comparing the mean HR values from data fusion methods described in section 9.4 to the mean HR from the reference ECG signal are shown in section 9.5.1.1. The results are summarised in Table 9-6.

9.5.1.1 BA plots

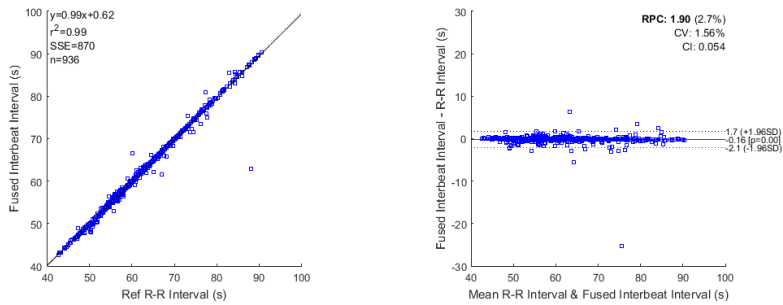
Mean HR for a 30 second window: Pulse Fusion method II (Method 3)



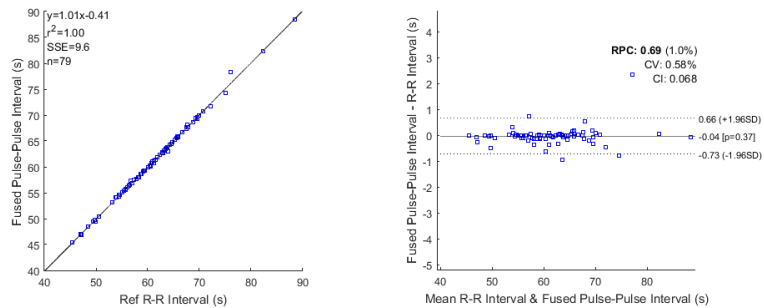
Mean HR for a 30 second window: ECG + PPG method II (Method 4)



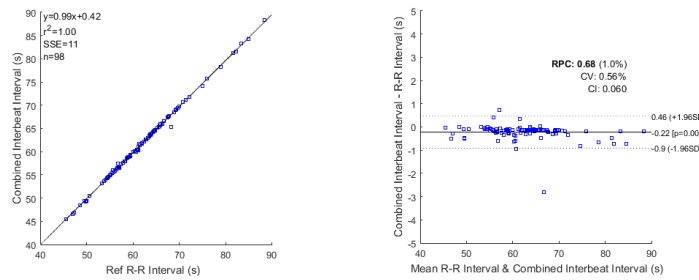
Mean HR for a 30 second window: ECG+PPG+fused method (Method 5)



Mean HR for a 5 minute window: Pulse Fusion method II (Method 3)



Mean HR for a 5 minute window: ECG + PPG method II (Method 4)



Mean HR for a 5 minute window: ECG+PPG+fused method (Method 5)

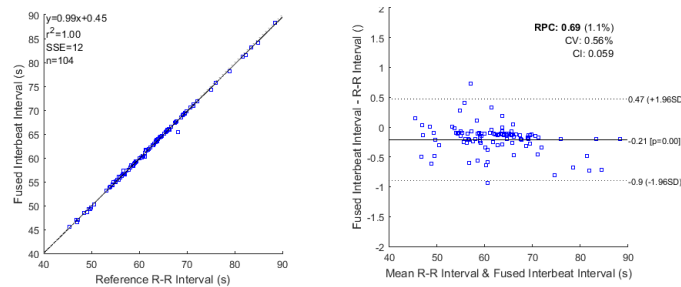


Figure 9-18 - BA plots for the mean HR estimation from the three data fusion methods (described in section 9.4) in comparison to the HR from the reference ECG signal. The window length for the figures were 30 seconds and 5 minutes.

Table 9-6 - Mean HR for data fusion methods

	Face ECG		PPG 1 st derivative		Pulse fusion II (Method 3)		ECG+PPG II (Method 4)		ECG + PPG + Fused (Method 5)	
	0.5	5	0.5	5	0.5	5	0.5	5	0.5	5
Window length (mins)										
RPC (CI)	1.91 (0.057)	0.71 (0.066)	1.27 (0.038)	0.68 (0.068)	2.00 (0.06)	0.69 (0.068)	1.90 (0.054)	0.68 (0.06)	1.90 (0.054)	0.69 (0.059)
CV (%)	1.54	0.57	1.05	0.57	1.65	0.58	1.56	0.56	1.56	0.56
Mean difference	-0.13*	0.19*	0.01	-0.06	0.01	-0.04	-0.16*	-0.22*	-0.16*	-0.21*
R ²	0.99	0.99	0.99	0.99	0.99	0.99	0.99	0.99	0.99	0.99
N	836	87	829	76	846	79	932	98	936	104

* Mean difference = 0 (p < 0.05)

9.5.1.2 Analysis and Discussion

Combining the mean HR information from different signals increased the amount of data from which accurate mean HR estimation occurred, without reducing the accuracy of the mean HR estimation. This is shown in Figure 9-18 and summarised in Table 9-6 where there is little difference in the R² and mean difference values from all data fusion methods

described in section 9.4 and from the ECG signal by itself. Additionally, the CV and RPC values are not significantly different for the different data fusion methods for both the 30 second and 5-minute windows, and are also not significantly different from the RPC values from the ECG signal. However, the number of windows where accurate mean HR estimation occurs is greater for the ECG+PPG method II (Method 4) and the ECG, PPG and fused method (Method 5), for both the 5 minute and 30 second windows. Additionally, although the number of windows where accurate mean HR estimation occurred in the Pulse Fusion method (Method 3) was larger than for the 1st derivative PPG method, the accuracy of the mean HR estimation is greater from the 1st derivative PPG HR signal than the HR signal from the Pulse Fusion method II (Method 3). However, Table 9-6 shows that the accuracy of the mean HR estimations from the Pulse Fusion method II (Method 3) is greater than from the face ECG signal, and the RPC and CV values are similar between the face ECG and Pulse Fusion method II (Method 3). This suggests that for estimating the mean HR, the Pulse Fusion method II (Method 3) is suitable.

The performance of Pulse fusion method II (Method 3) for estimating the mean HR was similar to the performance of the Pulse fusion method (Method 1), shown in Table 9-6. For both the Pulse fusion methods (Methods 1 and 3), the R^2 values of the HR estimations were equal to 0.99 for both 30 second and 5 minute windows. Over a 30 second window, Table 9-3 and Table 9-6 both show the mean differences from both methods were not significantly different from zero, and there were no significant differences between the RPC values from either data fusion method. However, over a 5 minute window, the mean difference was significantly smaller for Pulse fusion method II (Method 3) than for Pulse fusion method (Method 1), and similarly the RPC values were smaller for Pulse Fusion method II (Method 3) than for Method 1. This suggests that over a 30 second window there is no difference in the performance of the data fusion methods, however over a 5 minute window, Pulse Fusion method II (Method 3) produces a more accurate and repeatable mean HR estimation than Pulse fusion method (Method 1).

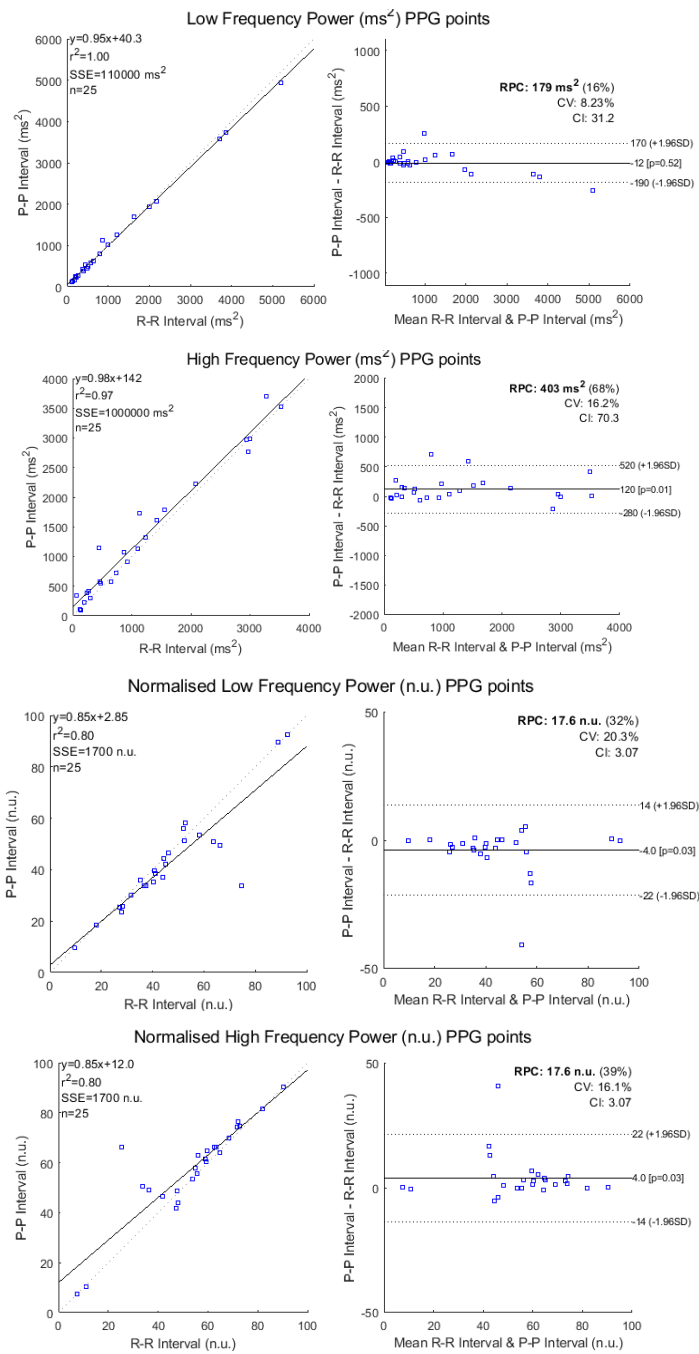
Similarly, there was little difference between the accuracy of the mean HR estimation from both ECG+PPG data fusion methods, Method 2 and Method 4. Comparing Table 9-3 and Table 9-6, there is no difference or little difference between the R^2 values and mean difference values for the two data fusion methods (Method 2 and Method 4). There is also no significant difference between the RPC values for both data fusion methods. This was true for both 30 second and 5 minute windows. This result as well as the results from the pulse fusion HR comparison suggest that the data fusion strategies described in section 9.2 will produce a mean HR accuracy with a similar level of performance to the data fusion strategies described in section 9.4.

9.5.2 HRV analysis

The BA plots comparing the HRV analysis results from the three data fusion methods described in section 9.4, to the HRV analysis results from the reference ECG, are shown in sections 9.5.2.1 and are summarised in Table 9-7, Table 9-8 and Table 9-9.

9.5.2.1 BA plots

9.5.2.1.1 Method 3: Pulse fusion method II



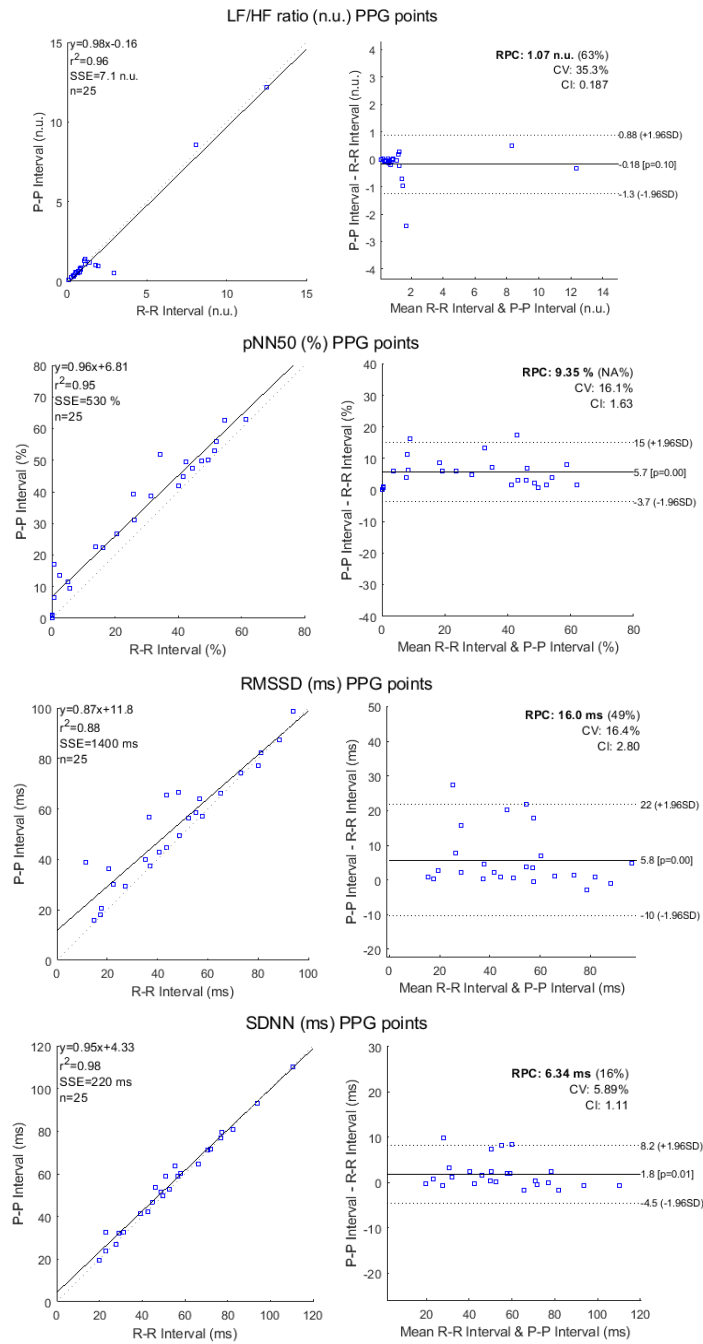


Figure 9-19 - BA plots for different HRV variables from BBI signals from the PPG data fusion method II (Method

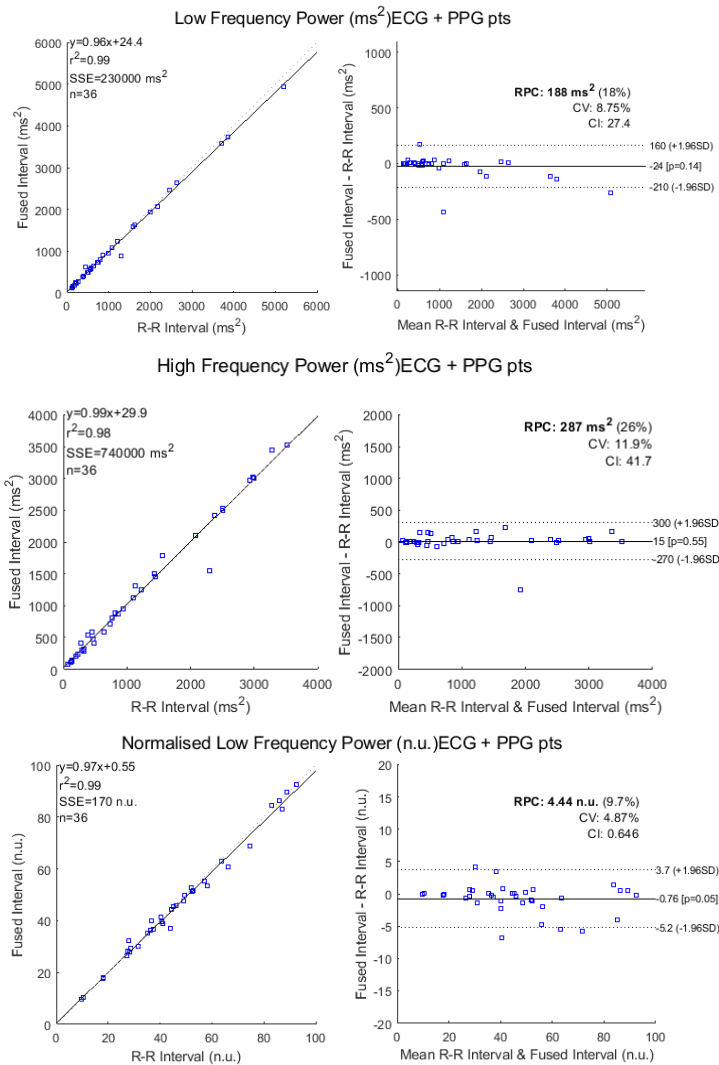
3)

Table 9-7 - HRV accuracy combining data from the Pulse Fusion method II (Method 3) (n=25)

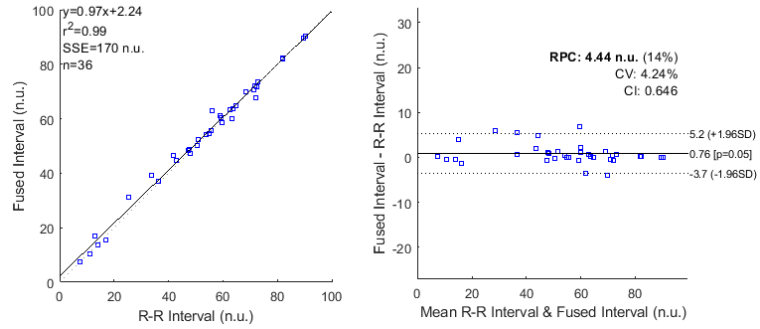
HRV variable	RPC (CI)	CV (%)	Mean difference	R ²
LF (ms ²)	179 (31.2)	8.23	-12	0.99
HF (ms ²)	403 (70.3)	16.2	120 *	0.97
LF n.u.	17.6 (3.08)	20.3	-4.0 *	0.8
HF n.u.	17.6 (3.07)	16.1	4.0*	0.8
LF/HF (n.u.)	1.07 (0.187)	35.3	-0.18	0.96
pNN50 (%)	9.35 (1.63)	16.1	5.7 *	0.95
RMSSD (ms)	16.0 (2.80)	16.4	5.8*	0.88
SDNN (ms)	6.34 (1.11)	5.89	1.8 *	0.98

* Mean difference not equal to 0 (p < 0.05)

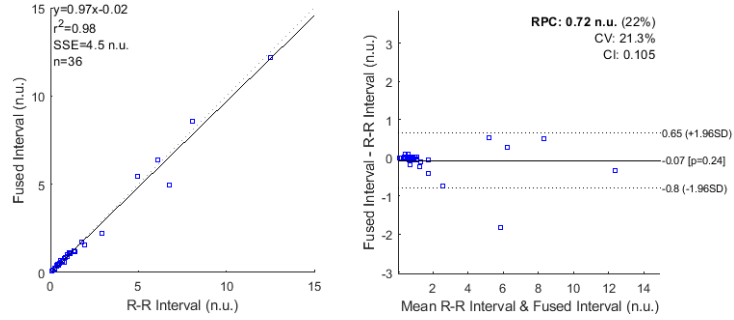
9.5.2.1.2 Method 4: ECG+PPG method II



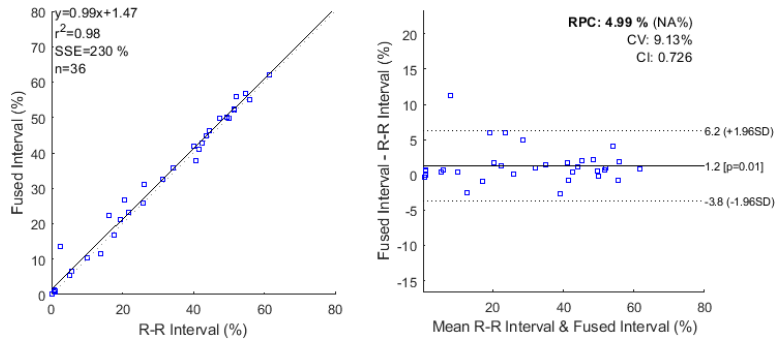
Normalised High Frequency Power (n.u.) ECG + PPG pts



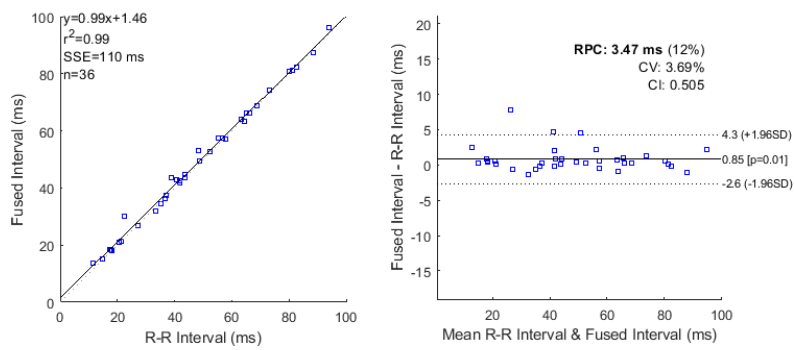
LF/HF ratio (n.u.) ECG + PPG pts



pNN50 (%) ECG + PPG pts



RMSSD (ms) ECG + PPG pts



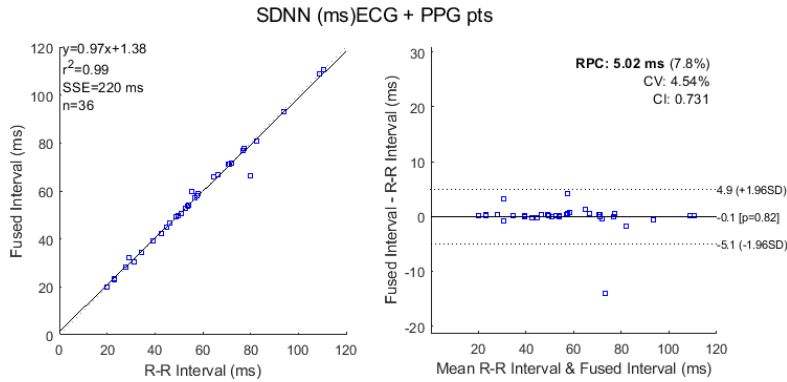


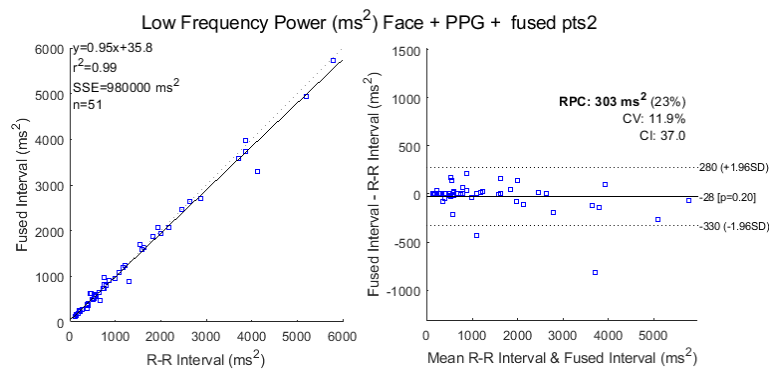
Figure 9-20 - BA plots for different HRV variables from BBI signals from the ECG+PPG data fusion method II (Method 4).

Table 9-8 - HRV accuracy combining data from the ECG+PPG HR (Method 4) signals (n=36)

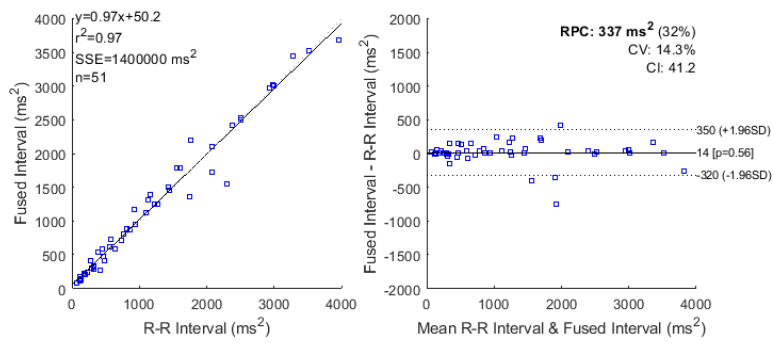
HRV variable	RPC (CI)	CV (%)	Mean difference	R ²
LF (ms ²)	188 (27.4)	8.75	-24	0.99
HF (ms ²)	287 (41.7)	11.9	15	0.98
LF n.u.	4.44 (0.646)	4.87	-0.76*	0.99
HF n.u.	4.44 (0.646)	4.24	0.76*	0.99
LF/HF (n.u.)	0.72 (0.105)	21.3	-0.07	0.98
pNN50 (%)	4.99 (0.726)	9.13	1.2 *	0.98
RMSSD (ms)	3.47 (0.505)	3.69	0.85*	0.99
SDNN (ms)	5.02 (0.731)	4.54	-0.1	0.99

* Mean difference not equal to 0 (p < 0.05)

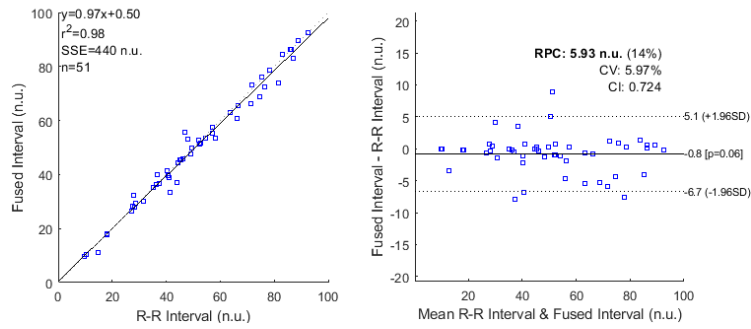
9.5.2.1.3 Method 5: ECG+PPG+fused method



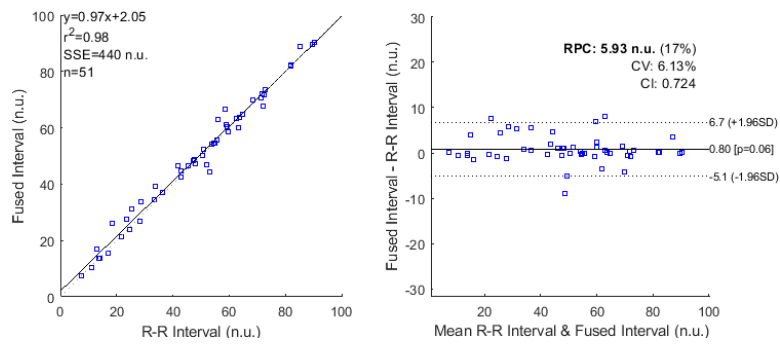
High Frequency Power (ms²) Face + PPG + fused pts2



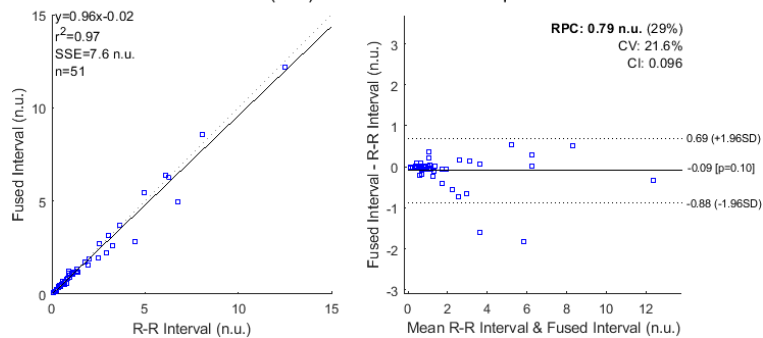
Normalised Low Frequency Power (n.u.) Face + PPG + fused pts2



Normalised High Frequency Power (n.u.) Face + PPG + fused pts2



LF/HF ratio (n.u.) Face + PPG + fused pts2



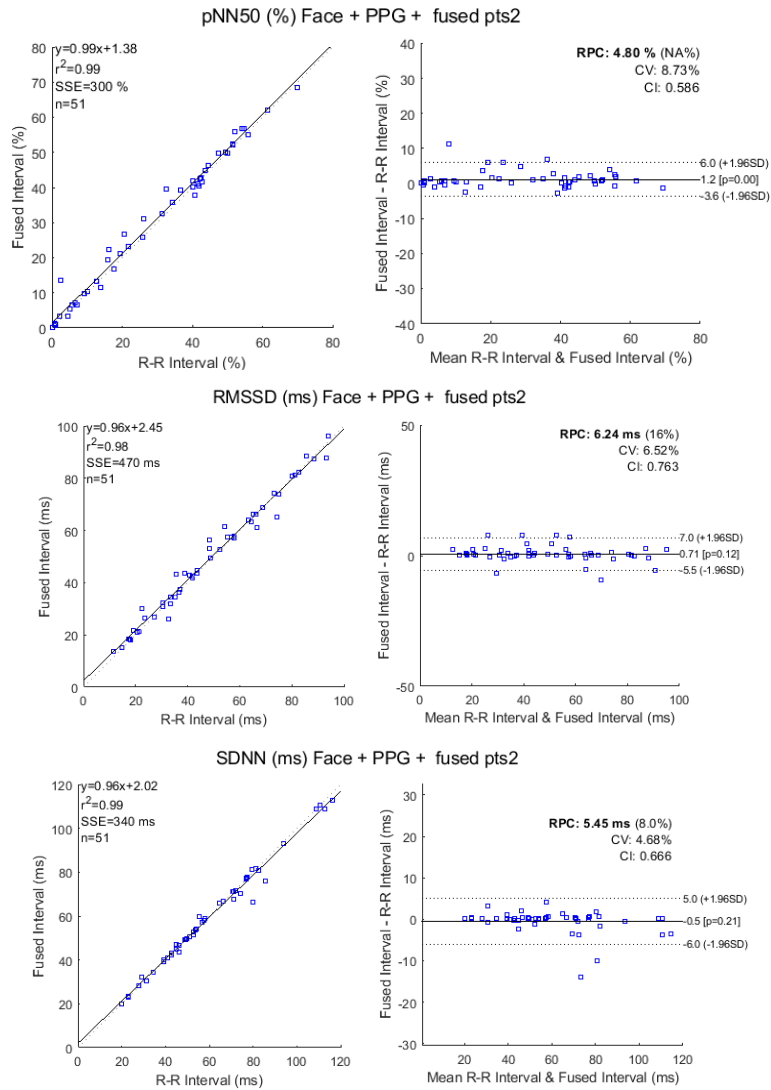


Figure 9-21 - BA plots for different HRV variables from BBI signals from the ECG+PPG+fused data fusion method (Method 5) before (left) and after (right) bad HRV windows are removed.

Table 9-9 - HRV accuracy combining data from the ECG, PPG and fused HR signals (Method 5) (n=51)

HRV variable	RPC (CI)	CV (%)	Mean difference	R ²
LF (ms ²)	303 (37.0)	11.9	-28	0.99
HF (ms ²)	337 (41.2)	14.3	14	0.97
LF n.u.	5.93 (0.724)	5.97	-0.8	0.98
HF n.u.	5.93 (0.724)	6.13	0.8	0.98
LF/HF (n.u.)	0.79 (0.096)	21.6	-0.09	0.97
pNN50 (%)	4.80 (0.586)	8.73	1.2*	0.99
RMSSD (ms)	6.24 (0.763)	6.52	0.71	0.98
SDNN (ms)	5.45 (0.666)	4.68	-0.5	0.99

* Mean difference not equal to 0 (p < 0.05)

9.5.2.2 Analysis and Discussion

The method of combining the HRV variables from the individual PPG HR signals (Method 3) is more accurate than the HRV variables from the Pulse Fusion method (Method 1). This is demonstrated in Figure 9-19 and summarised in Table 9-7, where all mean difference values are either less than or equal to corresponding mean difference values from the pulse fusion method (Method 1) in Table 9-4. Similarly, apart from the normalised LF and HF plots, the R² values were larger in Table 9-7 for Pulse fusion method II (Method 3) than from the pulse fusion method (Method 1) in Table 9-4. The RPC values were also significantly smaller for the HRV values from the Pulse fusion method II (Method 3) than from the pulse fusion method (Method 1). As was mentioned in section 9.3, the pulse fusion method (Method 1) produces HRV variables that are less accurate than the individual PPG signal HRV variables. Since the Pulse fusion method II (Method 3) is made up of HRV variables from either the maximum PPG HR or the 1st derivative PPG HR, it follows that combining the best data points from these two data sets results in more accurate HR and HRV values than the pulse fusion method (Method 1), as the HRV variables from this method were less accurate than from the maximum and the 1st derivative PPG heartbeats individually.

Similarly, there was little difference between the mean difference, R² values and RPC values from the Pulse fusion method II (Method 3) in Table 9-4 and from the 1st derivative PPG signal, shown in the previous chapter in Table 8-9 in section 8.2.4. This is because, of the 25 data points from the Pulse fusion method II (Method 3) HRV data, 24 of them come from the

1st derivative HRV data. This suggests that the most accurate method for combining two HR signals from the same PPG signal for HRV analysis is to calculate the HRV variables for the individual PPG signals and then combine the HRV data as described in section 9.4, instead of combining the BBI values into one BBI signal and then performing HRV analysis on the combined BBI signal, as described in section 9.2.

The method that had the highest accuracy of all fusion methods was the ECG+PPG method II (Method 4), with results given in Figure 9-20 and summarised in Table 9-8. Apart from the absolute LF component, the mean difference values for all HRV values in Table 9-8 were not largely different from the HRV values from the ECG signal, shown in Table 8.7 in section 8.2.4. Similarly, the RPCs from the ECG+PPG method (Method 4) HRV values were not significantly different to the RPCs of the HRV variables from the ECG signal, indicating no significant difference in repeatability between the two methods. However, the number of stages for HRV analysis for the ECG+PPG method II (Method 4) (41) was larger than for the ECG signal by itself (33), although it was lower than when the fused HR data was added ECG+PPG+fused method (Method 5) as shown in Table 9-9 (51). Hence this suggests that data fusion methods can be used to increase the amount of HRV data that can be accurately analysed from an ECG and PPG signal, without a significant reduction in the accuracy and repeatability of the results.

The HRV variables from the ECG+PPG+fused method (Method 5) was either more accurate than, or not significantly different to the HRV variables from the 1st derivative PPG HR signal, depending on the HRV variable analysed. This is shown in Figure 9-21 and is summarised in Table 9-9. However, the number of stages where HRV was calculated is much higher for Method 4 (51), than for the PPG HRV windows (21 and 23). The HRV variables from the ECG+PPG+fused method (Method 5) are more accurate than the 1st derivative HRV variables for the normalised LF and HF components, pNN50, and RMSSD. The reason these variables are significantly more accurate is unknown. The normalised HF, pNN50 and

RMSSD are all measures of short term variability, however there is no significant difference for absolute HF which is also a short term measure. The reason these variables are more accurate is more likely a result of the data being combined from different sources. This is because the normalised frequency components and the pNN50 values will not have as large a range as the absolute LF and HF components. This means that any outlier normalised HF or pNN50 values will have less of an effect on the confidence intervals of the RPC values, when compared with any outlier values from the absolute LF or HF components.

The reason that HRV analysis from the ECG+PPG HR signals (Method 4) shown in Table 9-8, may be more accurate than the method using ECG, PPG and the fused heartbeats (Method 5) shown in Table 9-9 is due to the HRV accuracy of the fused BBI values. The HRV data from the fused heartbeats are from stages where the accuracy of the ECG and PPG signals are not sufficient for HRV analysis, which means that any input data for the data fusion algorithm may also not be accurate. As such the output data will be less accurate than in other stages where the signal quality is higher. However as mentioned before the trade-off of this reduced accuracy is that reliable HRV analysis is able to be performed on more of the stage.

9.5.3 Results summary

The most accurate method for combining data for HRV analysis was achieved by using data from the ECG and PPG signals (ECG+PPG method (Method 4)) which was as accurate as the HRV analysis from the face ECG signal alone. However, to increase the amount of HRV data available, the HRV data from the fused HR signal (Method 5) can be added in cases when data from the ECG and PPG signals cannot be used for HRV analysis. Although a slight reduction in accuracy occurs, this method is still as accurate as using HRV analysis information from the 1st derivative PPG signal alone.

9.6 Discussion

Heartbeat data from the ECG and PPG signals were combined in an attempt to increase the accuracy of the HR and HRV analysis from the data. The information was also combined to increase the amount of accurate data on which reliable HR and HRV analysis could be performed. Using the heartbeats from the ECG and PPG signals, a common heartbeat signal was used to generate a fused BBI signal. From this fused signal, HR and HRV analysis was performed. HR and HRV information from the individual ECG, PPG and fused HR signals was also compared and the most accurate information from each signal was used to estimate the HR and HRV response for each participant.

The data fusion methods described in this chapter use signals that have a reasonably high accuracy level. As was seen in the previous chapter, for all BBI signals for all experiment stages, more than 90% of the heartbeats were correctly identified with less than 3% of the heartbeats being false positives. This means that if there is a temporary reduction in the signal quality in one of the signals, there is a reasonable chance that one of the other HR signals will be able to provide accurate HR information until the signal quality in the first signal is back to normal, which is why the data fusion method provides good results.

The data fusion methods described in this chapter were applied on heartbeats (and associated HRs) after the BBI correction algorithm (Section 6.6.1) had been applied. In theory, this means that there should be less false positives input to the data fusion algorithm, however as shown in the previous chapter there may also be less true heartbeats. If the data fusion algorithm was applied on the heartbeats before the BBI correction algorithm was applied it is unknown what the difference in the HR and HRV accuracy would be. For example, more false positives may result in more false positives in the fused BBI signal, or it may cause more true heartbeats to occur in the fused HR signal. This should be investigated in future work.

In the previous chapter it was discovered that the bi-level PAP mode causes a reduction in the signal quality of the PPG signal. Since all data fusion methods rely on heartbeats from the PPG signal, this means when bi-level mode is activated the accuracy and sensitivity may be reduced.

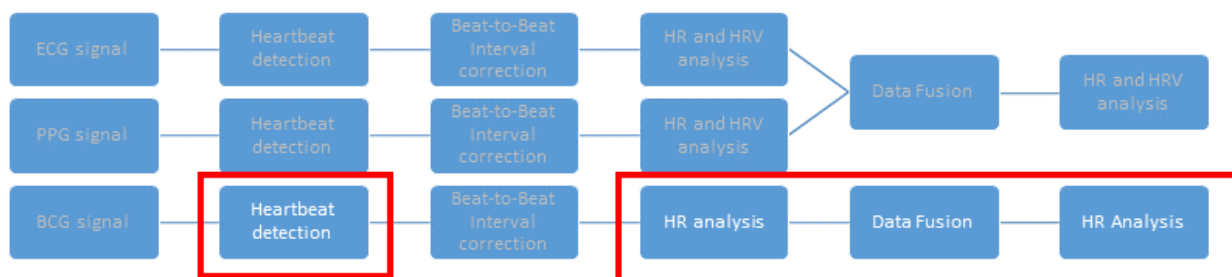
For the HRV analysis, stages that contained ectopic beats were manually excluded prior to the data fusion process. This was done since it is known that ectopic beats can cause inaccurate HRV measurements, and HRV analysis is rarely performed on a HR segment containing an ectopic heartbeat [8]. However, the ultimate aim of this work is to develop algorithms that can automatically determine whether a segment is acceptable for HRV analysis. Future work is recommended to develop a method for automatically identifying and discarding ectopic beats (such as described in [201]) to reduce the need for manual corrections of ectopic heartbeats.

The data fusion methods described in this paper were based on one HR from one ECG signal and three HRs from one PPG signal. It is unknown what the accuracy of these methods would be if other signals were used, or if multiple ECG or PPG signals were used. It is thought that, the higher the number of accurate signals, the greater the accuracy would be, however the data fusion methods may require some modifications to suit different numbers of input signals.

9.7 Conclusion

By combining the heartbeats from the ECG and PPG signals the amount of accurate HR data that was collected was increased in comparison with the HR from the individual signals, without any significant decrease in the accuracy of the HR. Additionally, by combining the HRV variables from the ECG and PPG signals, the number of accurate HRV windows was increased without a significant decrease in the HRV accuracy in comparison to just the ECG signal. Finally by combining the ECG, PPG and fused HRV data, the number of accurate

HRV windows can be further increased, with the accuracy of the resulting HRV variables being similar to the results of the HRV analysis of the PPG signals alone.



10. BCG testing

²The aim of this chapter was to measure Heart Rate (HR) using the gyroscope signals from the Inertial Measurement Unit (IMU) mounted on the Cardiomask, using a method called Ballistocardiography (BCG). As was mentioned in chapter 7, the gyroscope signals were used primarily to detect movement episodes to reduce the effect of motion artefacts on the ECG and PPG signal. However if the HR of the Cardiomask wearer can be detected from the Cardiomask gyroscope then this could provide another source of HR data which may be useful particularly for periods when the ECG or PPG signal quality is reduced. This chapter will discuss the following:

- Algorithm for detecting heartbeats from a gyroscope signal from a gyroscope embedded into the Cardiomask;
- Results of heartbeat detection algorithm on healthy participants;
- Description of two different data fusion algorithms used to improve the accuracy and consistency of the HR signal;
- Results from the two data fusion algorithms, including a comparison between them.

² Excerpts from this chapter have been taken from previous publications by the author from the following sources:

221. Gardner, M., et al. *Estimation of heart rate during sleep measured from a gyroscope embedded in a CPAP mask*. in *Biomedical Engineering and Sciences (IECBES), 2016 IEEE EMBS Conference on*. 2016. IEEE.

222. Gardner, M., et al. *A wearable device for monitoring patients during PAP therapy*. in *IEEE Life Science Conference*. 2017. Sydney, Australia: IEEE.

10.1 Introduction

As described in chapter 7, an IMU (MPU-9150) was attached to the Cardiomask (Figure 10-1). The sampling frequency of the gyroscope signals was 50 Hz.

The gyroscope signals were recorded simultaneously with the ECG and PPG signals that were discussed in chapters 8 and 9. A reference HR was measured from a reference ECG signal from electrodes located on the participant's hands and right foot. The reference ECG signal sampled was at 500Hz and heartbeats were detected using the Pan-Tompkins algorithm [185]. Participants lay on their back and sides for a period of 5 minutes each (stages 1-4), as well as simulating CPAP (stage 5) and bi-level PAP therapy (stage 6) for 5 minutes.

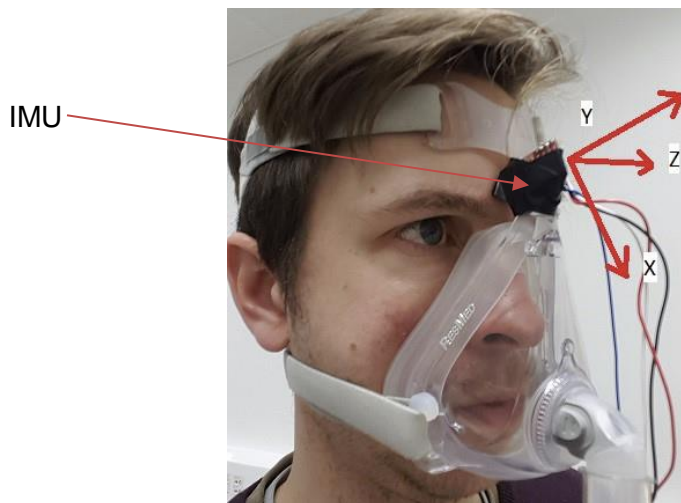


Figure 10-1 - Position and orientation of gyroscope axis in the IMU mounted on PAP mask

10.2 Identifying heartbeats in the BCG signal

To identify the heartbeats of the subject, the x, y, and z components of the gyroscope were analysed. A normalised signal was also calculated and was defined as

$$g_n = \sqrt{g_x^2 + g_y^2 + g_z^2} \quad (10.1)$$

where g_x , g_y , and g_z represent the x, y, and z components of the gyroscope, and g_n is the normalized gyroscope component. All 4 signals were resampled from 50Hz to 500 Hz, the

same frequency as the reference ECG signal. The signals were then transformed to make heartbeat detection easier as shown in Figure 10-2. The steps to transform the signals and identify the heartbeats are:

- A discrete Hilbert transform [223] was applied on the three gyroscope signals g_x , g_y , and g_z retroactively, using the standard Matlab 'hilbert' function. This transformation was applied as the movement caused by the BCG forces cause the head to wobble, which can be more difficult to reliably detect than a peak. The Hilbert transform was able to transform this 'wobble' into a peak, which is easier to detect. The Hilbert transform was not applied to the normalized gyroscope signal g_n , since during testing there was no significant improvement gained by transforming this signal.
- A 2nd order Butterworth filter with lower and upper cut-off frequencies of 0.5 and 10Hz was applied to remove high frequency motion artefacts, reduce vibration from unwanted sources, and remove baseline drift.
- A movement artefact threshold was calculated for each signal to remove large movement artefacts. Four different thresholds were calculated for each of the x, y, and z components as well as the normalised gyroscope component, and any part of the signal larger than the threshold for the specific component was set to zero. The thresholds were calculated in a 9 second initialisation period at the start of recording. The calculation was made by defining 6 non-overlapping consecutive windows of width 1.5 seconds. The maximum value for each window was calculated, and then the average of these maximum values was taken as the threshold for that component.
- Signals were squared to increase their SNRs.
- Signals were integrated using an integration window of 0.1 seconds to assist with peak detection by amplifying peaks but not noise. A width of 0.1 seconds was chosen, as based on early experimentation, this value provided the most accurate heart beat detection results.

- Peak detection algorithm was applied. Peaks were then categorised as heartbeats. The algorithm used to identify peaks from the integration window was derived from the peak detection section of the Pan-Tompkins QRS detection algorithm [185].
- The Beat-to-Beat Interval (BBI) correction algorithm described in section 6.6.2 (the combined threshold algorithm) was applied to all four resultant HR signals, to reduce the number of false positive heartbeats detected and improve the accuracy of the HR measurements.

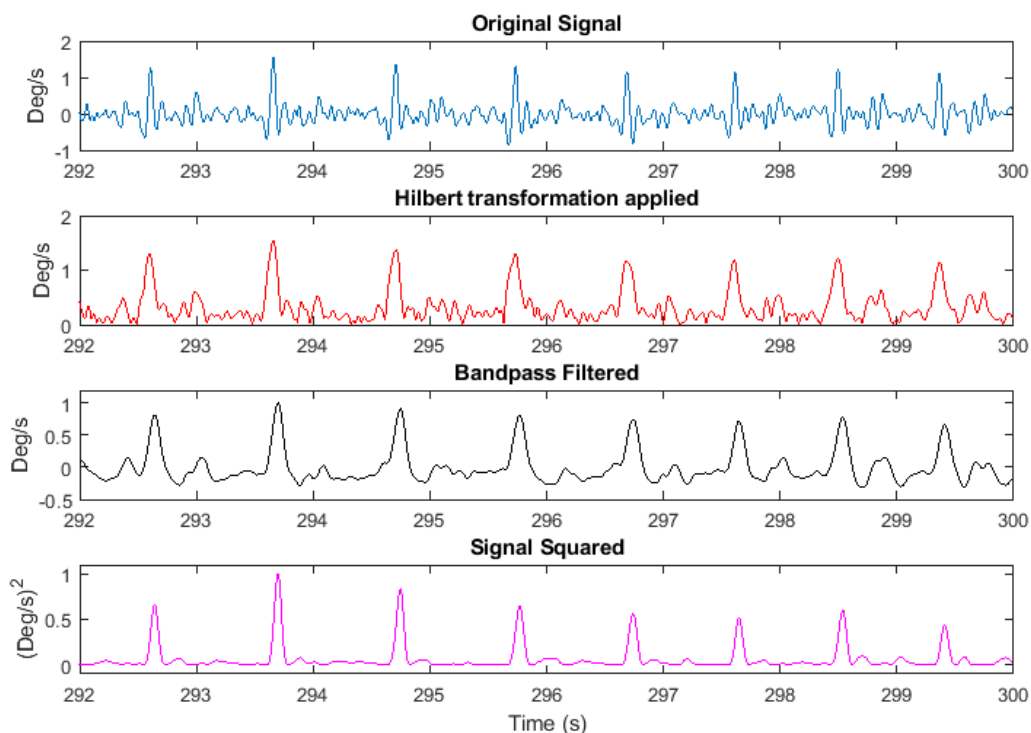


Figure 10-2 - An example of the signal processing steps that converts the raw gyroscope signal (top) to a signal where the heartbeats can be easily detected (bottom)

10.3 Experiment method

For the four HR signals from the different gyroscope signals (g_x , g_y , g_z and g_n), the number of correctly detected and falsely detected heartbeats were analysed. Additionally, Bland-Altman plots were constructed for the BBI values from each of the gyroscope signals to assess the accuracy of the measured BBI values in comparison to the reference ECG signal.

10.4 Results

10.4.1 Examples of BCG signals – Lying on Back

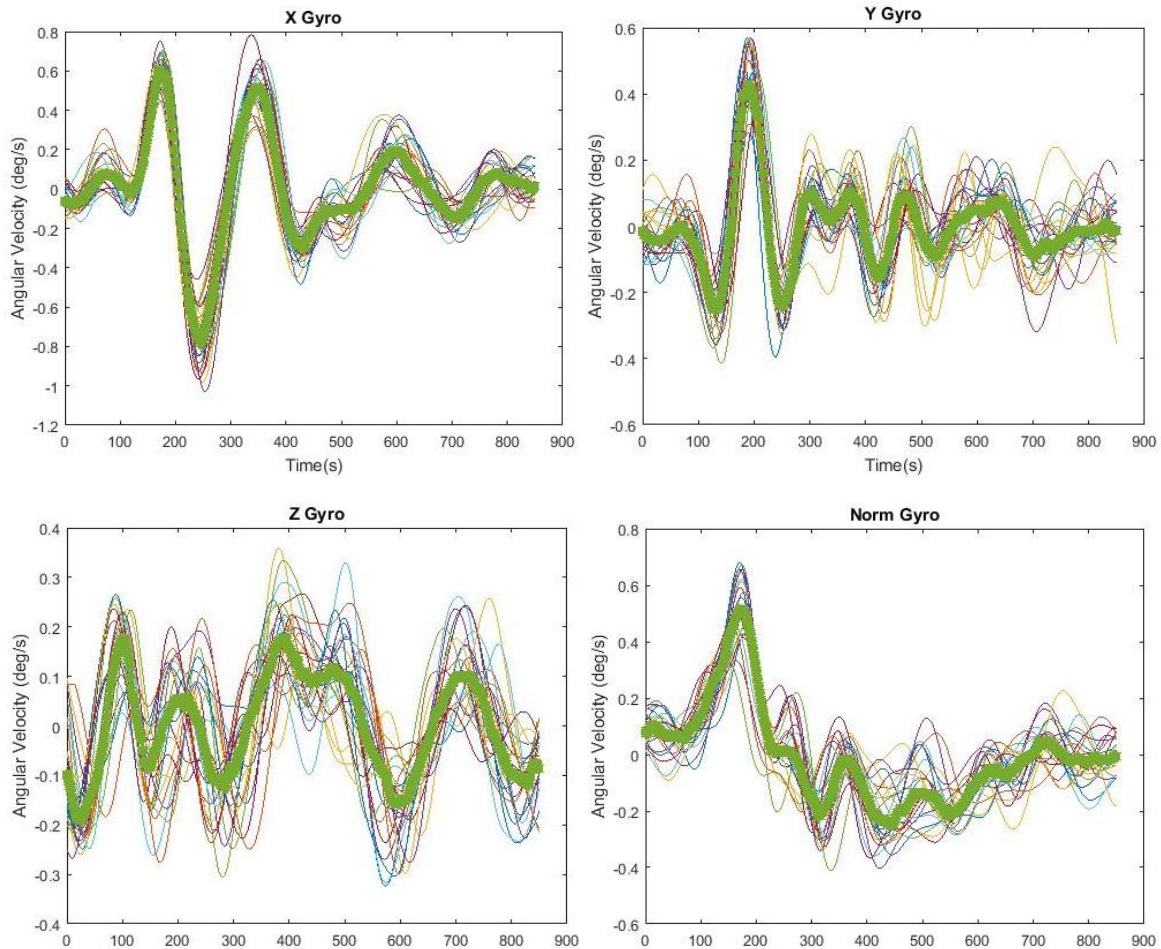


Figure 10-3 – Example of gyroscope signals caused by a heartbeat when participant was lying on their back. The averaged signal is shown as the thick green line in each plot.

An example of a BCG signal recorded from one participant is shown in Figure 10-3, and was recorded when the participant was lying on their back and when the PAP device was off. The X, and Y gyroscope signals both have a clear and distinct peak at around 200ms caused by the heartbeat, which causes a similar peak in the normalised gyroscope signal. According to Figure 10-1, the X gyroscope signal corresponds to rotation in the horizontal direction and the Y gyroscope signal corresponds towards rotation towards the shoulders. In the Z gyroscope signal, there was no distinct and obvious peak at this time point. This implies that the resulting movement caused by a heartbeat is not as strong in the Z direction (which Figure 10-1 shows is an up and downward movement of the head).

10.4.2 Examples of BCG signals – Lying on Side

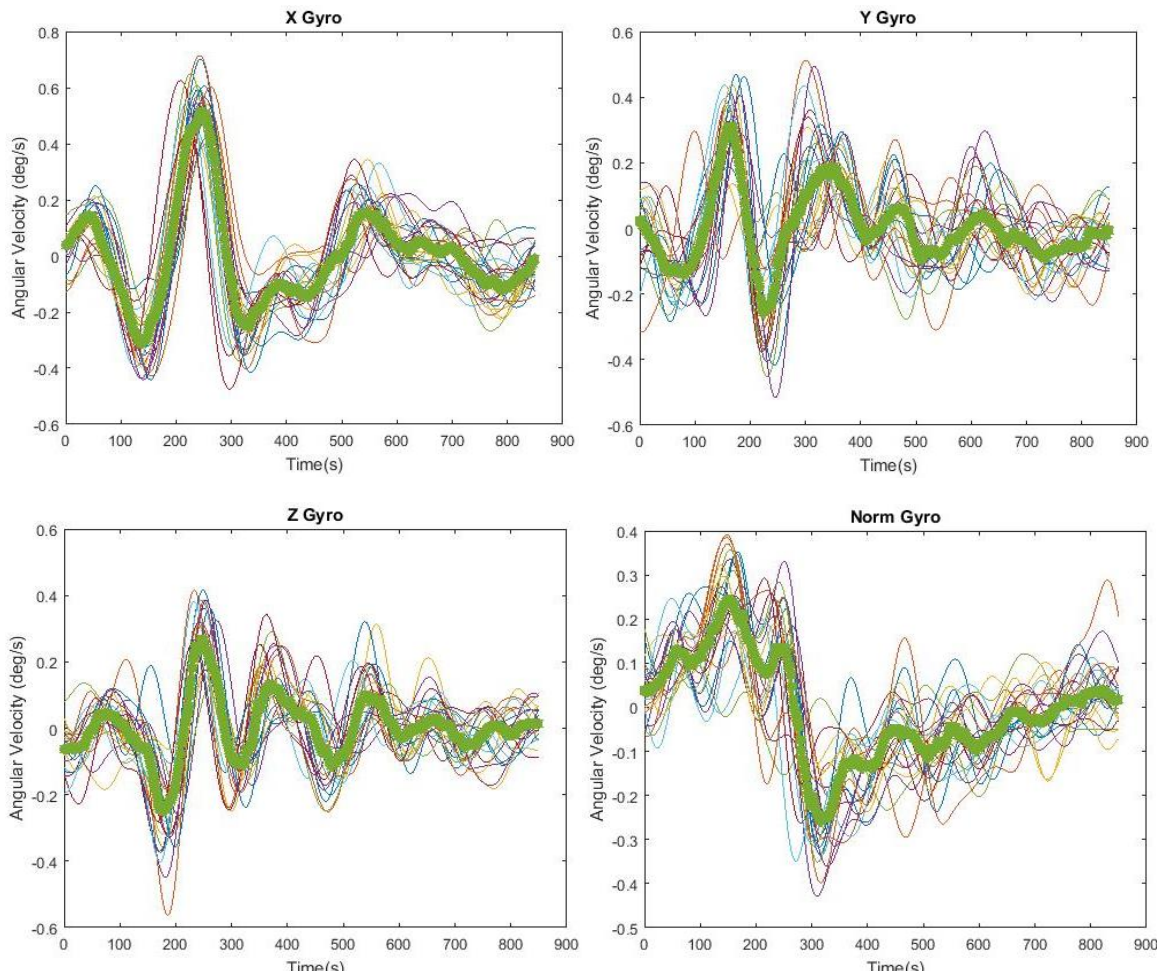


Figure 10-4 - Example of Gyroscope signals caused by a heartbeat when participant was lying on their left side. The averaged signal is shown as the thick green line in each plot.

An example of the BCG signal recorded when the same participant was lying on their left side is shown in Figure 10-4 and when they were lying on their right side in Figure 10-5. These figures, when compared with the BCG signal in Figure 10-3, show that there is a difference in the BCG signal when the participant was lying on the side compared with when they were lying on their back. There is a reduction in the peak magnitude when the participant was lying on their side, particularly in the X and Y gyroscope signals. Additionally, in Figure 10-3 when the participant is on their back the maximum value at 250ms is in the negative direction, however when the participant is lying on their left side (Figure 10-4) the maximum value is in the positive direction at that same time point. Furthermore the peak is not as distinctive in the X gyroscope signal in Figure 10-5. This shows that the shape of the

signals change with different sleeping positions, which is due to the differing dynamics of the movement of the participants with different sleeping positions. It is hence expected that the performance of the heartbeat detection algorithms will vary with different sleeping positions, and future work may look at the possibility of making custom heartbeat detection algorithms for different sleeping positions. In this thesis however, the same algorithm will be used for all sleeping positions.

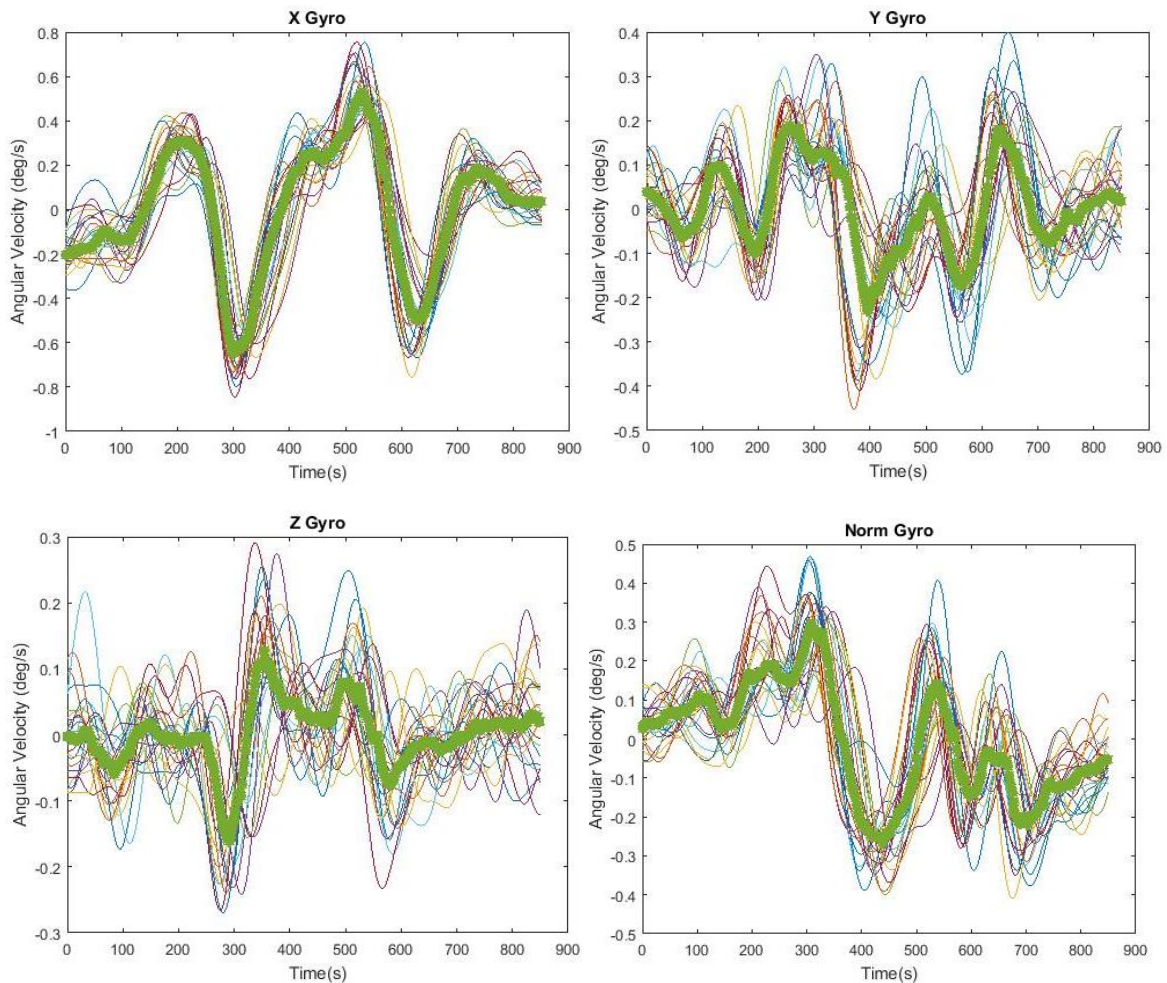


Figure 10-5 - Example of Gyroscope signals caused by a heartbeat when participant was lying on their right side. The averaged signal is shown as the thick green line in each plot.

10.4.3 Bland Altman plots

The Bland-Altman (BA) plots for the BBIs are shown in Figure 10-6 to Figure 10-9. These figures show that the BBIs measured from the BCG are accurate when compared to the reference ECG signal, mean difference values equal to 0.00 for all four BA plots. Comparing these BA plots to the BA plots for the ECG and PPG BBIs in the chapter 8 (Figures 8-1 to 8-

3), the correlation coefficients of the BCG heartbeat detection are lower. Additionally, the RPC values are higher for the BCG signals than the ECG and PPG signals, showing that the BBIs from the gyroscope are less repeatable. In Figure 10-7 the highest number of heartbeats were detected in the Y gyroscope signal, which also had a lower RPC value than the BA plots for the other gyroscope signals. This suggests that the heartbeat detection algorithm was most successful on the Y gyroscope signal (head rotation towards the shoulders) compared to the other signals.

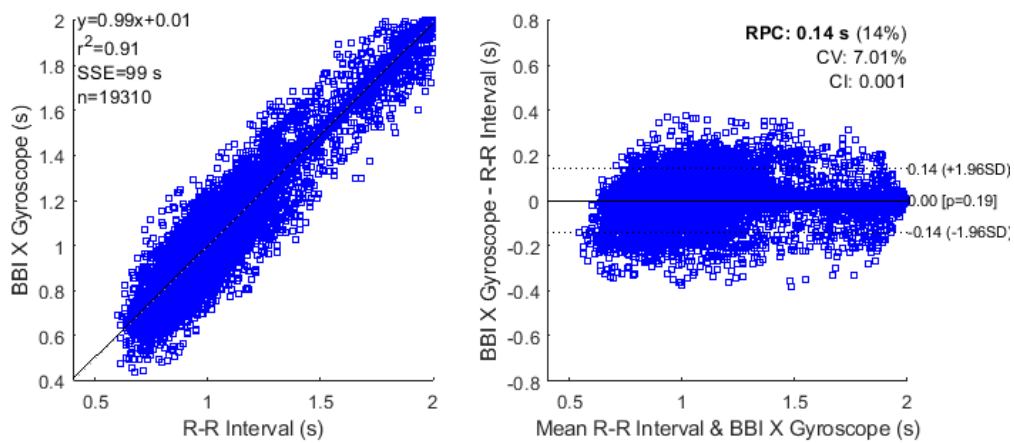


Figure 10-6 - Bland Altman plot of the BBIs from the X gyroscope signal compared with the reference ECG signal

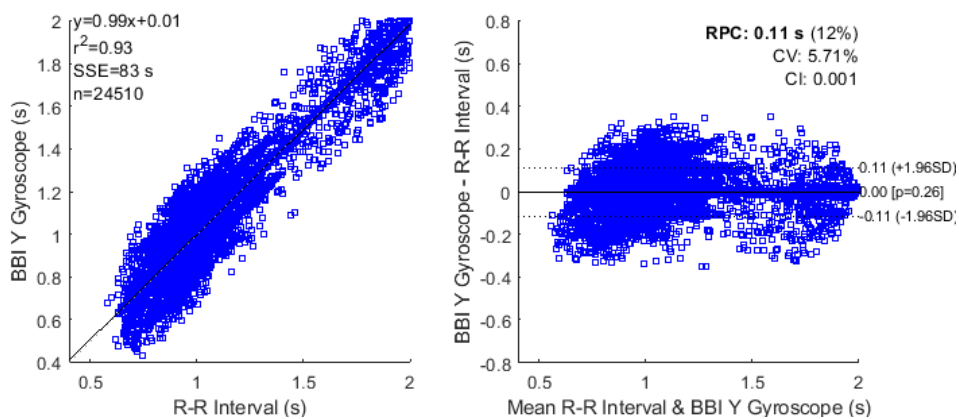


Figure 10-7 - Bland Altman plot of the BBIs from the Y gyroscope signal compared with the reference ECG signal

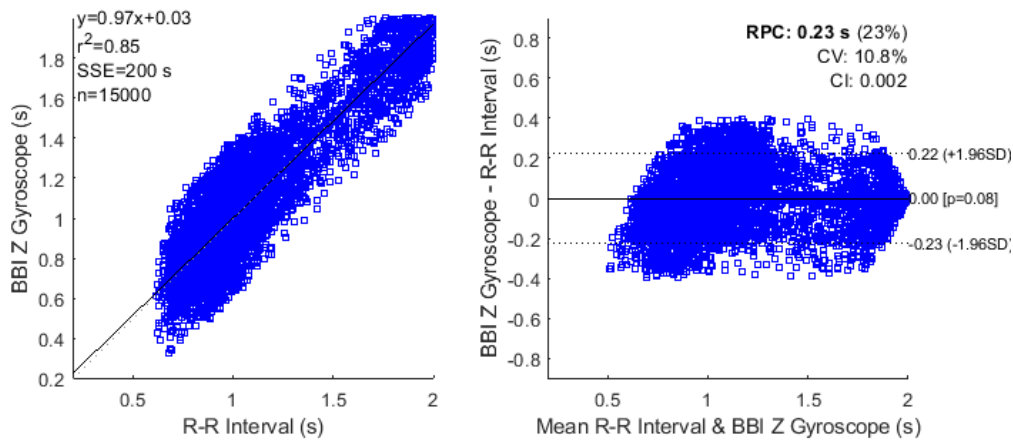


Figure 10-8 - Bland Altman plot of the BBIs from the Z gyroscope signal compared with the reference ECG signal

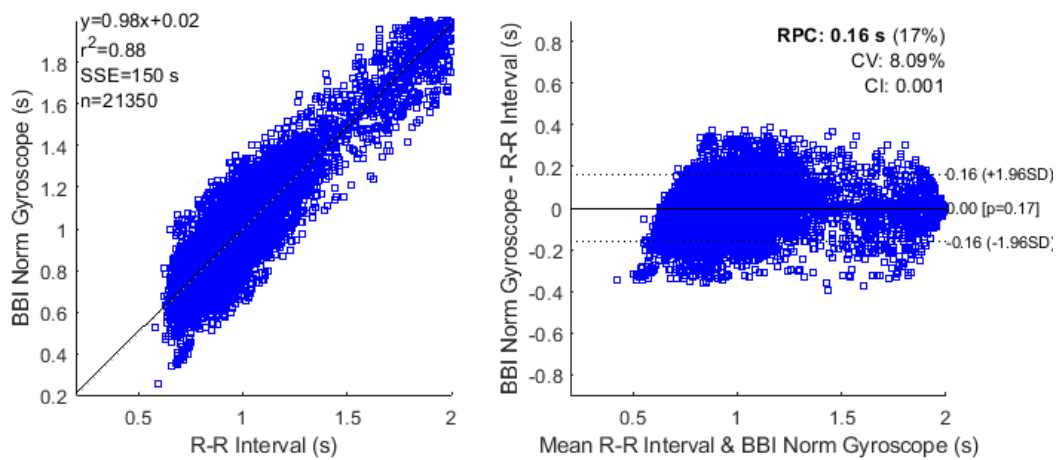


Figure 10-9 - Bland Altman plot of the BBIs from the normalised gyroscope signal compared with the reference ECG signal

10.4.4 Heartbeat detection sensitivity

The heartbeat detection algorithm had the highest sensitivity when applied to the Y gyroscope signal, regardless of sleeping position or PAP mode, as shown in Figure 10-10 and Table 10-1. Table 10-1 shows that for every stage the heartbeat detection sensitivity using the Y gyroscope signals was either significantly higher than the other gyroscope signals, or it was not significantly different to another equally high signal.

The Y gyroscope signal also had the lowest percentage of false heartbeats detected for all experiment stages as shown in Figure 10-11 and Table 10-2. Table 10-2 shows that for every stage the proportion of falsely detected heartbeats from the Y gyroscope signals was

either significantly lower than the other gyro signals, or it was not significantly different to another equally low signal.

Table 10-1 – Median (IQR) sensitivity (%) of heartbeat detection algorithm

	X Gyro	Y Gyro	Z Gyro	Normalised Gyro
Stage 1 (Lying on Back)	83.84 (28.02) *	94.28 (18.17)	72.88 (22.53) *	92.21 (15.13)
Stage 2 (Lying on Left side)	52.61 (20.80) *†	71.80 (33.11) †	56.23 (19.56) †	62.64 (32.01) †
Stage 3 (Lying on Right side)	59.44 (26.32) *†	76.82 (28.56) †	55.54 (19.21) *†	68.83 (18.23) †
Stage 4 (Lying on Back)	81.79 (25.97) *	90.65 (12.76)	66.19 (19.64) *	89.39 (25.36)
Stage 5 (CPAP mode on)	84.79 (25.06)	90.05 (17.76)	65.79 (22.94) *	90.69 (19.76)
Stage 6 (Bi-level mode on)	77.58 (26.25)	90.96 (16.18)	39.74 (26.17) *†	59.67 (33.11)*†

* Median % of heartbeats less than % detected in Y gyroscope signal (p<0.05)

† Decrease in heartbeat sensitivity compared with stage 1 (p<0.05)

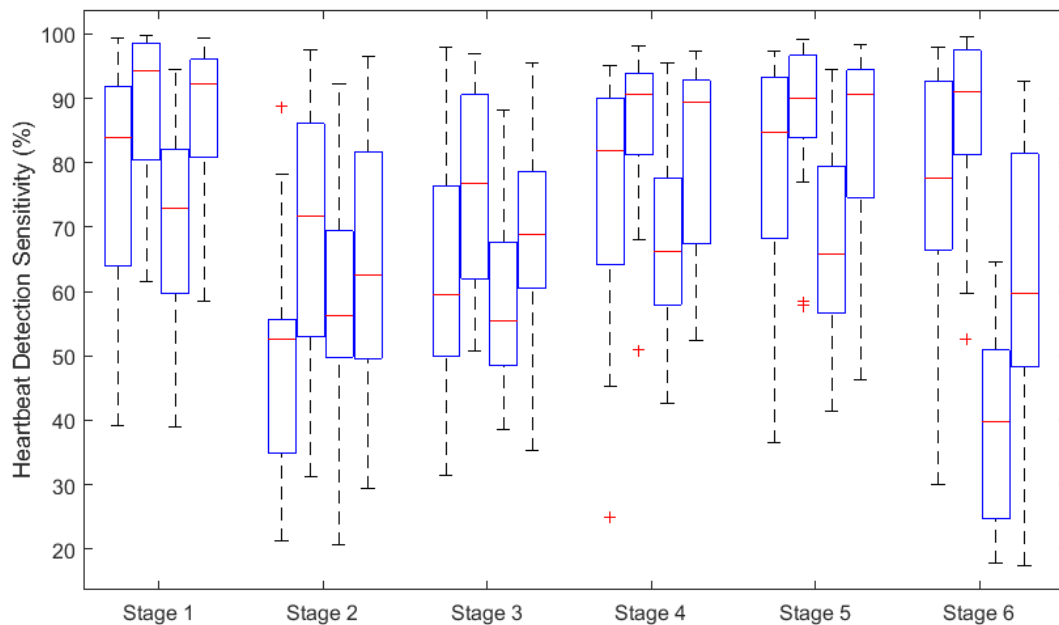


Figure 10-10 – Sensitivity of the heartbeat detection algorithm. Results are for (from left to right within each Stage) the X Gyro, Y gyro, Z Gyro and Normalised Gyroscope signals

Table 10-2 - Median (IQR) Percentage of heartbeats that were incorrectly classified as heartbeats by the heartbeat detection algorithm

	X Gyro	Y Gyro	Z Gyro	Normalised Gyro
Stage 1	12.51 (37.22)*	4.34 (7.10)	22.09 (25.08)*	5.91 (9.85)
Stage 2	42.42 (24.34) *†	16.63 (22.78) †	33.51 (25.68)* †	30.95 (32.63) †
Stage 3	29.98 (14.78) *	8.55 (17.46) †	31.05 (18.95)* †	22.09 (16.97)* †
Stage 4	11.17 (31.19) *	5.23 (11.55)	25.66 (25.13)*	6.81 (10.63)
Stage 5	14.87 (17.66) *	4.61 (12.33)	25.48 (21.10)*	6.23 (10.98)
Stage 6	17.86 (25.24) *	8.07 (13.79)	37.25 (22.46)* †	15.62 (13.36)* †

* Median % of heartbeats greater than % detected in Y gyroscope signal Y gyroscope signal ($p < 0.05$)
 † Increase in falsely detected heartbeats compared with stage 1 ($p < 0.05$)

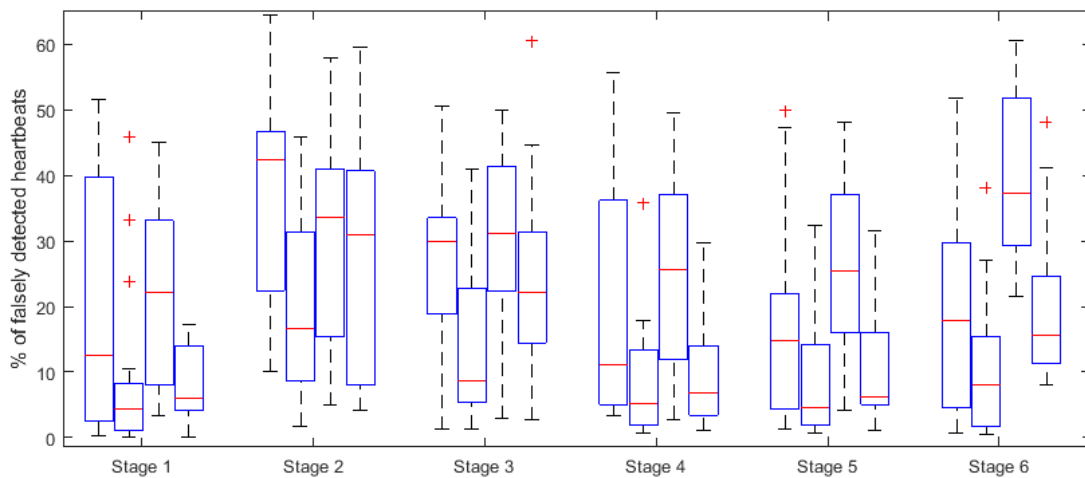


Figure 10-11 - The percentage of heartbeats detected by the heartbeat detection algorithm that were false positives. Results are for (from left to right) the X Gyro, Y gyro, Z Gyro and Normalised Gyroscope signals

Figure 10-10, Figure 10-11, Table 10-1 and Table 10-2 show that the heartbeat detection algorithm was most successful on the Y gyroscope (head tilted towards shoulder) signal, as it has the highest heartbeat detection sensitivity, and the lowest percentage of false positives detected. Looking at the results from Figure 10-3, one reason that the heartbeat detection algorithm is more successful for the Y gyroscope signal when compared with other signals is that it has a larger SNR than other gyroscope signals. This would make it easier to differentiate the heartbeats from the noise of the signal leading to more heartbeats being detected and fewer false positives.

Although there is a large peak in the X gyroscope signal (horizontal direction), there are also large peaks either side of the main peak which may reduce the effectiveness of the

heartbeat detection algorithm. However the signals in Figure 10-3 are from only one participant, so the signal features in that figure may not account for the results of all the participants shown in Figure 10-10, Figure 10-11, Table 10-1 and Table 10-2.

The signal with the worst performance was the Z gyroscope signal, which corresponds to a vertical head tilt (as shown in Figure 10-1). The heartbeat detection sensitivity was consistently the lowest for all stages, except when the participants were lying on their left side, as shown in Figure 10-10 and Table 10-1. Additionally, Figure 10-11 and Table 10-2 show that for all experiment stages the percentage of false positives from the Z gyroscope signal was either the highest or not significantly different to the percentage of false positives detected in the other gyroscope signals. A reason for this is the shape of the Z gyroscope signal, as seen in Figure 10-3, which as previously mentioned, does not have a distinct peak corresponding to the heartbeat. This makes it more difficult for the heartbeat detection algorithm to reliably detect the heartbeats in the signal, leading to a lower number of heartbeats correctly detected, and a higher number of false positives. The reason that there is not significant peak corresponding to the heartbeat in the Z gyroscope signal is not known, however it may be that for each heartbeat there is more linear movement and less rotational movement in the horizontal-vertical direction at the sensor location. Further testing would be required to attempt to maximise the efficiency of the heartbeat detection algorithm on the Z gyroscope signal, which may include using the signal from the accelerometer.

There was no significant difference in percentage of correctly or falsely detected heartbeats between when the PAP device was off (stage 4) compared to when the CPAP mode was on (stage 5) for any of the gyroscope signals. However, the rapid change in pressure that occurs during bi-level PAP therapy (stage 6) created motion artefacts in the Z gyroscope signals as shown in Figure 10-12. This resulted in a 36% decrease in the heartbeat detection sensitivity for the Z and normalised gyroscope signals when the bi-level mode was on (stage 6) compared with when the CPAP mode was on (stage 5) (see Table 10-1). Additionally,

Table 10-2 shows that for the Z and normalised gyroscope signals, there was a respective 12% and 9% increase in the proportion of false positives when the bi-level mode was on compared to when the CPAP mode was on. Since the normalised gyroscope signal is made of a combination of the X, Y, and Z signals, it is logical that if one of these signals is significantly affected, then there will also be a similar effect on the normalised gyroscope signal. Table 10-1 and Table 10-2 show that the percentage of correctly and falsely detected heartbeats from the X and Y gyroscope signals were not significantly affected by the activation of the bi-level mode.

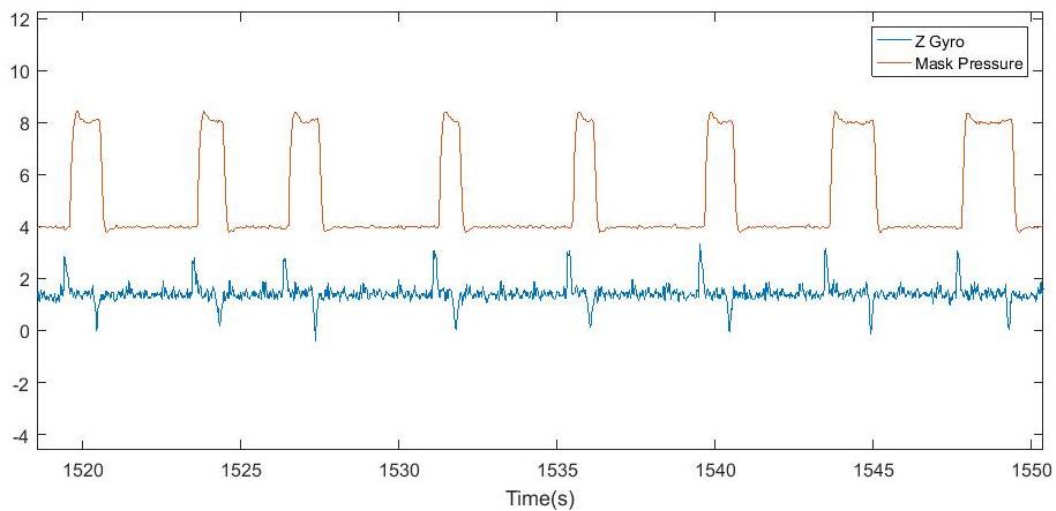


Figure 10-12 – An example of how the change in the applied mask pressure that occurs in the bi-level PAP mode can cause artefacts in the gyroscope signal.

There was a significant decrease in the sensitivity of the heartbeat detection algorithm when the participants were lying on their side in comparison to when they were lying on their back. For all signals there was a reduction of between 10-30% in the heartbeat detection sensitivity (Figure 10-10, Table 10-1) and an increase of between 5-30% in the percentage of false positives detected (Figure 10-11, Table 10-2) when the participant went from lying on their back (Stage 1) to lying on their side (Stage 2 and 3). Furthermore, when the participants went from lying on their right side (Stage 3) to lying on their back again (Stage 4), there was a 10-20% increase in the heartbeat detection sensitivity for the Y, Z and normalised gyroscope signal ($p < 0.05$ for Y gyroscope signal). Additionally, there was a

significant decrease in the proportion of false positives when the participant went from lying on their right side (Stage 3) to lying on their back (Stage 1) for the Y (5% reduction) and normalised gyroscope (15% reduction) signals ($p < 0.05$). However there was no significant difference in the heartbeat detection sensitivity or false positives for the Y, Z and normalised gyroscope signal when the participants went from lying on their left side (Stage 2) to their right side (Stage 3). These results indicate that when the participants were lying on their side, the sensitivity of the heartbeat detection algorithm decreases compared with when they were lying on their back.

When the participants were lying on the side (Figure 10-4 and Figure 10-5), the peaks of the BCG signal were not as well defined and the magnitudes were not as large as when the participants were lying on their back (Figure 10-3). This would make it more difficult for the heartbeat detection algorithm to find the peaks, as the SNR ratio was worse. This is the likely reason for the decrease in the sensitivity of the heartbeat detection algorithm when the participants were lying on their side.

There was a significant reduction in the sensitivity of the heartbeat detection algorithm on the X gyroscope signal when the participants were lying on their left side compared with when they were lying on their right side. This was shown in Figure 10-10 and Table 10-1 ($p = 0 < 0.05$) by a 5% reduction in the heartbeat detection sensitivity and Figure 10-11 and Table 10-2 ($p < 0.05$) by a 15% increase in the percentage of falsely detected heartbeats. However for the other signals, there was no significant difference between when the participants were lying on their left and right side ($p \geq 0.05$). Because the dynamics of how the ballistocardiographic forces affect head movement are not well understood, it is unclear if this is a result of a number of outlier values affecting the result, or whether the signal has a worse quality when the participants were lying on their left side in comparison with the right side.

10.4.5 Results Summary

While the heartbeat detection algorithm on the BCG signals shows promising results, the results are not consistent enough for continuous accurate HR monitoring, particularly when the participant was lying on their side or when the bi-level mode was activated. Given that from the gyroscope, four signals were recorded that all measure HR, the next logical step was to implement a data fusion method to investigate whether this would enable a consistent, accurate HR measurement from the BCG signals.

10.5 Data Fusion methods

Two different data fusion algorithms were developed; a Custom Weighted Average (CWA) algorithm, and a Kalman Filter (KF). These algorithms were chosen as similar approaches have been used to combine data from different sources [148, 168], as discussed in section 4.4.

For these data fusion algorithms the recording period was firstly divided into non-overlapping 1.5 second windows. A width of 1.5 seconds was chosen as it is large enough so that for a subject with a normal HR (>40bpm), there will be at least one heartbeat per window. For each window, all of the heartbeats inside that window were identified for each of the x, y, z and normalised gyroscope components, using the methods described in section 10.2. For each of the identified heartbeats, an instantaneous HR was then calculated using the currently identified heartbeat and the previous heartbeat for that component. If multiple HR values were identified in one window then the HR value closest to the previous HR estimation was used and all other HR values discarded.

After the heartbeats had been identified, outlier HR values were discarded. Outlier HRs were defined as an HR either greater than 200 BPM or less than 40 BPM. These values were

discarded as they can still contaminate the data fusion process, particularly when the gyroscope signal quality is low.

The data fusion methods are designed to take several instantaneous HR signals and output a single averaged HR at regular intervals. This averaged HR signal cannot be directly compared to the instantaneous HR values from the reference ECG signal. Hence the averaged HR values from the data fusion methods were compared with the averaged HR values over the same time period from the reference ECG HR. This can be used to determine which of the data fusion methods generate a more accurate HR signal. However, because an averaged HR is being used, HRV is not possible on the HR signal from the data fusion methods.

10.5.1 CWA Algorithm

In each window, the estimated HRs from all gyroscope signals were assigned a weighting between 0 and 1, calculated using an exponential formula based on the difference in HR between the currently estimated HR for that signal, and the previous output of the CWA algorithm. The weighting, $\sigma_{i,k}$ for signal i at time k , was calculated as

$$\sigma_{i,k} = e^{\frac{-|HR_{i,k} - \widehat{HR}_{k-1}|}{C}} \quad (10.2)$$

where \widehat{HR}_{k-1} was the previous estimation of the HR from the CWA algorithm, and $HR_{i,k}$ is the HR measurement from the k th window for signal i . To increase the speed of convergence of the algorithm for testing, the initial value of the HR (i.e. \widehat{HR}_0) was set as the first measured R-R interval from the reference ECG signal. The value of C was set to 0.15 which was determined experimentally to be the optimum value, the results of which are shown in Appendix D.

Finally, the HR for each window was estimated from the HRs in the defined windows and their corresponding weightings:

$$\widehat{HR}_k = \sum_{i=1}^4 \frac{\sigma_i^2 HR_{i,k}}{\sum_{j=1}^4 \sigma_j^2} \quad (10.3)$$

where $HR_{i,k}$ is the HR measurement from the k th window of one of the gyroscope signals.

The equation was derived from the work of Townsend [168].

10.5.2 KF algorithm

The KF is a signal fusion technique that is able to take measurements from several sources and make an estimation on the state of the defined system based on those measurements. KFs have been previously used for estimation of HR, especially from noisy sources, and for tracking of vital signs and reducing false alarms in intensive care [148, 149].

A KF consists of two sections: in the first, a prediction is made based on a defined model of the state that the filter is applied; in the second, the prediction is updated based upon observation measurements. For our system, the prediction is that the HR will remain constant with some small variation. A similar approach was made in [148].

For our system we assume that for time k

$$HR_k = HR_{k-1} + w_k \quad (10.4)$$

where w_k is the natural variation of the HR, which is modelled as zero mean Gaussian noise with covariance Q_k . At time k , the observation measurements is defined as

$$z_k = H_k x_k + v_k \quad (10.5)$$

where

$$H_k = \begin{bmatrix} 1 \\ 1 \\ 1 \\ 1 \end{bmatrix} \quad (10.6)$$

$$x_k = \begin{bmatrix} g_x \\ g_y \\ g_z \\ g_n \end{bmatrix} \quad (10.7)$$

and $g_{x,y,z}$ are the HR estimations from the x, y, and z components respectively, g_n is the HR estimation from the normalised gyroscope components. v_k is defined as the observation noise, which is assumed also to be Gaussian, with zero mean and noise R_k . The prediction equations for our system are

$$\hat{x}_{k|k-1} = \hat{x}_{k-1|k-1} + w_k \quad (10.8)$$

$$P_{k|k-1} = P_{k-1|k-1} + Q_k \quad (10.9)$$

where $\hat{x}_{k|k-1}$ is the estimation of the HR at time k , based on the information known at time $k-1$, and P is a measure of the accuracy of the prediction. From these equations the prediction is updated based on measurements taken at time k according to the following equations of a KF, shown in Appendix D.

Similarly to the CWA algorithm, the initial estimation of HR was taken from the reference ECG HR. The initial value of P was 0.1. Q_k was kept constant for all participants for the duration of the recording. The value for Q_k was set to 0.05, which was found experimentally to be the optimum value, the results of which are shown in Appendix D. R_k was defined as

$$R_k = \begin{bmatrix} \sigma_{x,k} & 0 & 0 & 0 \\ 0 & \sigma_{y,k} & 0 & 0 \\ 0 & 0 & \sigma_{z,k} & 0 \\ 0 & 0 & 0 & \sigma_{n,k} \end{bmatrix} \quad (10.10)$$

where

$$\sigma_k = |g_k - \hat{x}_{k-1|k-1}| \quad (10.11)$$

For this KF we assumed each time step corresponded to each observation window (of length 1.5 seconds). If a heartbeat is not detected in the window, then the matrices are resized so that any component that has no heartbeat in the window at time k , or has had a heartbeat discarded, is not considered in the calculations at time k . If the HR in the window at time k is equal to $\hat{x}_{k-1|k-1}$ then $\sigma_{i,k}$ is set to 0.01, to avoid a σ value of 0, which can cause problems when inverting certain matrices as part of the KF equations (see Appendix A).

An example of how the KF algorithm described is able to perform data fusion to estimate the HR is shown in Figure 10-13. This figure shows that even during periods where some of the HR information is not accurate the KF algorithm is able to produce an accurate HR estimate.

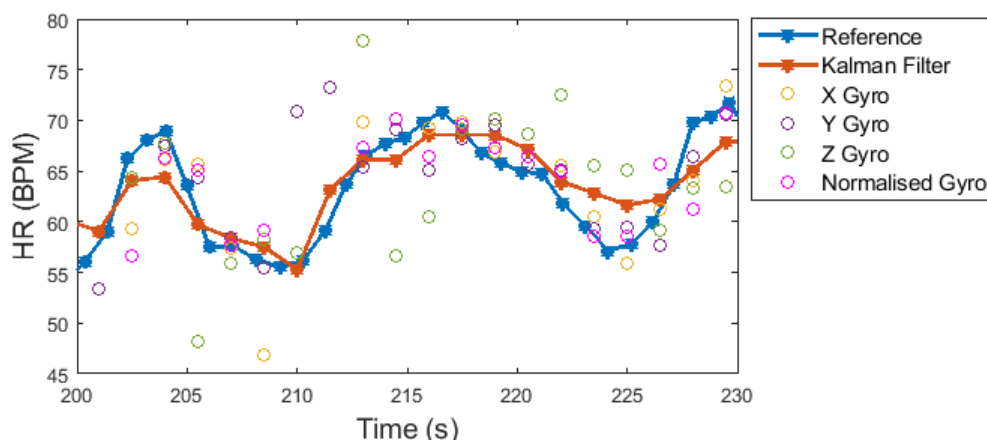


Figure 10-13 - An example of how the HR information from the gyroscope signals (coloured circles) are used to estimate the HR using the Kalman Filter (orange line), compared with the reference ECG HR (blue line)

10.6 Results

The mean and median errors produced by each of the data fusion algorithms are shown in Figure 10-14 and Figure 10-15 respectively, and tabulated in Table 10-3. The mean error of the HR estimation was significantly larger for the CWA algorithm than for the KF algorithm. This difference was greater when the participants were lying on their side (2.5 and 3BPM for right (stage 3) and left (stage 2) side respectively), compared with when they were lying on their back (stage 1) (1BPM). Since the mean HR error is much larger than the median HR error, this suggests that there are periods where the HR estimation from the CWA algorithm

is quite inaccurate, increasing the mean HR error without significantly increasing the median HR error. However, the mean HR error for the KF algorithm was either below or approximately 5 BPM, suggesting that these periods of inaccurate HR estimation are not as common for the KF algorithm. Hence based on the results of Figure 10-15 and Figure 10-14, it was determined that the KF algorithm was able to consistently provide a more accurate HR estimation than the CWA algorithm.

Table 10-3 – The median error (in BPM) for the optimum CWA and KF algorithms for all participants for each experiment stage. Values are mean (std).

	Experiment Stages					
	1	2	3	4	5	6
Median Error						
CWA	2.14 (1.06)	3.88 (3.27)†	3.46 (2.94)†	2.17 (1.24)	2.10 (1.03)	2.55 (1.86) ^a
KF	2.11 (1.00)	3.46 (2.59)†	3.01 (1.74)†	2.27 (1.15)	2.18 (1.14)	2.44 (1.41) ^a
Mean Error						
CWA	3.82 (2.48)	7.78 (5.37)†	6.66 (4.45)†	4.59 (2.71)	4.11 (2.42)	5.33 (4.05) ^a
KF	3.00 (1.75)*	4.70 (2.89)*†	4.09 (2.03)*†	3.38 (1.64)*	3.01 (1.50)*	3.36 (1.78)* ^a

*difference when compared to error from CWA algorithm (p<0.05)
 †stage 2 and 3 values significantly different to stage 5 value (p<0.05)
^astage 6 values not significantly different to stage 5 value (p>0.05)

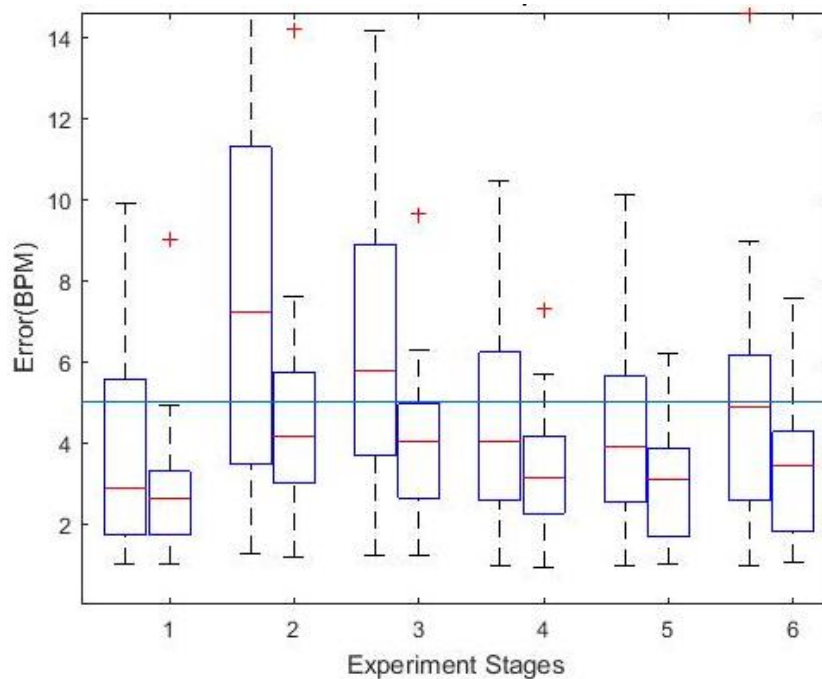


Figure 10-14 - The mean error for the optimum CWA (left) and KF (right) algorithms. A line indicating 5BPM is also shown (light blue)

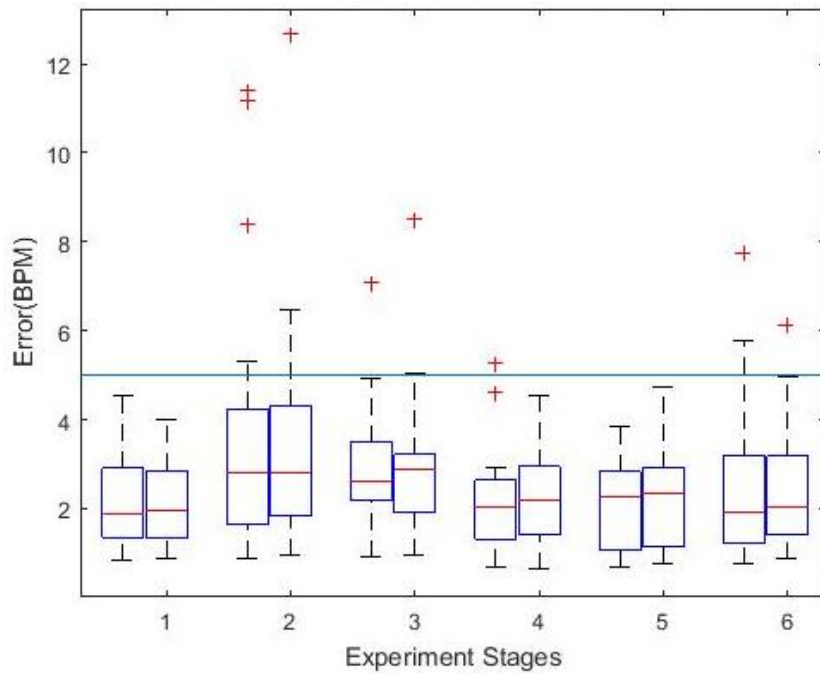


Figure 10-15 - The median error for the optimum CWA (left) and KF (right) algorithms. A line indicating 5BPM is also shown (light blue)

The median error for both the CWA and KF algorithms was under 5 BPM for most participants. This is shown in Figure 10-15, where there were a few outlier measurements above 5BPM, and in stage 2 (lying on their left side) and stage 6 (bi-level mode), the median error exceed 5BPM for some of the participants. This suggests that both CWA and KF data fusion methods are able to accurately estimate HR for the majority of 1.5 second windows when the participants are lying on their back, left and right side, and with different modes of the PAP device.

The accuracy of both HR estimation methods was reduced when the participants were lying on their side compared with when they were lying on their back. This is shown by the 1BPM increase in the median error in Figure 10-15 in stages 2 and 3 (lying on each side) compared with stages when they were lying on their back (stages 1 and 4). Similarly, this is also shown in the increase in mean error of between 2-4 BPM in Figure 10-14 and Table 10-3. There was no significant difference between when the participants were lying on their left (Stage 2) or right side (stage 3) for the median or mean error ($p \geq 0.3219$). These results are probably a reflection of the number of correctly and falsely detected heartbeats, as when analysing

these results, it was found that the sensitivity was also increased when the participants were lying on their back compared with when they were lying on their side. Since the data fusion algorithms inputs are the detected heartbeats, it follows that the data fusion algorithms accuracy would reflect the sensitivity of the heartbeat detection algorithm.

The activation of the bi-level mode (Stage 6) did not have a significant difference on the error of the KF or the CWA algorithm. Earlier results indicated that the bi-level reduced the sensitivity of the heartbeat detection algorithm on the Z and normalised gyroscope signals, so it was expected that there would also be a reduction in the error of the data fusion algorithms. However, Table 10-3 shows that for both the KF and CWA algorithm there was no significant difference in the mean or median error between when the CPAP mode (stage 5) was on and when the bi-level mode was on (stage 6). Hence although the bi-level mode induced artefacts in the gyroscope signal, it made no difference to the HR estimation accuracy of either the CWA or the KF fusion algorithms.

10.6.1 Results summary

The KF algorithm was able to produce a more accurate HR estimation than the CWA algorithm. The mean and median error for the HR estimation for the KF algorithm was below 5BPM for most of the participants. These results show that using a KF data fusion algorithm, a consistent and accurate HR signal can be measured from BCG signals.

10.7 Discussion

In this chapter, the gyroscope signals from the Cardiomask were analysed to estimate the HR of the wearer. A heartbeat detection algorithm was developed for identifying heartbeats in the gyroscope signals. Two data fusion algorithms were developed to attempt to provide a consistent and accurate HR signal. These data fusion algorithms were tested with healthy participants lying on their back and their side, and under different PAP modes.

The HR estimation error results in Figure 10-14 and Figure 10-15 has several outlier values for both the CWA and KF algorithms. These outliers are caused by periods where the signal

quality is poor, and no accurate HR values can be measured from any of the gyroscope signals. This leads to inaccurate HR values being input to the data fusion algorithms, causing an inaccurate HR estimation. However, Figure 10-14 and Figure 10-15 show that these cases are rare. Future work will look at developing more advanced strategies for dealing with periods where no accurate HR data are available to reduce the amount of outlier HR estimations that occur.

Since the BCG method for detecting heartbeats relies on detecting small movements of the subject's head, this technique is prone to errors from small motion artefacts. Other sources of vibrations or small movements could cause false detection of heartbeats, or for the heartbeat to be undetectable in the signal. Such examples of other sources include small movements of other parts of the body, such as the subject's arms or legs, or even potentially from Rapid Eye Movement (REM) that occurs during sleep. However, because participants were asked to lie as still as possible for the duration of the experiment, then there should not be many movement artefacts in the data shown in this chapter. Similarly, because the participants were not asleep, there would not have been any interference from any REM artefacts in the data.

For these small movements, it is possible that the signals from all three gyroscope axes are contaminated by movement artefacts. This would make it difficult for the data fusion algorithms to accurately estimate the HR of the wearer. For the KF, this would be reflected by a larger state covariance variable for the window in which the movement occurs. This large state covariance would mean that the estimated HR for the window with the corrupted movement would be closer to the previous HR estimation than a window with a small state covariance, reducing the HR estimation error caused by small movement artefacts.

The participants in this study were healthy and in the age range 19-48 years. A typical sleep apnoea user will likely be older [2] and have a higher BMI [224] than the participants involved in this experiment. As a result, it is unknown how well the algorithm will work on a

patient cohort with sleep disorders, and cardiac or respiratory problems. This will be investigated in future research.

Similarly, the participants of this test were awake during recording of the data. It is unknown whether there would be a change in signal quality when participants are asleep. It is possible that some signal quality variation may occur as a result of the change in muscle tone during sleep compared to wake [225], affecting the vibration pattern of the BCG signal of the head. Further work is needed to determine whether this change would have a significant effect on the signal quality.

The results from this study assume that the PAP mask was correctly and tightly fitted in the same manner for each participant. Although attempts were made to reduce any variation in how tightly the mask was fitted to the participants, it was very difficult to ensure that all of the PAP masks were fitted exactly the same, due to different head shapes and sizes, and different participant subjective preference.

For the BCG signal measurement it was assumed that the movement of the PAP mask where the gyroscope signal is measured from is the same as the movement of the participant's head. When the mask is tightly fitted this assumption is more likely to be correct. However if the mask is not tightly fitted then this assumption does not hold, and some of the BCG movements may be dampened by the PAP mask, reducing the BCG signal quality.

The model for the HR from both the KF and the CWA algorithms assume that the HR remains constant with some small level of variation. This assumption is true for most of the time during sleep, as the HR will usually not change too rapidly during normal sleep. However for periods where the HR will change more rapidly and by a larger amount, such as when the participant is moving or experiencing an arrhythmia episode, this assumption may

not hold, and hence the HR estimation methods may not be as accurate during those periods. Future research is needed to confirm the accuracy of the HR estimation algorithms during periods of rapidly changing HR.

As with all optimisation and training experiments, the CWA and KF variables were optimised for the training data. Although an attempt was made to get a variety of participants with different heights, genders, and weights, it may be possible that the CWA and KF variables were over fitted. Future testing is needed with more participants including OSA patients to confirm that the optimal values for the CWA and KF variables in this paper are suitable for the whole population, or for the sleep apnoea population.

For each participant, the KF and CWA variables were kept constant for the duration of the recording period. Additionally, the KF and CWA variables were the same for different participants and between different experiment stages (i.e. for different sleeping orientations and different PAP device modes). For the KF algorithm the results in Appendix D suggest that the HR estimation is more accurate when the KF variables are set as low as possible. It may be possible to increase the accuracy of the HR estimation for the CWA algorithms if the CWA variable were optimised for each participant or were optimised for different sleeping positions or PAP modes. The accuracy of the HR estimation may also be increased by varying the CWA variable for each interval, depending on the participant's HR, the signal quality or detected number of heartbeats in that interval.

The applied pressures that were used during the CPAP and bi-level modes were relatively low compared with those normally used during PAP therapy. These low pressures were used to ensure comfort for the participants, who may not have previously experienced PAP therapy. When the CPAP mode was activated, there was no significant difference in the HR estimation accuracy compared with when PAP device was off, with the exception of the

initial pressure artefact when the CPAP mode was first activated. It is unknown whether for higher CPAP pressures, the results would change significantly.

It was reported in the results that there was a decrease in the accuracy of the BCG measurement method when the participants were lying on their side compared with when they were lying on their back. One reason for this could be that when the participants are lying on their side, the small movements caused by BCG forces are being dampened. This effect may be increased as the participants were lying on a pillow which would absorb some small movements. However, it could also be a function of the placement of the gyroscope in relation to the participant's head, and future work should explore the optimal location for the gyroscope.

Few devices have been made for the purpose of monitoring HR during sleep that use only a BCG signal. Di Rienzo et al used a wearable device which contained an accelerometer located on the wearer's sternum [81] to monitor cardiac intervals during sleep [136]. However to monitor these intervals, the BCG signal information was combined with an ECG signal. Di Rienzo also used the ECG signal instead of the BCG signal to locate and identify the heartbeats. In this chapter, although an ECG signal was recorded from the Cardiomask in parallel with the BCG, the results show that a standalone BCG device can be used to estimate HR, although this does not have the same heartbeat detection accuracy as systems which use the ECG signal (such as [136]) to detect the heartbeats.

The method used to extract the HR from the Cardiomask was based on work conducted by Hernandez et al [146]. The algorithm developed by Hernandez et al. was designed such that an HR could be accurately measured when the participant was standing, sitting, and using the device in normal everyday life. This meant it needed to be much more resistant to movement artefacts than if it was designed for just sleep monitoring. As a result, Hernandez et al. did not collect beat-by-beat HR information, and instead used the peak signal

frequency over a 20 second interval as the HR value. This method for HR estimation was designed such that it would require low power and low computational cost.

Unlike in Hernandez's method [146], the HR estimation algorithm described in this chapter was designed for situations where the wearers are asleep, and not moving too much. This means that a shorter window length could be used for estimating the HR, as movement episodes are less likely. If there is a change in the HR of the wearer, it would in theory be able to be detected more quickly by the algorithm developed in this chapter than by Hernandez's algorithm. However the trade-off of the decrease in the signal window length is that there is a slight decrease in the accuracy of the HR estimation, although it is difficult to compare accuracies over different window lengths. Hernandez et al. was able to estimate the HR of the wearer to within 0.44 BPM of the reference HR value over a 20 second window when the participants were lying on their back. In contrast the mean error of the HR estimation from the CWA and KF algorithms when the participants were lying on their back (stage 1) was approximately 3 BPM over a 1.5 second window.

10.8 Conclusion

In this chapter the ability to accurately measure HR from a gyroscope attached to the Cardiomask has been established. An algorithm was developed for detecting the heartbeats for the x, y, z and normalised gyroscope signals. Two data fusion methods, a CWA and a KF algorithm, were also developed to further increase the accuracy and consistency of the HR estimation. The accuracy of the KF algorithm was greater than the CWA algorithm, and was able to estimate the HR with an error of ≤ 5 BPM regardless of the participant's sleeping position or the mode of the PAP device. For both data fusion algorithms there was a decrease in the HR estimation accuracy when the participants were lying on their side compared to lying on their back. The reason for this decrease is not known and will be the subject of future testing. Future testing will also involve testing the device on sleep apnoea patients during PAP therapy.

11. Discussion/Conclusion

11.1 Restatement of the aim

The aim of this thesis was to develop a device that can accurately and comfortably monitor the Heart Rate (HR) of a person during Positive Airway Pressure (PAP) therapy. In Chapter 5, a PAP device was modified to be able to accurately monitor the HR of the wearer (named the “Cardiomask”). It was thought that by integrating the HR sensors into the mask, the effectiveness, ease of use and relative comfort of the PAP therapy would not be affected. The methods used for measuring HR were ECG, PPG and BCG. The ability of these different methods to accurately measure HR was tested on healthy participants who lay in several sleeping positions and underwent two common PAP therapy modes. Various algorithms were also developed in an attempt to increase the accuracy of the HR and HRV analysis from the recorded signals. Data from different signals were also combined in an attempt to increase the consistency and accuracy of the HR measurement of the wearer. The main contributions of this thesis, and potential future outcomes are listed below.

11.2 Summary of Contributions

11.2.1 ECG Electrode position

In Chapter 5, a novel ECG setup was described in which custom made Stainless Steel electrodes were attached to the straps of the PAP mask in a way that the electrodes were positioned onto the wearer’s face and neck. The electrode locations were chosen to maximise the amplitude and quality of the ECG signal measured from possible locations on the head and neck. Preliminary testing showed that although an ECG signal could be measured from electrodes on the face and neck, the signal quality of the ECG signal measured from the face was lower than that of a reference signal measured from electrodes placed in traditional locations. Chapter 8 showed that this reduction in signal quality resulted in some errors in heartbeat detection.

Despite a reduced SNR, the results in chapter 7 show that for the different participants, heartbeats could be accurately detected from the face ECG signal, and accurate HR and HRV analysis was possible. Indeed in the face ECG signal the mean heartbeat detection sensitivity and false positive rate was larger than 95% and less than 2% respectively. This led to a mean HR error of less than 2BPM as well as a high level of accuracy in the HRV analysis. Hence an ECG setup was developed such that it was possible to accurately measure HR using dry ECG electrodes integrated into a PAP mask.

11.2.2 BBI correction methods

In chapter 6 a novel BBI correction algorithm (combined threshold algorithm) was developed and compared with known BBI correction algorithms, as well as some other BBI correction algorithms developed by the author. This algorithm was better than standard BBI correction algorithms (including the Wessel algorithm [201] and the commonly used threshold algorithm [195]) at reducing the HR and HRV error for a BBI signal containing artificially corrupted values. This algorithm was applied to the signals measured from the Cardiomask, and the results in section 8.2.2.1 show that the BBI correction algorithm was able to increase the heartbeat detection sensitivity and reduce the number of false positives detected from the face ECG and PPG signals. Since missed heartbeats as well as falsely detected heartbeats can lead to HR and HRV errors, this result would lead to an increased HR and HRV accuracy from the ECG and PPG signals. Hence this BBI correction method allowed for a more accurate measurement of HR from the ECG and PPG signals.

11.2.3 Simple methods for rejecting HR and HRV values

Although the BBI correction method was able to improve the accuracy of the detected heartbeats reducing the HR and HRV error, there were still some corrupted values in the HR and BBI analysis. In Chapter 7, a method was described for simple rejection of corrupted mean HR values for 30 second and 5 minute windows, as well as another method for simple rejection of HRV values calculated from a 5 minute window. The mean HR values were rejected based on the signal quality and number of BBI values in the window. HRV results were rejected if BBI values used for HRV analysis had too large a range, or if there were too

few BBI values. The results in Chapter 8 show that by combining the combined threshold BBI correction method with the method for rejecting corrupted mean HR and HRV values, it was possible to measure HR and HRV accurately from the signals from Cardiomask without the need for manual BBI correction. Reducing the need for manually checking and correcting data would reduce the time between signal measurement and providing a physician with the necessary patient information, leading to earlier intervention if a problem did exist.

11.2.4 Data fusion methods for reducing HR and HRV error

In Chapter 9 several data fusion methods were introduced with the aim of improving the accuracy and the consistency of the HR and HRV analysis of the ECG and PPG signals. The results in Chapter 9 demonstrated data fusion methods that were able to increase the amount of valid analysis data, such that greater periods of accurate HR and HRV analysis was possible, without significantly reducing the accuracy of the HR and HRV analysis when compared with the BBI signal from the individual ECG and PPG signals.

Previous applications of data fusion methods for accurate HR measurement were done in such a way that accurate HRV analysis was not possible on the output signal, as the data fusion method would output a periodically sampled signal, which contained smoothed or average BBI values. In contrast, the data fusion methods described in chapter 9 were developed in such a way that after combining the data from the different signals, accurate HRV analysis was still possible. Hence Chapter 9 shows that the data fusion methods allow for the analysis of a larger amount of accurate HR and HRV analysis data collected from the wearer of the Cardiomask. This allows for the use of several sensors which are less accurate, but more comfortable for the wearer, instead of using one accurate sensor.

11.2.5 BCG application & data fusion method

The final contribution of this thesis is the novel application and signal processing of the BCG signals. A signal processing method was developed for maximising the SNR of the heartbeats in the gyroscope signal to allow for simple heartbeat detection. This method was applied on gyroscope signals recorded from an IMU mounted onto the PAP mask. By using a Kalman Filter (KF), the HR measurements from the different gyroscope signals were

combined to produce an accurate and consistent HR estimate. Testing in Chapter 10 showed that for participants that were awake the mean accuracy of the HR estimate was ≤ 5 BPM, regardless of the sleeping position or the type of PAP therapy that was used, however the sleeping position did affect the accuracy of the estimation. The results of Chapter 10 show that the signal processing method and the application of the KF to the resultant signals is able to produce an accurate and consistent HR estimation for a participant wearing the Cardiomask during PAP therapy. Since the IMU is attached to the PAP mask and not in contact with the wearer, this makes this solution as comfortable as a normal unmodified PAP mask.

11.3 Future work

11.3.1 Further development of algorithms developed in thesis

In Chapter 6, an algorithm was chosen for correcting BBI signals that had been corrupted by false RRI values. However this algorithm could be further developed to improve the effectiveness of the BBI correction. An example of this is that for the results in Chapter 6, BBI segments containing ectopic heartbeats were manually detected and excluded. Future methods could look at currently available methods for excluding ectopic beats (as outlined by Nabil et al. [195]) and combining a BBI correction algorithm with an algorithm that can account for ectopic beats, such that the BBI corrections would be fully automatic.

In Chapter 10, simple models of the HR were used for the CWA and KF algorithms. It was stated in Chapter 10 that it may be possible to improve the accuracy of the KF algorithm by modifying the HR model by attempting to predict the HR based on the current HR and other factors such as respiration. Another modification to the KF algorithm could be to change the constants in the KF into variables specific for each participant, or values that changed under different conditions.

11.3.2 Testing on OSA patients who are asleep

The results in this thesis were obtained from healthy participants, as the purpose of the tests was prototype validation rather than clinical investigation. Future testing will need to be conducted on OSA patients to validate that a similar level of HR and HRV accuracy to healthy participants can be obtained from the Cardiomask signals. Additionally, the participants in this test were awake for the duration of testing. Future testing will need to be conducted on participants who are asleep to determine if there is a change in the quality of the measured signals from the Cardiomask or the HR accuracy when the Cardiomask wearers are asleep compared with when they are awake.

11.3.3 Replication of results on nasal mask

The tests in this thesis were conducted using a full face PAP mask as this has a more surface area for sensors to be attached. However there also exists nasal PAP masks, as shown in the Figure 11-1. These masks are commonly preferred, although they are not always appropriate for some patients [15]. Given the differences in the location of the mask straps and the surface area covered by the nasal mask, the ECG, PPG and BCG setup described in chapter 5 may not be possible on the nasal mask. Hence future work could look at new possible locations for the ECG electrodes, reflectance pulse oximeter and the IMU such that measurement of HR from these signals could be possible when wearing the nasal mask.

Image has been removed due to copyright restrictions

Figure 11-1 - An example of a nasal PAP mask, which differs from the full face mask as the air is applied through the nostrils only. Source: www.resmed.com

11.3.4 Effectiveness of Cardiomask on PAP therapy

One of the design considerations for the modifications made to the PAP mask was that the sensors should not affect the effectiveness of the PAP therapy. Although there is no clear reason why the sensors selected should affect PAP therapy, this will need to be tested.

11.3.5 Effect of Cardiomask on ease of use and comfort

The sensors were designed such that OSA patients could put on the Cardiomask as they normally would, as this would mean that the ease of use and comfort of the overall PAP therapy would not be affected by the HR measuring modifications made to the mask.

However, in the tests undertaken, the Cardiomask was fitted to the participants by the experiment investigator to ensure optimal sensor placement. Additionally the participants only wore the mask for a short period of time compared to normal PAP therapy and in a clinical trial environment and not the intended application environment such as an OSA patient's home. Hence it is not known whether the ease of use or comfort of the Cardiomask is significantly different to a PAP mask that has not been modified.

11.3.6 Practical Design Improvements

The current Cardiomask prototype was developed as a proof of concept to demonstrate feasibility of measuring HR and HRV from ECG, PPG and BCG sensors retrofitted on a commercially available mask. It is recommended that some design changes be implemented in future design iterations:

- Wireless transmission of either the measured signals from the Cardiomask or the HR and HRV data from the Cardiomask signals to an off-board receiver with the PAP device.
- Better integration of ECG electrodes/wires into the PAP mask straps to increase repeatability of results, improve the simplicity of the setup and improve overall aesthetic of the design
- A new more permanent method to attach the IMU sensor to the PAP mask. The current method involves using an adhesive to hold the sensor in place. Future designs should attempt to reduce the vibration of the sensor independently of the

PAP mask, such that the movement of the sensor resembles the head movement as closely as possible.

- General improvements in aesthetics to improve the acceptability of the device.

11.4 Final Statement

This thesis has demonstrated the ability of a PAP mask, modified by the inclusion of custom-made ECG sensors and PPG sensors, to accurately monitor HR and HRV. This thesis has also demonstrated the ability to monitor HR accurately using gyroscope signals measured from a PAP mask. By combining these signals with signal processing and data fusion algorithms for improving accuracy, the work in this thesis paves the way for in-home monitoring of cardiac status of patients undergoing PAP therapy.

12. Appendices

12.1 Appendix A - General Equations for a Kalman Filter

State Model:

$$x_k = F_k x_{k-1} + B_k u_k + w_k \quad (12.1)$$

Predicted State estimate:

$$\hat{x}_{k|k-1} = F_k \hat{x}_{k-1|k-1} + B_k u_k \quad (12.2)$$

Predicted Estimate covariance:

$$P_{k|k-1} = F_k P_{k-1|k-1} F_k^T + Q_k \quad (12.3)$$

Update estimations:

$$y_k = z_k - H_k \hat{x}_{k|k-1} \quad (12.4)$$

$$S_k = H_k P_{k|k-1} H_k^T + R_k \quad (12.5)$$

$$K_k = P_{k|k-1} H_k^T S_k^{-1} \quad (12.6)$$

$$\hat{x}_{k|k} = \hat{x}_{k|k-1} + K_k y_k \quad (12.7)$$

$$P_{k|k} = (I - K_k H_k) P_{k|k-1} \quad (12.8)$$

12.2 Appendix B – Individual HRV analysis results

Colour code for appendix plots:

- Red – Corrupted data
- Purple – Pattern Detection algorithm (Algorithm 1)
- Dark blue – Wessel algorithm (Algorithm 2)
- Light blue – Combined Wessel algorithm (Algorithm 5)
- Black – Threshold algorithm (Algorithm 3)
- Orange – Combined Threshold algorithm (Algorithm 5)

Note: any missing columns in Figure 12-1 to Figure 12-8 indicate a median and IQR percentage error of zero (due to use of log plots).

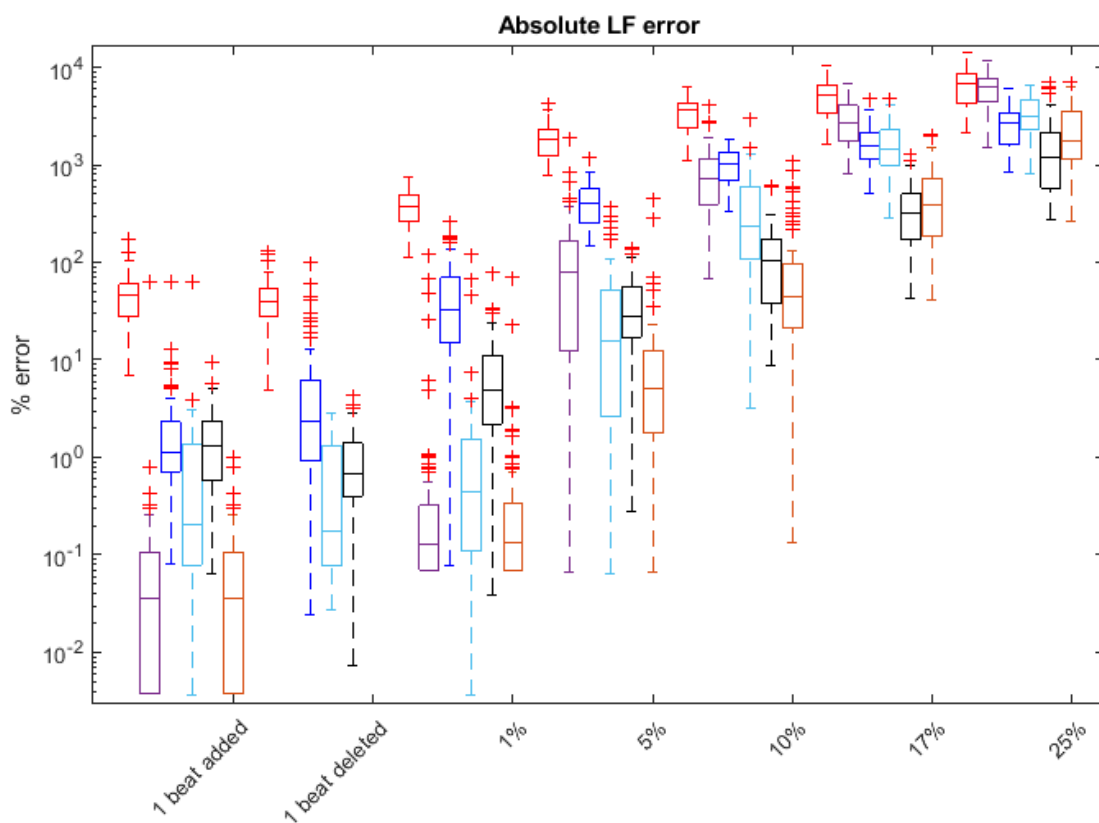


Figure 12-1 - Error of absolute LF component for each BBI correction algorithm in comparison to the reference HR

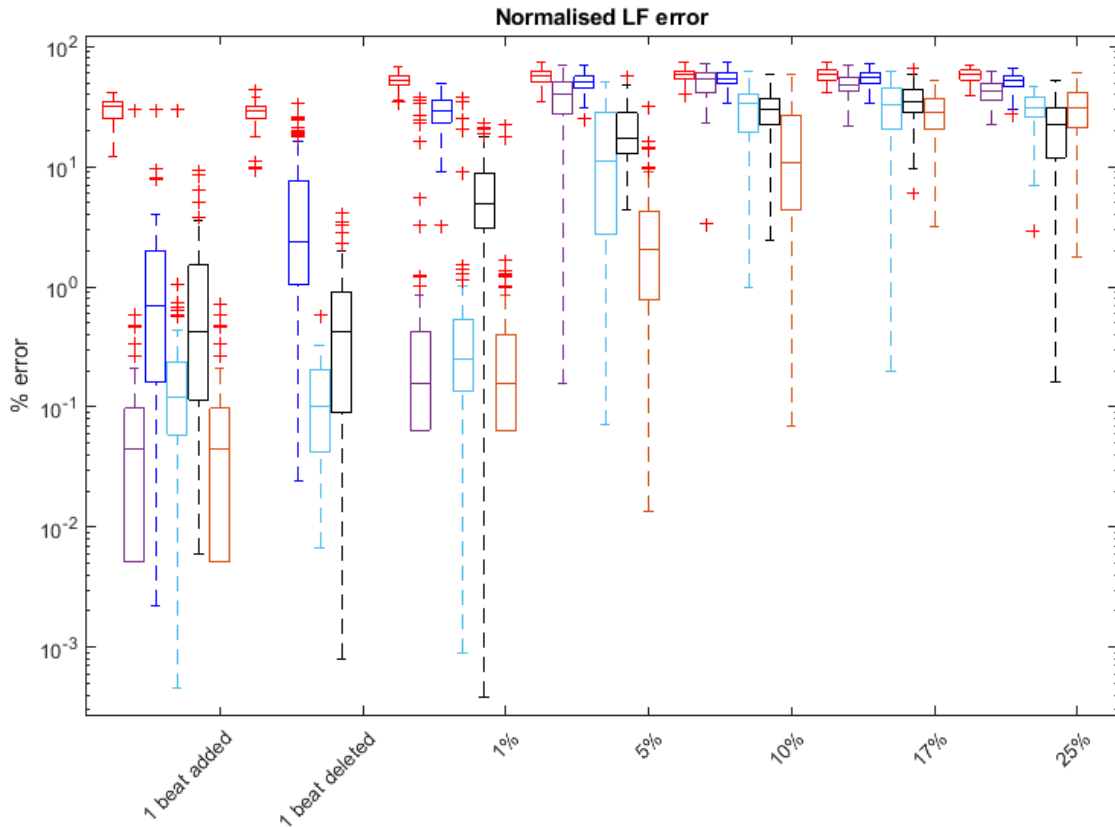


Figure 12-2 - Error of normalised LF component for each BBI correction algorithm in comparison to the reference HR

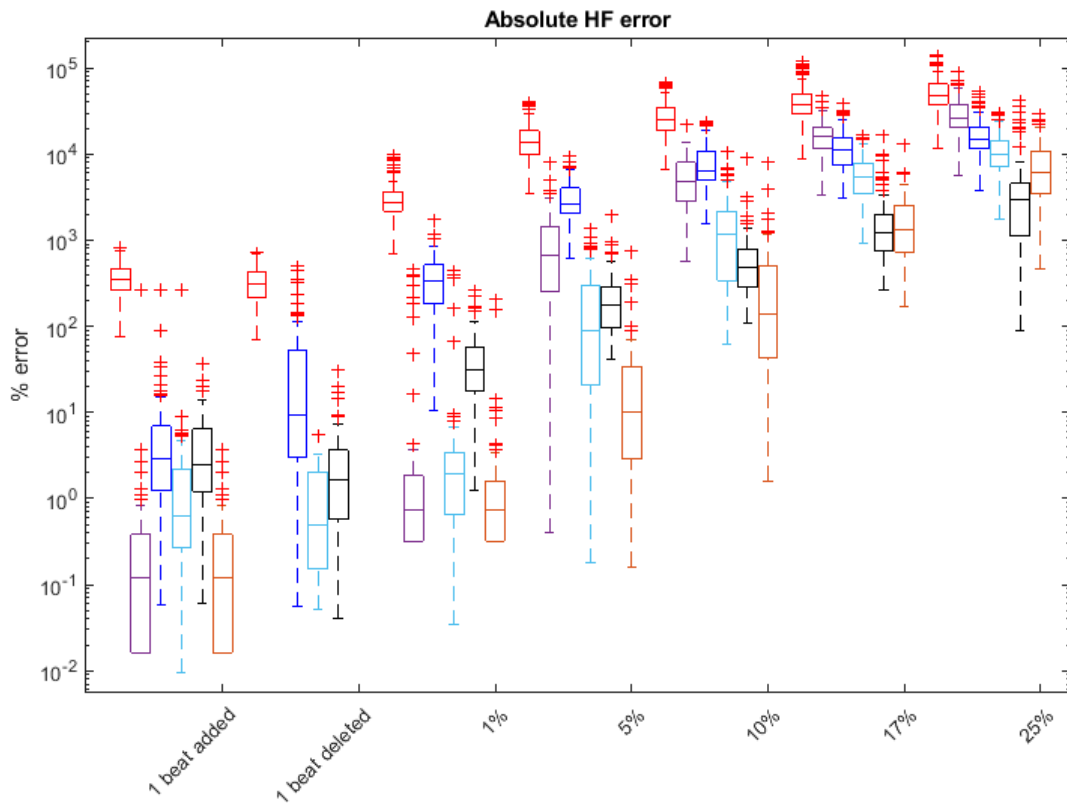


Figure 12-3 - Error of absolute HF component for each BBI correction algorithm in comparison to the reference HR

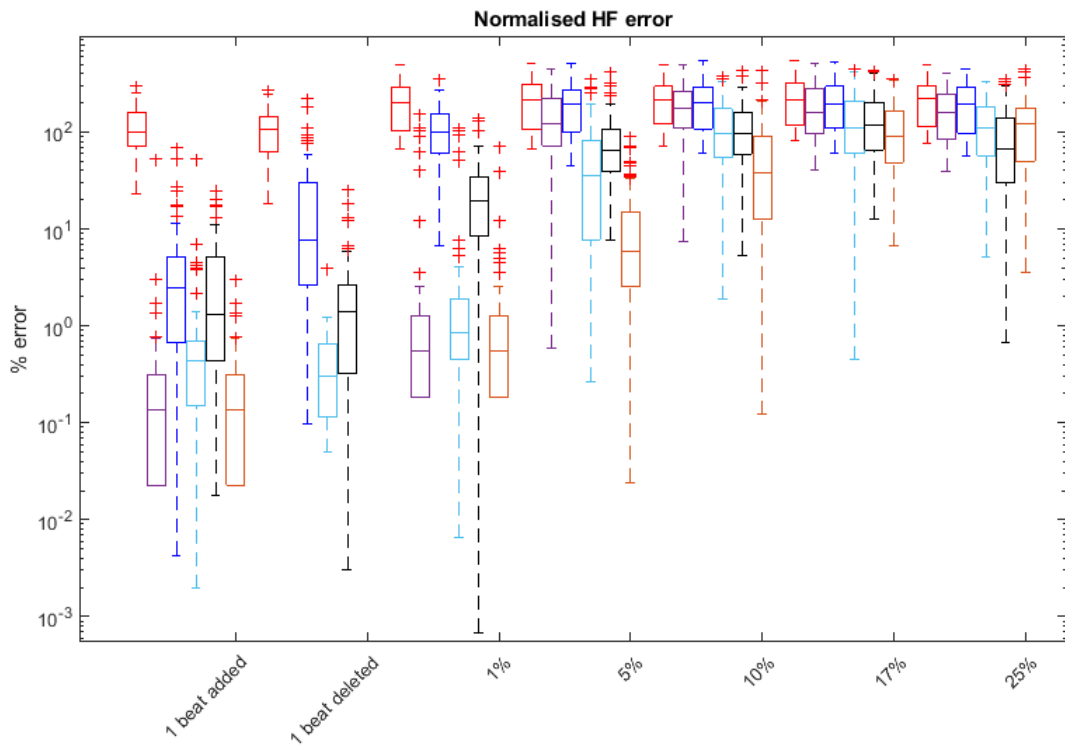


Figure 12-4 - Error of normalised HF component for each BBI correction algorithm in comparison to the reference HR

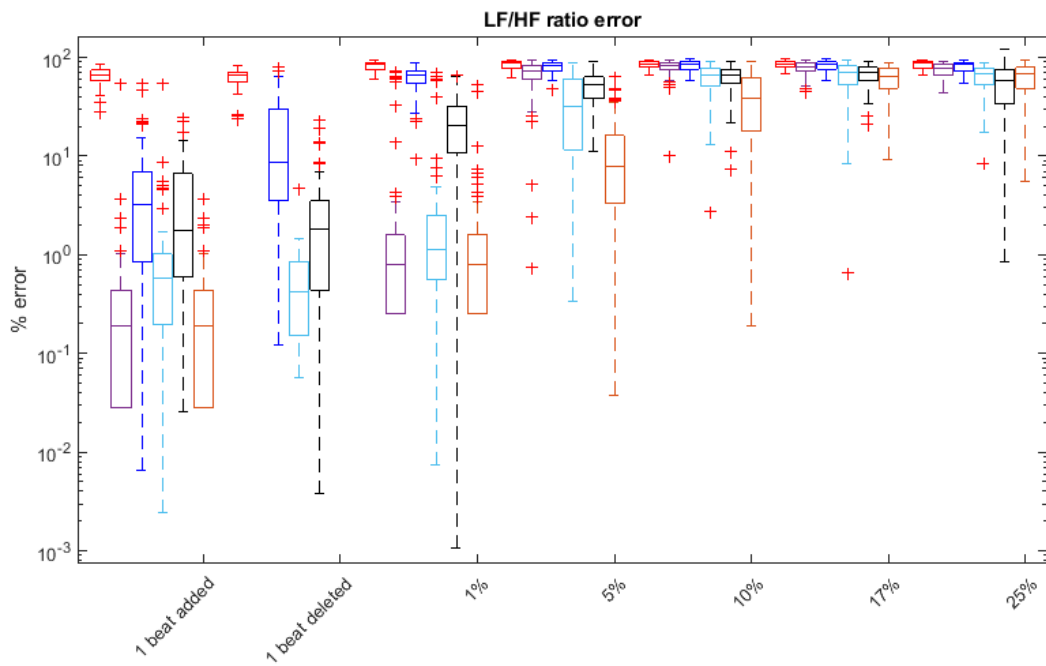


Figure 12-5 - Error of Frequency ratio component for each BBI correction algorithm in comparison to the reference HR

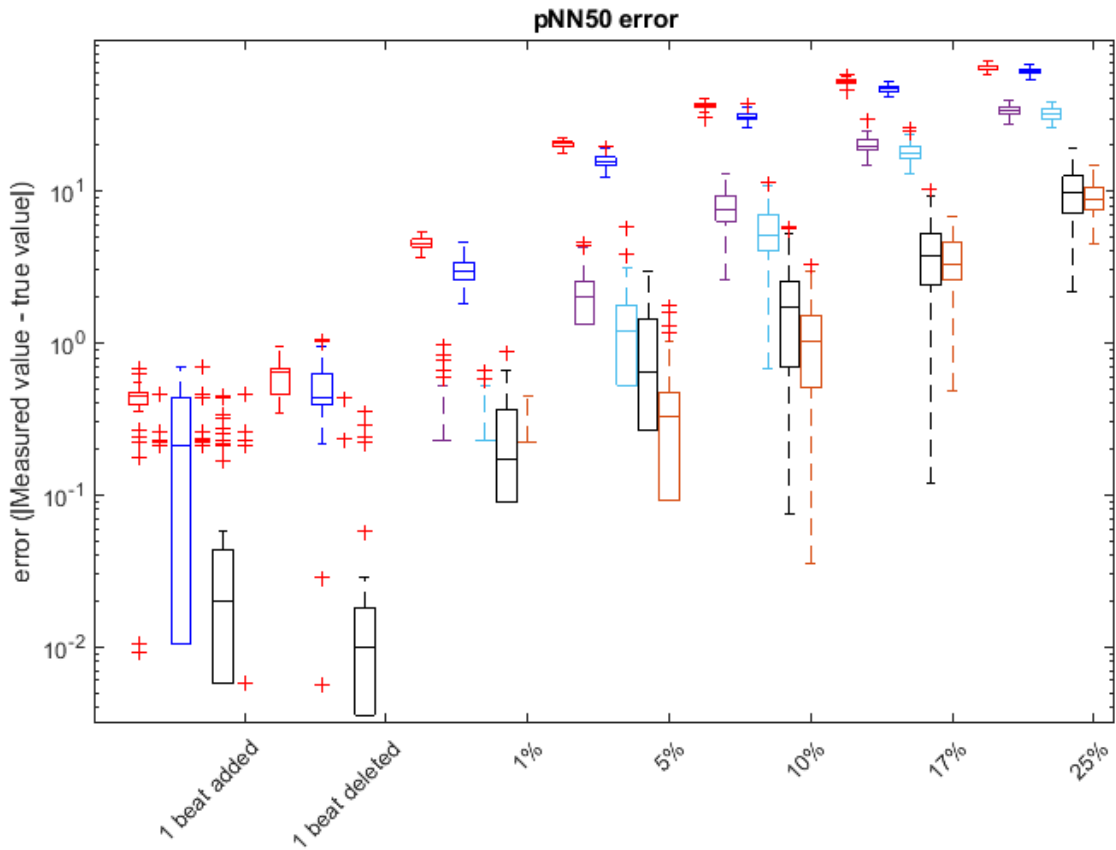


Figure 12-6 - Error of pNN50 component for each BBI correction algorithm in comparison to the reference HR

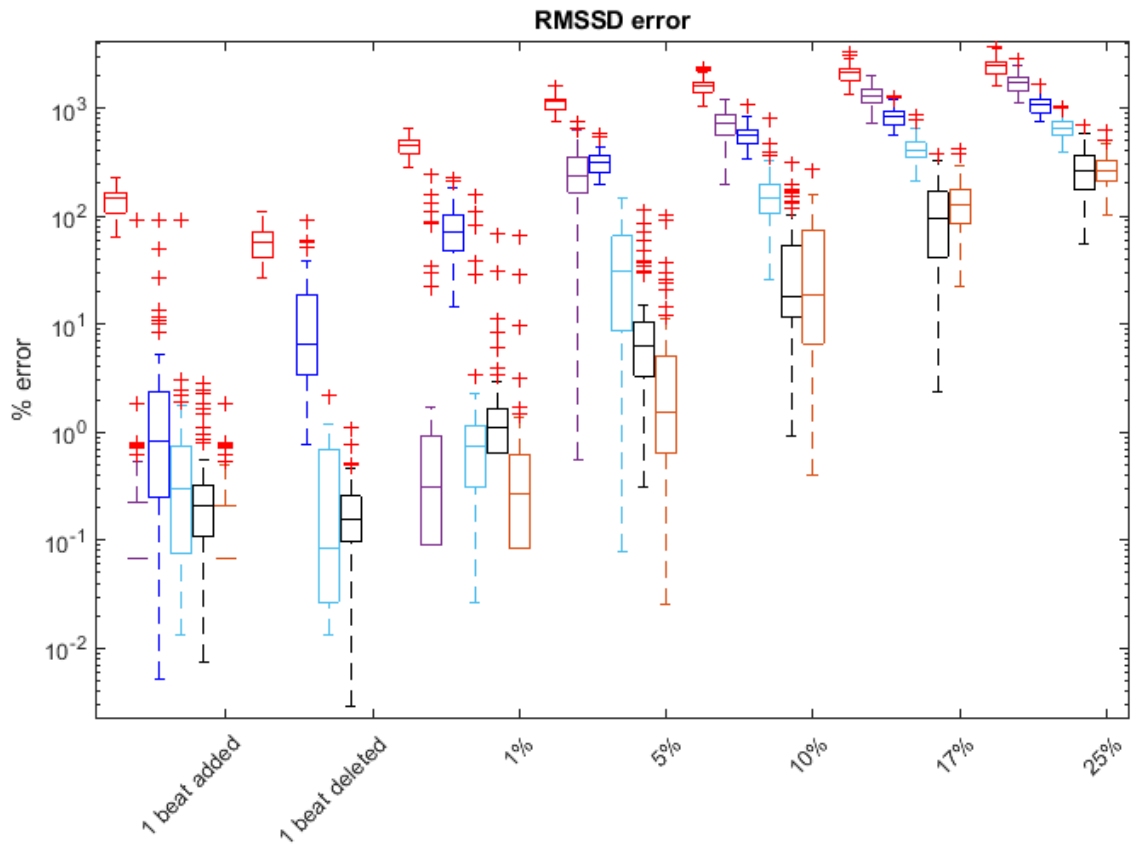


Figure 12-7 - Error of RMSSD component for each BBI correction algorithm in comparison to the reference HR

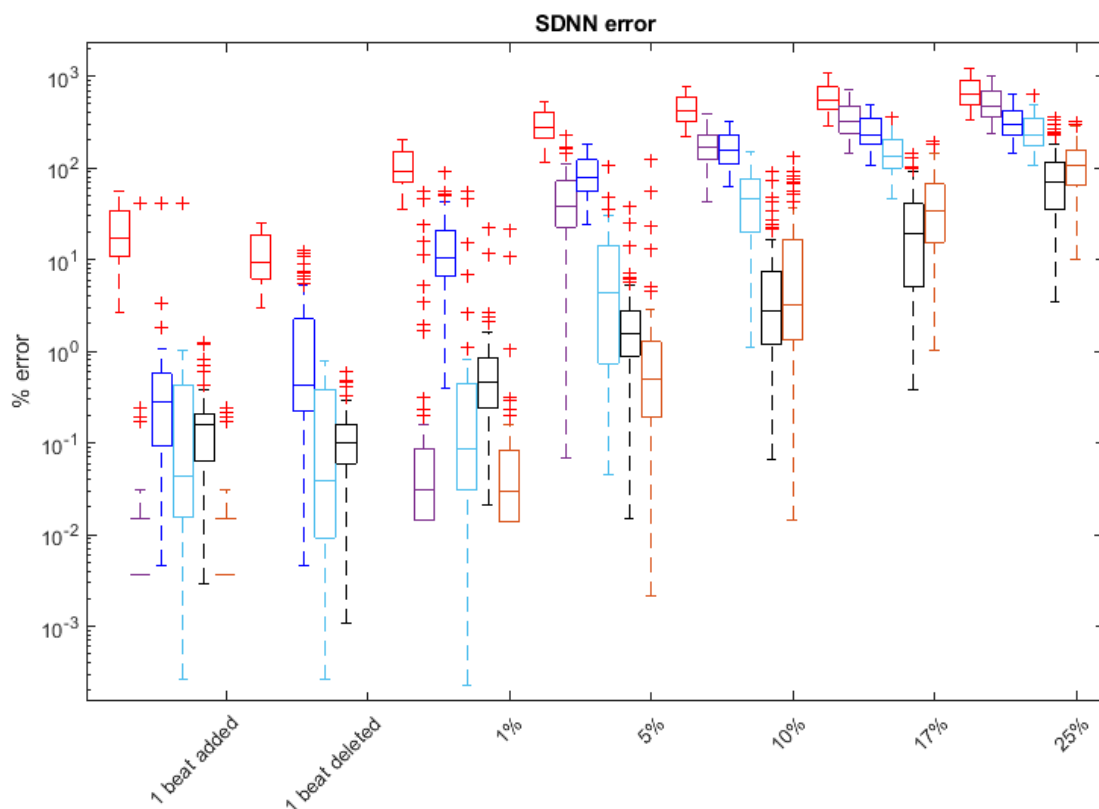


Figure 12-8 - Error of SDRR component for each BBI correction algorithm in comparison to the reference HR

From the HRV analysis of the corrupted BBI values, the magnitudes of the error values for the HF power components, as shown in Figure 12-3, are larger than the magnitudes of the error values for the LF power components, as shown in Figure 12-1 for all levels of corrupted BBI values ($p < 0.0001$). This suggests that having corrupted BBI values has a larger effect on the error of the power in the HF band than the LF band. This is because the addition of one or several false HR values will have a larger effect on the short term variation, which is represented by the HF power band, than the more long term variation, which is represented by the LF power band.

In figures 12-7 and 12-9, the error of the normalised LF and HF values remained constant when the number of corrupted BBI values beats was $\geq 10\%$ of the total BBI values. The error of the LF/HF ratio also remained constant for the same level of corrupted heartbeats, since the LF/HF ratio was calculated using the normalised LF and HF values. This trend in the error calculations is different to the error plot trends for other HRV variables (Figures 12-6,

12-8, 12-11 and 12-12), where when the number of corrupted BBI values was increased the HRV error increased, which occurs in all other HRV variables. The reason for this is shown in the formula for normalising the LF and HF components, which are:

$$LF_n = \frac{LF}{Total\ Power - VLF} = \frac{LF}{LF + HF}$$

$$HF_n = \frac{HF}{Total\ Power - VLF} = \frac{HF}{LF + HF}$$

Since the corrupted data will add more noise to the HF band than the LF band, as the data gets more corrupted, the HF power will increase at a larger rate than the LF power. As the difference between the LF and HF power increases, and the HF power gets sufficiently larger than the LF power, LF_n will tend asymptotically towards 0, and HF_n will tend asymptotically towards 1. Hence when the level of corrupted BBI values became larger, the difference between the power in the LF and HF power bands became larger, which caused the normalised LF and HF variables to approach constant values, as opposed to the other HRV errors which increased as the level of corrupted BBI values increased. This means that once the number of corrupted BBI values becomes larger than a certain value the normalised LF and HF values (and hence the error) will not change, even if the number of corrupted BBI values is increased.

In their results Peters et al. noted that the HF and LF/HF ratio are more effected by the missing BBI values than the LF [200]. A similar result occurred in the results for the results in this paper, and was also noted by Kim et al. [35]. For the original Threshold algorithm (Algorithm 3) when the number of corrupted heartbeats was $\geq 1\%$ of the total heartbeats, the error values for the LF analysis were significantly lower than the HF errors. This result also occurred for the LF and HF values for the Combined Threshold algorithm (Algorithm 5). This result is possibly due to the same reason that causes the magnitude of the HF error to be larger than the LF error in the corrupted BBI values analysis.

12.3 Appendix C –Ethics Submission

The experiment method described was approved by the Southern Adelaide Human Research Ethics Committee on the 2nd of December 2016.

The following pages relate to relevant ethics forms including:

- Patient information forms
- Personal information collection sheet
- Ethics approval letter



Participant Information Sheet/Consent Form

Non-Interventional Study - Adult providing own consent

Flinders University

Title	Feasibility testing of the Cardiomask: a device to monitor heart rate during sleep
Short Title	Testing of the Cardiomask
Ethics submission code	AU/1/39C7211
Project Sponsor	ResMed Ltd.
Coordinating Principal Investigator/ Principal Investigator	Prof. Karen Reynolds
Associate Investigator(s)	Mark Gardner
Location	Flinders University, Tonsley Campus

Part 1 What does my participation involve?

Introduction

You are invited to take part in this research project, "Feasibility testing of the Cardiomask." The research project is aiming to develop a device that is able to monitor heart rate of people during sleep. These devices are specifically designed to be used on patients undergoing treatment for sleep apnoea.

This Participant Information Sheet/Consent Form tells you about the research project. It explains the tests and research involved. Knowing what is involved will help you decide if you want to take part in the research.

Please read this information carefully. Ask questions about anything that you don't understand or want to know more about. Before deciding whether or not to take part, you might want to talk about it with a relative, friend or local doctor.

Participation in this research is voluntary. If you don't wish to take part, you don't have to. This will not affect your healthcare if you do not take part.

If you decide you want to take part in the research project, you will be asked to sign the consent section. By signing it you are telling us that you:

- Understand what you have read
- Consent to take part in the research project
- Consent to the tests and research that are described
- Consent to the use of your personal and health information as described.

You will be given a copy of this Participant Information and Consent Form to keep.

What is the purpose of this research?

The aim of this study is to determine how well our device, known as the “Cardiomask”, is able to monitor heart rate in a simulated sleeping environment. This device, if testing is successful, will be used to monitor the heart rate of patients who are being treated for sleep apnoea, a sleeping disorder that affects the ability of patients to breathe effectively whilst sleeping.

By monitoring a patient’s heart rate during sleep, we hope to gain more information about how the heart behaves not only during sleep, but also during therapy for sleep apnoea. Also, since it is common for sleep apnoea patients to have other heart related health problems, this device will potentially allow any heart problems to be detected before they become too severe.

This research is being conducted by Flinders University and in collaboration with ResMed Ltd. This research has been initiated by Professor Karen Reynolds. The results of this research will be used by the investigator Mark Gardner to obtain a Doctor of Philosophy (Engineering) degree.

What does participation in this research involve?

After you have read the required forms and given your consent the testing will begin. The initial steps will involve screening for eligibility and collecting some basic personal information. None of these criterion will be tested for prior to the commencement of this research, and it is asked that you read the following exclusion to see if any of these apply to you to the best of your knowledge.

Exclusion criteria includes:

- Women who are pregnant.
- Children and/or young people (i.e. <18 years).
- People highly dependent on medical care.
- People with a cognitive impairment, an intellectual disability or a mental illness.
- People with acute or chronic respiratory infection.
- People in which it is unsafe or who are unable to tolerate sleep apnoea therapy. These include people who have:
 - Severe Bullous lung disease
 - Pneumothorax or pneumomediastinum
 - pathologically low blood pressure, particularly if associated with intravascular volume depletion
 - dehydration
 - cerebrospinal fluid leak, recent cranial surgery, or trauma.
- Allergic or otherwise uncomfortable or harmful reaction to chemicals in Ag/AgCl electrode adhesive and hydrogel.
- People with soreness in their jaw, teeth or gums.

The personal information that will be collected will be age, gender, height and weight. These data will be collected on a separate form, which will be filled in after the consent form is signed.

You will then be fitted with the Cardiomask, which is a standard mask for sleep apnoea treatment that has been modified to monitor the wearer’s heart rate. You will also be asked to stick electrodes to your skin that will monitor a reference heart rate signal. These electrodes will be placed onto the back of both hands, as well as onto your right foot. If the Cardiomask or the applied electrodes make you feel uncomfortable or unwell then you may withdraw from this experiment at any time.



You will then be instructed to lie down onto the provided mattress and pillow and to assume a comfortable position lying on your back. The Cardiomask and the electrodes will then be connected to equipment that is used to record the data. Once the device is connected, a member of the research staff will ensure that the device and the reference signal are functioning correctly. Although the device is designed for monitoring participants during sleep, you will be asked to attempt to remain awake for the duration of the test so that you will be able to respond to the investigator's requests, and will be able to alert the investigator of any discomfort.

The Cardiomask will then be connected to a Positive Airway Pressure (PAP) device. This device is a medical device used to treat patients who have sleep apnoea, and functions by directing small amounts of air into the participant's airway in order to facilitate airflow. After the device is connected, the two modes that will be used during the test, the continuous mode and the bi-level mode, will be tested. If this device makes you feel uncomfortable or unwell then you may withdraw from this experiment. If the mask is not able to provide a sufficient seal and if there is significant air leakage from the mask then you may be asked to withdraw from this experiment.

The experiment will then begin. The experiment is divided into several stages. For the first stage you will be required to remain lying on your back for 5 minutes. You will then be instructed to roll over so that you are lying on your left side, and to remain in that position for 3 minutes, and then to repeat for your right side. After this you will be instructed to return to lying on your back.

The PAP device will then be turned on. The first mode of operation will be the continuous pressure mode. In this mode a constant air pressure will be pumped into the mask, however you will still be able to breathe normally. This may initially feel a little strange, however it should not cause any pain or discomfort. If you do experience any pain or discomfort, inform the research staff immediately. The device will be left in this mode for 3 minutes.

The second mode of operation will be the bi-level mode. In this mode the pressure being applied by the PAP device will vary depending on whether you are breathing in or breathing out. As with the constant pressure mode, you should still be able to breathe normally, although you may find that the PAP device will be assisting you in your breathing. If you do experience any pain or discomfort, inform the research staff immediately. The device will be left on this mode for 3 minutes.

At the completion of this final stage the test will then be complete. You are advised to remain lying down until a member of the research staff can assist you in removing the test equipment.

The total duration of the experiment should be no more than 20 minutes. After the test has been completed there will be no follow up stages to this test and you will not be required to complete any more tasks.

There are no costs associated with participating in this research project, nor will you be paid.

Do I have to take part in this research project?

Participation in any research project is voluntary. If you do not wish to take part, you do not have to. If you decide to take part and later change your mind, you are free to withdraw from the project at any stage.

If you do decide to take part, you will be given this Participant Information and Consent Form to sign and you will be given a copy to keep.



Your decision whether or not to take part, or to take part and then withdraw, will not affect your relationship with Flinders University, ResMed Ltd. or any of the staff or other members of these organisations.

What are the possible benefits of taking part?

There will be no clear benefit to you from your participation in this research. However your participation in this research may benefit the wider community, by improving our understanding and our ability to monitor cardiovascular diseases.

What are the possible risks and disadvantages of taking part?

While this research does not involve any interventional treatment, the processes may cause side effects. You may have none, some or all of the effects listed below, and they may be mild, moderate or severe. If you have any of these side effects, or are worried about them, talk with your investigator. Your investigator will also be looking out for side effects.

There may be side effects that the researchers do not expect or do not know about and that may be serious. Tell your investigator immediately about any new or unusual symptoms.

Many side effects go away shortly after treatment ends. However, sometimes side effects can be serious, long lasting or permanent. If a severe side effect or reaction occurs, your investigator may need to stop the experiment, and you may need to see your local physician for the best way to deal with these side effects.

Side Effect	Probability	Consequence	Duration
Discomfort from mask	Possible	Negligible	Duration of the test
Discomfort from PAP treatment	Unlikely	Minor incident	Duration of the test
Discomfort/pain from placing and/removing electrodes from skin	Likely	Negligible	Less than 1 second
Skin irritation from electrodes	Unlikely	Minor incident	2-3 days
Electric shock	Extremely Unlikely	Major injury-Fatality	-

Discomfort from the mask can arise from the mask being improperly fitted, and can lead to minor discomfort. If at any time during the experiment, the Cardiomask feels uncomfortable, inform the research staff and they can attempt to adjust the mask to be more comfortable.

Discomfort from the PAP treatment can arise due to abnormal circumstances. When the PAP device is on, the following side effects may arise:

- drying of the nose, mouth, or throat
- nosebleed
- bloating
- ear or sinus discomfort
- eye irritation
- skin rashes

If any of these symptoms occur during testing, inform the research staff as soon as possible.

The external electrodes contain an adhesive that is used to secure the electrodes to your skin. The process of removing these electrodes can irritate the surface layer of skin and remove some hairs, and as such, when removing these electrodes a small amount of pain can occur, however this pain will usually disappear within a few seconds.

In some participants, the chemicals in the adhesive used in the external electrodes may cause irritation of the skin, and may cause the skin to turn red, even after the electrodes have been removed. In most cases this should disappear within a few days, however if the irritation is severe then you should have the irritation site examined by your local physician.

The use of electrodes, both in the Cardiomask, and the external electrodes used for the reference heart rate signal, mean that you will be connected to an electrical circuit. This circuit is used to measure the electrical signals in your body that are generated by your heart. This means that there is a very small risk of electrocution, the consequences of which can vary from burns to death. Every attempt has been made to mitigate this risk, these steps include:

- Performing the experiments in a body protected area
- Having battery powered devices that are electrically isolated from large sources of voltage including mains power.
- Ensuring electrodes are properly secured onto your skin.

The mask that is going to be used may have been used by previous participants of this experiment. Every attempt has been made to prevent any spread of any infectious diseases that may be present on the test equipment. Such measures include:

- Cleaning of the Cardiomask with 70% Isopropyl alcohol wipes in between uses by each participant. Bacteria are unable to survive in environments containing 70% alcohol, and therefore any surfaces requiring direct patient contact will be wiped down with these alcohol wipes to prevent any bacteria being transmitted between patients.
- Using a disposable anti-bacterial filter that is placed in between the Cardiomask and the tubing of the CPAP device. The filter will be disposed of at the completion of every experiment, and a new filter will be applied before the CPAP tubing is connected to the Cardiomask. This filter will prevent any bacteria that is exhaled by the participant from infecting any other participants.

During analysis of the data, if results are discovered that may diagnose a previously unknown heart condition then you will be contacted and encouraged to visit your local physician. However the researchers conducting this investigation are not cardiologists, and the devices used in this experiment have not been approved as medical devices, and as such are not expert opinions and should not be treated as such.

If you become upset or distressed as a result of your participation in the research, the investigator will be able to arrange for counselling or other appropriate support. Any counselling or support will be provided by qualified staff who are not members of the research project team. This counselling will be provided free of charge.

What if I withdraw from this research project?

If you decide to withdraw from this research project, please notify a member of the research team. A member of the research team will inform you if there are any special requirements linked to withdrawing.

If you do withdraw your consent during the research project, the relevant study staff will not collect additional personal information from you, although personal information already collected will be retained to ensure that the results of the research project can be measured properly and to comply with law. You should be aware that data collected by the sponsor up to the time you withdraw will form part of the research project results. If you do not want them to do this, you must tell them before you join the research project.



Could this research project be stopped unexpectedly?

This research project may be stopped unexpectedly for a variety of reasons. These may include

- Unacceptable side effects
- The device being shown not to be effective
- Decisions made in the commercial interests of the sponsor or by local regulatory/health authorities.

Part 2 How is the research project being conducted?

What will happen to information about me?

By signing the consent form you consent to the relevant research staff collecting and using personal information about you for the research project. Any information obtained in connection with this research project that can identify you will remain confidential. All data will be stored in a secure drive, or a locked cabinet, accessible to only the research staff. The data will not contain any of your personal information. However a document linking your data to your email address will be kept in case analysis of the data reveals a cardiac abnormality or other significant event. This information will not be published in any format and will remain in the secure folder. Your information will only be used for the purpose of this research project and it will only be disclosed with your permission, except as required by law.

It is anticipated that the results of this research project will be published and/or presented in a variety of forums. In any publication and/or presentation, information will be provided in such a way that you cannot be identified, except with your permission. In the event that a participant is referred to individually in a publication, they will be assigned a number and referred to by that number e.g. participant 16. These numbers will be randomly assigned and will not in any way be connected to the order of the testing.

In accordance with relevant Australian privacy and other relevant laws, you have the right to request access to the information collected and stored by the research team about you. You also have the right to request that any information with which you disagree be corrected. Please contact the research team member named at the end of this document if you would like to access your information.

Any information obtained for the purpose of this research project that can identify you will be treated as confidential and securely stored. It will be disclosed only with your permission, or as required by law.

Complaints and compensation

If you suffer any injuries or complications as a result of this research project, you should contact the study team as soon as possible and you will be assisted with arranging appropriate medical treatment. If you are eligible for Medicare, you can receive any medical treatment required to treat the injury or complication, free of charge, as a public patient in any Australian public hospital.

In the event of loss or injury, the parties will be compensated by the Flinders insurance accident policy. If you are a student then the compensation is covered by the Student Personal Accident cover. For more details contact Steve Semmler at steve.semmler@flinders.edu.au or 82012618. For all participants, participation in this research does not mean you are waiving your right to legal compensation.



Who is organising and funding the research?

This research project is being conducted by Professor Karen Reynolds of Flinders University and is being funded by ResMed Ltd.

ResMed Ltd. and/or Flinders University may benefit financially from this research project if, for example, the project assists ResMed Ltd. and/or Flinders University to obtain approval for a new treatment and/or device.

You will not benefit financially from your involvement in this research project even if, for example, knowledge acquired from analysis of your data proves to be of commercial value to ResMed Ltd. and/or Flinders University.

In addition, if knowledge acquired through this research leads to discoveries that are of commercial value to ResMed Ltd. and/or Flinders University, the research staff or their institutions, there will be no financial benefit to you or your family from these discoveries.

Flinders University will receive a payment from ResMed Ltd. for undertaking this research project.

No member of the research team will receive a personal financial benefit from your involvement in this research project (other than their ordinary wages).

Who has reviewed the research project?

All research in Australia involving humans is reviewed by an independent group of people called a Human Research Ethics Committee (HREC). The ethical aspects of this research project have been approved by the HREC of Southern Adelaide Clinical Human Research Ethics Committee.

This project will be carried out according to the National Statement on Ethical Conduct in Human Research (2007). This statement has been developed to protect the interests of people who agree to participate in human research studies.

Further information and who to contact

The person you may need to contact will depend on the nature of your query.

If you want any further information concerning this project or if you have any medical problems which may be related to your involvement in the project (for example, any side effects), you can contact the principal investigator on +61 8 82015190 or any of the following people:

Associate Researcher

Name	Mark Gardner
Position	PhD Student
Telephone	+61448121126
Email	mark.gardner@flinders.edu.au

First aid officer

Name	Dr Nasser Asgari
Position	First aid Officer
Telephone	+61 8 82015059
Email	nasser.asgari@flinders.edu.au



Flinders University
The Medical Device
Research Institute

For matters relating to research at the site at which you are participating, the details of the local site complaints person are:

Complaints contact person

Name	Villis Marshall
Position	Director, Office for Research
Telephone	8204 6453
Email	Health.SALHNOfficeforResearch@sa.gov.au

If you have any complaints about any aspect of the project, the way it is being conducted or any questions about being a research participant in general, then you may contact:

Reviewing HREC approving this research and HREC Executive Officer details

Reviewing HREC name	Southern Adelaide Clinical Human Research Ethics Committee
HREC Executive Officer	Damian Creaser
Telephone	8204 6453
Email	Health.SALHNOfficeforResearch@sa.gov.au

Local HREC Office contact (Single Site -Research Governance Officer)

Position	Research Governance Officer
Telephone	8204 6453
Email	Health.SALHNOfficeforResearch@sa.gov.au

Consent Form - *Adult providing own consent*

Title Feasibility testing of the Cardiomask: a device to monitor heart rate during sleep
Short Title Testing of the Cardiomask
Ethics Submission Code AU/1/39C7211
Project Sponsor ResMed Ltd.
**Coordinating Principal Investigator/
Principal Investigator** Prof. Karen Reynolds
Associate Investigator(s) Mark Gardner
Location Flinders University, Tonsley Campus

Declaration by Participant

I have read the Participant Information Sheet or someone has read it to me in a language that I understand.

I understand the purposes, procedures and risks of the research described in the project.

I have had an opportunity to ask questions and I am satisfied with the answers I have received.

I freely agree to participate in this research project as described and understand that I am free to withdraw at any time during the project without affecting my relationship with Flinders University, the Medical Device Research Institute, or ResMed Ltd.

I understand that I will be given a signed copy of this document to keep.

Name of Participant (please print) _____

Signature _____ Date _____

Declaration by Study Doctor/Senior Researcher[†]

I have given a verbal explanation of the research project, its procedures and risks and I believe that the participant has understood that explanation.

Name of Study Doctor/
Senior Researcher[†] (please print) _____ Mark Gardner

Signature _____ Date _____

[†] A senior member of the research team must provide the explanation of, and information concerning, the research project.

Note: All parties signing the consent section must date their own signature.

Form for Withdrawal of Participation - *Adult providing own consent*

Title Feasibility testing of the Cardiomask: a device to monitor heart rate during sleep
Short Title Testing of the Cardiomask
Ethics Submission Code AU/1/39C7211
Project Sponsor ResMed Ltd.
**Coordinating Principal Investigator/
Principal Investigator** Prof. Karen Reynolds
Associate Investigator(s) Mark Gardner
Location Flinders University, Tonsley Campus

Declaration by Participant

I wish to withdraw from participation in the above research project and understand that such withdrawal will not affect my relationship with Flinders University, the Medical Device Research Institute, or ResMed Ltd.

Name of Participant (please print) _____
Signature _____ Date _____

Description of circumstances of withdrawal

Declaration by Study Doctor/Senior Researcher†

I have given a verbal explanation of the implications of withdrawal from the research project and I believe that the participant has understood that explanation.

Name of Study Doctor/
Senior Researcher† (please print) _____ Mark Gardner
Signature _____ Date _____

† A senior member of the research team must provide the explanation of and information concerning withdrawal from the research project.

Note: All parties signing the consent section must date their own signature.

- pathologically low blood pressure, particularly if associated with intravascular volume depletion

Yes

No

- cerebrospinal fluid leak, recent cranial surgery, or trauma.

Yes

No

- Acute or chronic respiratory infection?

Yes

No

The following questions should only be filled out on the day of testing:

Approximately how long has it been since you have washed your face with soap and water:

Less than 6 hours

Less than 12 hours

Greater than 12 hours

Since you have last washed your face with soap and water, have you applied any products to your face?

Yes

No

If you answered yes please list them below:

I declare that the information I have provided is accurate to the best of my knowledge

Signature: _____ Date: _____

Office for Research

Flinders Medical Centre
Ward 6C, Room 6A219
Flinders Drive, Bedford Park SA 5042
Tel: (08) 8204 6453
E: Health.SALHNOfficeforResearch@sa.gov.au



Government of South Australia

SA Health

Southern Adelaide Local Health Network

Final approval for ethics application

You are reminded that this letter constitutes **ethical** approval only. **Ethics approval is one aspect of the research governance process.**

You must not commence this research project at any SA Health sites listed in the application until a Site Specific Assessment (SSA), or Access Request for data or tissue form has been authorised by the Chief Executive or delegate of each site.

02 December 2016

Professor Karen Reynolds
Medical Device Research Institute
Flinders University
BEDFORD PARK SA 5042

Dear Professor Reynolds

The Southern Adelaide Clinical Human Research Ethics Committee (SAC HREC EC00188) have reviewed and provided ethical approval for this application which appears to meet the requirements of the *National Statement on Ethical Conduct in Human Research*.

Application Number: OFR # 326.16 - HREC/16/SAC/277

Title: Feasibility testing of the cardiomask: a device to monitor heart rate during sleep

Chief investigator: Professor Karen Reynolds

Approval Period: 02 December 2016 to 02 December 2019

The below documents have been reviewed and approved:

- NEAF dated 18 November 2016
- PICF Cardiac Mask v6.0 dated 11 August 2016
- Letter of Interest
- Information Collected Sheet

The following document has been noted:

- Filter Datasheet

TERMS AND CONDITIONS OF ETHICAL APPROVAL

As part of the Institution's responsibilities in monitoring research and complying with audit requirements, it is essential that researchers adhere to the conditions below and with the *National Statement chapter 5.5*.

Final ethical approval is granted subject to the researcher agreeing to meet the following terms and conditions:

1. The approval only covers the science and ethics component of the application. A SSA will need to be submitted and authorised before this research project can commence at any of the approved sites identified in the application.
2. If University personnel are involved in this project, the Principal Investigator should notify the University before commencing their research to ensure compliance with University requirements including any insurance and indemnification requirements.
3. Compliance with the *National Statement on Ethical Conduct in Human Research (2007)* & the *Australian Code for the Responsible Conduct of Research (2007)*.

4. To immediately report to SAC HREC anything that may change the ethical or scientific integrity of the project.
5. Report Significant Adverse events (SAE's) as per SAE requirements available at our website.
6. Submit an annual report on each anniversary of the date of final approval and in the correct template from the SAC HREC website.
7. Confidentiality of research participants MUST be maintained at all times.
8. A copy of the signed consent form must be given to the participant unless the project is an audit.
9. Any reports or publications derived from the research should be submitted to the Committee at the completion of the project.
10. All requests for access to medical records at any SALHN site must be accompanied by this approval email.
11. To regularly review the SAC HREC website and comply with all submission requirements, as they change from time to time.
12. Once your research project has concluded, any new product/procedure/intervention cannot be conducted in the SALHN as standard practice without the approval of the SALHN New Medical Products and Standardisation Committee or the SALHN New Health Technology and Clinical Practice Innovation Committee (as applicable) Please refer to the relevant committee link on the SALHN intranet for further information.

Kind Regards

A handwritten signature in black ink, appearing to read 'Bernadette Richards', written in a cursive style.

A/Professor Bernadette Richards
Chair, SAC HREC

12.4 Appendix D – Optimisation of data fusion constants

12.4.1 Variable optimisation

To test for the optimal values of C from the CWA algorithm (which shall be denoted as the CWA variable) and Q_k from the KF algorithm (which shall be denoted as the KF variable), both variables were varied from 0.05 to 1.5 via a step of 0.05. Then the HR was estimated using the KF and CWA algorithms with the new KF and CWA variables respectively. The error of the HR was compared for each variable to determine which value gave the lowest error for both variables.

12.4.2 Results

12.4.2.1 KF results

The performance of the HR estimation algorithms was evaluated for different CWA and KF variables.

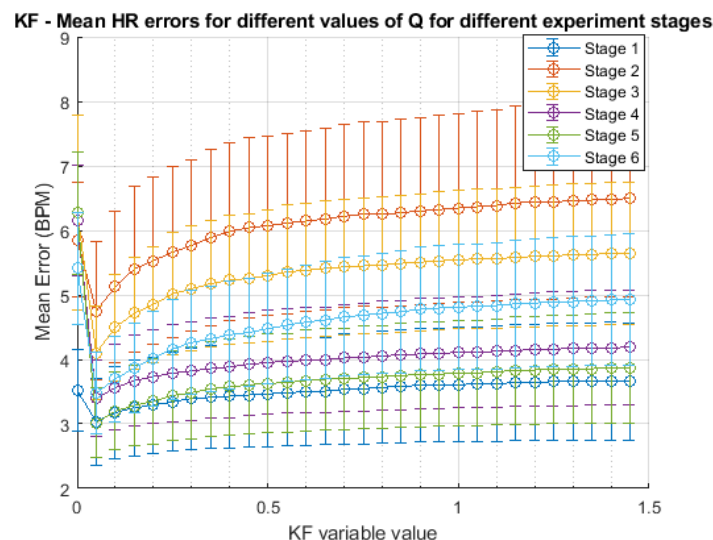


Figure 12-9 - The change in the average HR error over different participants with different KF variable values.

For the KF variable, the lower the value, the lower the HR estimation error. This is shown in Figure 12-9, where for all stages the mean and median HR error values for all participants' increases as the KF variable increases, as long as the KF variable is greater than 0. This figure shows that in order to reduce the median and mean HR error the KF variable should be set to a value as small as possible. This value relates to the covariance of the process noise of the KF or the random noise added to the state model to account for the natural variation of the HR, as shown in equation 12.3 in Appendix A.

However the effect of changing the KF variable is minimal. Mean and median error values from the KF algorithm from different participants using KF variables that would give the minimum (0.05), maximum (1.5) as well as an in between value (0.75) are shown in Figure 12-10. This comparison shows that for the participant data collected, the difference between the best and worst choice of the KF variable was between 0.6 and 1.7BPM, depending on the experiment stage. Whilst the difference in HR error between the best and worst case values for the KF variable was statistically significant ($p \leq 0.0023$), the effect of using a different KF variable was less than the interpatient variability and the different experiment stages had a larger effect on the error of the KF HR estimation algorithm.

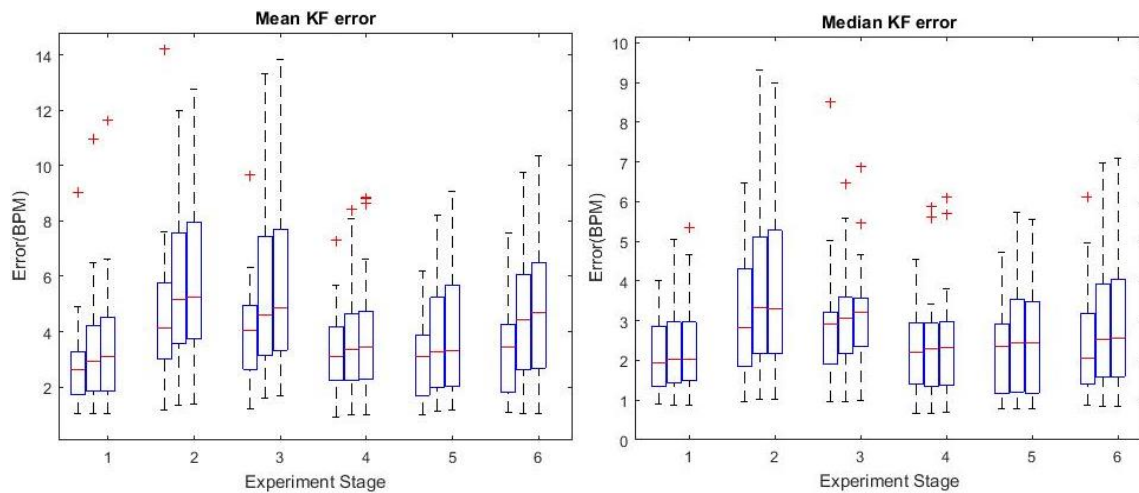


Figure 12-10 – Mean and median HR estimation error using the KF algorithm for each experiment stage for different Q values. Left Q = 0.05, middle Q = 0.75, right Q = 1.5

12.4.2.2 CWA results

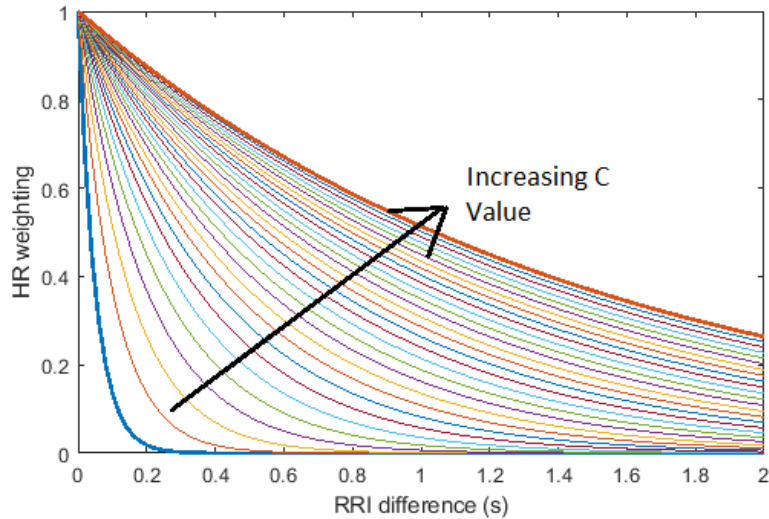


Figure 12-11 - Change in HR weighting with different C values ranging from 0.05 (thick blue line) to 1.5 (thick orange line).

For the CWA algorithm, the variation of the relationship between the weighting values and the difference in RRI values, caused by different CWA variable values, is shown in Figure 12-11. As expected this figure shows that for a large CWA variable (C), a larger weighting is given to a large difference in RRI value and vice versa. Figure 12-11 also shows why extreme values of the CWA variable may be impractical, as when the variable was set to a large value large RRI differences would be assigned relatively high weighting, which will cause outlier HR values to introduce errors into the HR estimation. The variation of the KF variable, and how it affected the HR covariance was more complex (see eqn. 13.3 in Appendix A) than for the CWA algorithm which is why it was not plotted.

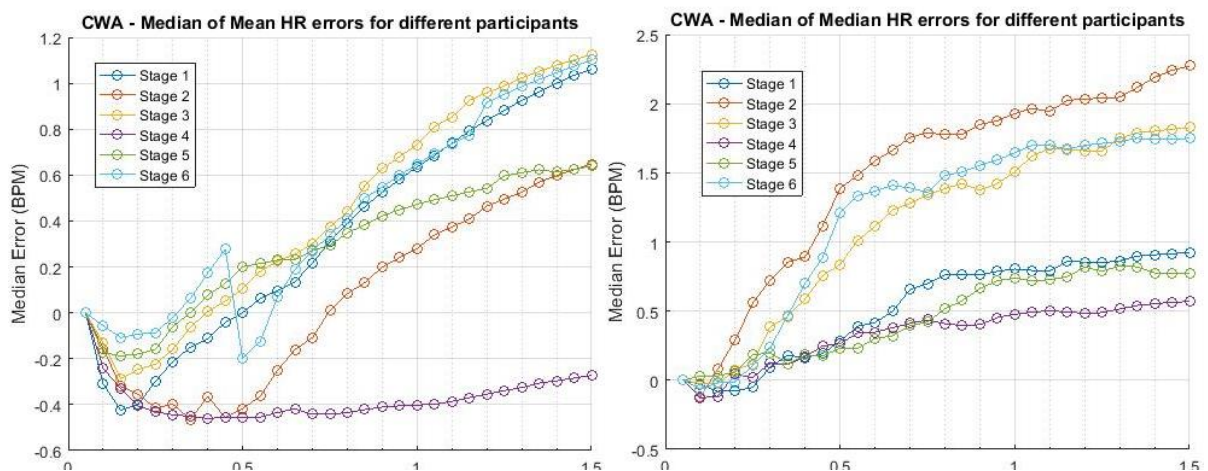


Figure 12-12 - The change in the mean (left) and median (right) HR error for different participants with different CWA variable values.

The relationship between the CWA variable and the HR estimation error as shown in Figure 12-12 was more complex than for the KF variable in Figure 12-9. Figure 12-12 shows that the optimum value for the CWA algorithm for reducing the HR estimation error is somewhere between 0 and 0.5, as when the CWA variable was larger than 0.5, the error increased as the CWA variable increased. This may be due to how the HR weighting is calculated, as Figure 12-11 shows how the HR weighting relationship changed with different CWA variable values. However from Figure 12-12, the CWA value that produced the lowest HR estimation error was approximately 0.15.

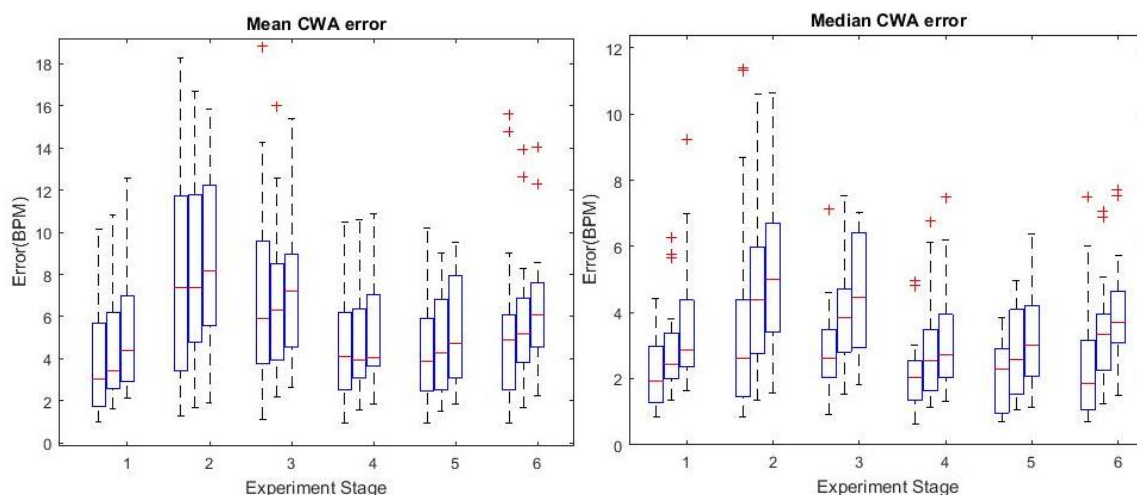


Figure 12-13 - Mean and median HR estimation error using the CWA algorithm for each experiment stage for different C values. Left C = 0.15, middle C = 0.7 right C = 1.5

Similarly to the KF HR estimation algorithm the effect that the CWA variable has on the HR estimation accuracy is not very large in comparison to the interpatient variability and the change in HR error between different experiment stages. The change in the error with the CWA variables that would theoretically give the maximum (C = 1.5) and minimum error (C = 0.15), as well as a value in between the maximum and minimum (C = 0.7) are shown in Figure 12-13. This figure shows that the difference between the median HR error for the theoretical best and worst CWA variables is larger (1-1.5BPM) than the difference between the best and worst values in Figure 12-10 (0.2-0.7BPM). Unlike in Figure 12-10 there is a large difference between the mean and median HR error values, even when the optimal CWA value is used. This implies that there are small amounts of periods where the HR error

is significantly larger than normally, and the distribution of the HR error from the CWA algorithm is non-normal.

13. References

1. Iskandar, A.A., et al. *A wearable 1-lead necklace ECG for continuous heart rate monitoring*. in *2016 IEEE 18th International Conference on e-Health Networking, Applications and Services, Healthcom 2016*. 2016.
2. Peppard, P.E., et al., *Increased prevalence of sleep-disordered breathing in adults*. *American journal of epidemiology*, 2013. **177**(9): p. 1006-1014.
3. Balachandran, J.S. and S.R. Patel, *Obstructive Sleep Apnea*. *Annals of internal medicine*, 2014. **161**(9): p. ITC1-ITC1.
4. Sullivan, C., et al., *Reversal of obstructive sleep apnoea by continuous positive airway pressure applied through the nares*. *The Lancet*, 1981. **317**(8225): p. 862-865.
5. Force, A.O.S.A.T. and A.A.o.S. Medicine, *Clinical guideline for the evaluation, management and long-term care of obstructive sleep apnea in adults*. *Journal of clinical sleep medicine: JCSM: official publication of the American Academy of Sleep Medicine*, 2009. **5**(3): p. 263.
6. Stanfield, C.L., et al., *Principles of human physiology*. 2011: Pearson/Benjamin Cummings.
7. Wesley, K., *Huszar's Basic Dysrhythmias and Acute Coronary Syndromes: Interpretation and Management, 4th Edition*. 2010, China: Elsevier Inc.
8. Camm, A., et al., *Heart rate variability: standards of measurement, physiological interpretation and clinical use*. *Task Force of the European Society of Cardiology and the North American Society of Pacing and Electrophysiology*. *Circulation*, 1996. **93**(5): p. 1043-1065.
9. Jose, A.D. and D. Collison, *The normal range and determinants of the intrinsic heart rate in man*. *Cardiovascular research*, 1970. **4**(2): p. 160-167.
10. Jay S. Balachandran, M. and M. Sanjay R. Patel, MS, *Obstructive Sleep Apnea*. *Annals of Internal Medicine*, 2014. **161**(9).
11. Gottlieb, D.J., et al., *Prospective study of obstructive sleep apnea and incident coronary heart disease and heart failure the sleep heart health study*. *Circulation*, 2010. **122**(4): p. 352-360.
12. Guilleminault, C., et al., *OBSTRUCTIVE SLEEP-APNEA AND CARDIAC INDEX*. *Chest*, 1986. **89**(3): p. 331-334.
13. Andreas, S., et al., *Changes in heart rate during obstructive sleep apnoea*. *European Respiratory Journal*, 1992. **5**(7): p. 853-857.
14. Yusuf, S., et al., *Global burden of cardiovascular diseases part I: general considerations, the epidemiologic transition, risk factors, and impact of urbanization*. *Circulation*, 2001. **104**(22): p. 2746-2753.
15. Gay, P., et al., *Evaluation of positive airway pressure treatment for sleep related breathing disorders in adults*. *Sleep*, 2006. **29**(3): p. 381-401.
16. Benjafield, A., et al., *0531 Compliance with Positive Airway Pressure Therapy after Switching from CPAP to Bilevel for Non-compliant OSA Patients: A Big Data Analysis*. *Sleep*, 2018. **41**(suppl_1): p. A198-A199.
17. Luo, F., et al., *Invasive versus non-invasive ventilation for acute respiratory failure in neuromuscular disease and chest wall disorders*. *Cochrane Database of Systematic Reviews*, 2017(12).
18. Criner, G.J., et al., *COPD Home Oxygen Therapy and Home Mechanical Ventilation: Improving Admission-Free Survival in Persistent Hypercapnic COPD*. *Chest*, 2018. **153**(6): p. 1499-1500.
19. Medicine, A.A.o.S. and C. Iber, *The AASM manual for the scoring of sleep and associated events: rules, terminology and technical specifications*. 2007: American Academy of Sleep Medicine.
20. Altevogt, B.M. and H.R. Colten, *Sleep Disorders and Sleep Deprivation: An Unmet Public Health Problem*. 2006: National Academies Press.

21. Zee, P.C. and P. Manthena, *The brain's master circadian clock: implications and opportunities for therapy of sleep disorders*. Sleep medicine reviews, 2007. **11**(1): p. 59-70.
22. Smolensky, M., et al., *Circadian rhythmic aspects of human cardiovascular function: a review by chronobiologic statistical methods*. Chronobiologia, 1975. **3**(4): p. 337-371.
23. Portaluppi, F. and R.C. Hermida, *Circadian rhythms in cardiac arrhythmias and opportunities for their chronotherapy*. Advanced drug delivery reviews, 2007. **59**(9): p. 940-951.
24. Burgess, H.J., et al., *Sleep and circadian influences on cardiac autonomic nervous system activity*. American Journal of Physiology-Heart and Circulatory Physiology, 1997. **273**(4): p. H1761-H1768.
25. Portaluppi, F., et al., *Diurnal blood pressure variation and hormonal correlates in fatal familial insomnia*. Hypertension, 1994. **23**(5): p. 569-576.
26. Thormann, J., M. Schlepper, and W. Kramer, *Diurnal changes and reproducibility of corrected sinus node recovery time*. Catheterization and cardiovascular diagnosis, 1983. **9**(5): p. 439-451.
27. Kong, T.Q., et al., *Circadian variation in human ventricular refractoriness*. Circulation, 1995. **92**(6): p. 1507-1516.
28. Muller, J.E., et al., *Circadian variation in the frequency of sudden cardiac death*. Circulation, 1987. **75**(1): p. 131-138.
29. Flemons, W.W., et al., *Access to diagnosis and treatment of patients with suspected sleep apnea*. American journal of respiratory and critical care medicine, 2004. **169**(6): p. 668-672.
30. Kapit, W., R.I. Macey, and E. Meisami, *The Physiology coloring book*. 2nd ed. 2000, California: Addison Wesley Longman Inc.
31. Mehra, R., et al., *Association of nocturnal arrhythmias with sleep-disordered breathing: The Sleep Heart Health Study*. American journal of respiratory and critical care medicine, 2006. **173**(8): p. 910-916.
32. Somers, V.K., et al., *Sleep apnea and cardiovascular disease: An american heart association/american college of cardiology foundation scientific statement from the american heart association council for high blood pressure research professional education committee, council on clinical cardiology, stroke council, and council on cardiovascular nursing in collaboration with the national heart, lung, and blood institute national center on sleep disorders research (national institutes of health)*. Journal of the American College of Cardiology, 2008. **52**(8): p. 686-717.
33. Abe, H., et al., *Efficacy of continuous positive airway pressure on arrhythmias in obstructive sleep apnea patients*. Heart and vessels, 2010. **25**(1): p. 63-69.
34. Harbison, J., P. O'Reilly, and W.T. Mc Nicholas, *Cardiac rhythm disturbances in the obstructive sleep apnea syndrome: effects of nasal continuous positive airway pressure therapy*. Chest, 2000. **118**(3): p. 591-595.
35. Kim, K.K., et al., *The effect of missing RR-interval data on heart rate variability analysis in the frequency domain*. Physiological measurement, 2009. **30**(10): p. 1039.
36. Kim, K.K., et al., *Effect of missing RR-interval data on heart rate variability analysis in the time domain*. Physiological measurement, 2007. **28**(12): p. 1485.
37. Kleiger, R.E., et al., *Decreased heart rate variability and its association with increased mortality after acute myocardial infarction*. The American Journal of Cardiology, 1987. **59**(4): p. 256-262.
38. Nolan, J., et al., *Prospective study of heart rate variability and mortality in chronic heart failure: Results of the United Kingdom heart failure evaluation and assessment of risk trial (UK-Heart)*. Circulation, 1998. **98**(15): p. 1510-1516.
39. La Rovere, M.T., et al., *Baroreflex sensitivity and heart-rate variability in prediction of total cardiac mortality after myocardial infarction*. Lancet, 1998. **351**(9101): p. 478-484.

179. Inan, O., et al., *Robust ballistocardiogram acquisition for home monitoring*. Physiological measurement, 2009. **30**(2): p. 169.
180. Zink, M.D., et al., *Unobtrusive Nocturnal Heartbeat Monitoring by a Ballistocardiographic Sensor in Patients with Sleep Disordered Breathing*. Scientific Reports, 2017. **7**(1): p. 13175.
181. Logier, R., et al. *A multi sensing method for robust measurement of physiological parameters in wearable devices*. in *2014 36th Annual International Conference of the IEEE Engineering in Medicine and Biology Society, EMBC 2014*. 2014.
182. Tarvainen, M.P., et al., *Time-varying analysis of heart rate variability signals with a Kalman smoother algorithm*. Physiological Measurement, 2006. **27**(3): p. 225-239.
183. Wolkove, N., et al., *Long-term compliance with continuous positive airway pressure in patients with obstructive sleep apnea*. Canadian respiratory journal, 2008. **15**(7): p. 365-369.
184. Cullen, D., *Printed Circuit Board Surface Finishes*, in *Printed Curcuits Handbook*, J. Clyde F. Coombs, Editor. 2008, McGraw-Hill Companies: United States of America. p. 32.1-32.23.
185. Pan, J. and W.J. Tompkins, *A real-time QRS detection algorithm*. Biomedical Engineering, IEEE Transactions on, 1985(3): p. 230-236.
186. Shelley, K.H., *Photoplethysmography: beyond the calculation of arterial oxygen saturation and heart rate*. Anesthesia & Analgesia, 2007. **105**(6): p. S31-S36.
187. Jo, E., et al., *Validation of biofeedback wearables for photoplethysmographic heart rate tracking*. Journal of Sports Science and Medicine, 2016. **15**(3): p. 540-547.
188. Curative, *Lotus CPAP System: Cloud Based Sleep Patient Management Platform*, C.M.D. gmbh, Editor.
189. *Xpod Model 3011LP & 3012LP Specification and Technical Information*. 2011: Plymouth, Minnesota USA.
190. Suhrbier, A., et al., *Comparison of three methods for beat-to-beat-interval extraction from continuous blood pressure and electrocardiogram with respect to heart rate variability analysis/Vergleich von drei Methoden der Schlag-zu-Schlag-Intervall-Extraktion aus kontinuierlichen Blutdruckverläufen und Elektrokardiogrammen zur Herzratenvariabilitätsanalyse*. Biomedizinische Technik, 2006. **51**(2): p. 70-76.
191. Posada-Quintero, H., et al., *Evaluation of pulse rate variability obtained by the pulse onsets of the photoplethysmographic signal*. Physiological measurement, 2013. **34**(2): p. 179.
192. Ferrer-Mileo, V., et al. *Accuracy of heart rate variability estimation by photoplethysmography using an smartphone: Processing optimization and fiducial point selection*. in *Engineering in Medicine and Biology Society (EMBC), 2015 37th Annual International Conference of the IEEE*. 2015. IEEE.
193. Sadeh, A. and C. Acebo, *The role of actigraphy in sleep medicine*. Sleep Medicine Reviews, 2002. **6**(2): p. 113-124.
194. Kalman, R.E., *A new approach to linear filtering and prediction problems*. Journal of basic Engineering, 1960. **82**(1): p. 35-45.
195. Nabil, D. and F.B. Reguig, *Ectopic beats detection and correction methods: A review*. Biomedical Signal Processing and Control, 2015. **18**: p. 228-244.
196. Albaghli, R. and K.M. Anderson. *A vision for heart rate health through wearables*. in *UbiComp 2016 Adjunct - Proceedings of the 2016 ACM International Joint Conference on Pervasive and Ubiquitous Computing*. 2016.
197. Gula, L.J., et al., *Heart rate variability in obstructive sleep apnea: A prospective study and frequency domain analysis*. Annals of Noninvasive Electrocardiology, 2003. **8**(2): p. 144-149.
198. Bakker, J.P., et al., *A pilot study investigating the effects of continuous positive airway pressure treatment and weight-loss surgery on autonomic activity in obese obstructive sleep apnea patients*. Journal of Electrocardiology, 2014. **47**(3): p. 364-373.

40. Stein, P.K. and Y. Pu, *Heart rate variability, sleep and sleep disorders*. Sleep Medicine Reviews, 2012. **16**(1): p. 47-66.
41. Sannino, G., et al., *Short term Heart Rate Variability to predict blood pressure drops due to standing: A pilot study*. BMC Medical Informatics and Decision Making, 2015. **15**(3).
42. Metelka, R., *Heart rate variability-current diagnosis of the cardiac autonomic neuropathy. A review*. Biomedical Papers, 2014. **158**(3): p. 327-338.
43. La Rovere, M.T., et al., *Short-term heart rate variability strongly predicts sudden cardiac death in chronic heart failure patients*. Circulation, 2003. **107**(4): p. 565-570.
44. Bigger, J., et al., *The ability of several short-term measures of RR variability to predict mortality after myocardial infarction*. Circulation, 1993. **88**(3): p. 927-934.
45. Malik, M. and A.J. Camm, *Components of heart rate variability—what they really mean and what we really measure*. The American journal of cardiology, 1993. **72**(11): p. 821-822.
46. Billman, G.E., *The LF/HF ratio does not accurately measure cardiac sympatho-vagal balance*. Frontiers in Physiology, 2013. **4 FEB**.
47. Smith, A.-L., *Using very short-term heart rate variability to monitor fentanyl-induced changes in the autonomic nervous system preceding respiratory depression HRV and opioid-induced loss of airway tone*, in *School of Computer Science, Engineering and Mathematics*. 2011, Flinders University of South Australia.
48. Moody, G.B. *Spectral analysis of heart rate without resampling*. in *Computers in Cardiology 1993, Proceedings*. 1993. IEEE.
49. Laguna, P., G.B. Moody, and R.G. Mark, *Power spectral density of unevenly sampled data by least-square analysis: performance and application to heart rate signals*. Biomedical Engineering, IEEE Transactions on, 1998. **45**(6): p. 698-715.
50. Huikuri, H.V., et al., *Circadian rhythms of frequency domain measures of heart rate variability in healthy subjects and patients with coronary artery disease. Effects of arousal and upright posture*. Circulation, 1994. **90**(1): p. 121-126.
51. Žemaitytė, D., G. Varoneckas, and E. Sokolov, *Heart rhythm control during sleep*. Psychophysiology, 1984. **21**(3): p. 279-289.
52. Farrell, T.G., et al., *Risk stratification for arrhythmic events in postinfarction patients based on heart rate variability, ambulatory electrocardiographic variables and the signal-averaged electrocardiogram*. Journal of the American College of Cardiology, 1991. **18**(3): p. 687-697.
53. Odemuyiwa, O., et al., *Comparison of the predictive characteristics of heart rate variability index and left ventricular ejection fraction for all-cause mortality, arrhythmic events and sudden death after acute myocardial infarction*. The American journal of cardiology, 1991. **68**(5): p. 434-439.
54. Cripps, T., et al., *Prognostic value of reduced heart rate variability after myocardial infarction: clinical evaluation of a new analysis method*. British heart journal, 1991. **65**(1): p. 14-19.
55. Fries, R., S. Hein, and J. König, *Reversed circadian rhythms of heart rate variability and morning peak occurrence of sustained ventricular tachyarrhythmias in patients with implanted cardioverter defibrillator*. Medical Science Monitor, 2002. **8**(11): p. CR751-CR756.
56. Saul, J.P., et al., *Analysis of long term heart rate variability: methods, 1/f scaling and implications*. Computers in cardiology, 1988. **14**: p. 419-422.
57. Patrino, V., et al., *Acute effects of autoadjusting and fixed continuous positive airway pressure treatments on cardiorespiratory coupling in obese patients with obstructive sleep apnea*. European Journal of Internal Medicine, 2014. **25**(2): p. 164-168.
58. Karasulu, L., et al., *Improving heart rate variability in sleep apnea patients: Differences in treatment with auto-titrating positive airway pressure (APAP) versus conventional CPAP*. Lung, 2010. **188**(4): p. 315-320.

59. Hayano, J., et al., *Stability over time of circadian rhythm of variability of heart rate in patients with stable coronary artery disease*. American heart journal, 1997. **134**(3): p. 411-418.
60. Fioranelli, M., et al., *Analysis of heart rate variability five minutes before the onset of paroxysmal atrial fibrillation*. Pacing and clinical electrophysiology, 1999. **22**(5): p. 743-749.
61. Furlan, R., et al., *Continuous 24-hour assessment of the neural regulation of systemic arterial pressure and RR variabilities in ambulant subjects*. Circulation, 1990. **81**(2): p. 537-547.
62. Jurysta, F., et al., *A study of the dynamic interactions between sleep EEG and heart rate variability in healthy young men*. Clinical neurophysiology, 2003. **114**(11): p. 2146-2155.
63. Jurysta, F., et al., *Long-term CPAP treatment partially improves the link between cardiac vagal influence and delta sleep*. BMC Pulmonary Medicine, 2013. **13**(1).
64. Christian Guilleminault, S.C., Roger Winkle, Kenneth Melvin, Ara Tilikian, *CYCLICAL VARIATION OF THE HEART RATE IN SLEEP APNOEA SYNDROME*. The Lancet, 1984. **323**(8369): p. 126-131.
65. Allen, J., *Photoplethysmography and its application in clinical physiological measurement*. Physiological measurement, 2007. **28**(3): p. R1.
66. Gertsch, M., *Theoretical Basics*, in *The ECG*. 2004, Springer-Verlag: Berlin Heidelberg. p. 3-11.
67. Winter, B.B. and J.G. Webster, *Driven-right-leg circuit design*. IEEE Transactions on Biomedical Engineering, 1983(1): p. 62-66.
68. Berry, R.B., *Fundamentals of sleep medicine*. 2011: Elsevier Health Sciences.
69. McAdams, E., *Bioelectrodes*, in *Encyclopedia of Medical Devices and Instrumentation*. 2006, John Wiley & Sons, Inc.
70. Searle, A. and L. Kirkup, *A direct comparison of wet, dry and insulating bioelectric recording electrodes*. Physiological Measurement, 2000. **21**(2): p. 271.
71. Wheelwright, C.D., *Physiological sensors for use in project Mercury*. Vol. 1082. 1962: National Aeronautics and Space Administration.
72. Avenel-Audran, M., et al., *Contact dermatitis from electrocardiograph-monitoring electrodes: role of p-tert-butylphenol-formaldehyde resin*. Contact dermatitis, 2003. **48**(2): p. 108-111.
73. Meziane, N., et al., *Dry electrodes for electrocardiography*. Physiological Measurement, 2013. **34**(9): p. R47-R69.
74. Uter, W. and H. Schwanitz, *Contact dermatitis from propylene glycol in ECG electrode gel*. Contact Dermatitis, 1996. **34**(3): p. 230-231.
75. Chi, Y.M., T.-P. Jung, and G. Cauwenberghs, *Dry-contact and noncontact biopotential electrodes: methodological review*. Biomedical Engineering, IEEE Reviews in, 2010. **3**: p. 106-119.
76. Muhlsteff, J., et al. *Wearable approach for continuous ECG-and activity patient-monitoring*. in *Engineering in Medicine and Biology Society, 2004. IEMBS'04. 26th Annual International Conference of the IEEE*. 2004. IEEE.
77. Hoffmann, K.-P., R. Ruff, and W. Poppendieck. *Long-term characterization of electrode materials for surface electrodes in biopotential recording*. in *Engineering in Medicine and Biology Society, 2006. EMBS'06. 28th Annual International Conference of the IEEE*. 2006. IEEE.
78. Meziane, N., et al., *Simultaneous comparison of 1 gel with 4 dry electrode types for electrocardiography*. Physiological Measurement, 2015. **36**(3): p. 513-529.
79. Geddes, L. and M. Valentinuzzi, *Temporal changes in electrode impedance while recording the electrocardiogram with "dry" electrodes*. Annals of biomedical engineering, 1973. **1**(3): p. 356-367.
80. Jourand, P., H. De Clercq, and R. Puers, *Robust monitoring of vital signs integrated in textile*. Sensors and Actuators, A: Physical, 2010. **161**(1-2): p. 288-296.

81. Di Rienzo, M., et al. *MagIC system: A new textile-based wearable device for biological signal monitoring. Applicability in daily life and clinical setting.* in *Annual International Conference of the IEEE Engineering in Medicine and Biology - Proceedings.* 2005.
82. Gandhi, N., et al. *Properties of dry and non-contact electrodes for wearable physiological sensors.* in *Proceedings - 2011 International Conference on Body Sensor Networks, BSN 2011.* 2011.
83. Yoo, J., et al., *A wearable ECG acquisition system with compact planar-fashionable circuit board-based shirt.* *IEEE Transactions on Information Technology in Biomedicine*, 2009. **13**(6): p. 897-902.
84. Xie, L., et al. *A system-on-chip and paper-based inkjet printed electrodes for a hybrid wearable bio-sensing system.* in *Engineering in Medicine and Biology Society (EMBC), 2012 Annual International Conference of the IEEE.* 2012. IEEE.
85. Schijvenaars, B.J., G. van Herpen, and J.A. Kors, *Intraindividual variability in electrocardiograms.* *Journal of Electrocardiology*, 2008. **41**(3): p. 190-196.
86. Yong Gyu Lim, K.K.K., and Kwang Suk Park, *ECG Measurement on a Chair Without Conductive Contact.* *IEEE TRANSACTIONS ON BIOMEDICAL ENGINEERING*, 2006. **53**(5): p. 956-959.
87. Aleksandrowicz, A. and S. Leonhardt, *Wireless and Non-contact ECG Measurement System—the “Aachen SmartChair”.* *Acta Polytechnica*, 2007. **47**(4-5).
88. Lim, Y.G., K.K. Kim, and K.S. Park, *ECG recording on a bed during sleep without direct skin-contact.* *Biomedical Engineering, IEEE Transactions on*, 2007. **54**(4): p. 718-725.
89. Ueno, A., et al., *Capacitive sensing of electrocardiographic potential through cloth from the dorsal surface of the body in a supine position: A preliminary study.* *IEEE Transactions on Biomedical Engineering*, 2007. **54**(4): p. 759-766.
90. Ottenbacher, J. and S. Heuer. *Motion artefacts in capacitively coupled ECG electrodes.* in *World Congress on Medical Physics and Biomedical Engineering, September 7-12, 2009, Munich, Germany.* 2009. Springer.
91. Chapman, D., *ResMed Research-Guiding Document.* 2010, Flinders University: MDPP.
92. Farrugia, S.P. and D.G. Chapman, *Method and apparatus for detecting cardiac signals.* 2011, Google Patents.
93. He, D., E.S. Winokur, and C.G. Sodini. *A continuous, wearable, and wireless heart monitor using head ballistocardiogram (BCG) and head electrocardiogram (ECG).* in *Engineering in Medicine and Biology Society, EMBC, 2011 Annual International Conference of the IEEE.* 2011. IEEE.
94. He, D.D., E.S. Winokur, and C.G. Sodini, *An Ear-Worn Vital Signs Monitor.* *Biomedical Engineering, IEEE Transactions on*, 2015. **62**(11): p. 2547-2552.
95. Zhang, Q., et al., *A machine learning-empowered system for long-term motion-tolerant wearable monitoring of blood pressure and heart rate with ear-ECG/PPG.* *IEEE Access*, 2017. **5**: p. 10547-10561.
96. Yang, H.-C., et al., *Study of Single-Arm Electrode for ECG Measurement Using Flexible Print Circuit.* Department of Electrical Engineering, Southern Taiwan University.
97. Zhang, H., et al. *A novel Motion and Noise Artifacts Reduction Mechanism (MNARM) for wearable PPG-based heart rate extraction.* in *IET Conference Publications.* 2015.
98. Shin, J.H., et al., *Nonconstrained sleep monitoring system and algorithms using air-mattress with balancing tube method.* *IEEE Transactions on Information Technology in Biomedicine*, 2010. **14**(1): p. 147-156.
99. Korhonen, I. and A. YLI-HANKALA, *Photoplethysmography and nociception.* *Acta Anaesthesiologica Scandinavica*, 2009. **53**(8): p. 975-985.
100. Sinex, J.E., *Pulse oximetry: principles and limitations.* *The American journal of emergency medicine*, 1999. **17**(1): p. 59-66.

101. Schäfer, A. and J. Vagedes, *How accurate is pulse rate variability as an estimate of heart rate variability?: A review on studies comparing photoplethysmographic technology with an electrocardiogram*. International journal of cardiology, 2013. **166**(1): p. 15-29.
102. Netzer, N., et al., *Overnight pulse oximetry for sleep-disordered breathing in adults: a review*. CHEST Journal, 2001. **120**(2): p. 625-633.
103. Johansson, A. and P. Öberg, *Estimation of respiratory volumes from the photoplethysmographic signal. Part I: experimental results*. Medical & biological engineering & computing, 1999. **37**(1): p. 42-47.
104. Elgendi, M., *On the analysis of fingertip photoplethysmogram signals*. Current cardiology reviews, 2012. **8**(1): p. 14-25.
105. Tur, E., et al., *Basal perfusion of the cutaneous microcirculation: measurements as a function of anatomic position*. Journal of investigative dermatology, 1983. **81**(5): p. 442-446.
106. Baek, H.J., et al., *Photoplethysmogram measurement without direct skin-to-sensor contact using an adaptive light source intensity control*. IEEE Transactions on Information Technology in Biomedicine, 2009. **13**(6): p. 1085-1088.
107. Nilsson, L., et al., *Combined photoplethysmographic monitoring of respiration rate and pulse: a comparison between different measurement sites in spontaneously breathing subjects*. Acta Anaesthesiologica Scandinavica, 2007. **51**(9): p. 1250-1257.
108. Charkoudian, N. *Skin blood flow in adult human thermoregulation: how it works, when it does not, and why*. in *Mayo Clinic Proceedings*. 2003. Elsevier.
109. Curative, *Lotus CPAP System: Cloud Based Sleep Patient Management Platform*, C.M.D. gmbh, Editor.
110. Sugino, S., et al., *Forehead is as sensitive as finger pulse oximetry during general anesthesia*. Canadian Journal of Anesthesia, 2004. **51**(5): p. 432-436.
111. Schallom, L., et al., *Comparison of forehead and digit oximetry in surgical/trauma patients at risk for decreased peripheral perfusion*. Heart & Lung: The Journal of Acute and Critical Care, 2007. **36**(3): p. 188-194.
112. Cheng, E.Y., M.B. Hopwood, and J. Kay, *Forehead pulse oximetry compared with finger pulse oximetry and arterial blood gas measurement*. Journal of clinical monitoring, 1988. **4**(3): p. 223-226.
113. Shelley, K.H., et al., *The effect of venous pulsation on the forehead pulse oximeter wave form as a possible source of error in Spo2 calculation*. Anesthesia & Analgesia, 2005. **100**(3): p. 743-747.
114. Chiu, Y.C., et al., *Determination of pulse wave velocities with computerized algorithms*. American heart journal, 1991. **121**(5): p. 1460-1470.
115. Kazanavicius, E., et al., *Mathematical methods for determining the footpoint of the arterial pulse wave and evaluation of proposed methods*. Information Technology and control, 2005. **34**(1): p. 29-36.
116. Giardino, N.D., P.M. Lehrer, and R. Edelberg, *Comparison of finger plethysmograph to ECG in the measurement of heart rate variability*. Psychophysiology, 2002. **39**(2): p. 246-253.
117. Khandoker, A.H., C.K. Karmakar, and M. Palaniswami, *Comparison of pulse rate variability with heart rate variability during obstructive sleep apnea*. Medical engineering & physics, 2011. **33**(2): p. 204-209.
118. Hayano, J., et al., *Assessment of pulse rate variability by the method of pulse frequency demodulation*. Biomedical engineering online, 2005. **4**(1): p. 62.
119. Milnor, W.R., *Hemodynamics*. 1982, Baltimore: Williams & Wilkins.
120. Shan, S.-M., et al. *Reliable PPG-based algorithm in atrial fibrillation detection*. in *Biomedical Circuits and Systems Conference (BioCAS), 2016 IEEE*. 2016. IEEE.
121. Paradkar, N. and S.R. Chowdhury. *Cardiac arrhythmia detection using photoplethysmography*. in *Engineering in Medicine and Biology Society (EMBC), 2017 39th Annual International Conference of the IEEE*. 2017. IEEE.

122. Hayes, M.J. and P.R. Smith, *A new method for pulse oximetry possessing inherent insensitivity to artifact*. Biomedical Engineering, IEEE Transactions on, 2001. **48**(4): p. 452-461.
123. Kim, S.H., D.W. Ryoo, and C. Bae. *U-healthcare system using smart headband*. in *Engineering in Medicine and Biology Society, 2008. EMBS 2008. 30th Annual International Conference of the IEEE*. 2008. IEEE.
124. Comtois, G., Y. Mendelson, and P. Ramuka. *A comparative evaluation of adaptive noise cancellation algorithms for minimizing motion artifacts in a forehead-mounted wearable pulse oximeter*. in *Engineering in Medicine and Biology Society, 2007. EMBS 2007. 29th Annual International Conference of the IEEE*. 2007. IEEE.
125. Khan, E., et al., *A robust heart rate monitoring scheme using photoplethysmographic signals corrupted by intense motion artifacts*. IEEE Transactions on Biomedical Engineering, 2016. **63**(3): p. 550-562.
126. Temko, A. *Estimation of heart rate from photoplethysmography during physical exercise using Wiener filtering and the phase vocoder*. in *Proceedings of the Annual International Conference of the IEEE Engineering in Medicine and Biology Society, EMBS*. 2015.
127. Mendelson, Y., R.J. Duckworth, and G. Comtois. *A wearable reflectance pulse oximeter for remote physiological monitoring*. in *Annual International Conference of the IEEE Engineering in Medicine and Biology - Proceedings*. 2006.
128. Cha, J.Y., et al. *Unconstrained respiration and heart rate monitoring system based on a PPG pillow during sleep*. in *Proceedings of the 30th Annual International Conference of the IEEE Engineering in Medicine and Biology Society, EMBS'08 - "Personalized Healthcare through Technology"*. 2008.
129. Tamura, T., et al., *Wearable photoplethysmographic sensors—past and present*. Electronics, 2014. **3**(2): p. 282-302.
130. He, D., et al. *The ear as a location for wearable vital signs monitoring*. in *Engineering in Medicine and Biology Society (EMBC), 2010 Annual International Conference of the IEEE*. 2010. IEEE.
131. Poh, M.-Z., et al., *Cardiovascular monitoring using earphones and a mobile device*. IEEE Pervasive Computing, 2012. **11**(4): p. 18-26.
132. Kim, C.-S., et al., *Ballistocardiogram: Mechanism and potential for unobtrusive cardiovascular health monitoring*. Scientific reports, 2016. **6**.
133. Mukai, T., et al. *Determination of locations on a tactile sensor suitable for respiration and heartbeat measurement of a person on a bed*. in *Engineering in Medicine and Biology Society (EMBC), 2014 36th Annual International Conference of the IEEE*. 2014. IEEE.
134. Mack, D.C., et al. *A passive and portable system for monitoring heart rate and detecting sleep apnea and arousals: Preliminary validation*. in *Conference Proceedings - 1st Transdisciplinary Conference on Distributed Diagnosis and Home Healthcare, D2H2 2006*. 2006.
135. Nukaya, S., et al., *Noninvasive bed sensing of human biosignals via piezoceramic devices sandwiched between the floor and bed*. IEEE Sensors Journal, 2012. **12**(3): p. 431-438.
136. Di Rienzo, M., et al., *Wearable seismocardiography for the beat-to-beat assessment of cardiac intervals during sleep*. Conference proceedings : ... Annual International Conference of the IEEE Engineering in Medicine and Biology Society. IEEE Engineering in Medicine and Biology Society. Annual Conference, 2014. **2014**: p. 6089-6091.
137. Jia, W., et al. *Estimation of heart rate from a chest-worn inertial measurement unit*. in *4th International Symposium on Bioelectronics and Bioinformatics, ISBB 2015*. 2015.
138. Jafari Tadi, M., et al., *Gyrocardiography: A New Non-invasive Monitoring Method for the Assessment of Cardiac Mechanics and the Estimation of Hemodynamic Variables*. Scientific Reports, 2017. **7**(1): p. 6823.

139. Wiens, A.D., A. Johnson, and O.T. Inan, *Wearable Sensing of Cardiac Timing Intervals From Cardiogenic Limb Vibration Signals*. IEEE Sensors Journal, 2017. **17**(5): p. 1463-1470.
140. Tavakolian, K., *Characterization and analysis of seismocardiogram for estimation of hemodynamic parameters*. 2010, Applied Science: School of Engineering Science.
141. Kim, C., et al., *Ballistocardiogram as Proximal Timing Reference for Pulse Transit Time Measurement: Potential for Cuffless Blood Pressure Monitoring*. Biomedical Engineering, IEEE Transactions on, 2015. **62**(11): p. 2657-2664.
142. Neary, J.P., et al., *Assessment of mechanical cardiac function in elite athletes*. Open Sports Med J, 2011. **5**: p. 26-37.
143. Etemadi, M., et al. *Tracking clinical status for heart failure patients using ballistocardiography and electrocardiography signal features*. in *Engineering in Medicine and Biology Society (EMBC), 2014 36th Annual International Conference of the IEEE*. 2014. IEEE.
144. Inan, O.T., et al., *Novel wearable seismocardiography and machine learning algorithms can assess clinical status of heart failure patients*. Circulation: Heart Failure, 2018. **11**(1): p. e004313.
145. Balakrishnan, G., F. Durand, and J. Guttag. *Detecting pulse from head motions in video*. in *Computer Vision and Pattern Recognition (CVPR), 2013 IEEE Conference on*. 2013. IEEE.
146. Hernandez, J., et al. *BioGlass: Physiological parameter estimation using a head-mounted wearable device*. in *Wireless Mobile Communication and Healthcare (Mobihealth), 2014 EAI 4th International Conference on*. 2014. IEEE.
147. Bruser, C., et al., *Adaptive beat-to-beat heart rate estimation in ballistocardiograms*. Information Technology in Biomedicine, IEEE Transactions on, 2011. **15**(5): p. 778-786.
148. Li, Q., R.G. Mark, and G.D. Clifford, *Robust heart rate estimation from multiple asynchronous noisy sources using signal quality indices and a Kalman filter*. Physiological measurement, 2008. **29**(1): p. 15.
149. Ebrahim, M.H., J.M. Feldman, and I. Bar-Kana, *A robust sensor fusion method for heart rate estimation*. Journal of Clinical Monitoring, 1997. **13**(6): p. 385-393.
150. Ansermino, J.M., et al., *An evaluation of a novel software tool for detecting changes in physiological monitoring*. Anesthesia and Analgesia, 2009. **108**(3): p. 873-880.
151. Yang, P., G. Dumont, and J.M. Ansermino, *Adaptive change detection in heart rate trend monitoring in anesthetized children*. IEEE Transactions on Biomedical Engineering, 2006. **53**(11): p. 2211-2219.
152. Sayadi, O. and M.B. Shamsollahi, *Life-threatening arrhythmia verification in ICU patients using the joint cardiovascular dynamical model and a bayesian filter*. IEEE Transactions on Biomedical Engineering, 2011. **58**(10 PART 1): p. 2748-2757.
153. Yang, P., G.A. Dumont, and J.M. Ansermino, *Sensor fusion using a hybrid median filter for artifact removal in intraoperative heart rate monitoring*. Journal of Clinical Monitoring and Computing, 2009. **23**(2): p. 75-83.
154. Foussier, J., et al., *An adaptive Kalman filter approach for cardiorespiratory signal extraction and fusion of non-contacting sensors*. BMC Medical Informatics and Decision Making, 2014. **14**(1).
155. Andreotti, F., et al. *Improved heart rate detection for camera-based photoplethysmography by means of Kalman filtering*. in *2015 IEEE 35th International Conference on Electronics and Nanotechnology, ELNANO 2015 - Conference Proceedings*. 2015.
156. Bruser, C., et al., *Improvement of force-sensor-based heart rate estimation using multichannel data fusion*. IEEE Journal of Biomedical and Health Informatics, 2015. **19**(1): p. 227-235.
157. Castanedo, F., *A review of data fusion techniques*. The Scientific World Journal, 2013. **2013**.

158. Kamen, E.W. and J.K. Su, *Kalman Filter Applications*, in *Introduction to Optimal Estimation*. 1999, Springer London: London. p. 225-267.
159. Novak, V., et al., *Influence of respiration on heart rate and blood pressure fluctuations*. *Journal of Applied Physiology*, 1993. **74**(2): p. 617-626.
160. Sforza, E., et al., *Cardiovascular variability during periodic leg movements: a spectral analysis approach*. *Clinical neurophysiology*, 2005. **116**(5): p. 1096-1104.
161. Hayano, J., et al., *Screening for obstructive sleep apnea by cyclic variation of heart rate*. *Circ Arrhythm Electrophysiol*, 2011. **4**(1): p. 64-72.
162. Julier, S.J. and J.K. Uhlmann. *New extension of the Kalman filter to nonlinear systems*. in *Signal processing, sensor fusion, and target recognition VI*. 1997. International Society for Optics and Photonics.
163. Jarisch, W. and J.S. Detwiler, *Statistical Modeling of Fetal Heart Rate Variability*. *IEEE Transactions on Biomedical Engineering*, 1980. **BME-27**(10): p. 582-589.
164. Li, Q., R.G. Mark, and G.D. Clifford, *Artificial arterial blood pressure artifact models and an evaluation of a robust blood pressure and heart rate estimator*. *Biomedical engineering online*, 2009. **8**(1): p. 13.
165. Arnold, M., et al., *Adaptive AR modeling of nonstationary time series by means of Kalman filtering*. *IEEE Transactions on Biomedical Engineering*, 1998. **45**(5): p. 553-562.
166. McSharry, P.E., et al., *A dynamical model for generating synthetic electrocardiogram signals*. *Biomedical Engineering, IEEE Transactions on*, 2003. **50**(3): p. 289-294.
167. McNames, J. and M. Aboy, *Statistical modeling of cardiovascular signals and parameter estimation based on the extended kalman filter*. *IEEE Transactions on Biomedical Engineering*, 2008. **55**(1): p. 119-129.
168. Townsend, N., *Merging multiple estimates to form a single estimate*. 2001, Oxford:Department of Engineering Science, University Oxford.
169. Nemati, S., A. Malhotra, and G.D. Clifford, *Data Fusion for Improved Respiration Rate Estimation*. *EURASIP journal on advances in signal processing*, 2010. **2010**: p. 926305.
170. Liu, N.T., et al., *Reliable real-time calculation of heart-rate complexity in critically ill patients using multiple noisy waveform sources*. *Journal of Clinical Monitoring and Computing*, 2014. **28**(2): p. 123-131.
171. A F Pimentel, M., et al., *Heart beat detection in multimodal physiological data using a hidden semi-Markov model and signal quality indices*. *Physiological Measurement*, 2015. **36**(8): p. 1717-1727.
172. Clifford, G.D., et al., *Signal quality indices and data fusion for determining clinical acceptability of electrocardiograms*. *Physiological Measurement*, 2012. **33**(9): p. 1419-1433.
173. Li, Q. and G. Clifford, *Signal quality indices and data fusion for determining acceptability of electrocardiograms collected in noisy ambulatory environments*. *Computing in Cardiology*, 2011. **38**.
174. Behar, J., et al. *A single channel ECG quality metric*. in *Computing in Cardiology*. 2012.
175. Clifford, G.D., et al. *Signal quality indices and data fusion for determining acceptability of electrocardiograms collected in noisy ambulatory environments*. in *Computing in Cardiology*. 2011.
176. Sukor, J.A., S. Redmond, and N. Lovell, *Signal quality measures for pulse oximetry through waveform morphology analysis*. *Physiological measurement*, 2011. **32**(3): p. 369.
177. Li, Q. and G. Clifford, *Dynamic time warping and machine learning for signal quality assessment of pulsatile signals*. *Physiological measurement*, 2012. **33**(9): p. 1491.
178. Zong, W., G. Moody, and R. Mark, *Reduction of false arterial blood pressure alarms using signal quality assessment and relationships between the electrocardiogram and arterial blood pressure*. *Medical and Biological Engineering and Computing*, 2004. **42**(5): p. 698-706.

199. Rand, J., et al., *Real-time correction of heart interbeat intervals*. Biomedical Engineering, IEEE Transactions on, 2007. **54**(5): p. 946-950.
200. Peters, C., et al., *The effect of artifact correction on spectral estimates of heart rate variability*. Conference proceedings : ... Annual International Conference of the IEEE Engineering in Medicine and Biology Society. IEEE Engineering in Medicine and Biology Society. Conference, 2008: p. 2669-2672.
201. Wessel, N., et al., *Nonlinear analysis of complex phenomena in cardiological data*. Herzschrittachertherapie und Elektrophysiologie, 2000. **11**(3): p. 159-173.
202. Tarkiainen, T.H., et al., *Comparison of methods for editing of ectopic beats in measurements of short-term non-linear heart rate dynamics*. Clinical physiology and functional imaging, 2007. **27**(2): p. 126-133.
203. Goldberger, A.L., et al., *Physiobank, physiotoolkit, and physionet components of a new research resource for complex physiologic signals*. Circulation, 2000. **101**(23): p. e215-e220.
204. Silva, I. and G.B. Moody, *An open-source toolbox for analysing and processing physionet databases in matlab and octave*. Journal of open research software, 2014. **2**(1).
205. Nunan, D., G.R. Sandercock, and D.A. Brodie, *A Quantitative Systematic Review of Normal Values for Short-Term Heart Rate Variability in Healthy Adults*. Pacing and clinical electrophysiology, 2010. **33**(11): p. 1407-1417.
206. dos Santos, L., et al., *Application of an automatic adaptive filter for heart rate variability analysis*. Medical engineering & physics, 2013. **35**(12): p. 1778-1785.
207. Dantas, E.M., et al., *Spectral analysis of heart rate variability with the autoregressive method: What model order to choose?* Computers in biology and medicine, 2012. **42**(2): p. 164-170.
208. Berger, R.D., et al., *An Efficient Algorithm for Spectral Analysis of Heart Rate Variability*. IEEE Transactions on Biomedical Engineering, 1986. **BME-33**(9): p. 900-904.
209. Iozzia, L., L. Cerina, and L. Mainardi, *Relationships between heart-rate variability and pulse-rate variability obtained from video-PPG signal using ZCA*. Physiological Measurement, 2016. **37**(11): p. 1934-1944.
210. Koenig, N., et al., *Validation of a new heart rate measurement algorithm for fingertip recording of video signals with smartphones*. Telemedicine and e-Health, 2016. **22**(8): p. 631-636.
211. Barbieri, R. and E.N. Brown, *Correction of erroneous and ectopic beats using a point process adaptive algorithm*. Conference proceedings : ... Annual International Conference of the IEEE Engineering in Medicine and Biology Society. IEEE Engineering in Medicine and Biology Society. Conference, 2006: p. 3373-3376.
212. Brennan, M., M. Palaniswami, and P. Kamen. *A new model-based ectopic beat correction algorithm for heart rate variability*. in *Annual Reports of the Research Reactor Institute, Kyoto University*. 2001.
213. Mateo, J. and P. Laguna, *Analysis of heart rate variability in the presence of ectopic beats using the heart timing signal*. IEEE Transactions on Biomedical Engineering, 2003. **50**(3): p. 334-343.
214. Solem, K., P. Laguna, and L. Sörnmo, *An efficient method for handling ectopic beats using the heart timing signal*. IEEE Transactions on Biomedical Engineering, 2006. **53**(1): p. 13-20.
215. Force, P.A.P.T.T., et al., *Clinical guidelines for the manual titration of positive airway pressure in patients with obstructive sleep apnea*. Journal of Clinical Sleep Medicine, 2008. **4**(02): p. 157-171.
216. He, T., G. Clifford, and L. Tarassenko, *Application of independent component analysis in removing artefacts from the electrocardiogram*. Neural Computing & Applications, 2006. **15**(2): p. 105-116.
217. Busek, P., et al., *Spectral analysis of heart rate variability in sleep*. Physiological research, 2005. **54**(4): p. 369.

218. Mendez, M., et al. *Time-varying analysis of the heart rate variability during REM and non REM sleep stages*. in *Engineering in Medicine and Biology Society, 2006. EMBS'06. 28th Annual International Conference of the IEEE*. 2006. IEEE.
219. Escalona, O.J., et al., *Wrist and Arm Body Surface Bipolar ECG Leads Signal and Sensor Study for Long-term Rhythm Monitoring*. *Computing*, 2017. **44**: p. 1.
220. Kruskal, W.H. and W.A. Wallis, *Use of ranks in one-criterion variance analysis*. *Journal of the American statistical Association*, 1952. **47**(260): p. 583-621.
221. Gardner, M., et al. *Estimation of heart rate during sleep measured from a gyroscope embedded in a CPAP mask*. in *Biomedical Engineering and Sciences (IECBES), 2016 IEEE EMBS Conference on*. 2016. IEEE.
222. Gardner, M., et al. *A wearable device for monitoring patients during PAP therapy*. in *IEEE Life Science Conference*. 2017. Sydney, Australia: IEEE.
223. King, F.W., *Hilbert Transforms*. *Encyclopedia of Mathematics and its Applications*. Vol. 2. 2009: Cambridge University Press.
224. Resta, O., et al., *Sleep-related breathing disorders, loud snoring and excessive daytime sleepiness in obese subjects*. *International Journal of Obesity & Related Metabolic Disorders*, 2001. **25**(5).
225. Purves, D., et al., *Physiological Changes in Sleep States*, in *Neuroscience*. 2001, Sinauer Associates: Sunderland (MA).